

**Palaeolimnology of high and low altitude sites in
Ethiopia: Diatom and geochemistry records from
Garba Guracha and Lake Babogaya**

David Anton Ieuan Grady

A thesis submitted in fulfilment of the requirements for the degree of
Doctor of Philosophy

March 2020

Aberystwyth University

Supervisors: Dr Sarah Davies & Professor Henry Lamb



Word Count of thesis: DECLARATION	79, 119
This work has not previously been accepted in substance for any degree and is not concurrently submitted in candidature for any degree.	
Candidate name	David Anton Ieuan Grady
Signature:	
Date	31/03/2020

STATEMENT 1

This thesis is the result of my own investigations, except where otherwise stated. Where ***correction services** have been used, the extent and nature of the correction is clearly marked in a footnote(s).

Other sources are acknowledged by footnotes giving explicit references. A bibliography is appended.

Signature:	
Date	31/03/2020

[*this refers to the extent to which the text has been corrected by others]

STATEMENT 2

I hereby give consent for my thesis, if accepted, to be available for photocopying and for inter-library loan, and for the title and summary to be made available to outside organisations.

Signature:	
Date	31/03/2020

NB: *Candidates on whose behalf a bar on access (hard copy) has been approved by the University should use the following version of Statement 2:*

I hereby give consent for my thesis, if accepted, to be available for photocopying and for inter-library loans after expiry of a bar on access approved by Aberystwyth University.

Signature:	
Date	31/03/2020

i Dad a Maddie

Acknowledgments

Thank you first and foremost to my two amazing supervisors Dr. Sarah Davies and Professor Henry Lamb. They have offered me some of the best guidance I could have asked for over the last three years. Through some very bad times during this PhD they have been there for me without fail with a happy smile, full of advice and kind words. A thanks also to Dr. Patrick Robson, Dr. Graciela Gil-Romera and Lucas Bittner who have literally been my inspiration through my three years at Aberystwyth and listened to my woes without fail. Because of them I have not felt alone in the wild world of academia. Hollie Wynne was also the difference for me in the labs at Aberystwyth University, not only in the company but with her lab expertise, so a huge thank you for that.

I'm very grateful to the Mountain Exile Hypothesis Group for welcoming me into the team and dealing with my fussy eating habits at 4,000 m altitude. A huge thank you especially to Mekbib Fekadu who seamlessly helped coordinate the logistics in Ethiopia of such a huge project. A thanks also to the Masonic Charitable Foundation, the QRA and INQUA that helped fund various aspects of my research. A thank you also to Professor Frank Schabitz for allowing me to use, and funding radiocarbon dates on the Lake Babogaya core. A big thank you to the staff at the Royal Botanic Garden Edinburgh, especially Frieda Christie, for their assistance for the week that I took over their microscopes. Also, a large thank you to Rosa and David for the months of help in identifying a new diatom species at one of my sites.

A little odd, but I would like to thank Chef Gordon Ramsey, Grubby and the team at Game Grumps for their shows and streams that I watched/listened to in the microscope room and during some very difficult periods on my first and second years. Always managed to perk my mood back up and get me going on the right track again!

My family and friends deserve a huge thanks for their encouragement and time listening to things that they likely didn't quite understand regarding mud and algae. Twm, Jordan, Cynan and Josh especially were there for me during some very tough times and done an amazing job of groomsmen despite my "diatom-talk" the day before my wedding. My dad and my darling wife Maddie have been monumental in helping me through everything so far. I can never be grateful enough to them for all their love, care and support.

"Winners win. Losers let it happen."

– Mr. Rees (Blwyddyn 9-11, YGCR)

Abstract

Palaeoenvironmental studies at high altitude in eastern Africa are rare. As a result, our understanding of contemporary climate change in the region is limited. This study presents high-resolution, multi-proxy (diatoms and core geochemistry) palaeolimnological reconstructions at sites located at contrasting altitudes: Garba Guracha a cirque lake >3950 m above sea level spanning the last 16,000 years, and since the mid-Holocene at Lake Babogaya a crater lake on the western escarpment of the Main Ethiopian Rift (1800 m above sea level).

These palaeo-records broadly exhibit the same glacial-interglacial dynamics and sub-millennial shifts in climate found in other palaeolimnological records from across eastern Africa. However, these shifts are more muted at Garba Guracha. Furthermore, the precise timing and expression of these climatic events is not always synchronous between the Lake Babogaya and Garba Guracha records as well as other records across eastern Africa.

The Garba Guracha sediment geochemistry and diatom record is typical of a dry, post-glacial and sparsely vegetated environment with the dominance of Fragilarioid taxa and high terrigenous input. Due to the poorly developed post-glacial landscape at Garba Guracha, any Younger Dryas-like drying signal would have been superimposed on to high soil erosion and a poorly productive lake environment. The retreat of a nearby ice mass may also have over-ridden any catchment development related to the start of the African Humid Period. However, in response to increased moisture availability and warming at Garba Guracha after 10,250 cal BP, catchment productivity considerably increases with a large increase in diatom productivity and organic matter content and remains

high for the majority of the remaining African Humid Period interval. The termination of the African Humid Period is clear in the Garba Guracha diatom record at around 5,500 cal BP, with a second phase of change to an environment similar to the modern day after 4,500 cal BP, potentially representing the Meghalayan. Drier conditions around the Meghalayan is also documented in the Lake Babogaya record with the deposition of a Gastropod shell layer. A reduction in organic matter content following the deposition of this layer likely represents reduced productivity and a destabilising catchment under a drier climate. These drier conditions culminate in the deposition of coarse grained, terrigenous material between 3,600 and 3,300 cal BP. Following high lake nutrient content and deepening of the lake between 3,300 cal BP and 1,750 cal BP, the Lake Babogaya record suggests a relatively stable, deep lake, with only brief intervals of shallower waters, until the top of the core (~600 cal BP). The diatom record after 560 cal BP at Garba Guracha is characterised by a dominance of aerophilous taxa such as *Nitzschia amphibia* and Cymbelloid taxa driven by an increased growing season and nutrient loading under a drier climate.

These records further reinforce the reported heterogeneous pattern of climate across the region and the significance of site-specific dynamics in the responses of catchments to regional drivers. The data produced in this study may be used to inform future climate modelling and perform more complete regional downscaling, while also furthering our understanding of palaeoenvironmental change in eastern Africa, at a variety of altitudes.

Key words: Ethiopia, Garba Guracha, Lake Babogaya, palaeolimnology, diatoms, XRF geochemistry.

Table of Contents

Chapter 1 : Research Context & Aims	1
1.1 Contemporary climate change.....	1
1.2 Lake sediments as archives of palaeoenvironmental data.....	3
1.3 Records of environmental change in Ethiopia.....	5
1.4 Aims & Objectives	8
1.5 Thesis structure.....	10
Chapter 2 : Hydrological Change in eastern Africa	11
2.1 Reconstructing Palaeoenvironments in eastern Africa	12
2.1.1 Chronological controls	15
2.1.2 Issues with proxies	18
2.2 Overview of eastern African climatology	20
2.2.1 Long-term controls on eastern African climate.....	22
2.3 Heinrich Stadial 1 (18,000 – 15,000 BP) and eastern Africa	23
2.4 The African Humid Period (15,000 – 5,000 BP)	25
2.4.1 The Younger Dryas (12,700 – 11,800 BP).....	26
2.4.2 Resumption of the AHP in the Early Holocene.....	30
2.4.3 Termination of the AHP	34
2.5 The Meghalayan	37
2.6 The Last Millennium	41
2.7 Summary.....	46
Chapter 3 : The Physical Environment of Ethiopia & Study Sites	47
3.1 Geology of Ethiopia	47
3.2 Ethiopian Climate.....	48
3.3 The Bishoftu Crater Lakes	50
3.3.1 Study Site 1: Lake Babogaya	55
3.4 The Bale Mountains	61
3.4.1 Study site 2: Garba Guracha	63
3.4.1.1 Environmental change at Garba Guracha since the Late Pleistocene....	68

Chapter 4 : Study Methods.....	73
4.1 Field sampling.....	74
4.1.1 Core retrieval.....	74
4.2 Laboratory methods	77
4.2.1 Core lithology and chronology	77
4.2.2 Water chemistry	82
4.2.3 X-ray fluorescence (XRF) scanning.....	82
4.2.4 Isotopic analysis of bulk organic material.....	84
4.3 Diatoms.....	84
4.3.1 Diatoms and environmental change.....	86
4.3.2 Diatom-based research in eastern Africa.....	92
4.3.2.1 Understanding transfer functions in eastern Africa	93
4.3.3 Diatom sample preparation and analysis	96
4.3.3.1 Diatom identification and taxonomy.....	98
4.3.3.2 Microscopy and photography	99
4.3.3.3 Taxonomy of problematic species	101
4.3.3.3.1 <i>Nitzschia</i> Hassall	101
4.3.3.3.2 <i>Fragilaria</i> Lyngbye	107
4.4 Numerical methods.....	113
Chapter 5 : Constructing the Babogaya composite core depth model ...	122
5.1 Initial core description and section correlation	123
5.2 Section correlation by XRF data	125
5.3 Section correlation using visual stratigraphic markers	125
5.3.1 Matching core stratigraphy to XRF data.....	125
5.3.2 Core section correlation using Dynamic Time Warping.....	129
5.4 Conclusion: final composites	131
Chapter 6 : Results - Lake Babogaya	135
6.1 Core lithology.....	135
6.1.1 Composite core (0.68 – 8.30 m)	135
6.1.2 Floating core.....	138
6.2 Chronology.....	139
6.3 Core chemistry.....	143
6.3.1 Composite core data	144

6.3.2 Floating core data.....	148
6.4 The diatom record.....	152
6.4.1 Composite core data	152
6.4.2 Floating core data.....	156
6.4.3 Laminae diatom counts.....	159
6.4.4 Diatom ordination	159
6.5 Interpretation of the Babogaya sedimentary record	165
6.6 Summary of the palaeolimnological Lake Babogaya record	182
Chapter 7 : Results – Garba Guracha.....	185
7.1 Modern aquatic environment	185
7.2 Modern diatom ecology.....	187
7.3 Master core creation and lithology.....	189
7.4 Core chronology	191
7.4.1 Sediment-water interface.....	191
7.4.2 Main core.....	193
7.5 Core geochemistry	194
7.6 The diatom record.....	199
7.6.1 Garba Guracha diatom principal curve and quantitative data.....	207
7.7 Interpretation of the Garba Guracha sedimentary record.....	210
7.8 Summary of the palaeolimnological record of BAL-GGU17-1AB	221
Chapter 8 : Discussion of Findings	224
8.1 Consideration of methods and avenues of further research.....	224
8.2 Late Pleistocene/Early Holocene environmental change at Garba Guracha.....	226
8.2.1 Younger Dryas-type hydrological change at Garba Guracha?	228
8.3 Onset of humid conditions at Garba Guracha – delayed AHP?	229
8.4 Abrupt changes in the Holocene?	231
8.4.1 Termination of the African Humid Period	233
8.4.2 The Meghalayan (4,200 BP to present day).....	237
8.5 Post-4.2 ka BP event change	239
8.5.1 Modern rapid change in eastern Africa	243
8.6 Anthropogenic impacts	244

Chapter 9: Conclusions	246
9.1 Palaeolimnological change at Lake Babogaya and Garba Guracha	246
References.....	249
Appendices.....	291
Appendix 1	291
Appendix 2	323
Thesis plates	331

List of Figures

Chapter 1 : Research Context & Aims

Figure 1.1: Number of studies at various sites with published lacustrine sediment records. 8

Chapter 2 : Hydrological Change in eastern Africa

Figure 2.1: Eastern Africa and neighbouring countries, with major lakes in light blue. The boxed area forms the main focus of this review, with some relevant analogues from other regions also discussed where appropriate. 13

Figure 2.2: Comparison of East African palaeoclimate, the Dongge cave (southeast Asia) and NGRIP records. 16

Figure 2.3: Simplified models for depositions of a calcareous organic (mixed) varve (left) and a clastic varve (right; Zolitschka *et al.*, 2015). 17

Figure 2.4: Seasonal climatology (December, January and February; DJF, March, April and May; MAM, June, July and August; JJA and September, October and November; SON) for tropical Africa, including precipitation rates (Mitchell & Jones, 2005), surface wind (Kalnay *et al.* 1996), and the approximate locations of the ITCZ (solid line) and CAB (dotted line). Dashed red box corresponds to the boxed area in Figure 2.1. Adapted from Tierney *et al.* (2011b). 22

Figure 2.5: Change in summer insolation for North Africa (20°N; top) and African lake level status from an updated OLLD (Tierney *et al.*, 2011a; bottom). Adapted from deMenocal & Tierney (2012). 24

Figure 2.6: Comparison of some palaeoenvironmental records around the YD interval (yellow), with blue highlighting earlier/later changes in certain records. 31

Figure 2.7: Proxy lake status reconstructions from the Oxford Lake Level Database (Street-Perrott *et al.*, 1989), updated with more recent lake level reconstructions in Tierney *et al.* (2011b), for 9,000 BP (A) and 6,000 BP (B). Dashed red box corresponds to the boxed area in Figure 2.1. Adapted from Tierney *et al.* (2011b). 32

Figure 2.8: Rolling 200 year mean of Manning & Timpson's (2014) summed probability distribution analyses using all ¹⁴C dates in their three correlating regions (Eastern and Central Sahara and the 'Atlas Hoggar').. 33

Figure 2.9: Comparison of the AHP represented in palaeoclimate records across Africa. 36

Figure 2.10: Regional time slices of ΔD_{wax} across eastern African sites between 14,000 and 5,000 BP (Costa *et al.*, 2014) showing the influence of the CAB in regional hydrological changes. 37

Figure 2.11: Comparison of climatic conditions 9000 BP to present in East Africa showing increased variability from the end of the AHP. 40

Figure 2.12: 1,100-year historical (1883 AD-present) and sedimentology-inferred lake level (arrow and dashed line indicate overflow period) and salinity (diatom-inferred conductivity) record for the Crescent Island crater basin in Lake Naivasha, Kenya, compared with a decadal record of atmospheric ¹⁴CO₂ production as a proxy for solar radiation, with periods of solar minima also noted..... 42

Figure 2.13: Qualitative comparison of African lake levels 9,000 BP vs. present levels. Reconstructed from the OLLD (COHMAP members, 1988; Street-Perrott *et al.*, 1989) updated with lake-level data generated in the last twenty years by Tierney *et al.* (2011b).....43

Chapter 3 : The Physical Environment of Ethiopia & Study Sites

Figure 3.1: Simplified geological map of Ethiopia redrawn from Tadesse *et al.* (2003).....48

Figure 3.2: The seasonal precipitation cycle in Ethiopian rainfall zones adapted from Viste *et al.*, 2013)..... 50

Figure 3.3: Bishoftu Crater Lakes location within Ethiopia (red point in inset map) and the Bishoftu area (black lines indicate roads). 51

Figure 3.4: Mean (\pm standard deviation) monthly rainfall (blue) and average air temperature (orange) data for 1951-2003 (missing 1991-1993) and 1952-2005, respectively, from the Debre Zeit Research Centre meteorological station in Awulachew *et al.* (2006). 53

Figure 3.5: Aragonite laminations in freeze-dried section of Lake Hora core HG98-1 (top; scale in cm). Scanning electron microscope images of aragonite crystals (bottom; 5 μ m scale) from (Lamb *et al.* 2002). 56

Figure 3.6: Bathymetric scans and images of Lake Babogaya (Schaebitz unpubl. data). The photograph was taken by H. Lamb from the south-eastern shore of the lake..... 58

Figure 3.7: Seasonal characteristics of Lake Babogaya waters adapted from Lamb *et al.* (2002). Temperature profiles April 1964 - September 1966. All profiles are between 19° and 20°C at 30 m depth, with vertical grids spaced at 1°C intervals (top). Dissolved oxygen content of Lake Babogaya to a depth of 60 m, May 1964 - October 1966 (bottom). Red line highlights the general level of lake anoxia. 60

Figure 3.8: Bale Mountains, and surrounding major towns, location within Ethiopia. Faded contour lines, between bold 1000 m lines, denote changes of 200 m..... 62

Figure 3.9: Schematic SW–NE profile of the Bale Mountains to show altitudinal zonation of regional vegetation by Umer *et al.* (2007). 63

Figure 3.10: Rainfall (blue) and temperature (orange) of areas in, and around, the Bale Mountains. A – Dinsho, B – Rira (6°46.3'N, 39°43.5'E), C – Goba and D – Dola-Mena (for settlement locations see Figure 3.8).. 64

Figure 3.11: Garba Guracha location within the Bale mountains (left) and cross-sectional view of basin characteristics (right; Tiercelin *et al.*, 2008). Sample locations in Tiercelin *et al.* (2008) are shown..... 65

Figure 3.12: Outlet point from Garba Guracha into the Togona valley (arrow) overflowing in 2001 (Tiercelin *et al.*, 2008; left) and desiccated in 2017 (right), with the lake level considerably lower than during overflow periods (red line indicates overflow shoreline level) and far from the outlet point (bottom). Sand is evident on the very outer lake edge, with organic-rich muds towards the centre. 67

Figure 3.13: Environmental proxies from Garba Guracha in Umer *et al.* (2007) and Tiercelin *et al.* (2008)..... 72

Chapter 4 : Study Methods

Figure 4.1: Sample locations around Garba Guracha in the 2001 field campaign (in Tiercelin *et al.*, 2008), with sample and spring locations in 2017 also shown (this study). Due to the small size of springs 2 and 3, possibly due to the dry conditions, a small pool where both streams merged downstream was sampled..... 75

Figure 4.2: Bathymetry of Lake Babogaya, with core sample locations during the 2011 coring campaign (Schäbitz, unpublished data.) 77

Figure 4.3: Diatom morphology of three example species from the centrics (left) and both araphid (middle) and raphid pennates (right). Diatom images include those taken under a light microscope (top) and a scanning electron microscope (bottom). Scale bars at 10 µm. 85

Figure 4.4: Simplified diagram showing the influence of changing precipitation and evaporation on the physical and chemical characteristics of a lake, and the effect this has on the diatom assemblage of that lake..... 86

Figure 4.5: The salinity ranges (horizontal line) and salinity optima (circle) of selected diatom species from the Northern Great Plains, North America, generated from a survey of water chemistry and diatoms in the surface sediments of 55 regional lakes. 89

Figure 4.6: Simplified diagram of the process of deriving quantitative reconstructions of past lake characteristics from biostratigraphical palaeolimnological data using transfer functions by Juggins & Birks (2012)..... 90

Figure 4.7: Changes in Moon Lake log diatom-inferred salinity estimates (g/L; solid line) redrawn from Laird *et al.* (1998). This diatom-inferred salinity record is compared with a Bhalme-Mooley Drought Index (BMDI; dotted) based on Oladipo (1986) BMDI equation for the Great Plains region and monthly summer (April–September) precipitation records from nearby climate stations..... 91

Figure 4.8: DARES protocol for counting broken valves..... 101

Figure 4.9: Images of similar diatoms in the literature. *Nitzschia amphibia*. f. *rostrata* (left; A), *Nitzschia lancettula* (middle; B) and *Nitzschia vanoyei* (right; C). Images taken from Krammer & Lange-Bertalot (1997: 373, pl. 78, figs. 22-23), Hustedt (1949: pl. 13, figs. 39-47) and Cholnoky (1954: 421, pl. 2, figs. 75-81), respectively..... 106

Figure 4.10: Common forms of *Nitzschia abonouensis* (A), *Nitzschia mediocris* (B), *Nitzschia etoshensis* (C), *Nitzschia palea* (D) and *Nitzschia paleacea* (E). Images from sources cited in Table 4.2. Scale bars = 10 µm. No scale given in Hustedt (1949) and Krammer & Lange-Bertalot (1988) for B and E..... 109

Figure 4.11: <i>Nitzschia fabiennejansseniana</i> under LM. 2-15 = valve view, 16-18 = girdle view. 27a = zoomed view of the valve (accompanying scale bar for this figure is 5 μ m) to illustrate the central gap between fibulae (arrow)	110
Figure 4.12: Example principal curve through the Abernethy pollen dataset (Birks & Mathewes, 1978), as in Simpson & Birks (2012), created in R.	116
Figure 4.13: Squared residual length for the fossil assemblages down the Garba Guracha core	120
Figure 4.14: Squared chord distance for the fossil assemblages down the Garba Guracha core.....	121

Chapter 5 : Constructing the Babogaya composite core depth model

Figure 5.1: Flowchart of determining final core stratigraphy for analysis of the Lake Babogaya core.....	123
Figure 5.2: Stratigraphy of core BA-LC-2011 plotted against field depth.	124
Figure 5.3: Use of XRF in supporting visual core features	127
Figure 5.4: Marked peaks in Ti are used to identify an overlap between sections 8B and 9A, following carbonate rich sediments in 8B (blue arrow), in the absence of apparent visual tie points.	128
Figure 5.5: Concept of DTW functions for various time series, with dotted and solid lines representing reference and query time series, respectively	130
Figure 5.6: Three-way DTW plots for potential overlaps between 9B and 10A (first 'missing' section; A), 9B and a subset of 10A (B), 9B and section 10 (C), 11A and 9B (D), 11A and 10B (second 'missing' section; E).	132
Figure 5.7: BA-LC-2011 sections (numbered in red) plotted by composite depth. Section overlaps are highlighted (blue) which led to the formation of the composite core, with sediment unused in the composite shown as grey..	134

Chapter 6 : Results - Lake Babogaya

Figure 6.1: Lake Babogaya composite core lithology.	137
Figure 6.2: Lake Babogaya floating composite core lithology.	139
Figure 6.3: Bayesian age-depth model of four micro-charcoal AMS ¹⁴ C dates from composite Babogaya core, constructed in BACON for R.	141
Figure 6.4: Bayesian age-depth model of three micro-charcoal AMS ¹⁴ C dates from the floating composite Babogaya core, constructed in BACON for R.	142
Figure 6.5: Organic carbon and XRF-derived peak area geochemical data for the Babogaya composite core	146

Figure 6.6: Pearson's correlation matrix of selected elements in the Babogaya composite core derived from XRF scanning.....	147
Figure 6.7: Organic carbon and XRF-derived peak area geochemical data for the Babogaya floating core	149
Figure 6.8: Pearson's correlation matrix of selected elements in the Babogaya composite core derived from XRF scanning.....	150
Figure 6.9: Diatom diagram for the Lake Babogaya composite core by depth (age as secondary axis).....	154
Figure 6.10: Diatom diagram for the Lake Babogaya floating core by depth (age as secondary axis).....	158
Figure 6.11: Diatom diagram for Lake Babogaya laminated section (89.7-90.8 cm composite depth) counts by depth	160
Figure 6.12: Diatom diagram for Lake Babogaya laminated section (491.49-492.39 cm composite depth) counts by depth	160
Figure 6.13: Diatom diagram for Lake Babogaya laminated section (442.28-443.08 cm composite depth) counts by depth	161
Figure 6.14: Principal curve (blue) of the Babogaya diatom data. Taxa scores in (PCA) ordination space are denoted by red crosses, with the main taxa labelled. The start of the curve (A; 0 PrC score) and end of the curve (B; 1 PrC score) are also shown.	162
Figure 6.15: Quantitative diatom data for the Lake Babogaya composite core.....	163
Figure 6.16: Quantitative diatom data for the Lake Babogaya floating core	164
Figure 6.17: Synthesis of diatom, XRF-derived peak area and organic geochemical for the Lake Babogaya core.....	166
Figure 6.18: Lake Babogaya bathymetry (left) and cross sections of three transects across this data (cross sections shown on the right)	174

Chapter 7 : Results - Garba Guracha

Figure 7.1: Composition of the Garba Guracha diatom flora around the lake (left), with sample locations also shown (right)	188
Figure 7.2: Garba Guracha master core (BAL-GGU17-1AB) lithostratigraphy (Bittner <i>et al.</i> , submitted.).....	190
Figure 7.3: Fallout radionuclide concentrations in short core taken from Garba Guracha showing (a) total ²¹⁰ Pb, (b) unsupported ²¹⁰ Pb, and (c) ¹³⁷ Cs and ²⁴¹ Am concentrations versus depth (top). Radiometric chronology showing the CRS model ²¹⁰ Pb dates and sedimentation rates for the Garba Guracha short core (bottom).....	193
Figure 7.4: Bayesian age-depth model of fourteen bulk AMS ¹⁴ C dates from core BAL-GGU17, constructed in Bittner <i>et al.</i> (submitted) using BACON for R.....	196

Figure 7.5: XRF-derived peak area geochemical data for the Garba Guracha core.....	200
Figure 7.6: Pearson’s correlation matrix of selected elements in the Garba Guracha core derived from XRF scanning.....	201
Figure 7.7: Diatom diagram for the Garba Guracha core by depth (age as secondary axis)	203
Figure 7.8: Principal curve (blue) of the Garba Guracha diatom data. Taxa scores in (PCA) ordination space are denoted by red crosses, with the main taxa labelled. ‘A’ denotes the beginning of the curve (i.e. lowest principal curve scores) and ‘B’ representing the end of the curve (i.e. highest principal curve scores).....	208
Figure 7.9: Quantitative diatom data for the Garba Guracha core	209
Figure 7.10: Synthesis of both XRF-derived peak area geochemical and diatom data for the Garba Guracha core.....	211
Figure 7.11: Pollen diagram from Garba Guracha from Umer <i>et al.</i> (2007). Percentages are calculated from the sum of all pollen grains and fern spores counted. The red line denotes the increase in Ericaceous vegetation cover.....	213

Chapter 8 : Discussion of Findings

Figure 8.1: Lake levels around Africa at 9,000 BP (redrawn from Tierney <i>et al.</i> , 2011b). The red dashed box outlines the region of eastern Africa region as defined in Chapter 2, with the solid black circle the location of Garba Guracha.....	230
Figure 8.2: Termination of the AHP across multiple sites in much of Africa as determined by Shanahan <i>et al.</i> (2015), including the locations and timings of the termination of the AHP at the study sites included in this study	235
Figure 8.3: Comparison of Lake Babogaya records with similar records from relatively nearby Lake Abiyata (Chalie & Gasse, 2018; note reverse scale) and Chew Bahir (Foerster <i>et al.</i> , 2012; note reverse scale), with ENSO activity as recorded in the Laguna Pallacacocha red colour intensity record (Moy <i>et al.</i> , 2002) also shown	241
Figure 8.4: Comparison of Garba Guracha records discussed in text with similar records from relatively close sites (the Gulf of Aden (Tierney <i>et al.</i> , 2015) Chew Bahir (Foerster <i>et al.</i> , 2012; note reverse scale) and Lake Challa (Tierney <i>et al.</i> , 2011b) in easternmost areas where moisture from the Indian Ocean is important and ENSO activity as recorded in the Laguna Pallacacocha red colour intensity record (Moy <i>et al.</i> , 2002).....	242

List of Tables

Chapter 2 : Hydrological Change in eastern Africa

Table 2.1: Main study sites discussed in this review with corresponding site numbers plotted in Figure 2.1. * - marine core record..... 14

Chapter 3 : The Physical Environment of Ethiopia & Study Sites

Table 3.1: Hydrological characteristics of Lake Hora (HO) and Lake Babogaya (BA; Lamb *et al.*, 2002). Direct rainfall (DR), groundwater (GW), evaporation (Evap.) and chlorine (Cl). 52

Table 3.2: Oxygen and carbon isotope values (V-PDB) for aragonite from individual year-assigned laminae in the sediments of Lake Hora (Lamb *et al.*, 2002)..... 56

Table 3.3: Hydrochemistry of the Debre Zeit area groundwater (Gr) and Lake Babogaya (BA) surface water in 1998¹ from Lamb *et al.* (2002) and 2001² for Lake Babogaya surface waters to 50 m depth by Lemma (2009). 57

Table 3.4: Lake Garba Guracha hydrochemistry in May 2001 from Tiercelin *et al.* (2008). Sampling locations in relation to Lake Garba Guracha are shown in Figure 3.8. Trace concentrations are represented by a '+'. 69

Chapter 4 : Study Methods

Table 4.1: Range (mean \pm s.d) of *Nitzschia fenestralis* measurements (under LM; in μm) of 50 valves in a sample dominated by the species compared to similar looking species. * - Measurements of *Nitzschia amphibia* used, as source: Hustedt (1959) is currently unavailable. ** - Based on his own observations, Hustedt (1949) argues this is not the full size range of the species and that *Nitzschia lancettula forma minor* (bracketed measurements) described by Müller (1905) are incorrect. Numbers next to species names correspond to the images in Figure 4.9..... 105

Table 4.2: Range (1 d.p; mean \pm s.d: 2 d.p) of *Nitzschia fenestralis* measurements (under LM and SEM; in μm) of 200 valves (10 in SEM) in samples dominated by the species, compared to morphologically similar species. All measurements are given in μm . * n = the 10 samples measured under SEM. nd = not determined/documented. Images of each species can be found in Figure 5.11 and 5.12..... 108

Table 4.3: Variance explained by the PrC compared with PCA/CA axes 1 and 2 for both Lake Babogaya and Garba Guracha. All data have been rounded to 3 decimal places... 117

Table 4.4: Performance statistics for WA and WA-PLS models for conductivity transfer functions using the Garba Guracha fossil diatom data. 119

Chapter 5 : Constructing the Babogaya composite core depth model

Table 5.1: Visual and geochemical tie points identified to create a composite..... 133

Chapter 6 : Results - Lake Babogaya

Table 6.1: AMS radiocarbon chronology for Lake Babogaya composite and floating cores (* omitted dates). Radiocarbon ages were calibrated in CALIB (v. 7.1; Stuiver & Reimer, 1993) using the IntCal13 calibration curve (Reimer *et al.*, 2013)..... 140

Chapter 7 : Results - Garba Guracha

Table 7.1: Garba Guracha hydrochemistry in February 2017. Sampling locations around the lake are shown in Figure 4.1. 186

Table 7.2: ²¹⁰Pb chronology of Garba Guracha sediment-water interface core..... 192

Table 7.3: AMS radiocarbon dates in order of depth for the Garba Guracha core. 195

Chapter 1 :

Research Context & Aims

This research aims to present detailed, long-term palaeoenvironmental reconstructions from a low and high-altitude site in eastern Africa to provide a perspective of change through time across altitude on the continent which is currently lacking in the wider literature. This chapter serves as an introduction to the main themes, topics and discussions of this thesis. Within this introduction the rationale, main aims and objectives of this research are outlined, with a summary of the thesis structure also provided. 'BP' throughout this thesis indicates calibrated years before 1950.

1.1 | Contemporary climate change

Increased environmental pollution, rising temperatures and associated climate change are now firmly established as a reality (IPCC, 2013). The consequences of recent change are already evident (Parmesan & Yohe, 2003). A variety of emergent challenges will face societies in the coming decades, with many suggesting multiple 'planetary boundaries' have already been traversed (Steffen *et al.*, 2015). At least 0.5°C of warming has already been experienced across sub-Saharan Africa in the past century (Niang *et al.*, 2014), which is one of the regions most vulnerable to a changing climate as an estimated 386 million individuals live on less than US\$1.25/day, with a mean poverty line of US\$2.25/day (Ravallion, 2012). In combination with this low capacity for adaptation, agriculture is a major economic sector in the region, and is projected to be severely impacted, with recent

estimates suggesting wheat yields across East Africa, for example, may decline by up to 72% as a result of a changing climate (Adhikari *et al.*, 2015).

Furthermore, the tropics play a key role in the global moisture and heat budget (Yin & Battisti, 2001; Weldeab *et al.*, 2007), and in the stability of higher latitude ice masses both in the present (Ding *et al.*, 2014) and the past (Trauth *et al.*, 2003). Environmental and climatic change in the African tropics holds significant implications for the global system, as well as the inhabitants of the region, underlining the need to fully understand change in this region. However, despite an expansion of research teams and programmes such as the ‘PEP III Pole-Equator-Pole transect through Europe and Africa’, generating a vast expansion of quantitative data regarding past hydrological and climatic change in the African tropics (see Chapter 2), the region remains under-represented due to the scarcity of long-term records, in comparison with higher-latitudes. As a result our current understanding of past and ongoing climatic change in the region remains uncertain (Giannini *et al.*, 2008; Dosio & Panitz, 2016). For example, despite a gradual reduction in precipitation across the Horn of Africa, potentially as a consequence of recent anthropogenic climate change (Liebmann *et al.*, 2014; Tierney *et al.*, 2015), recent modelling by Tierney *et al.* (2015) suggests the region will have become considerably wetter by the end of the 21st century. Conversely, precipitation across the more southerly countries of the eastern African tropics such as Mozambique and Malawi is projected to decline as a result of a changing climate (Niang *et al.*, 2014). The production of further high-resolution, long-term records of environmental change is essential to fully understand how lower latitude atmospheric components respond to major forcing factors, and also the role of the tropics within the global climate system.

1.2 | Lake sediments as archives of palaeoenvironmental data

Lakes accumulate sediments continually, an ongoing process since their formation, in many cases for thousands to millions of years. This accumulation archives numerous physical, chemical and biological proxies. Recent developments such as non-destructive x-ray fluorescence (XRF) scanning techniques, can combine to facilitate a multi-proxy, holistic approach to reconstruct past environmental conditions for an area. The sedimentary archives of the numerous lake basins across the African tropics offer the potential to produce long-term records of environmental and climatic change over both spatial and temporal scales (Verschuren & Russell, 2009).

The extensive research effort to reconstruct the past African climate has gradually produced a detailed outline of past hydrological change since the Last Glacial Maximum (LGM; 23,000-19,000 BP), which was characterised by arid conditions and low lake levels (Gasse, 2000). During the last glacial-interglacial transition conditions gradually became more humid, with a considerable shift to significantly humid conditions at the start of the so-called African humid period (AHP), associated with enhanced monsoonal activity, and marked by a widespread increase in lake levels across the continent and the 'greening' and populating of the Sahara (Tierney *et al.*, 2011b; Manning & Timpson, 2014). This period of enhanced humidity terminated around 6,000-5,000 years ago, although the rapidity of this termination is uncertain with multiple contradictory records from archives across the region suggesting either an abrupt (deMenocal *et al.*, 2000; Tierney *et al.*, 2008; Marshall *et al.*, 2009; Garcin *et al.*, 2012; Tierney & deMenocal, 2013) or

gradual termination (Kröpelin *et al.*, 2008; Marshall *et al.*, 2011; Foerster *et al.*, 2012; Junginger & Trauth, 2013).

As the number and resolution of palaeoenvironmental records from across the region has increased it has become clear that these millennial-scale variations in climate have been punctuated by abrupt climatic shifts towards dry conditions, which appear to be global in nature: Heinrich event 1 (H1; ~18,000-15,000 BP) and the Younger Dryas (YD; 12,700-11,500 BP). Present conditions in many parts of the African tropics are dry, however these conditions are relatively mild in comparison to the dry conditions experienced during H1. Multiple lake records across the region, such as lakes Victoria (Talbot & Lærdal, 2000; Stager *et al.*, 2002), Tanganyika (Tierney *et al.*, 2008), Malawi (Brown *et al.*, 2007), Bosumtwi, Ghana (Brooks *et al.*, 2005; Shanahan *et al.*, 2015), Tana, northern Ethiopia (Lamb *et al.*, 2007; Marshall *et al.*, 2011), suggest substantial lake level lowering or desiccation coinciding with the H1 event in the Northern Hemisphere (Hemming, 2004). Similarly, the YD represents a brief return to arid conditions from the AHP, recorded in the sediments of multiple lakes such as Chew Bahir (Foerster *et al.*, 2012), Challa (Tierney *et al.*, 2011b), Tanganyika (Tierney *et al.*, 2008), Victoria (Stager *et al.*, 2002) and Malawi (Barker *et al.*, 2007). The exact timing of both the onset and termination of the YD is uncertain, with some studies displaying contradictory records (e.g. Lézine *et al.*, 2005; Marshall *et al.*, 2009; Ivory *et al.*, 2012; Tierney & deMenocal, 2013). Further abrupt, short-lived arid intervals have also been identified in multiple palaeoenvironmental reconstructions during the Holocene around 4,000 years BP and potentially around 8,200 years BP (e.g. Thompson *et al.*, 2002; Powers *et al.*, 2005; Tierney *et al.*, 2011b; Marshall *et al.*, 2011).

The Milankovitch precessional cycle (19-23 ka) forcing of summer insolation is considered to be the dominant mechanism for these millennial-scale hydrological changes since the LGM (Kutzbach & Street-Perrott, 1985; Trauth *et al.*, 2003). Multiple feedback processes are required to fully explain these non-linear climatic transitions in the last 20,000 years, including changes in vegetation cover, ice sheet dynamics and SSTs of the Atlantic and Pacific (Renssen *et al.*, 2006; Tierney *et al.*, 2008; Timm *et al.*, 2010).

Dearing (2013) highlights the potential for lacustrine archives to provide useful data for contemporary societies in facing future environmental change by producing highly resolved time-series of data, and also provide essential long-term perspectives for complex socio-ecological systems, especially at regional scales. For example, Dearing *et al.* (2008) argue multiple records of environmental change and human activity, including lake sedimentary records, in southwest China for the past ~9,000 years, provided valuable insights into the future resilience and sustainability of the modern agricultural system, by illustrating the importance of adapting local anthropogenic activities and anticipating the behaviour of the summer monsoon. Furthermore, palaeoclimate data obtained from lacustrine records may ultimately be used to constrain and calibrate model simulations of past and future climate (Anderson *et al.*, 2006; Dearing, 2013).

1.3 | Records of environmental change in Ethiopia

Ethiopia is positioned between the climatic boundary of the humidity associated with the tropics and the semi-arid and arid climate of the eastern Sahel. This geographical positioning also places Ethiopia on the northernmost limit of the Inter Tropical Convergence Zone (ITCZ), where even a slight reduction of the northern

penetration of the ITCZ would lead to drastic reductions, and even failures, in rainfall. Furthermore, much of the country, like the rest of the Horn of Africa region, is sensitive to variations in moisture sources from the Indian Ocean, especially further east where little or moisture is received from the Congo Basin (Tierney *et al.*, 2011b).

The Main Ethiopian Rift (MER) Valley region has been a key point of focus for reconstructing past environmental conditions. However, long, high-resolution records in the Ethiopian rift are lacking, with many key studies relying on shorelines of former lakes (e.g. Gillespie *et al.*, 1983; Johnson *et al.*, 2001). Exploitation of Ethiopia's sedimentary lake archives for long, continuous paleoenvironmental reconstructions has been increasing over the past couple of decades with studies at multiple sites including lakes Tilo (Telford & Lamb, 1999), Abiyata (Chalié & Gasse, 2002) and Chew Bahir (Foerster *et al.*, 2012) in the very south of the MER.

Crater lakes have small, well-defined catchments, simple basin morphologies, and are often associated with rapid rates of sediment accumulation making them able to provide some of the best sedimentary records of environmental change (Williams *et al.*, 1993). The record from Lake Tilo (Telford *et al.*, 1999) highlights the utility of crater lakes in studying palaeoenvironmental change in the MER region. North of Lake Tilo on the western escarpment of the rift, southeast of Addis Ababa, Lamb *et al.* (2002) demonstrate that the biochemical varves evident in the lake sediments of Lake Hora (and likely nearby Lake Babogaya), are deposited annually and are linked to the annual cycle of lake stratification and mixing. A high-resolution record from these laminated sediments would contribute to the current understanding of environmental change across the MER region.

Recently, sedimentary archives in highland lakes in the north (Lamb *et al.*, 2007; Marshall *et al.*, 2009; 2011; Loakes *et al.*, 2018) and south of Ethiopia (Umer *et al.*, 2007; Tiercelin *et al.*, 2008; Gil-Romera *et al.*, 2019) have also been used to reconstruct past environmental change. A limited amount of research had previously been done in eastern Africa, with higher altitude sites still rare (Figure 1.1), despite their sensitivity to climatic change (e.g. Thompson *et al.*, 2005; Camarero *et al.*, 2015; Vanneste *et al.*, 2017) and potential importance as refugia for early human populations (Ossendorf *et al.*, 2019). Further comparisons can be made of the impacts of climatic changes between higher altitude sites and the plethora of sites at lower elevations. Inevitably the availability and accessibility of lower altitude sites has contributed to a greater wealth of studies at lower altitude sites in the region. These recent studies at higher altitudes in Ethiopia have been invaluable in offering perspectives on environmental change across altitudinal ranges in the region.

Garba Guracha is a small cirque lake sitting above the afro-alpine zone in the Bale Mountains, southern Ethiopia, a region known to be occupied to some degree during the Middle Stone Age (47,000 to 31,000 BP) at the Fincha Habera rock shelter ~20 km to the north east (Ossendorf *et al.*, 2019). Garba Guracha also represents a site on the eastern edge of Atlantic moisture sources and thus able to offer a perspective of a changing climatically driven hydrological cycle sourced by the Indian Ocean at high altitude. The site has previously been studied by Umer *et al.* (2007) and Tiercelin *et al.* (2008), but much of this focus was on catchment changes (i.e. the development of the post-glacial environment and vegetational change) as opposed to primarily understanding hydrological and limnological changes at Garba Guracha.

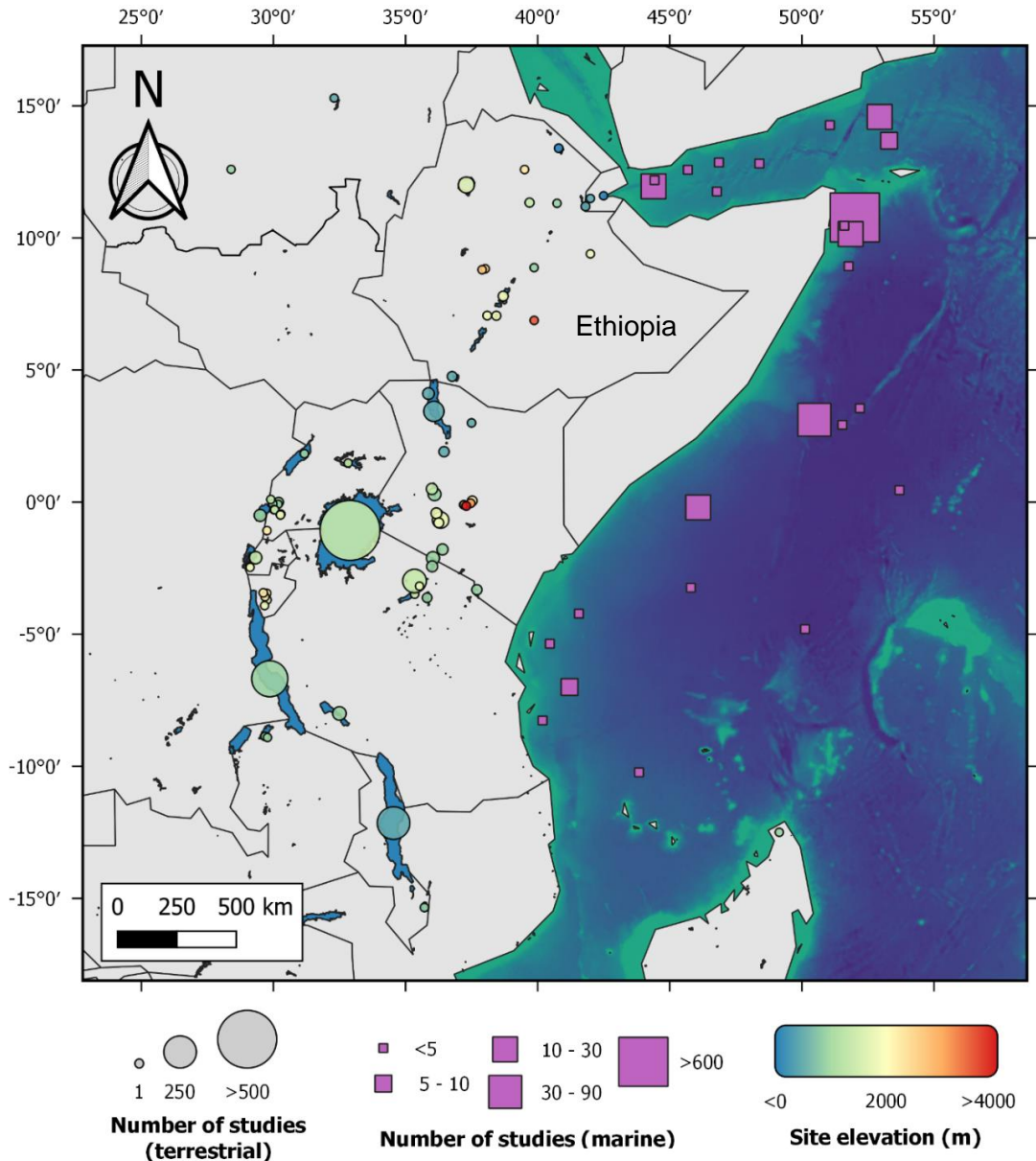


Figure 1.1: Number of studies at various sites with published lacustrine sediment records. Data was acquired using database searches for keywords for each site (e.g. “Lake Victoria” AND “sediment”) for sites listed in the NOAA and Neotoma databases. Created using QGIS (v. 2.18.15).

1.4 | Aims & Objectives

The aim of this research is to provide detailed, long-term palaeoenvironmental reconstructions from eastern Africa. Sedimentary records from two sites are investigated utilising a multi-proxy approach: Lake Babogaya, a crater lake in

central Ethiopia (1800 m elevation) and Garba Guracha, a high-altitude (3950 m elevation), cirque lake in the Bale Mountains. Of particular interest in this work is to compare the expression of past climate change recorded at these two contrasting sites (in terms of elevation and environmental history) in order to further our limited understanding of past (as well as contemporary) climate change dynamics across a range of elevations.

Specific research questions addressed in this thesis include:

- Is there palaeolimnological evidence to suggest millennial scale hydrological changes since the last glaciation and significant hydrological changes during the Holocene?
- How is the termination of the African Humid Period expressed at Garba Guracha and Lake Babogaya?
 - Was the termination abrupt or gradual?
- How do the findings from the sites compare to other records from Ethiopia, the Horn of Africa and subtropical Africa?
 - Is there a difference in the expressions of climate change at the higher altitude site in comparison to the lower altitude site and others in the region?
 - What are the possible mechanisms controlling the expression of climatic events at Lake Babogaya and Garba Guracha?
- Is there palaeolimnological evidence of anthropogenic impacts to the lake catchment?
 - To what extent have humans impacted the lake catchments through time?

1.5 | Thesis structure

This thesis is divided into eight chapters. This first chapter has provided the context and main aims of this research. The issues and topics outlined in this chapter will then be addressed in Chapter 2, which provides a comprehensive review of the current literature regarding the past hydrological climate of the eastern African tropics since H1. Ultimately, this review aims to provide a regional context for the results of this study to be compared against.

The climate and geology of Ethiopia is described in Chapter 3, with the specific climate, hydrochemistry and underlying geology of the study sites also presented within this national context. In Chapter 4 the methodological approach adopted in this study is discussed, with a context and rationale for these methods also provided. The results acquired through utilising these methods are presented and interpreted in Chapter 5 (Garba Guracha) and Chapter 6 (Lake Babogaya). Due to issues encountered in core retrieval and correlation, Chapter 7 provides an outline of the methodical approach taken to correlate the Lake Babogaya core.

Results from both sites are discussed in reference to one another, as well as the wider literature in Chapter 8, with a consideration of methods used and further work also given. This thesis concludes in Chapter 9 by outlining the key findings of the research in reference to the original research questions posed and highlighting the contribution of this study to our understanding of the long-term climate history of Ethiopia.

Chapter 2 :

Hydrological Change in eastern Africa

Since early work by researchers such as Livingstone (1967), Grove & Goudie (1971), and Gasse & Street (1978), understanding of the palaeoenvironment of eastern Africa continues to significantly improve. This chapter aims to review the current literature regarding our understanding of climatic variability across eastern Africa (see Figure 2.1), since the last glacial maximum. It builds upon the earlier reviews of Gasse (2000), Peyron *et al.* (2000), Marchant & Hooghiemstra (2004), Kiage & Liu (2006) and Nash *et al.* (2016). While these reviews provide extensive analyses, some are either spatially or temporally limited in their reviews, or concentrate on specific environmental proxies or conditions. This chapter builds on these earlier syntheses to reflect the latest methodological advancements in palaeoenvironmental reconstructions, and the considerable effort by multiple researchers at new sites, especially across Ethiopia and the Horn of Africa region over the past decade (Figure 2.1; Table 2.1). Since the earlier reviews of Gasse (2000) and Kiage & Liu (2006), there have been numerous methodological advances, including non-destructive XRF scanning facilitating extensive multi-proxy approaches (see Davies *et al.*, 2015). Calibration datasets have been developed, and continue to improve, to constrain the ecological indicator value of lacustrine biological proxies (e.g. Eggermont *et al.*, 2006; 2010), and innovative organic biomarker proxies have been identified (e.g. δD_{wax} , Tex_{86} and BIT-indices¹)

¹ TEX_{86} is based on the degree of cyclisation of membrane lipids, specifically isoprenoid glycerol dialkyl glycerol tetraethers (GDGTs) from Thaumarchaeota in lake sediments with the BIT (Branched and Isoprenoid Tetraether) index reflecting the input of GDGTs from terrestrial soil bacteria (Powers *et al.*, 2010).

which have begun to allow new temperature and moisture balance reconstructions (Verschuren & Russell, 2009).

In combination with the chapter 3, this review of past hydrological change across East Africa since the end of the last glacial maximum ultimately provides a framework which facilitates the comparison and validation of the new findings of this research with other research from the region.

2.1 | Reconstructing Palaeoenvironments in eastern Africa

Traditionally, reconstructing past environmental change in tropical Africa was significantly hindered by the rarity of instrumental and documentary records prior to European colonisation in the 19th Century (Nash & Adamson, 2014). The opportunities to utilise longer-term, natural archives commonly used in the higher latitudes (e.g. tree ring and ice core records) are limited in tropical Africa (Verschuren, 2003), with a Holocene Kilimanjaro ice core record the sole example in this region (Thompson *et al.*, 2002). Lake sedimentary archives have therefore long been recognised as “the principal source of information” in reconstructing the past climate and environments of tropical Africa (Verschuren, 2003: 315).

Lacustrine records from multiple sites across eastern Africa have been analysed using a multitude of different proxies and have provided an environmental record for the past 17,000 years (Figure 2.2) and beyond. The focus of these reconstructions has varied from long-term glacial-interglacial dynamics through the Quaternary, to short-term centennial to inter-annual scales in order to understand the regional responses to natural shifts in climate; relevant to current anthropogenic climate change and the role of climate in the development and evolution of humans through time.

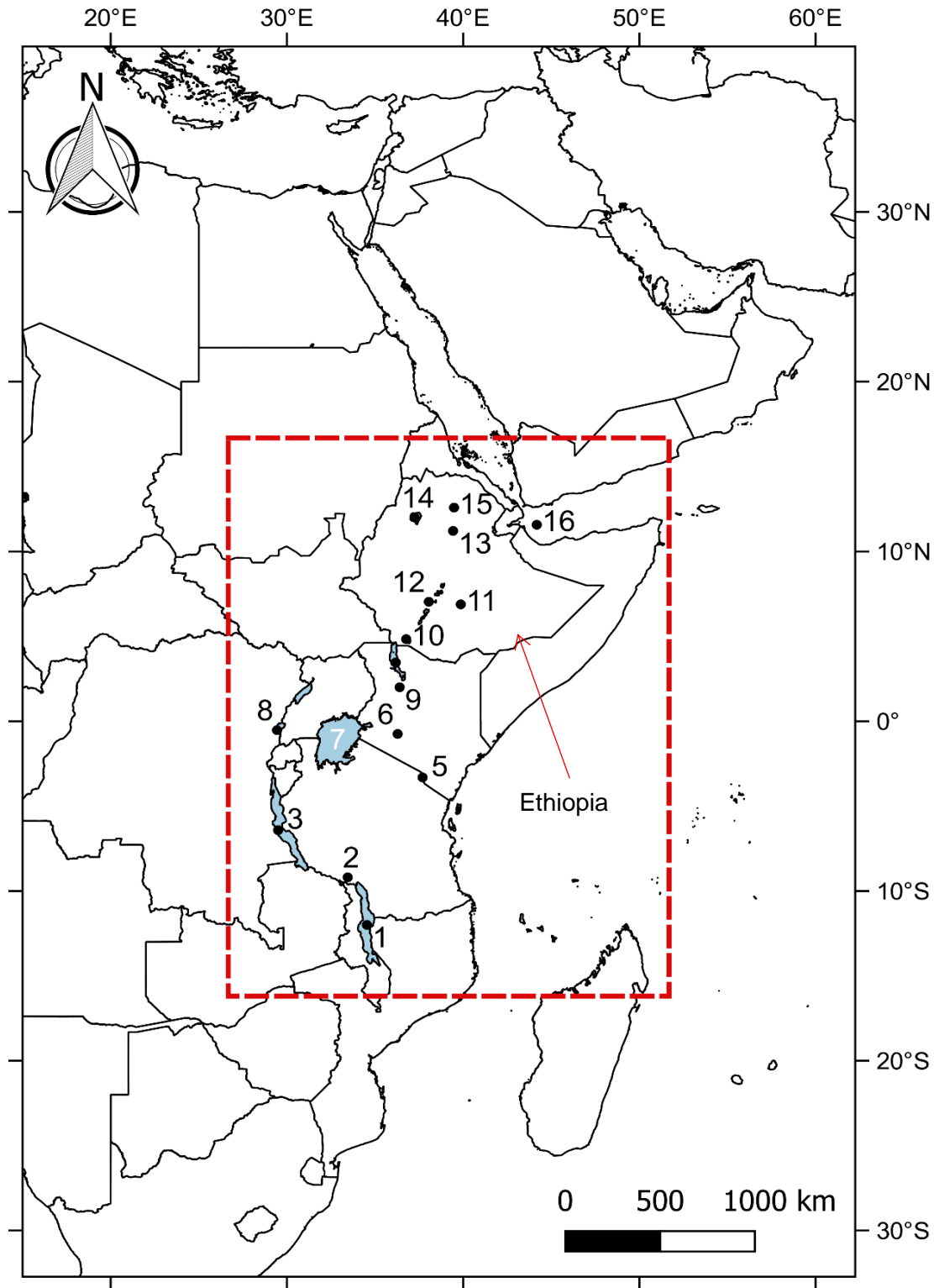


Figure 2.1: Eastern Africa and neighbouring countries, with major lakes in light blue. The boxed area forms the main focus of this review, with some relevant analogues from other regions also discussed where appropriate. The approximate coring locations of some of the main sites of discussion in the review are also numbered 1-16, and listed in Table 2.1.

Table 2.1: Main study sites discussed in this review with corresponding site numbers plotted in Figure 2.1. * - marine core record.

	Site	Elevation (m.a.s.l)	Citation(s)
1	Malawi	475	(Powers <i>et al.</i> , 2005; Brown <i>et al.</i> , 2007; Barker <i>et al.</i> , 2007; Castañeda <i>et al.</i> , 2009; Woltering <i>et al.</i> , 2011; Ivory <i>et al.</i> , 2012)
2	Masoko	840	(Vincens <i>et al.</i> , 2007; Garcin <i>et al.</i> , 2007a; 2007b)
3	Tanganyika	770	(Stager <i>et al.</i> , 2009; Tierney <i>et al.</i> , 2008; 2010)
4	Turkana	360	(Garcin <i>et al.</i> , 2012; van der Lubbe <i>et al.</i> , 2017)
5	Challa	880	(Tierney <i>et al.</i> , 2011b; Buckles <i>et al.</i> , 2016)
6	Naivasha	1880	(Verschuren <i>et al.</i> , 2000)
7	Victoria	1135	(Talbot & Lærdal, 2000; Stager <i>et al.</i> , 2002; 2005; Berke <i>et al.</i> , 2012)
8	Edward	910	(Russell & Johnson, 2005; 2007)
9	Suguta	300	(Garcin <i>et al.</i> , 2009; Borchardt & Trauth, 2012; Junginger & Trauth, 2013)
10	Chew Bahir	575	(Foerster <i>et al.</i> , 2012; 2014)
11	Garba Guracha	3950	(Umer <i>et al.</i> , 2007; Tiercelin <i>et al.</i> , 2008)
12	Tilo	1545	(Lamb <i>et al.</i> , 2000; 2004)
13	Hayq	1905	(Lamb <i>et al.</i> , 2007a; Loakes, 2015)
14	Tana	1790	(Lamb <i>et al.</i> , 2007b; Marshall <i>et al.</i> , 2011; Costa <i>et al.</i> , 2014; Loomis <i>et al.</i> , 2015)
15	Ashenge	2440	(Marshall <i>et al.</i> , 2009)
16	Site P178-15P*	-	(Tierney & deMenocal, 2013; Tierney <i>et al.</i> , 2015)

Several authors have provided site locations and syntheses of hydrological change across the African continent in their reviews (e.g. Gasse, 2000). The Oxford Lake-Level Database (OLLD; COHMAP members, 1988; Street-Perrott *et al.*, 1989), recently updated by Tierney *et al.* (2011b), provides an extensive database of relative lake levels. These lake levels are categorised as ‘low’ when a lake is dry and/or at its most saline, and/or within 0–15% of its total altitudinal range of fluctuation; ‘intermediate’ when a lake is within 15–70% of its altitudinal range and/or ambiguously rising or falling, and ‘high’ when a lake is within 70–100% of its altitudinal range and/or overflowing, and/or at its deepest/freshest state. However, as Gasse (2000) highlights, the original papers used for each lake level status reconstruction should also be consulted as the term “lake status” is an interpretation which sometimes deviates from that in the original works.

2.1.1 | Chronological controls

Accurate and reliable chronologies are crucial in being able to interpret changes in a sedimentary record and relate these changes to those inferred elsewhere. Varves are defined as containing at least two or more seasonal laminae which distinctly contrast in properties such as colour, composition, texture, structure and/or thickness. Due to the manner of their seasonal deposition varved sediments can be used to construct high-resolution chronologies. Although the succession and characteristics of seasonally deposited laminae are varied across the globe, reflective of a repetitive, site specific, annual cycle, it is possible to broadly categorise laminae as clastic (physical), biogenic (biological) or endogenic (chemical), but are known to often be a combination of these components (O’Sullivan, 1983; Zolitschka *et al.*, 2015; Figure 2.3).

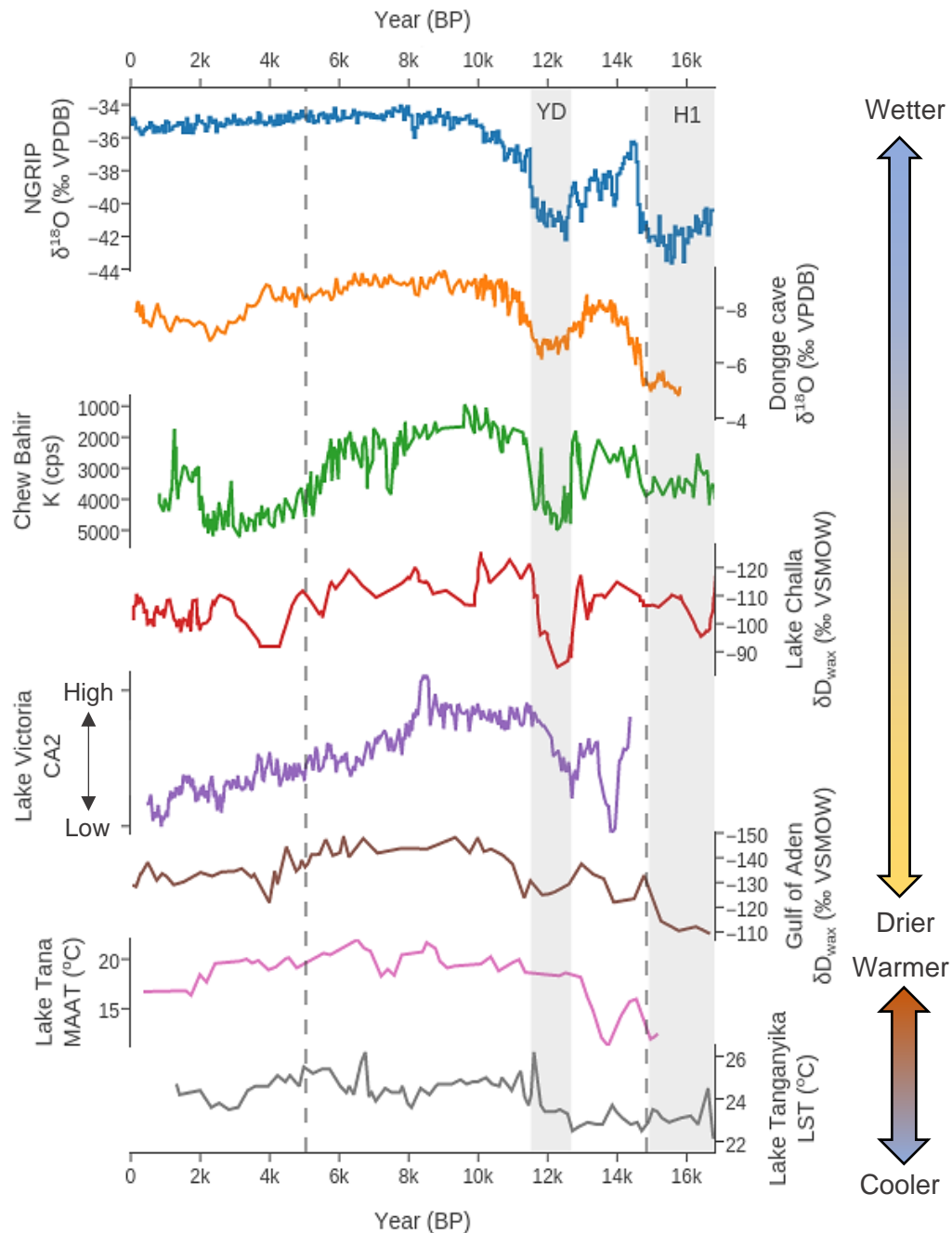


Figure 2.2: Comparison of East African palaeoclimate, the Dongge cave (southeast Asia) and NGRIP records. Records (from top to bottom) include: $\delta^{18}\text{O}$ data from the NGRIP (Andersen *et al.*, 2004); $\delta^{18}\text{O}$ data from Dongge cave (Dykoski *et al.*, 2005; reverse scale); Chew Bahir potassium (K) record (Foerster *et al.*, 2012; reverse scale); Lake Challa $\delta\text{D}_{\text{wax}}$ record (Tierney *et al.*, 2011b; reverse scale); Lake Victoria CA2 record (shallow:deep water diatoms serving as a proxy for lake water depth; Stager *et al.*, 2002); Gulf of Aden $\delta\text{D}_{\text{wax}}$ record (Tierney & deMenocal, 2013; reverse scale); mean average air temperature (MAAT) temperature records from Lake Tana (Loomis *et al.*, 2015) and lake surface temperature (LST) records from Lake Tanganyika (Tierney *et al.*, 2008) inferred from Tex_{86} and BIT-indices. Shading indicates the Younger Dryas (YD) and Heinrich 1 (H1), with dashed lines indicating approximate interval of the African Humid Period.

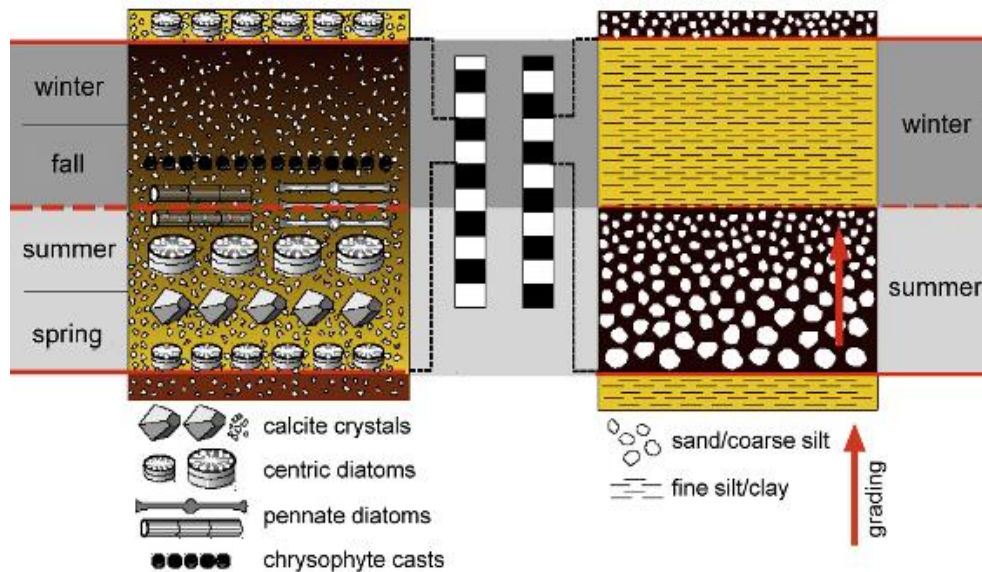


Figure 2.3: Simplified models for depositions of a calcareous organic (mixed) varve (left) and a clastic varve (right; Zolitschka *et al.*, 2015).

Due to this high-resolution, continuously varved sediments are the obvious preference for reconstructing climate variability at a century-decadal time scale. However, such continuous records in intertropical Africa are uncommon due to the complexity and variability of the seasonal monsoonal cycle and their preservation in sediments (Verschuren, 2003). Some rare examples of sites where truly annually laminated sediments have been found in eastern Africa include Lakes Malawi (Johnson *et al.* 2002), Hora (Lamb *et al.*, 2002b) and Challa (Wolff *et al.*, 2011).

Lead-210 (^{210}Pb) is a naturally-produced radionuclide, derived from atmospheric fallout (termed unsupported ^{210}Pb). Caesium-137 (^{137}Cs) and Americium-241 (^{241}Am) are artificially produced radionuclides, introduced to the environment by atmospheric fallout from nuclear weapons testing and nuclear reactor accidents (since 1954 AD, with known, pronounced peaks of ^{137}Cs in the Northern Hemisphere at 1959 and 1963 AD). Due to the recent known anthropogenic emission of these radionuclides, they have been successfully utilised to produce high-resolution chronologies for sedimentary sequences, but their utility only

extends to more-modern sediments (back ~150 years for ^{210}Pb and ~50 years for ^{137}Cs and ^{241}Am) due to the timing of these anthropogenic emissions (Appleby, 2001).

Producing core chronologies based on radiocarbon dates (^{14}C) is the most common, and using terrestrial macrofossils (i.e. twigs, leaves needles of trees, charcoal from these materials and identifiably terrestrial insect parts) as material for ^{14}C dating has long been recognised as key to establishing reliable and accurate chronologies in sedimentary archives. However, whilst macrofossils are considered the obvious, 'gold-standard' preference for ^{14}C dating, it is common for lake sediments to be lacking sufficient macrofossil materials to be dated (Zimmerman & Myrbo, 2015).

Bulk sediment samples, of organic matter or carbonates, can provide radiocarbon dates, but are not as reliable as dating macrofossil samples (Törnqvist *et al.*, 1992). Generally, sources of error include: (i) contamination by younger carbon through root penetration and/or bioturbation; (ii) contamination by old 'dead' carbon; (iii) the lake reservoir effect and (iv) the hardwater reservoir effect (Björck & Wohlfarth, 2001). Discrepancies in the accuracy between dating certain materials, as well as multiple sources of error and issues of contamination, has often made it necessary to re-date, or offset dates in, a sedimentary sequence to establish a more accurate chronology (Stager *et al.*, 2003; Stager *et al.*, 2009).

2.1.2 | Issues with proxies

An additional complicating factor in interpreting eastern African lacustrine records is the often uncertain relationship between sedimentary climate-proxy indicators (physical, chemical or biological), and the primary climate variables of temperature,

precipitation and wind (Verschuren, 2003). In contrast to lakes in the northern temperate regions, where a range of climate proxies can be assumed to be directly controlled by variations in temperature, a reliable proxy of temperature change in Africa has only recently been developed (Verschuren & Russell, 2009). Several eastern African lake temperature records have now been produced through the application of innovative new proxies such as TEX₈₆ (e.g. Powers *et al.*, 2005; Berke *et al.*, 2012), but this may not be as reliable in small lakes where the signal may be compounded by substantial amounts of isoprenoid tetraether compounds derived from soil (Powers *et al.*, 2010).

Reconstructions of past climate therefore rely on inferring and calibrating the relationship between the sediment, water column and climate. For example, diatom-inferred conductivity based on such calibrations of this relationship has been used to infer past environmental conditions across eastern Africa (diatom-based research in eastern Africa is discussed in greater detail than here in Chapter 5). However, the robustness and sensitivity of calibrations and training sets remains disputed as the calculation of ecological optima sometimes gives results that are quite different for the same species, when derived from large local to regional datasets (Mills & Ryves, 2012). Furthermore, changes in lake sediment composition in eastern Africa is not necessarily predominantly driven by climatic change, with non-climatic factors (e.g. volcanism and human activity) a considerable influence, or in some cases overriding climate (Telford *et al.*, 1999; Mills *et al.*, 2014; Votava *et al.*, 2017). Multi-proxy approaches are commonly used in palaeolimnology as they provide additional, independent lines of evidence, facilitating a more holistic and thorough investigation of lake-catchment system

responses to climate, and other potential external forces such as anthropogenic activities (e.g. agricultural practices and land clearance; Birks & Birks, 2006).

2.2 | Overview of eastern African climatology

The climate of eastern Africa is characterised by strong rainfall seasonality, heavily influenced by the annual migration of the Intertropical Convergence Zone (ITCZ) between 10° North and South, following the zenithal position of the sun (Figure 2.4; Nicholson, 1996). The Congo Air Boundary (CAB; Figure 2.4) is also highly influential in defining the climate of eastern Africa. The location of the CAB is partly determined by orographical constraints including the Ethiopian and Kenyan Highlands and marks the confluence of moisture derived from the Atlantic Ocean and the Indian Ocean. Recent isotope analyses and meteorological station data suggest that convergent, unstable air within the CAB serves as an important source of seasonal rainfall in, for example, Ethiopia (Levin *et al.*, 2009) and Tanzania (Mapande & Reason, 2005).

The Horn of Africa and coastal eastern Africa are orographically isolated from convergence along the CAB; as a result these regions experience more arid conditions. The aridity of eastern Africa can also be attributed to micro-orographical effects such as leeward rain shadows east of the topographical highs of Mt. Kenya and Mt. Kilimanjaro, and the influence of divergent, dry lower-level winds that move parallel to the eastern African shore from June–September and December–February (Nicholson, 1996).

The migration of the ITCZ and CAB throughout the year skews the seasonal distribution of precipitation in eastern Africa towards October–May. Most of the region experiences a well-pronounced dry season from June to August, followed

by either two rainy seasons for northern areas and areas close to the equator, with peak rains in November and April, or an extended rainy season from October–May for areas farther south of the equator (Tierney *et al.*, 2011b; Figure 2.4). An exception to this rule, for example, is Ethiopia, which experiences slightly different seasonal shifts in climate than the rest of eastern Africa (Figure 2.4). Drier conditions prevail between October and May, with the wettest months between June and August.

On an interannual timescale, variations in eastern African precipitation is sensitive to both Atlantic Ocean and Indian Ocean climate dynamics. For areas receiving precipitation from the CAB, interannual changes in Atlantic Ocean sea surface temperatures (SSTs) and SST gradients can modulate the strength of the trade winds and the advection of moisture into equatorial Africa (Tierney *et al.*, 2011a). Furthermore, a flattening of the meridional gradient in Atlantic SSTs, such as warmer South Atlantic SSTs, typically results in anomalously high precipitation rates (Camberlin *et al.*, 2001). Shifts in the Walker circulation over the Indian Ocean basin cause large interannual fluctuations in precipitation. A flattening of the zonal SST gradient in the Indian Ocean, and subsequent reversal of the Walker circulation, typically causes anomalous convergence and rainfall in the western Indian Ocean extending into eastern Africa (Tierney *et al.*, 2011a). Such shifts in zonal circulation can be caused by anomalously warm SSTs in the western Indian Ocean (Ummenhofer *et al.*, 2009), positive Indian Ocean Dipole events (IOD), and the El Niño-Southern Oscillation (ENSO; Camberlin *et al.*, 2001; Diro *et al.*, 2011).

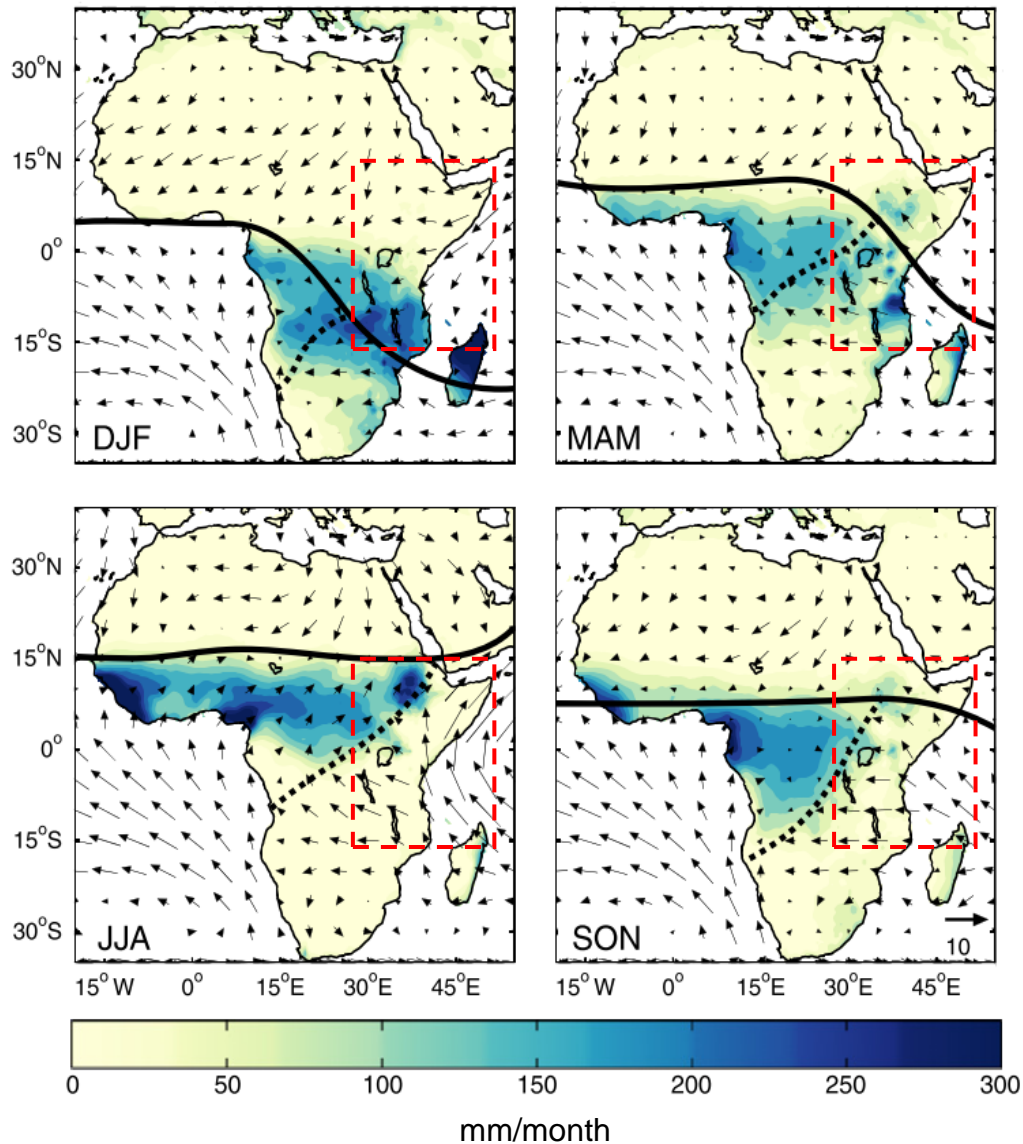


Figure 2.4: Seasonal climatology (December, January and February; DJF, March, April and May; MAM, June, July and August; JJA and September, October and November; SON) for tropical Africa, including precipitation rates (Mitchell & Jones, 2005), surface wind (Kalnay *et al.*, 1996), and the approximate locations of the ITCZ (solid line) and CAB (dotted line). Dashed red box corresponds to the boxed area in Figure 2.1. Adapted from Tierney *et al.* (2011b).

2.2.1 | Long-term controls on eastern African climate

The Milankovitch precessional cycles (23-19 ka) are the dominant control on long-term variations in climate, and regulate moisture availability in Africa (Kutzbach & Street-Perrott, 1985; Trauth *et al.*, 2003). The precessional control on tropical

moisture has been illustrated through the climate modelling undertaken by Clement *et al.* (2004) which showed that a 180° shift in precession out of phase with the modern could alter boreal summer precipitation in eastern Africa by 100-200 mm. Periods of increased humidity over the past 20,000 years have been linked to orbitally-forced radiation maxima, and as a result considerably influenced lake-levels at various sites across eastern Africa (Gasse, 2000; Trauth *et al.*, 2003; Barker *et al.*, 2004; Figure 2.5).

However, lacustrine records in the African tropics and recent simulations have also shown that climate does not respond linearly to precessional insolation change. The abruptness and onset of these climatic transitions can only be fully explained when climate-biophysical feedbacks are accounted for (Renssen *et al.*, 2006; Timm *et al.*, 2010). In conjunction with orbitally-forced variability, centennial-scale variations such as Heinrich events and the Younger Dryas are also considered a significant influence on climatic change. Changes in Atlantic and Indian Ocean SSTs, related to the thermohaline circulation and often associated with these events, also have a considerable influence on African climate (Gasse & van Campo, 1994; Gasse, 2000; Tierney *et al.*, 2008).

2.3 | Heinrich Stadial 1 (18,000 – 15,000 BP) and eastern Africa

Heinrich events are generally associated with ice-rafted debris (IRD) archived in the sediments of North Atlantic marine cores dated between 70,000 BP and 14,000 BP (Hemming, 2004). Heinrich event 1 (~18,000-15,000 BP; Heinrich, 1988; Bond *et al.*, 1992; Broecker *et al.*, 1992) is the most recent of these distinctive cold periods in the North Atlantic region.

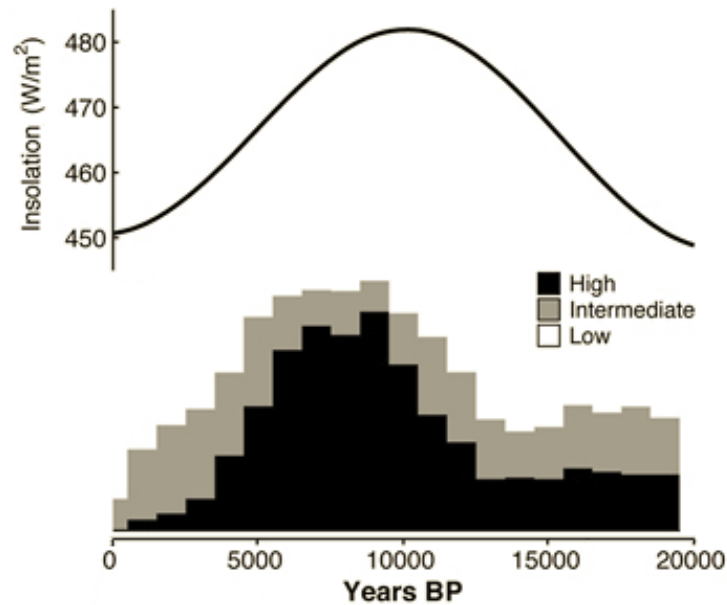


Figure 2.5: Change in summer insolation for North Africa (20°N; top) and African lake level status from an updated OLLD (Tierney *et al.*, 2011a; bottom). Adapted from deMenocal & Tierney (2012).

Palaeoceanographic records suggest a connection between the abrupt climate changes towards cold, arid conditions during these events and variations in North Atlantic Deep Water (NADW) formation and the Atlantic Meridional Overturning Circulation (AMOC; McManus *et al.*, 2004), following the abrupt input of freshwater associated with ice sheet instability and these ice-rafts (Hemming, 2004). Despite being largely associated with the North Atlantic, numerous studies suggest H1 had some impact on the hydrological climate of eastern Africa (e.g. Figure 2.2). For example, improved chronological controls and re-examination of records from widely distributed cores at Lake Victoria by Stager *et al.* (2002) suggests that the lake was desiccated at least once during this period. Seismic reflection data further north at Lake Tana shows that the lake was completely desiccated during H1 some time between 18,700 and 16,700 BP. Peaty sediments at the base of a core from the deepest part of the lake centre contain high concentrations of periphytic and planktonic diatoms and high concentrations of *Poaceae* and *Cyperaceae* pollen.

This sediment overlies the compacted silt sediment, the desiccation layer revealed by reflector data, which indicates that lake desiccation was followed by the development of shallow-water environments and papyrus swamp isolated in the lake centre between 16,700 and 15,100 BP (Lamb *et al.*, 2007; Marshall *et al.*, 2011).

2.4 | The African Humid Period (15,000 – 5,000 BP)

The African Humid Period (AHP) began following the drier conditions associated with H1 (Hemming, 2004). The AHP has been strongly linked with the precessional increase in the Northern Hemisphere insolation during low eccentricity (deMenocal *et al.*, 2000; Shanahan *et al.*, 2015). By 11,000–10,000 BP, summer insolation in the northern hemisphere had risen to peak levels ~8% greater than today due to the Earth's orbital precession. This gradually aligned the boreal summer solstice with the perihelion, strengthening the summer monsoon systems and consequently increasing precipitation across much of Africa, by as much as 35–45% over North Africa (Prell & Kutzbach, 1987; Berger & Loutre, 1991; deMenocal & Rind, 1993; Figure 2.5). However, recent simulations suggest a more complex trigger for the onset of the AHP by showing that the magnitude and extent of reconstructed hydrological and ecological changes can only be reproduced when land surface and ocean feedbacks are included (Timm *et al.*, 2010).

Although the mechanism for the onset of the AHP remains unclear, the associated hydrological changes across Africa are evident in multiple palaeoenvironmental archives. Despite the lack of continuous local palaeoenvironmental data, Junginger & Trauth (2013) conclude from their hydro-balance model for palaeo-Lake Suguta that only an abrupt onset (~300 years) prior to 14,800 BP could have led to the

high lake levels recorded after ~14,000 BP. They find that the onset of the AHP must have significantly and abruptly increased local precipitation (+26% in comparison to the present day) to lead to the higher lake levels recorded. Marine $\delta^{18}\text{O}_{\text{seawater}}$ records suggest that the outflow waters of the rivers Niger and Sanaga around the onset of the AHP sharply decrease in salinity (~0.8‰ change; Weldeab *et al.*, 2005; Weldeab *et al.*, 2007). Eastern African lacustrine records also document an abrupt shift in climate; for example, K content sharply reduces at Chew Bahir (~4000 to ~2000 cps at the onset of the AHP at ~15,000 BP), suggesting decreased aridity (Foerster *et al.*, 2012). Diatom analyses on the northern basin of Lake Malawi by Gasse *et al.* (2002) similarly suggest more humid conditions and that the lake level was high from 15,700 to 13,000 BP and likely overflowed. Similarly, $\delta^{13}\text{C}$ values decrease abruptly at ~15,000 BP at Lake Victoria, marking a shift to deeper-water conditions and algal-dominated lake production (Talbot & Lærdal, 2000). Temperature reconstructions based on microbial membrane lipid structures at Lakes Tana (Loomis *et al.*, 2015) and Malawi (Powers *et al.*, 2005; Woltering *et al.*, 2011) suggest an increase in temperature of ~3-4°C at ~15,000-14,000 BP.

2.4.1 | The Younger Dryas (12,700 – 11,800 BP)

Kiage & Liu (2006) highlight variations in vegetation across eastern Africa may indicate the presence of Younger Dryas (YD)-like conditions, but argue that further work was required before the occurrence of the YD in eastern Africa could be confirmed. However, the occurrence of the YD interval in eastern Africa is a research gap that has now largely been addressed. In eastern Africa, arid conditions of the YD punctuate the warm, wet AHP (Figure 2.2). Tex_{86} records at

Lake Malawi suggest an abrupt air temperature decrease of $\sim 2^{\circ}\text{C}$ (Powers *et al.*, 2005; Woltering *et al.*, 2011) at $\sim 12,500$ BP.

Arid conditions are represented by forest decline and increases in grasses inferred from lignin phenol records and $\delta^{13}\text{C}$ values at Lake Malawi (Castañeda *et al.*, 2009), and from other terrestrial sedimentary archives across eastern Africa (e.g. Ryner *et al.*, 2006; Rucina *et al.*, 2009). This pattern is also represented in the highlands of Ethiopia in a pro-glacial lake in the Bale Mountains (Umer *et al.*, 2007). $\delta\text{D}_{\text{wax}}$ records from Lakes Challa (Tierney *et al.*, 2011b) and Tanganyika (Tierney *et al.*, 2008) suggest decreased precipitation during this period, with the highest $\delta^{18}\text{O}_{\text{diatom}}$ value ($+39.7\text{‰}$) recorded at $\sim 12,000$ BP in sediments from Lake Malawi (Barker *et al.*, 2007), reflecting this period of aridity. Furthermore, peaks of K at Chew Bahir (Foerster *et al.*, 2012) and increased Zr:Ti ratios at Lake Malawi (Brown *et al.*, 2007), reflect dry windy conditions and increased soil erosion.

However, some records suggest that environmental characteristics associated with the YD in the African tropics were not uniform across the continent. For example, a pollen record from Site GeoB 12624-1, off the Rufiji River delta, eastern Africa shows a heterogeneous vegetation pattern with alterations between dry and humid taxa presenting no clear climatic signal for the YD (Bouimetarhan *et al.*, 2015). Similarly, in a clear contrast to the observed YD cooling observed elsewhere, pollen assemblages from Lake Masoko document an expansion of tropical seasonal forests during the YD period, representing more humid conditions (Garcin *et al.*, 2007a; Vincens *et al.*, 2007). However, recent pollen analyses at Lake Malawi identify two phases of aridification where the expansion of these drought-intolerant forest taxa were likely restricted to areas of favourable edaphic conditions along permanent waterways between 13,000 and 12,300 BP, before

being succeeded by grassland and woodland (12,300-11,800 BP) reflecting gradually increasing aridity across the YD (Ivory *et al.*, 2012).

Furthermore, the exact timing and duration of the YD across the African tropics may be more uncertain than previously thought. A stable isotope record from Lake Ashenge (Marshall *et al.*, 2009) suggests an early initiation of the YD in the region roughly 900 years before it is identified in the Greenland ice cores (~12,700-11,500 BP; Alley, 2000) and the start of the YD at other African sites (Figure 2.2; Figure 2.6). A sedimentary hiatus from 11,760-7,560 BP impedes the full interpretation of the environmental characteristics of the YD and subsequent Pleistocene/Holocene transition. However, the lake experienced severely arid conditions from 13,600-11,800 BP, evident from the highest, and sustained, $\delta^{18}\text{O}$ and $\delta^{13}\text{C}$ values throughout the core and enhanced precipitation of aragonite during this period (D in Figure 2.6).

Uncertainties in the timing of the YD cooling in the eastern African tropics has also been identified in marine sediment records. DeMenocal *et al.* (2000) document increased terrigenous sedimentation at ODP Site 658C off Cap Blanc, Mauritania (20°45'N, 18°35'W) ~800 years before the YD identified in the Greenland ice cores (12,700-11,500 BP). They suggest this offset can be accounted for by marine ^{14}C reservoir discrepancies due to changes in deep ocean circulation and related changes in ocean-atmosphere radiocarbon partitioning during this period. They argue that large increases in *Globigerina bulloides* abundances at their site during this interval would be consistent with increased regional upwelling and older apparent ^{14}C ages at this time (deMenocal *et al.*, 2000). However, microalgae and pollen records at Site KW31, in the Gulf of Guinea (3°31'1N, 05°34'1E), suggest

enhanced aridity between 13,400 to 12,100 BP, 700 years prior to the YD proper (Lézine *et al.*, 2005).

Leaf wax data by Tierney & deMenocal (2013) in marine sediments from Site P178-15P in the Gulf of Aden also show a contrasting YD record. Their results show that the termination of the YD in the Gulf of Aden record occurs later in all iterations (median = 10,850 BP) than the YD proper documented in leaf wax records at other African sites such as Lake Challa (Tierney *et al.*, 2011b) and Tanganyika (Tierney *et al.*, 2008). Like DeMenocal *et al.* (2000), Tierney & DeMenocal (2013) suggest ^{14}C reservoir offsetting may be inaccurately representing this termination, but acknowledge they currently lack sufficient information to constrain how the Gulf of Aden ^{14}C reservoir has evolved through time to fully address this.

Marshall *et al.* (2009) speculate that, assuming that this early initiation is not a result of inaccurate ^{14}C dates, the early initiation of the YD at sites north of $\sim 10^\circ\text{N}$ may be associated with a southerly suppression of the ITCZ. This suppression of the ITCZ is attributed to gradual cooling at high northerly latitudes prior to the onset of the established YD chronozone $\sim 12,700$ years ago (Alley, 2000). Loomis *et al.* (2015), upon identifying a lack of abrupt and significant YD cooling (between -0.3°C and $+0.3^\circ\text{C}$ change across 12.7-11.5 ka) at Lake Tana (Figure 2.2), suggest that climatic changes in northeast Africa during this period were more strongly influenced by large variations in atmospheric circulation such as the incursions of highly influential Congo Basin air masses, as opposed to changes in CO_2 and insolation, than locations to the south and west.

However, the aridification associated with the YD is evident in magnetic and geochemical core data from Lake Tana (Marshall *et al.*, 2011), with no early onset

such as that at Ashenge despite a similar latitude (Figure 2.1). Furthermore, the hypotheses by Marshall *et al.* (2009) and Loomis *et al.* (2015) offer little explanation for sites further south such as KW31 (Lézine *et al.*, 2005) or the potential late termination of the YD at another site laying north of 10°N: Site P178-15P (Tierney & deMenocal, 2013).

Evidently, our understanding of the YD in eastern Africa has progressed since Kiage & Liu (2006). However, the exact timing and effects of the YD may be unclear, with varied responses from different sites. This may be attributed to inaccuracies in ¹⁴C chronologies, with reservoir discrepancies a prevalent issue in marine core records (e.g. Tierney & deMenocal, 2013) or that only bulk samples were used by Marshall *et al.* (2009), for example. However, it may also reflect the diverse location and topography of sites across the region, which may have created unique hydrological conditions, associated with variations in moisture sources, at some sites producing locally distinct/regionally contrasting expressions of the Younger Dryas.

2.4.2 | Resumption of the AHP in the Early Holocene

Despite some uncertainty regarding the exact timing of the YD, the abrupt resumption of the AHP is evident in multiple palaeoenvironmental records in the African tropics (e.g. Junginger & Trauth, 2013; Tierney & deMenocal, 2013). As discussed previously, at around 11,000 to 10,000 BP insolation reached a maximum, influencing lake-levels at various sites across eastern Africa (Figure 2.5). By 9,000 BP multiple lakes experienced higher water levels across most of the African continent as a result of this increased moisture availability, even in the now arid Sahara (A in Figure 2.7).

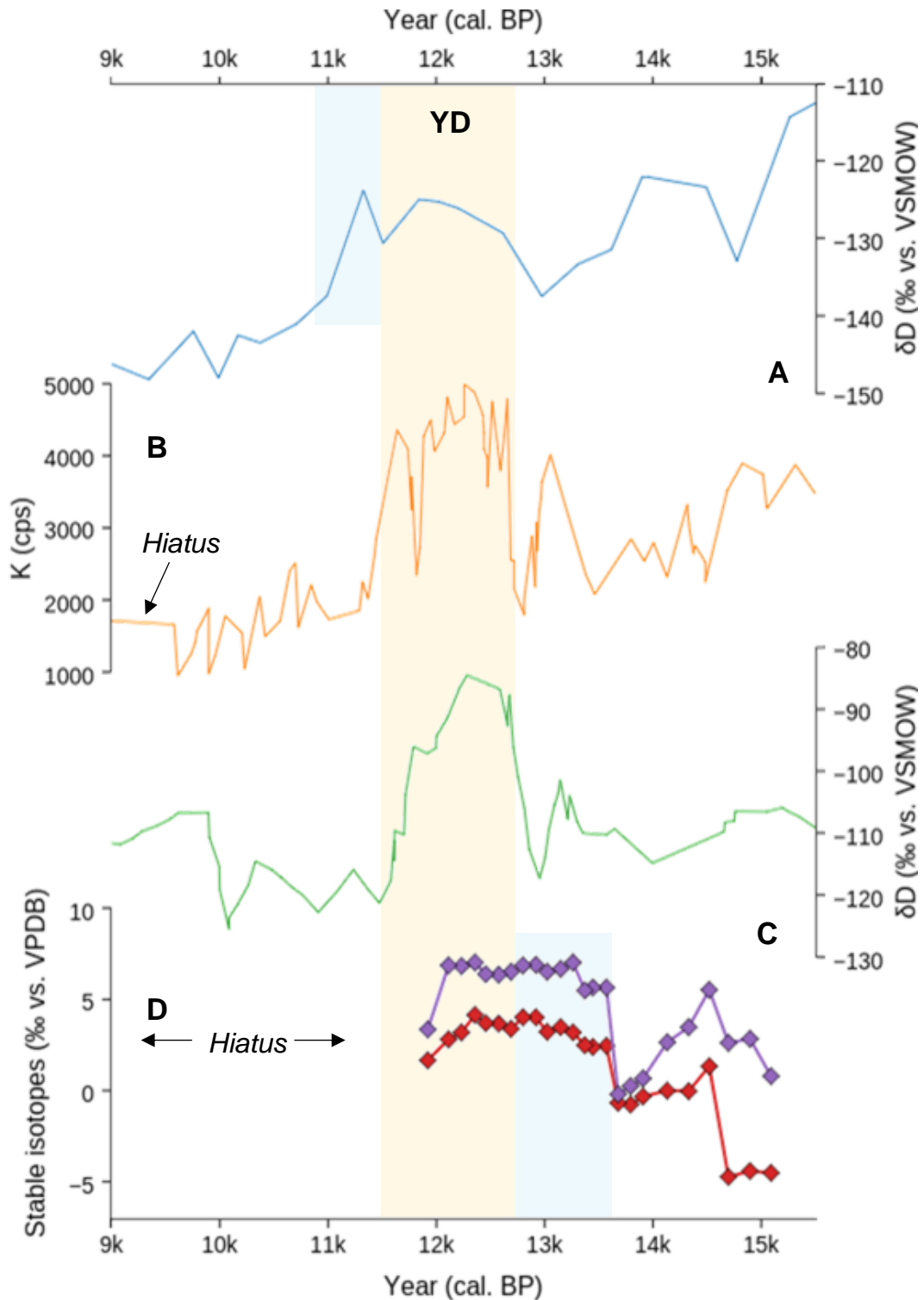


Figure 2.6: Comparison of some palaeoenvironmental records around the YD interval (yellow), with blue highlighting earlier/later changes in certain records. Late termination of the YD as identified at Site P178-15P (A) by Tierney & deMenocal (2013), Chew Bahir (B) by Foerster *et al.* (2012) and Lake Challa (C) by Tierney *et al.* (2011b) which display the YD proper (Figure 2.2), and the early initiation of the YD in Marshall *et al.* (2009) is also shown by sustained high stable isotope values at Lake Ashenge (D).

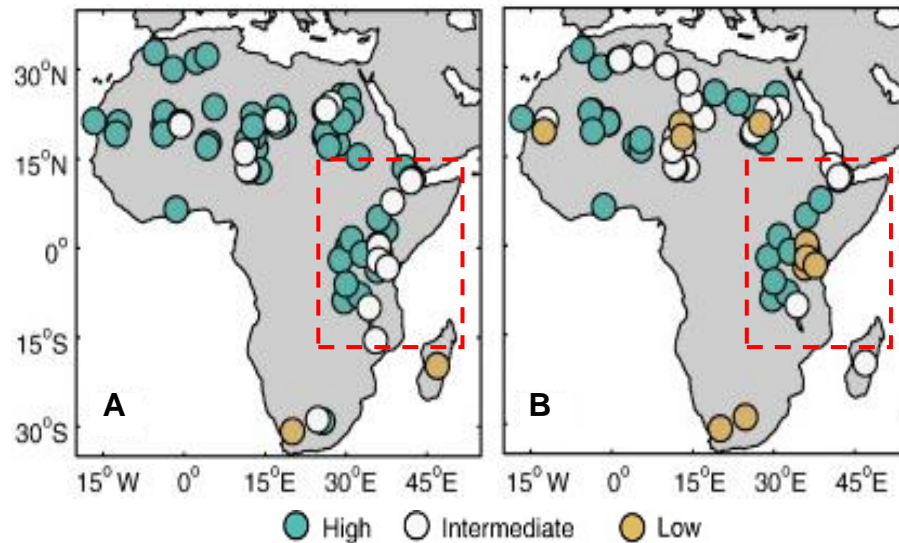


Figure 2.7: Proxy lake status reconstructions from the Oxford Lake Level Database (Street-Perrott *et al.*, 1989), updated with more recent lake level reconstructions in Tierney *et al.* (2011b), for 9,000 BP (A) and 6,000 BP (B). Dashed red box corresponds to the boxed area in Figure 2.1. Adapted from Tierney *et al.* (2011b).

In combination with multiple sedimentary records of hydrological change from palaeo-Lake Suguta (e.g. Garcin *et al.*, 2009; Junginger & Trauth, 2013), evapotranspiration estimates generated from remote sensing data and using the *Surface Energy Balance Algorithm for Land* for the Suguta basin suggest that the region during the AHP must have experienced ~20% more precipitation than today (Borchardt and Trauth, 2012). Similarly, hydrological modelling by Garcin *et al.* (2012) shows that the water level of Lake Turkana increased to the point of overflowing around the resumption of the AHP.

In the Ethiopian highlands, clastic input at Lake Garba Guracha reduces after 11,800 BP, to negligible and consistently low concentrations by 10,000 BP, corresponding to a sharp ~10% increase in TOC at 10,000 BP, reflecting the transition from a glacier-fed lake to an open lacustrine domain characterised by increased local precipitation, temperature and organic productivity (Tiercelin *et al.*, 2008). This was also represented by an increase in woody vegetation, soil

stabilisation, and increased leaf litter and soil humus content inferred from a pollen stratigraphy of the same core (Umer *et al.*, 2007).

In conjunction with these palaeoenvironmental records, occupation of the Sahara is evident from the various occurrences of rock art that are scattered throughout the upland regions of the desert, illustrating a lush environment with Sahelian and riverine fauna and scenes of large-game hunting, livestock herding and religious ceremony (e.g. di Lernia & Gallinaro, 2010). Archaeological evidence from past settlement sites across the region has shown evidence for intensive occupation, initially by pottery-using hunter-gatherers, and then by increasingly mobile pastoralists after the introduction of domestic livestock at ~8,000-7,500 BP (Kuper & Kröppelin, 2006; Dunne *et al.*, 2012; [Figure 2.8](#)).

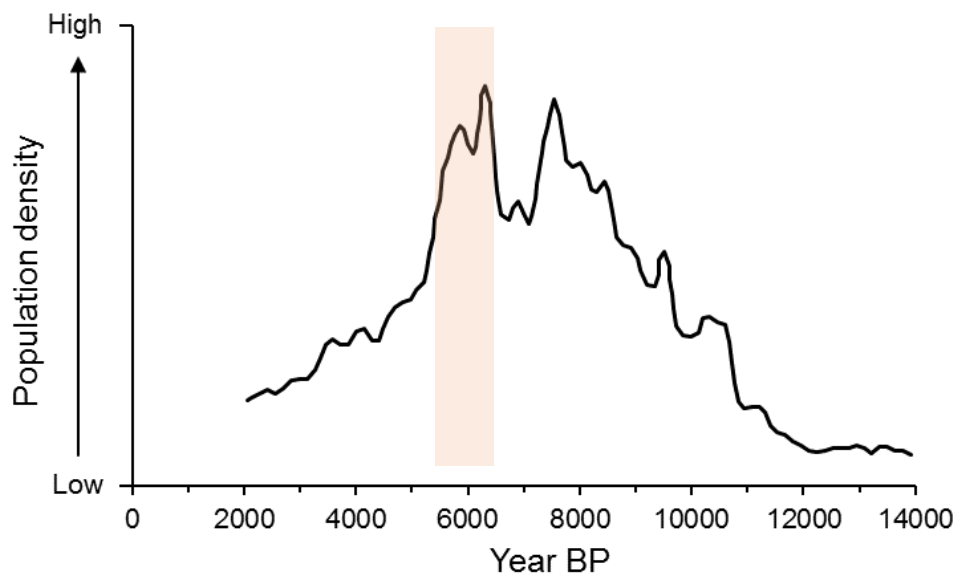


Figure 2.8: Rolling 200 year mean of Manning & Timpson's (2014) summed probability distribution analyses using all ^{14}C dates in their three correlating regions (Eastern and Central Sahara and the 'Atlas Hoggar'). Shading indicates general period of environmental degradation associated with the termination of the AHP as identified by the studies cited in this chapter. Redrawn from Manning & Timpson (2014).

A detailed re-examination of the Chew Bahir K record between 11,000 BP and 4,000 BP reveals a distinctive drought event at ~8,150 BP (Trauth *et al.*, 2015).

This drought event is the first of five events, as part of a stepwise increase in aridity. More stable, humid conditions re-establish between for ~600 years at 7,750 BP, before returning to a period of instability with abrupt wet-dry shifts, with a drought event at 7,150 BP. A one-thousand year long, gradual drying of the region, punctuated by extreme arid intervals, is also identifiable in the record after 5,950 BP. In total, at least 19 events of extreme aridity are represented in the Chew Bahir K record between 8,200 BP and 5,000 BP, which were between 20 and 80 years long and recurring every 160 ± 40 years. (Trauth *et al.*, 2015). However, despite some arid intervals during the AHP such as these, moisture availability presumably remained relatively high to at least 6,000 BP (Figure 2.5).

2.4.3 | Termination of the AHP

As highlighted by Claussen *et al.* (1999), the termination of the AHP and subsequent desertification of multiple regions of Africa, especially the Sahara, during the Holocene, was undeniably a crucial period for human society. This reversal of humid conditions, favourable for growth and expansion, has been the hypothesised predominant driving force behind large population declines across most of the Sahara (Figure 2.8), but may have also been the stimulus leading to the foundation of civilizations near relatively moist refugia such as the Nile valley (Kuper & Kröpelin, 2006; Manning & Timpson, 2014; Castañeda *et al.*, 2016).

Much like the YD, the termination of the AHP highlights the contradictory data from various sources regarding the dynamics of wet-dry cycles in Africa (Foerster *et al.*, 2012). The results of multiple studies suggest an abrupt termination to the AHP (within just two centuries in some cases; e.g. Marshall *et al.*, 2009). Abrupt terminations have been documented in a variety of archives including: marine

sedimentary records off the west (deMenocal *et al.*, 2000; Adkins *et al.*, 2006; McGee *et al.*, 2013) and east coasts (Tierney & deMenocal, 2013) of Africa; terrestrial sedimentary derived records of δD_{wax} at Lakes Tanganyika and Tana (Tierney *et al.*, 2008; Costa *et al.*, 2014), palaeo-shoreline and strontium isotope records from Lake Turkana (Garcin *et al.*, 2012; van der Lubbe *et al.*, 2017), and a stable isotope record at Lake Ashenge (Marshall *et al.*, 2009). Furthermore, a Lake Tana δD_{wax} record also suggests an early, as well as abrupt, termination of the AHP around 8,000 BP (Costa *et al.*, 2014).

Conversely, Ethiopian speleothem records (Asrat *et al.*, 2007; Baker *et al.*, 2010) and records from Chew Bahir (Foerster *et al.*, 2012; Trauth *et al.*, 2015), palaeo-lake Suguta (Junginger & Trauth, 2013), Lake Tilo (Lamb *et al.*, 2004), Lake Yao and Lake Chad, the latter two on the peripheries of the Sahara (Kröpelin *et al.*, 2008; Amaral *et al.*, 2013), suggest a more gradual transition to a more arid climate from the wet conditions of the AHP.

Findings from multiple climate models similarly present a contradictory account with, for example, Renssen *et al.* (2006) and Hély *et al.* (2009) suggesting an abrupt transition in West Africa and a gradual termination of humid conditions in the east, or Liu *et al.* (2007) proposing an abrupt vegetation collapse followed by a gradual precipitation decline. In their synthesis of hydrological reconstructions across Africa, Shanahan *et al.* (2015) propose that the termination of the AHP was locally abrupt in some areas, such as at Lake Bosumtwi, Ghana, but occurred progressively later at other sites in lower latitudes (Figure 2.9). They argue that the time-transgressive termination of the AHP reflects declining rainfall intensity as a result of decreased summer insolation and the southward migration of the ITCZ during this period.

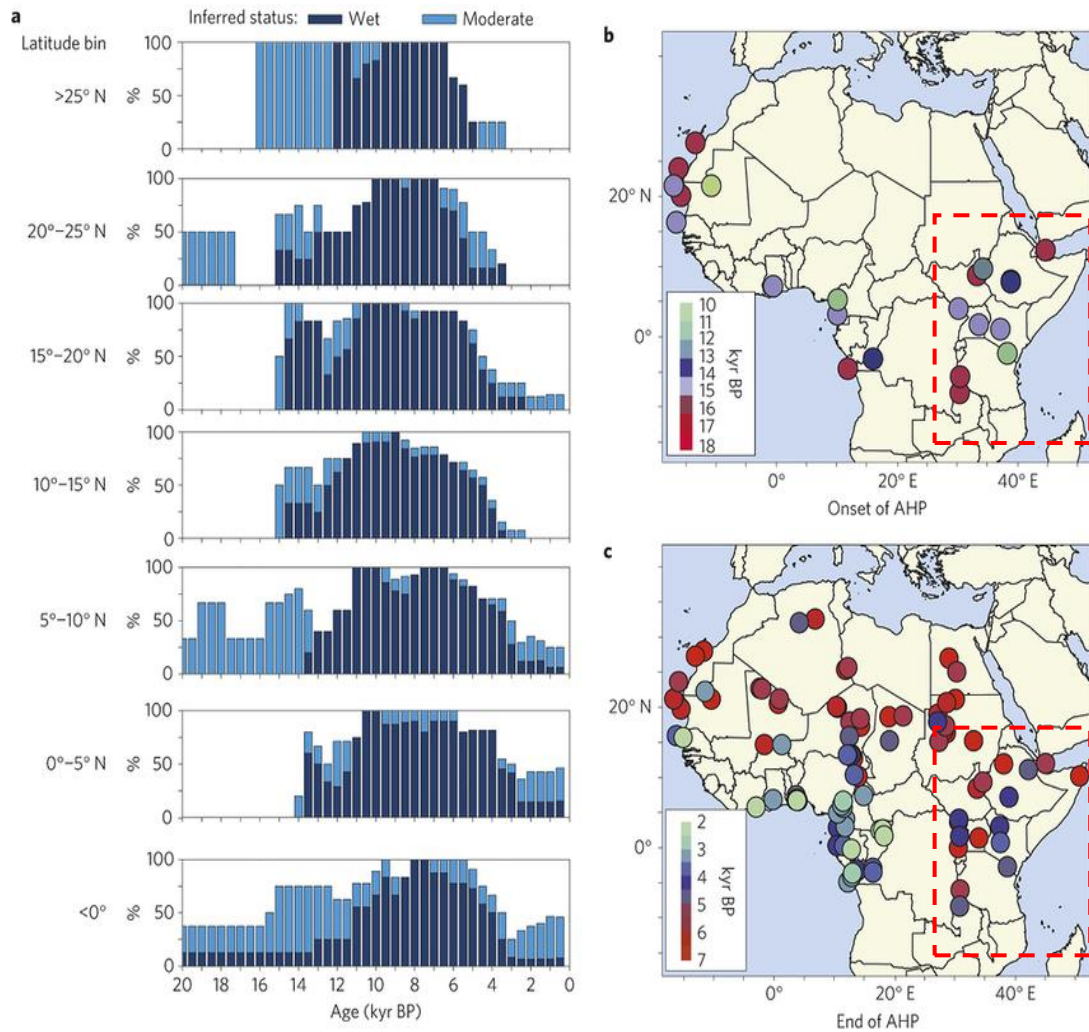


Figure 2.9: Comparison of the AHP represented in palaeoclimate records across Africa. Shown are: frequency histograms for included records indicate wet or moderate conditions, binned at 5° latitude intervals (in descending order; a) and the timing of changes in water balance at the beginning (b) and end (c) of wet, AHP-like conditions. Dashed red box corresponds to the boxed area in Figure 2.1. Adapted from Shanahan *et al.* (2015).

Modelling past hydrological changes at palaeo-Lake Suguta (Junginger & Trauth, 2013) show that the termination of the AHP was gradual, but after an abrupt rainfall decrease, which they, like many other studies (e.g. Tierney *et al.*, 2011b; Costa *et al.*, 2014; Liu *et al.*, 2017) attribute to changes in the ITCZ, but also migration of the CAB (Figure 2.10). Further potential influences on AHP responses have also been highlighted.

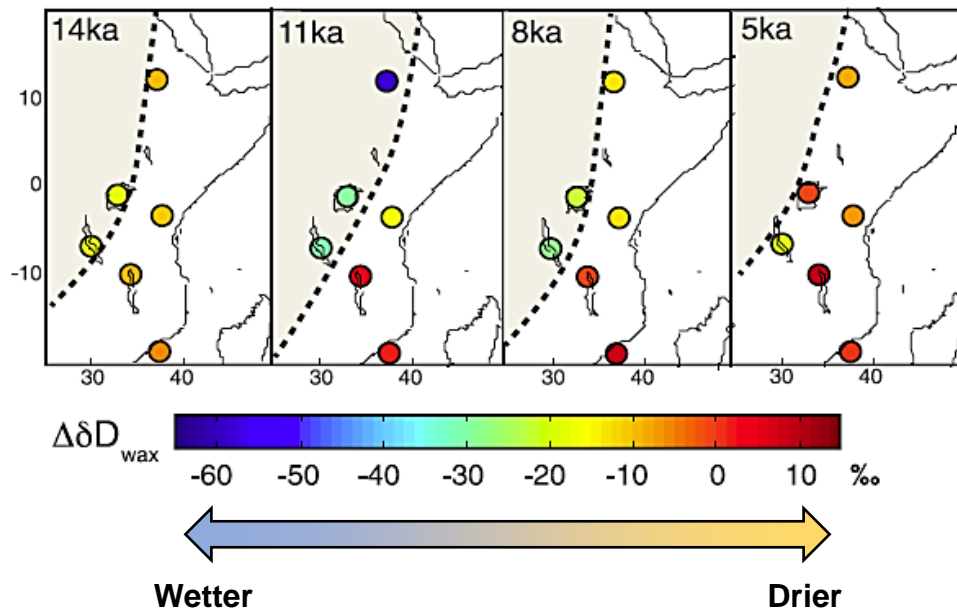


Figure 2.10: Regional time slices of ΔD_{wax} across eastern African sites between 14,000 and 5,000 BP (Costa *et al.*, 2014) showing the influence of the CAB in regional hydrological changes. Shading indicates the regions influenced by Congo Basin sourced precipitation, with the dotted line representing the CAB. The area shown largely corresponds to the boxed area in Figure 2.1, with Lake Tana to the north and the Zambezi fan the southernmost site. Adapted from Costa *et al.* (2014).

These include changes in the intensity of the African Easterly Jet stream, Indian Ocean SSTs and feedbacks between coastal upwelling and the monsoons, as well as migrations of the ITCZ and the CAB (Tierney *et al.*, 2008; 2011a; Liu *et al.*, 2017). Furthermore, changes in regional hydroclimates may also have been amplified by influences such as vegetation feedbacks (Renssen *et al.*, 2006) and local groundwater conditions (Lézine *et al.*, 2011).

2.5 | The Meghalayan

The final subdivision of the Holocene: the Meghalayan (Middle–Late Holocene Boundary), is based on the widespread 4.2 ka event (Walker *et al.*, 2012). Various sedimentary records from across the region highlight a period of pronounced aridity from around 4,200 BP (Gasse, 2000). For example, partially laminated sediments

from the northern Red Sea suggest anomalous changes in evaporation and water salinity (Arz *et al.*, 2006). This aridity is also reflected in dust records from Kilimanjaro ice cores (Thompson *et al.*, 2002). However, an isotopic stalagmite record from Dante Cave in northeastern Namibia suggests a potentially more complex 4.2 ka event in Africa. Two pulses of wetter conditions between 4,150 and 3,930 BP are represented by a $\sim 2\text{‰}$ decrease in $\delta^{18}\text{O}$ values (Railsback *et al.*, 2018).

Following the termination of the AHP, arid conditions were established and remained relatively stable, with some records and lake-level reconstructions largely suggesting prolonged periods of uninterrupted aridity until the present (e.g. Richardson & Dussinger, 1986; Tiercelin *et al.*, 2008; Marshall *et al.*, 2009). Millennial-scale aridity during these periods is also documented in the sediments of the Nile deep-sea fan (Blanchet *et al.*, 2013; 2014) and speleothem records in southeastern Ethiopia (Asrat *et al.*, 2007; Baker *et al.*, 2010), with this aridification epitomised by the establishment of the modern Sahara around 2,700 BP (Kröpelin *et al.*, 2008), illustrating the regional extent of this pronounced dry interval.

However, instability and variations in this aridity throughout the Late Holocene have also been shown (Figure 2.11). Short-lived, abrupt reversals towards more humid conditions at $\sim 3,000$ BP are evident in records from Chew Bahir and Lake Challa (Tierney *et al.*, 2011b; Foerster *et al.*, 2012; Figure 2.11), with this reversal less short-lived, lasting $\sim 1,000$ -1,500 years, for example, in the Ziway-Shala lake basin system (Gillespie *et al.*, 1983). Such a reversal is also evident in leaf wax records from the Gulf of Aden from around 3,500 to 2,000 BP (Tierney & deMenocal, 2013) and records of increased convective precipitation inferred from $^{18}\text{O}_{\text{diatom}}$ values from

2,900 to 1,900 BP at Small Hall Tarn and Simba Tarn, Mt. Kenya (Barker *et al.*, 2001).

Furthermore, from 2,000 BP in many records this wet-dry variability increases (Figure 2.11). At Chew Bahir a humid interval began abruptly around 2,000 BP, with a sharp increase in inferred humidity at ~1,500 BP, before a rapid termination just a few centuries later (Foerster *et al.*, 2012). Similarly, leaf wax records at Lakes Tana (Costa *et al.*, 2014), Challa (Tierney *et al.*, 2011) and Victoria (Berke *et al.*, 2012), and a BIT-index record at Lake Challa (Buckles *et al.*, 2016), display similar increases in moisture availability beginning at around 2,000 BP. Leaf wax records from Lake Tanganyika displays a similar shift to more humid conditions at ~1,500 BP (Tierney *et al.*, 2010), following a period of abrupt wet-dry shifts.

As the ENSO cycle has such an influential role in the climate of eastern Africa, many authors have speculated that changes in the ENSO cycle were likely a major influence on these marked perturbations in moisture availability at, and after, 4,000 BP (Tierney *et al.*, 2011a; Foerster *et al.*, 2012). In their review, Donders *et al.* (2008) find that around 3,000 BP the ENSO-teleconnected regions were characterised by an increased impact of ENSO, comparable to the present-day high-amplitude fluctuations of ENSO, with multiple terrestrial archives around the Pacific Basin suggesting an increased frequency of ENSO events in the Late Holocene (e.g. Sandweiss *et al.*, 1996; Rodbell *et al.*, 1999; Donders *et al.*, 2005; Conroy *et al.*, 2008).

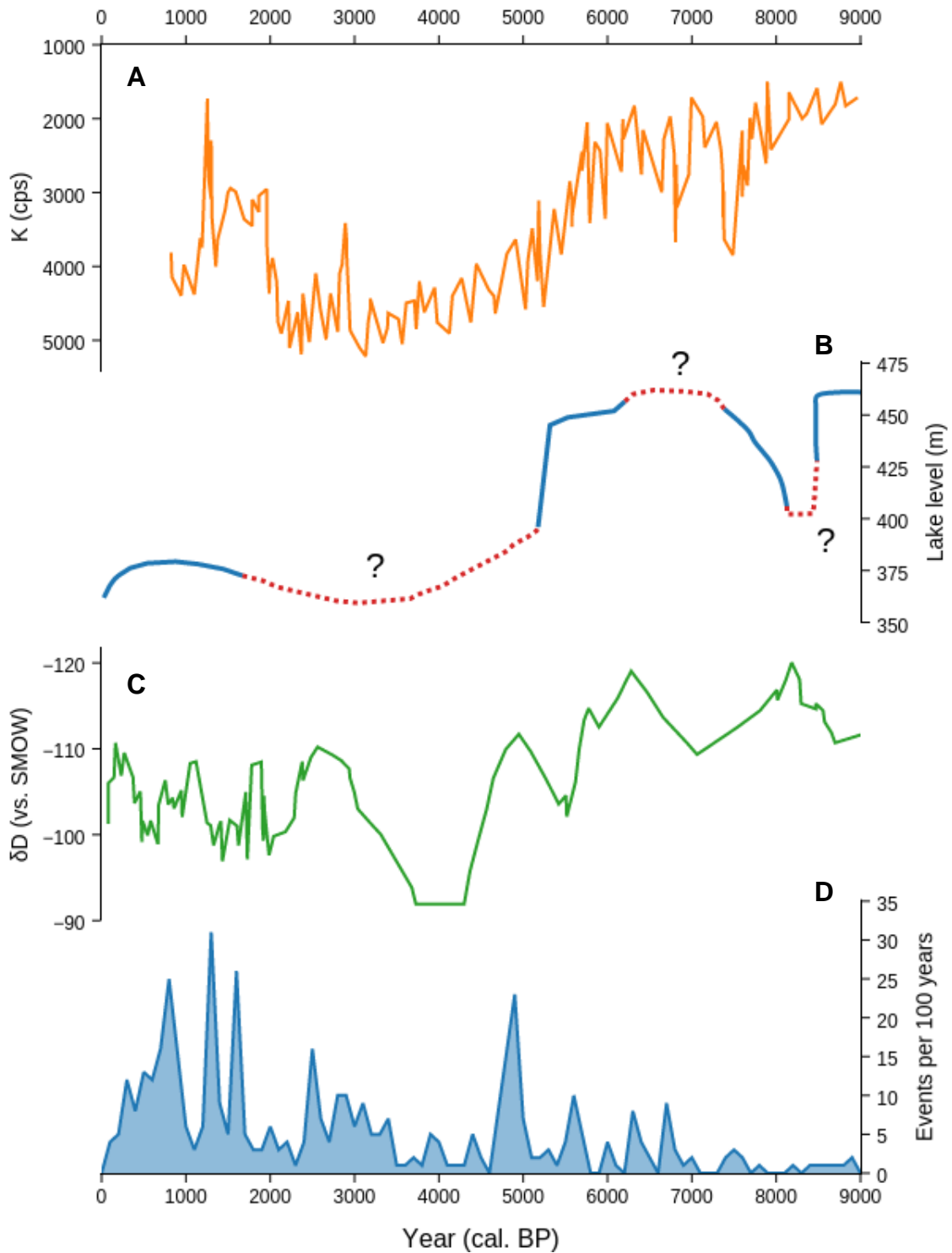


Figure 2.11: Comparison of climatic conditions 9000 BP to present in East Africa showing increased variability from the end of the AHP. Chew Bahir K record (A; Foerster *et al.*, 2012), palaeo-shoreline reconstructions of South Island, Lake Turkana (B; Garcin *et al.*, 2012; dashed lines and '?' denote uncertainty in water-level reconstruction), leaf wax records from Lake Challa (C; Tierney *et al.*, 2011b) and the palaeo-ENSO record from Laguna Pallcacocha, Ecuador (D; Moy *et al.*, 2002).

For example, Moy *et al.* (2002) show, using sediments from Laguna Pallcacocha, southern Ecuador, increased frequency of ENSO events between 3,000 and 2,500 BP and around 1,500 BP (Figure 2.11). It is important to note, that although fossil coral records from the Pacific do contradict these findings (see Cobb *et al.*, 2013), they do still highlight periods of variability in ENSO frequency throughout the Late Holocene.

2.6 | The Last Millennium

Verschuren *et al.* (2000), from the partially submerged Crescent Island crater basin in Lake Naivasha, provide a high resolution record of the climate of equatorial eastern Africa for the past 1,100 years. A combination of sediment-inferred lake depth reconstructions and local ecological assemblage (diatoms and chironomids) compositions and distributions revealed considerable perturbations in local hydrological conditions over the past millennium (Figure 2.12). Local conditions were likely dry at Lake Naivasha with a persistent, saline lowstand from ~1000 to 1270 AD, interrupted by only a brief (~50 years) freshwater interval at ~1220 AD.

Conditions during this period have also been recorded using a variety of proxies across numerous other archives throughout eastern Africa in the Gulf of Aden (Tierney *et al.*, 2015), several Ugandan maar lakes (Russell *et al.*, 2007; Mills *et al.*, 2014) and at Sacred Lake, Mt. Kenya (Konecky *et al.*, 2014), Lakes Victoria (Stager *et al.*, 2005), Edward (Russell & Johnson, 2005), Hayq (Lamb *et al.*, 2007a; Loakes, 2015), Challa (Buckles *et al.*, 2016) and Tanganyika (Stager *et al.*, 2009). These conditions fall within the anomalously warm period across much of the globe (Mann *et al.*, 2009) commonly known as the Medieval Climate Anomaly (MCA).

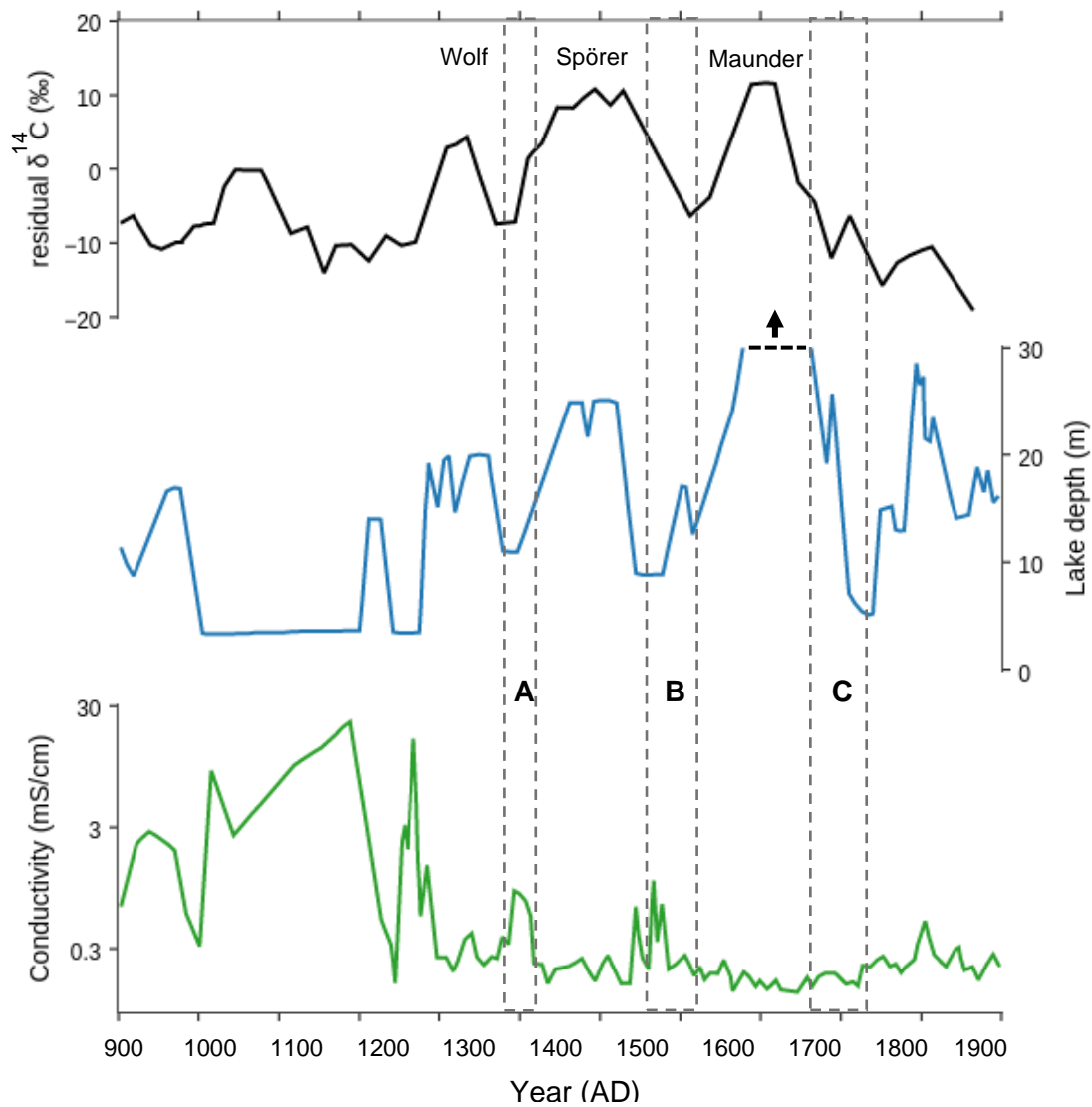


Figure 2.12: 1,100-year historical (1883 AD-present) and sedimentology-inferred lake level (arrow and dashed line indicate overflow period) and salinity (diatom-inferred conductivity) record for the Crescent Island crater basin in Lake Naivasha, Kenya, compared with a decadal record of atmospheric $^{14}\text{CO}_2$ production as a proxy for solar radiation, with periods of solar minima also noted. The dashed bars represent known periods of severe aridity and societal change recorded through oral tradition: the Wamara (A), Nyarubanga (B), and Lapanarat-Mahlatule (C) droughts. Redrawn from Verschuren *et al.* (2000).

For example, in easternmost equatorial eastern Africa, the Lake Challa BIT-index record suggests that abrupt aridification between 1150 CE and 1200 resulted in peak MCA drought, which was maintained until 1300 CE (Buckles *et al.*, 2016). On the western edges of the eastern Africa region, an increased ratio of Mg to Ca in

authigenic calcite (%Mg) in Lake Edward's sediments suggests the area experienced significantly arid periods between around 1050 to 1200 CE (Russell & Johnson, 2007).

At Site P178-1, in northern eastern Africa, drier conditions were maintained from ~950 to 1200 CE, culminating in abrupt, marked perturbations (leaf wax value change from -123 to -137 within 20 years) between wet and dry conditions centred around 1200 CE. The modern climate of eastern Africa is considerably dry, especially in comparison to the peak humid conditions of the AHP (Figure 2.13), with records from, for example, Lake Hayq (Lamb *et al.*, 2007) and the Gulf of Aden (Tierney *et al.*, 2015) suggesting even drier conditions than the MCA, with Lamb *et al.* (2007a) noting that the Hayq $\delta^{18}\text{O}$ record only displays two periods with drier climate than present conditions centred at 800 AD and 1750–1880 AD.

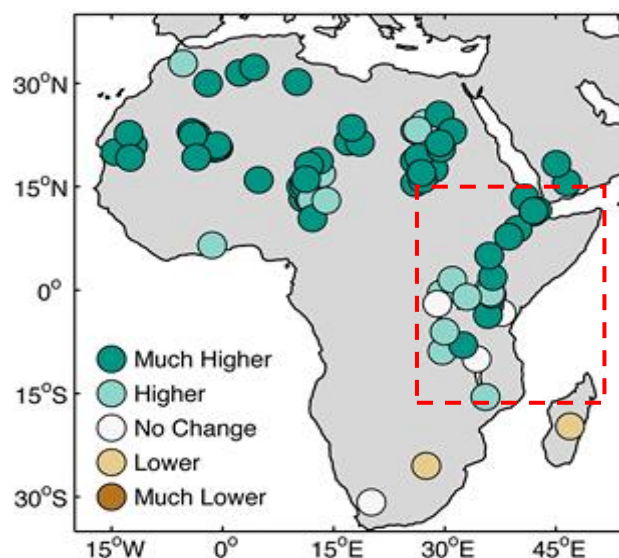


Figure 2.13: Qualitative comparison of African lake levels 9,000 BP vs. present levels. Reconstructed from the OLLD (COHMAP members, 1988; Street-Perrott *et al.*, 1989) updated with lake-level data generated in the last twenty years by Tierney *et al.* (2011b). Adapted from deMenocal & Tierney (2012). Dashed red box corresponds to the boxed area in Figure 2.1.

The wettest period of the last 2,000 years in numerous records in eastern Africa occurred during the LIA (~1450-1800 AD). Following the drier conditions of the MCA, the Naivasha record, like many of the other records discussed above, suggests more humid conditions by displaying an establishment of freshwater conditions, highlighted by the gradual reduction and disappearance of more saline-tolerant taxa (e.g. *Craticula elkab*, *Kiefferulus disparillis*) and the expansion of freshwater taxa (e.g. *Psectrocladius viridescens*). However, two brief (~40 year) intervals of drier conditions, represented by reductions in lake depth and increased salinity, which are also documented in local indigenous cultures as significant drought periods and cultural change, are also evident (Figure 2.12). The latter of these dry intervals are followed by a highstand (above the historical maximum of 1894 AD) between 1670 and 1770 AD at which point the lake overflowed. Similar conditions during the LIA period have been reported from other records across eastern Africa (e.g. Ashley *et al.*, 2004; Konecky *et al.*, 2014; Tierney *et al.*, 2015; Buckles *et al.*, 2016). However, based on a synthesis of lacustrine proxy and instrumental climate data, and by applying Empirical Orthogonal Function approaches, Tierney *et al.* (2013) exhibits that the region of eastern Africa that may have experienced a predominantly wet rather than dry climate during the main phase of the LIA, extended along the eastern coast from 7°S northward to the Horn of Africa, and inland to ~35-34°E over northern Kenya and Ethiopia. This finding was recently reinforced by the leaf wax record of Tierney *et al.* (2015) which suggests wetter conditions peaked in the early 17th century as far along the eastern African coast north as the Gulf of Aden.

Despite exhibiting a similar trend to eastern sites during the MCA, and post-MCA, palaeoenvironmental reconstructions at locations farther to the west, such as the

Ugandan crater lakes in Russell *et al.* (2007) and Mills *et al.* (2014), Lakes Edward (Russell & Johnson, 2007), Masoko (Garcin *et al.*, 2007b) and Tanganyika (Tierney *et al.*, 2010) have displayed a return to drier conditions during the LIA. For example, the increase in %Mg in the Lake Edward record suggests that regional aridity during this period was comparable to that experienced during the MCA (Russell & Johnson, 2007). However, lacustrine records at some sites, such as at Lakes Victoria (Stager *et al.*, 2005) and Hayq (Lamb *et al.*, 2007a), seem to present an intermediate pattern between these 'eastern' and 'western' histories. During the main-phase LIA the climate at these sites was drier than during the early LIA, but still wetter than both peak MCA drought or the 20th century average. For example, the percentage change in shallow water diatoms at Lake Victoria, positioned geographically between eastern and western eastern Africa, suggests the lake reached its highest levels between 1400 and 1600 AD, followed by a decline and a more modest lake level at around 1700 AD (Stager *et al.*, 2005).

In their study, Tierney *et al.* (2013) demonstrated that the development of a coastal (eastern)-interior (western), wet-dry dipole was driven mainly by temporal variations in Indian Ocean SSTs, with the importance of Indian Ocean SSTs also demonstrated in simulations by Klein *et al.* (2016). Furthermore, Nash *et al.* (2016) highlight the influence of variability in the ENSO cycle in the creation of this spatial dichotomy, as suggested by Russell & Johnson (2007), is not inconsistent with this mechanism. Additionally, the CAB may have also played an important role in LIA climate, with either a westward shift (Russell & Johnson, 2007), or a weakened convergence (Tierney *et al.*, 2011a), during the main-phase LIA, which may have contributed towards the formation of this eastern-western dipole, and intermediate

responses at sites such as Lake Victoria (Stager *et al.*, 2005) with influences from both the Indian and Atlantic oceans.

2.7 | Summary

The climate of eastern Africa has varied considerably, both temporally and spatially, over the past 15,000 years, driven by a complex interplay of orbitally-forced variability, land surface changes, migration of the ITCZ and the CAB and changes in SSTs in the Atlantic, Pacific and Indian Oceans. Since the earlier reviews of Gasse (2000) and Kiage & Liu (2006), our knowledge of the eastern African hydroclimate has expanded considerably. Further research questions have developed regarding past hydrological change in eastern Africa, such as spatial extent of the LIA wet-dry dipole, the exact nature and timing of the YD, termination of the AHP and the cause of these changes/patterns. These past perturbations in climate significantly influenced the spatial distribution and development of early cultures and civilisations (e.g. Figure 2.8), underlining the importance of fully understanding the nature and timing of these wet-dry cycles and of identifying the underlying circulation patterns and feedbacks that respond to and amplify orbitally-forced changes in eastern Africa. Further work with these questions in mind may provide useful insights into current and future environmental changes, both natural and anthropogenic, and the associated impacts and contemporary societies

Chapter 3 :

The Physical Environment of Ethiopia & Study Sites

In this chapter, the geology and climate of Ethiopia are outlined, followed by a detailed description of the two study areas within this context. This includes seasonal variations in climate, underlying geology and hydrochemistry of the individual lakes sampled in this study. Previous palaeoenvironmental investigations in the vicinity of each study site are also discussed in the context of the broader review of palaeoclimatic research introduced in Chapter 2.

3.1 | Geology of Ethiopia

The geodynamic and geomorphic processes since the Oligocene have produced the diverse Ethiopian landscape. The south-eastern section of the territory is largely homogenous, mainly consisting of Late Palaeozoic, Mesozoic and Cenozoic continental and marine sediments. Due to sustained tectonic action for millions of years associated with the position of the region on the Somali and Nubian minor plates, illustrated by the abundance of geological faults, volcanic rocks are common across the country (Tadesse *et al.*, 2003; Figure 3.1).

The main Ethiopian rift (MER) is a central valley connected to the southern corner of the Afar Triple Junction, and is a predominant feature of the Ethiopian landscape. The MER is roughly 80 km in width and ~330 km long, bisecting the country from northeast to southwest. It continues to widen since the initial rifting in the southern and central MER between 18 and 15 Ma; extension in the northern Main Ethiopian rift commenced after 11 Ma, at a rate of about 2.5 mm/yr (Wolfenden *et al.*, 2004; Chorowicz, 2005).

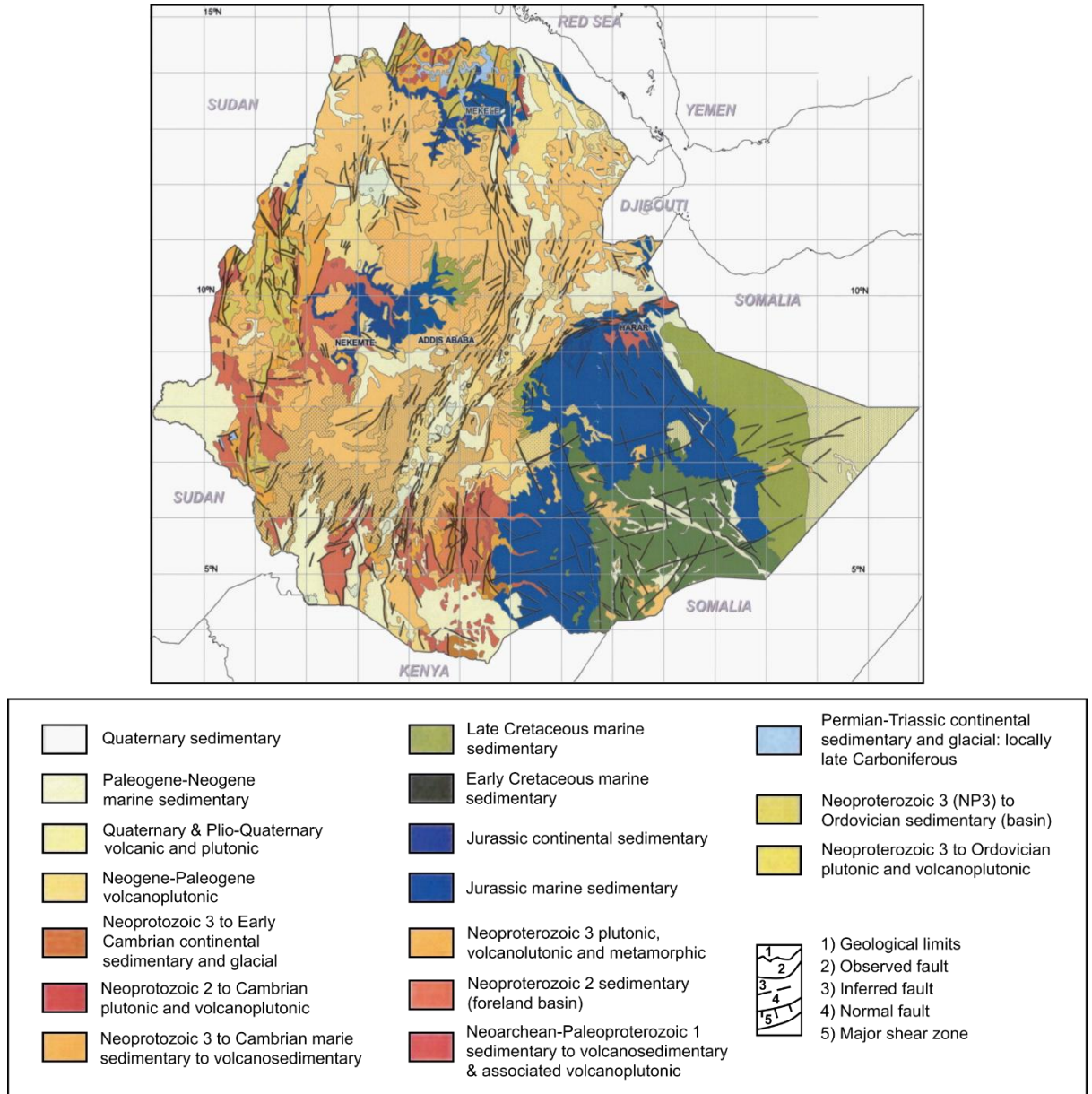


Figure 3.1: Simplified geological map of Ethiopia redrawn from Tadesse *et al.*, (2003).

3.2 | Ethiopian Climate

The Ethiopian National Meteorology Agency (NMA 2013) highlights that from a meteorological point of view, there are three seasons in Ethiopia, with the monthly and seasonal rainfall outlined by Viste *et al.* (2013) in Figure 3.2:

- 1) As the Arabian high weakens and moves toward the Indian Ocean, the ITCZ migrates northwards, causing a short rainy season from February to May (*Belg*) over much of the *Belg*-growing areas. In the south-western

areas of the country it denotes the beginning of the long rainy season, starting in March and peaking in April. For the western parts of the country, the rainy season starts during March/April. However, further north of the western section of the country, this season is predominantly dry except for the month of May.

- 2) From June to September the main rainy season begins (*Kiremt*) associated with a movement of the ITCZ northwards, with a higher magnitude rainfall in comparison to the other seasons. This period of increased rainfall accounts for up to three quarters of the annual rainfall in the north-western highlands (Korecha & Barnston, 2007; Figure 3.2). However, the southern and south-eastern lowlands of Ethiopia receive very little rain during this period, with only a small amount of rain towards the end of the season.
- 3) A dry season (*Bega*), associated with a southward migration of the ITCZ, characterised by cool nights and warm days, is experienced from October to December/January. However, short rains are experienced over some southern parts of the country, with occasional showers over central and northern regions of the country, depending on influences from mid-latitude rain-bearing systems.

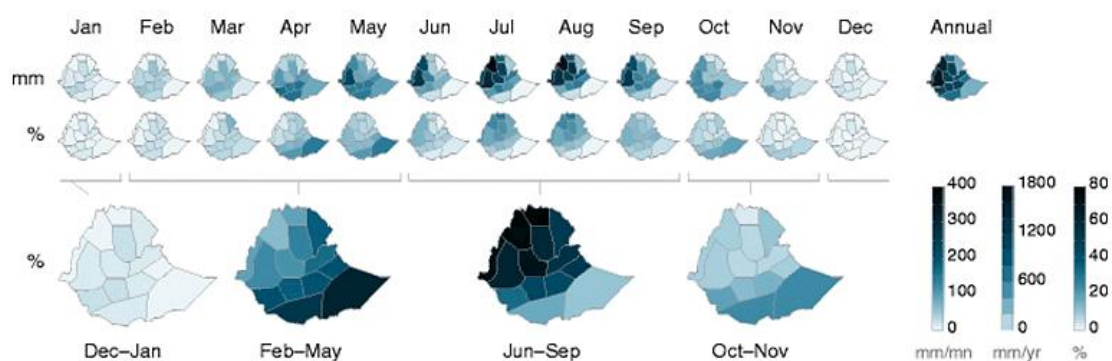


Figure 3.2: The seasonal precipitation cycle in Ethiopian rainfall zones adapted from *Viste et al.*, 2013). 1971–2000 monthly mean (mm/mn) and annual precipitation (mm/yr), and seasonal and monthly percentage of annual precipitation corresponding to their respective colour gradient bars.

3.3 | The Bishoftu Crater Lakes

The Bishoftu Crater Lakes (BCLs) lie in a group of maars on the western escarpment of the MER at Bishoftu[†] at an altitude of 1860 m above sea level, ~45 km southeast of Addis Ababa, Ethiopia (Figure 3.3). The local bedrock is composed of 10-9 Ma-old basalts and 1-4 Ma-old acid volcanics. These 1-4 Ma eruptions led to the formation of the central volcanoes Yerer, Bede Gebabe and Zikwala. The maars, cinder cones and lava flows represent relatively more recent (10 ka) volcanic activity (Gasparon *et al.*, 1993 in Kebede *et al.*, 2002). The transmissivity of the older basaltic aquifers ranges between 389 and 21,600 m²/day. The younger basic pyroclastic rocks, interbedded with minor acidic products, comprise the largest part of the local Bishoftu Crater Lakes area, with transmissivities of 1,100 up to 18,000 m²/day (Gasparon *et al.*, 1993; Ali, 1999 in Kebede *et al.*, 2002). The scoria cones and volcanic domes are believed to be the major zones of groundwater recharge, and as the static groundwater level is

[†] Also known as Debre Zeit (or alternatively spelt Debre Zeyt/Zeyit).

above the local lake levels, the importance of groundwater inflow to the lakes is evident (Gasparon *et al.*, 1993; Ali, 1999 in Kebede *et al.*, 2002; Table 3.1).

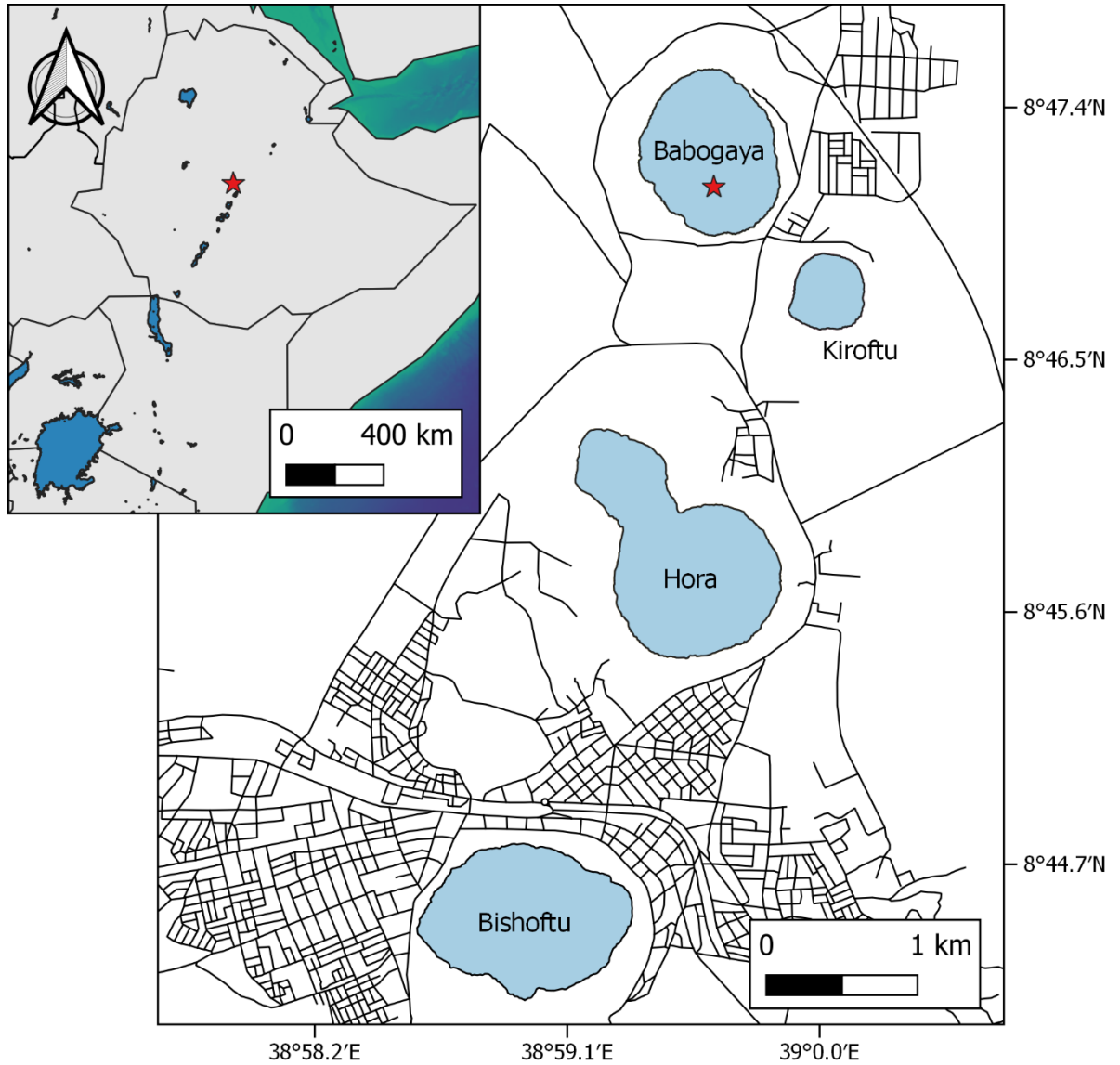


Figure 3.3: Bishoftu Crater Lakes location within Ethiopia (red point in inset map) and the Bishoftu area (black lines indicate roads).

The local climate is monsoonal with distinct, pronounced wet and dry seasons, corresponding to the three seasons outlined above. Local rainfall is highest during the *Kiremt* with highest mean monthly rainfall in July and August (up to 300 mm in some years).

Table 3.1: Hydrological characteristics of Lake Hora (HO) and Lake Babogaya (BA; Lamb *et al.*, 2002). Direct rainfall (DR), groundwater (GW), evaporation (Evap.) and chlorine (Cl).

	% inflow			% outflow		Residence time (years)	
	DR	Runoff	GW	Evap.	GW	Water	Cl
HO	47	10	43	97	3	6	500
BA	38	6	56	79	21	10	81

These humid conditions in the *Kiremt* contrasts the relative aridity experienced during the *Bega* with recorded monthly rainfall below 50 mm between October and January from 1951 to 2003. Seasonal variations in mean air temperature are low, with mean annual air temperature varying around 19°C by roughly $\pm 0.5^\circ\text{C}$. Lowest temperatures occur at night throughout the dry season, with the highest temperatures experienced through the *Belg* and the beginning of the wet season (Figure 3.4).

The past natural vegetation of the area was likely *Acacia albida* savanna, with *Juniperus procera* forest at higher elevations. The contemporary landscape is increasingly urbanised and dominated by agriculture, principally the cultivation of tef. Trees and shrubs including: *Eucalyptus*, *Casuarina equisetifolia*, *Schinus molle* and *Opuntia* have been planted around the lakes (Lamb *et al.*, 2002).

Multiple researchers have conducted comprehensive investigations into the limnology of the BCLs (Baxter *et al.*, 1965; Wood *et al.*, 1976; Wood *et al.*, 1984; Wood & Talling, 1988; Lamb *et al.*, 2002; Lemma, 2009), and as a result the seasonal variations in lake characteristics are well understood.

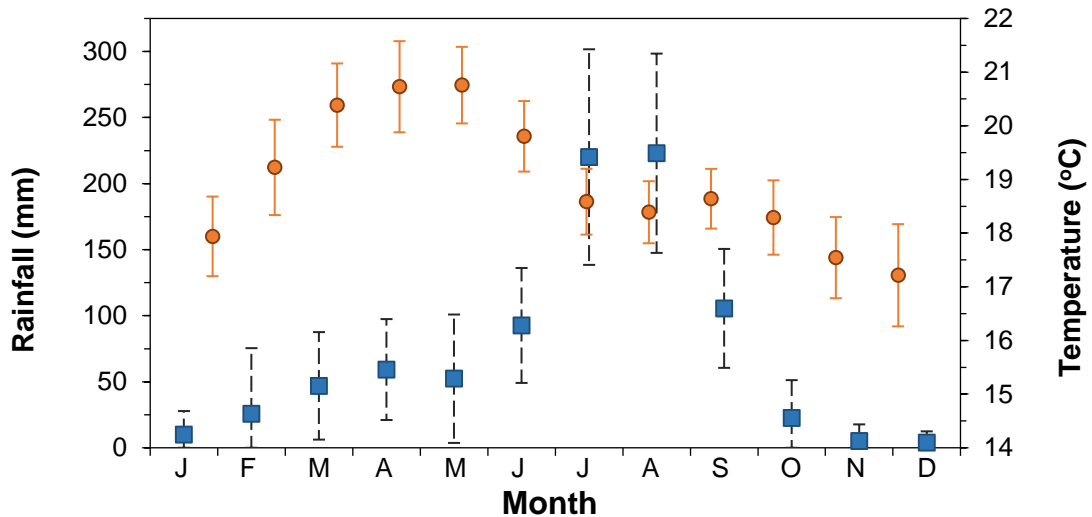


Figure 3.4: Mean (\pm standard deviation) monthly rainfall (blue) and average air temperature (orange) data for 1951-2003 (missing 1991-1993) and 1952-2005, respectively, from the Debre Zeit Research Centre meteorological station in Awulachew *et al.* (2006).

Carbonate laminations, alternating between isotopically different (more ^{18}O and ^{13}C enriched light layers; Table 3.2) dark and light layers, are present in the stratigraphy of Lake Hora (Lamb *et al.*, 2002; Figure 3.5). In contrast to the mechanisms controlling varve formation in temperate-zone lakes where seasonal changes in temperature controls stratification and productivity, the low variations in temperature at Bishoftu suggests rather different mechanisms of seasonal stratification and mixing as the dominant control on lake productivity and the formation of these laminae. Small amounts of aragonite are present in the dark organic layers, which suggests that aragonite deposition occurs throughout the year, but the rate of precipitation increases and/or deposition of organic material ceases during the stratification cycle.

The lighter layers, composed of authigenic aragonite crystals, are precipitated during algal photosynthetic uptake of dissolved CO_2 (Lamb *et al.*, 2002). This occurs during the dry-season when lake waters are mixed due to reduced

insulative cloud cover. During the wet season the insulative cloud cover promotes thermal stratification. This mixing promotes algal photosynthesis and aragonite precipitation by bringing Ca and other nutrients from the hypolimnion to the surface. This mixing also potentially causes lighter algal detritus to be retained in suspension through the water column while the denser aragonite falls to the lake floor, which is supported by the higher densities of algal matter during the dry season (Lamb *et al.*, 2002). Furthermore, in support of this mechanism, the isotopic composition of aragonite layers sampled by Lamb *et al.* (2002) at Lake Hora in the January dry season corresponds to the surface water samples taken simultaneously. Similarly, the isotopic depletion of dark layer aragonite laminations also supports a wet-season dark layer, dry season light layer model (Table 3.2). There is also a close similarity between the estimated sediment accumulation rates derived from lamina counts (2.9 mm/year) and from a ^{210}Pb chronology (2.2-2.9 mm/year) confirming that these laminae are deposited annually, and highlighting their potential to reconstruct environmental change at a high resolution.

The numerous detailed investigations and descriptions of the BCLs highlight similarities in limnological behaviour, and as Lamb *et al.* (2002) suggest, it is reasonable to assume that the BCLs share comparable seasonal dynamics. As a result, they suggest that the wet-dry cycle of aragonite deposition and laminae formation evident at Lake Hora may also be used to explain the light-dark laminae evident in the sediments of Lake Babogaya. In support of this hypothesis, for example, Mg plays an important role in the precipitation of calcium carbonates in water (Folk, 1974; Kelts & Hsü, 1978), and much like Lake Hora, the Mg:Ca ratio

of Lake Babogaya waters is greater than 3 (Table 3.3), conditions in which aragonite is typically precipitated by algal photosynthesis (Lamb *et al.*, 2002).

3.3.1 | Study Site 1: Lake Babogaya

Lake Babogaya is the northern-most lake of the BCLs (Figure 3.2). The lake has a surface area of 0.58 km², maximum and mean depth of 65 m and 38 m, respectively, with a volume of 0.022 km³ (Figure 3.6). Characteristic of many crater lakes, Lake Babogaya has steep slopes with a very small catchment area and no inflowing rivers or streams. During the rainy season, the lake is fed by a combination of rainfall, runoff and underground inflows (Table 3.1). A small submerged volcanic cone is also present in the lake (Wood & Talling, 1988; Lamb *et al.*, 2002; Lemma, 2009). The modern lake environment is the site of multiple hotels.

The lake develops thermal stratification during March through to November, leading to the formation of indistinct thermoclines at 11-16 m depth late in the summer wet season (Figure 3.7). The waters of Babogaya mix through November to February, during the dry season, associated with the evaporative and night-time radiative cooling under conditions of low humidity and low cloud cover (Lamb *et al.*, 2002). Oxygen supersaturation develops in the upper layer of the lake during the wet season, due to algal photosynthetic activity. Epilimnetic oxygen minima coincide with dry-season mixing, and occur occasionally during the wet season when the thermocline deepens (e.g. July-August 1966; Figure 3.7). Secchi disk measurements in March of 2001 and the end of February 2002 (both the *Belg* season) reveal the upper ~150-170 cm of lake waters are transparent (Lemma, 2009).

Table 3.2: Oxygen and carbon isotope values (V-PDB) for aragonite from individual year-assigned laminae in the sediments of Lake Hora (Lamb *et al.* 2002).

Year	Light layers		Dark layers	
	$\delta^{18}\text{O}$	$\delta^{13}\text{C}$	$\delta^{18}\text{O}$	$\delta^{13}\text{C}$
1997	6.54	10.30	-	-
1996	6.30	10.93	-	-
1995	6.37	10.53	-	-
1994	6.38	10.32	-	-
1993	6.06	10.41	-	-
1992	6.78	10.83	-	-
1991	7.01	10.70	-	-
1990	7.06	10.86	-	-
1989	7.26	10.71	-	-
1988	6.89	10.16	-	-
1987	7.09	10.70	5.9	9.3
1986	6.49	10.73	-	-
1985	6.75	10.55	-	-
1984	6.65	10.87	-	-
1983	7.03	10.63	-	-
1982	7.42	10.65	-	-
1981	7.63	10.60	5.1	8.0
1980	7.21	10.57	-	-
1979	7.23	10.12	5.1	7.5
1978	6.87	10.41	-	-
1977	7.08	10.21	3.8	6.3
1976	6.99	10.17	4.2	6.3
1975	6.94	10.00	5.2	7.9
1974	6.76	10.34	-	-
1973	6.65	10.36	-	-
1972	7.26	10.12	5.7	8.1
1971	6.87	9.98	5.0	6.6
1970	7.15	9.99	-	-
1969	6.87	9.82	-	-
1968	7.11	9.68	-	-
1967	7.15	9.73	3.5	0.8
1966	6.99	9.72	3.8	5.5
1965	6.87	9.51	2.7	0.7
1964	6.72	9.66	3.3	-0.7
1963	6.84	9.91	4.6	6.1
1962	7.43	9.47	4.7	6.3

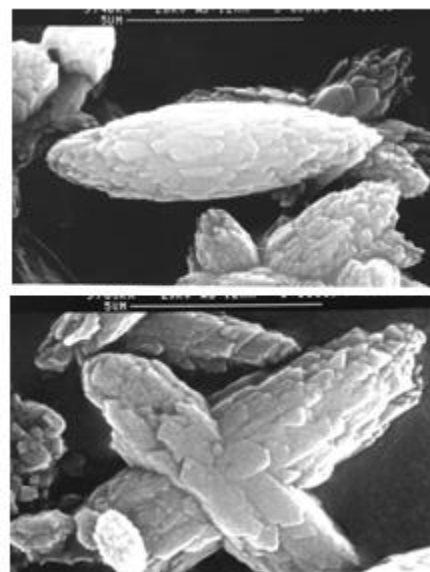
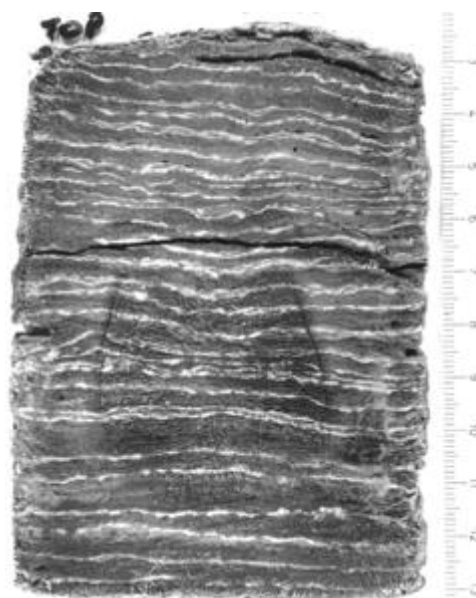


Figure 3.5: Aragonite laminations in freeze-dried section of Lake Hora core HG98-1 (top; scale in cm). Scanning electron microscope images of aragonite crystals (bottom; 5 μm scale) from (H. Lamb *et al.* 2002).

Table 3.3: Hydrochemistry of the Debre Zeit area groundwater (Gr) and Lake Babogaya (BA) surface water in 1998¹ from Lamb *et al.* (2002) and 2001² for Lake Babogaya surface waters to 50 m depth by Lemma (2009).

	Conductivity (k20 μ S/cm)	pH	HCO ₃ ⁻ (meq/L)	Cl ⁻ (meq/L)	SO ₄ ²⁻ (meq/L)	CO ₃ ⁻ (meq/L)	K ⁺ (meq/L)	Na ⁺ (meq/L)	Ca ²⁺ (meq/L)	Mg ²⁺ (meq/L)	
Gr ¹	685	7.3	2.62	0.42	-	-	-	0.42	1.98	2.52	
BA ¹	776	8.7-9.2	7.67	0.69	-	-	-	3.74	0.22	3.74	
BA ²	0 m	850 (\pm 30)	-	2.55	0.06	4.09	2.70	0.37	2.33	0.84	3.72
	3 m	841 (\pm 28)	-	4.20	0.11	3.51	3.00	0.72	4.97	0.80	3.92
	6 m	829 (\pm 15)	-	4.30	0.11	2.28	2.90	0.76	4.97	0.60	4.64
	16 m	859 (\pm 14)	-	4.60	0.11	2.68	2.60	0.62	4.58	0.68	4.36
	30 m	959 (\pm 12)	-	5.99	0.10	2.79	1.90	0.45	2.84	0.68	4.72
	50 m	-	-	5.49	0.10	2.08	1.70	0.42	2.52	0.60	4.52

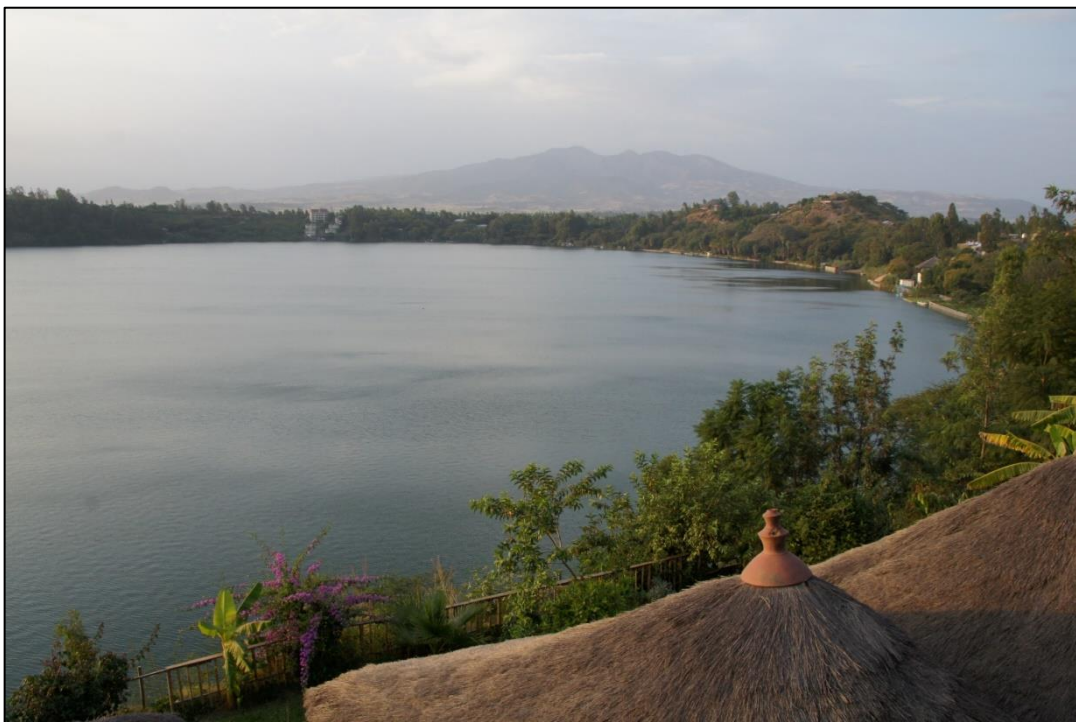
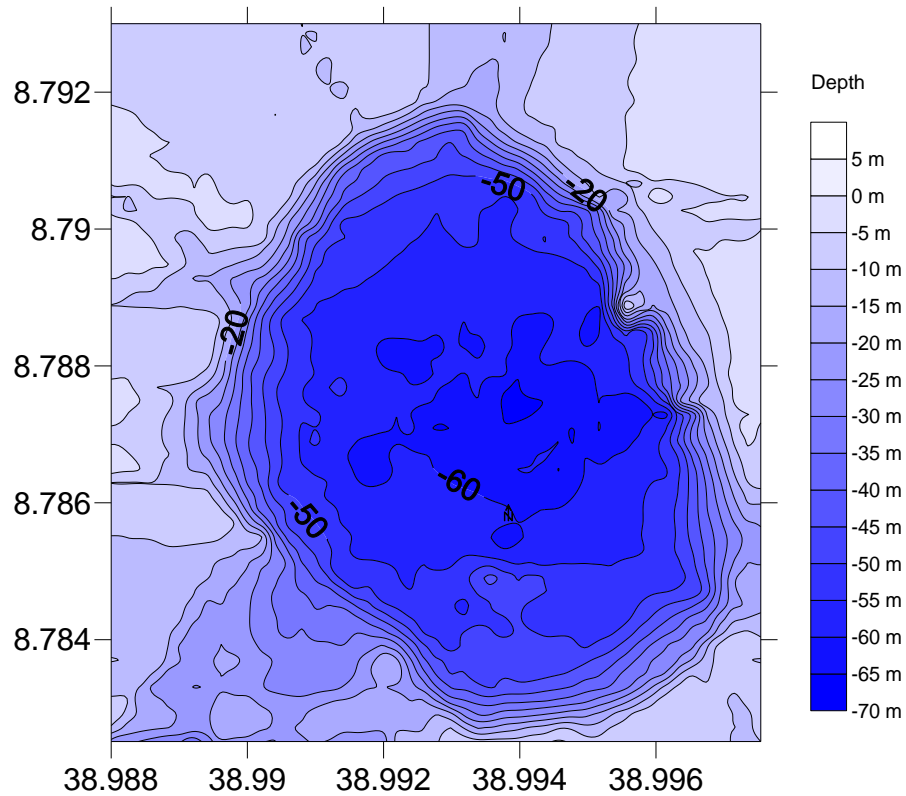


Figure 3.6: Bathymetric scans and images of Lake Babogaya (Schaebitz unpubl. data). The photograph was taken by H. Lamb from the south-eastern shore of the lake.

Conductivity is slightly higher at the surface (850 $\mu\text{S}/\text{cm}$), likely due to higher surface water temperatures, and remains around 830-860 $\mu\text{S}/\text{cm}$ between 0 and

16 m, due to cooler and calmer waters. However, conductivity below 16 m is higher as substances slowly sink. Despite peak salinity at 40 m depth (~1000 $\mu\text{S}/\text{cm}$) is significantly less than that of nearby Lake Hora (~2300 $\mu\text{S}/\text{cm}$; Lemma, 2009). Surface pH usually varies between 8.7 and 9.2, decreasing with depth to pH 8.4 in stratified conditions. Calcium (Ca) concentration is higher in the epilimnion, associated with the photosynthetic precipitation of aragonite, with a negligible increase of magnesium (~1 meq/L) with depth (Lamb *et al.*, 2002; Lemma, 2009; Table 3.3).

Between 1963 and 1966, and in 1980, Wood & Talling (1988) report that the dominant algae at Lake Babogaya was *Microcystis aeruginosa*. However, little is known of the diatom communities at Lake Babogaya, with Lemma (2009: 232) simply stating “a few diatoms” are known to be present. Belay (2007) reported that between June 2006 and April 2007 the following diatoms species were present: *Cyclotella planctonica*, *Cymbella cistula*, *Fragilaria capucina*, *Fragilaria ulna*, *Surirella linearis*, *Synedra dorsiventralis*, *Nitzschia nyassensis* and *Nitzschia vermicularis*, with the latter two being the most dominant species. T. Pinches of Aberystwyth University (BSc student unpub. data.) describes the diatom stratigraphy of a 1.15 m core taken in 1998, which represents the past ~400 years (assuming a similar sedimentation rate to that of nearby Lake Hora; Lamb *et al.*, 2002). Thirty species were identified, however only a few of these were present above 2% of the entire core assemblage, leaving eight dominant species: *Cymbella fonticola*, *Cymbella affinis*, *Cymbella microcephala*, *Achnanthes minutissima*, *Navicula cryptocephala*, *Nitzschia amphibia*, *Nitzschia palea* and *Nitzschia fonticola*.

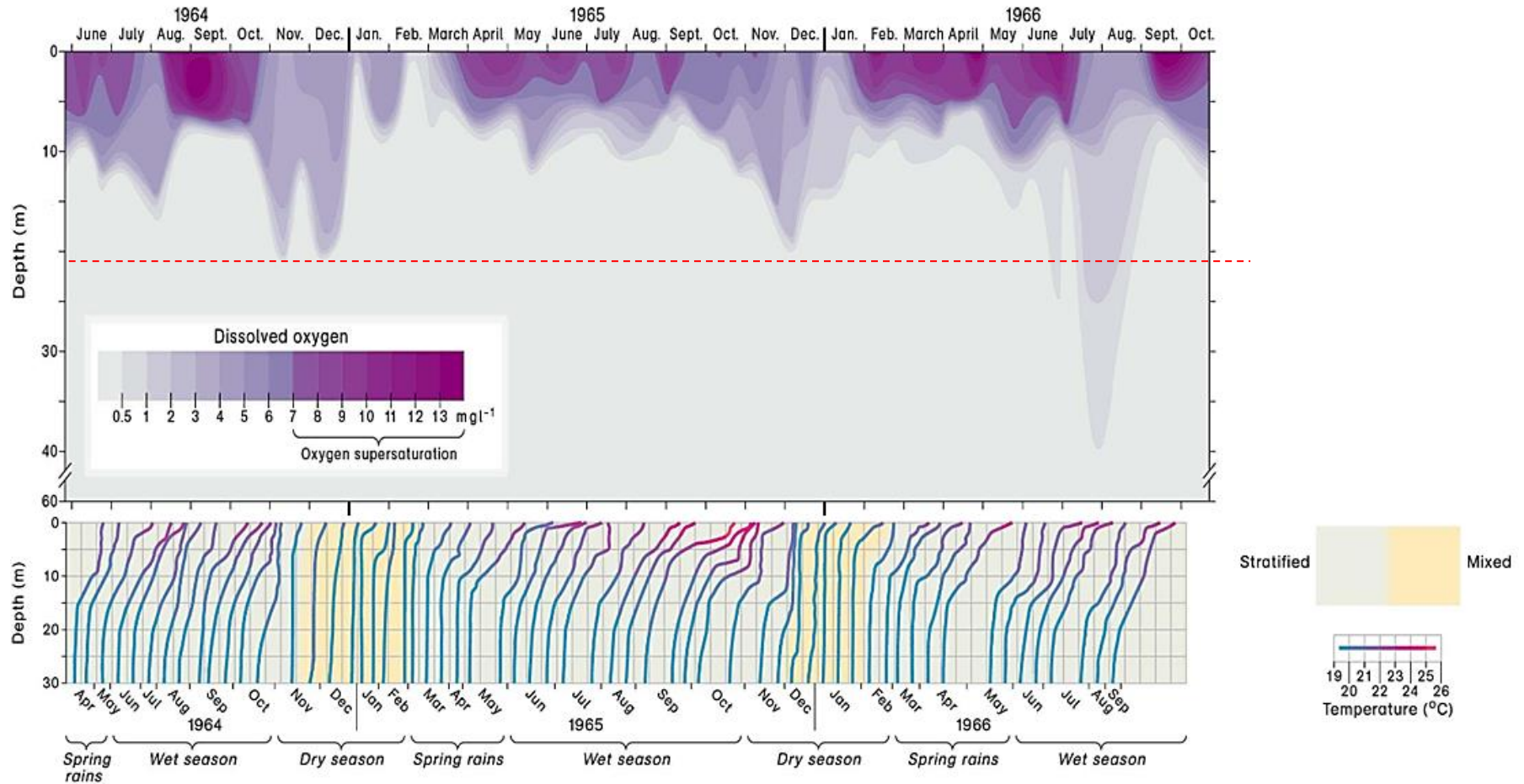


Figure 3.7: Seasonal characteristics of Lake Babogaya waters adapted from Lamb *et al.* (2002). Temperature profiles April 1964 - September 1966. All profiles are between 19° and 20°C at 30 m depth, with vertical grids spaced at 1°C intervals (top). Dissolved oxygen content of Lake Babogaya to a depth of 60 m, May 1964 - October 1966 (bottom). Red line highlights the general level of lake anoxia.

3.4 | The Bale Mountains

The Bale Mountains (between roughly 6°40'-7°10' N and 39°30'-40°00' E; Figure 3.8), in the Oromia Region of southeast Ethiopia, belong to the Bale-Arsif massif that forms the western section of the south-eastern Ethiopian highlands and consists of Miocene basalt and trachyte lavas overlying Mesozoic marine sediments (GSE, 1996; Figure 3.1). The Sanetti Plateau is a major landform of the Bale Mountains with altitudes around 4000-4200. Multiple peaks above 4000 m rise above the plateau including Mount Batu (4350 m) and Tullu Dimtu (~4400 m), the latter being the second highest peak in Ethiopia.

Vegetation across the plateau is mainly characterised by Afroalpine dwarf scrub and isolated *Erica* shrubs, which is surrounded by an *Ericaceous* belt (Figure 3.9; Umer *et al.*, 2007). However, disturbance by cutting, burning and domestic stock grazing has increased over the last few decades with multiple grazing grounds and transhumant settlements scattered across the plateau.

The alternating wet-dry cycle at the Bale Mountains, much like the rest of the Horn of Africa, corresponds to the movements of the ITCZ throughout the year. Average annual rainfall (1971-2000) from various stations from the surrounding region in Viste *et al.* (2013) indicates rainfall is highest through the *Kiremt* and *Belg* (42% and 39% of total annual rainfall, respectively), in contrast to the arid *Bega* season which experiences only 19% of total rainfall through the four months from October through to January (Figure 3.4).

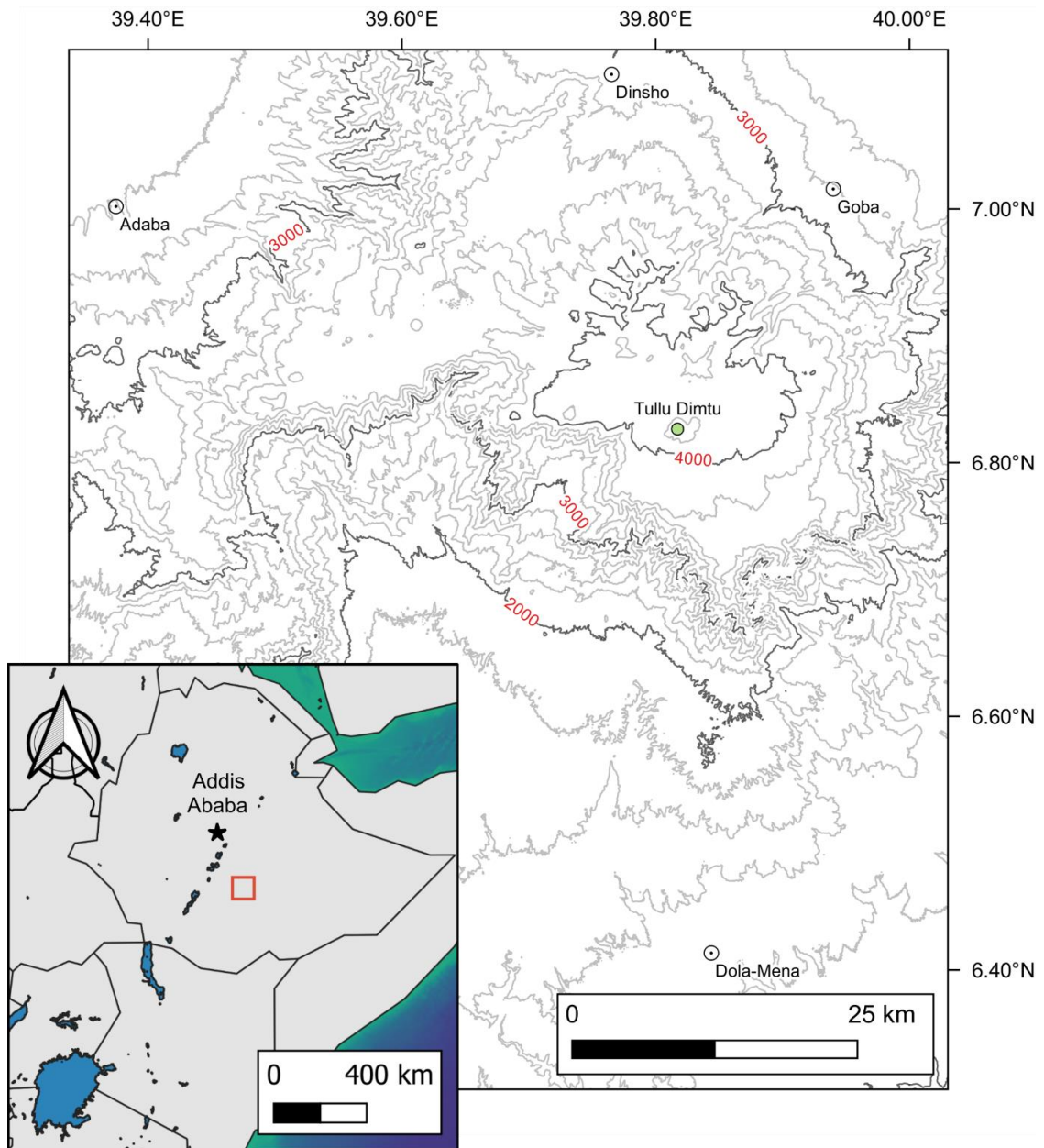


Figure 3.8: Bale Mountains, and surrounding major towns, location within Ethiopia. Faded contour lines, between bold 1000 m lines, denote changes of 200 m.

The effects of altitude are evident on the distribution of rainfall across the Bale Mountains, with rainfall generally higher on the northern slopes (~1000 mm) than the southern slopes (~800 mm; Figure 3.10). The effects of altitude also influence the diurnal variation in air temperature, with frost common at 4000-4200 m.

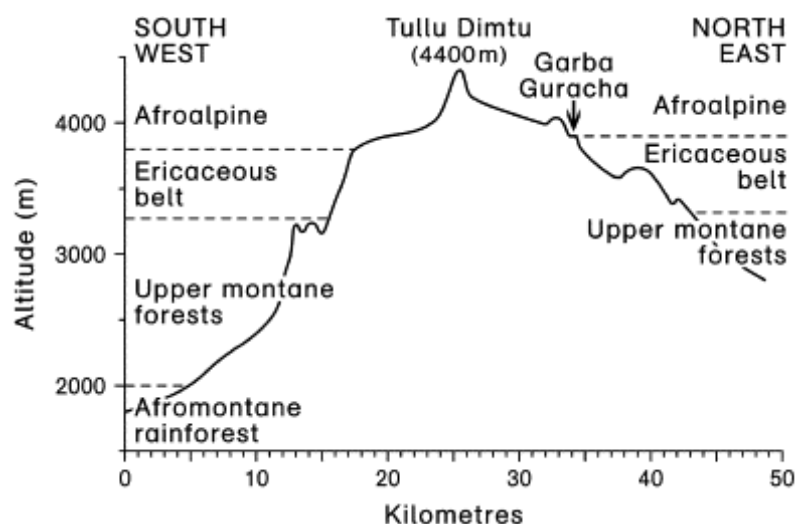


Figure 3.9: Schematic SW–NE profile of the Bale Mountains to show altitudinal zonation of regional vegetation by Umer *et al.* (2007).

During the LGM, the most recent estimates suggest that around 180 km² of ice covered the mountains with a central 30 km² ice cap centered around Tullu Dimtu and multiple glaciated valleys in the north (Osmaston *et al.*, 2005). The area contains numerous peat bogs and glacial lakes, some of which have been the focus of palaeoenvironmental studies (e.g. Umer & Bonnefille, 1998; Umer *et al.*, 2007; Tiercelin *et al.*, 2008).

3.4.1 | Study site 2: Garba Guracha

Garba Guracha (6°52' N, 39°49' E) is a small (500 m length, 300 m width, 6 m deep) NNE-orientated rounded spearhead-shape lake lying in a cirque at the end of a side valley of the upper Togona valley at an altitude of ~3950 m (Figure 3.11). Preliminary depth measurements from 7 transects (February 2017) indicate that the lake floor gently slopes down from the margins, with the exception of the western margin bounded by a vertical slope, with waters of >5 m deep in the very centre. In comparison to the rift system lakes, few limnological studies have been conducted at Garba Guracha (Werdecker, 1962 and Löffler, 1978 are rare examples).

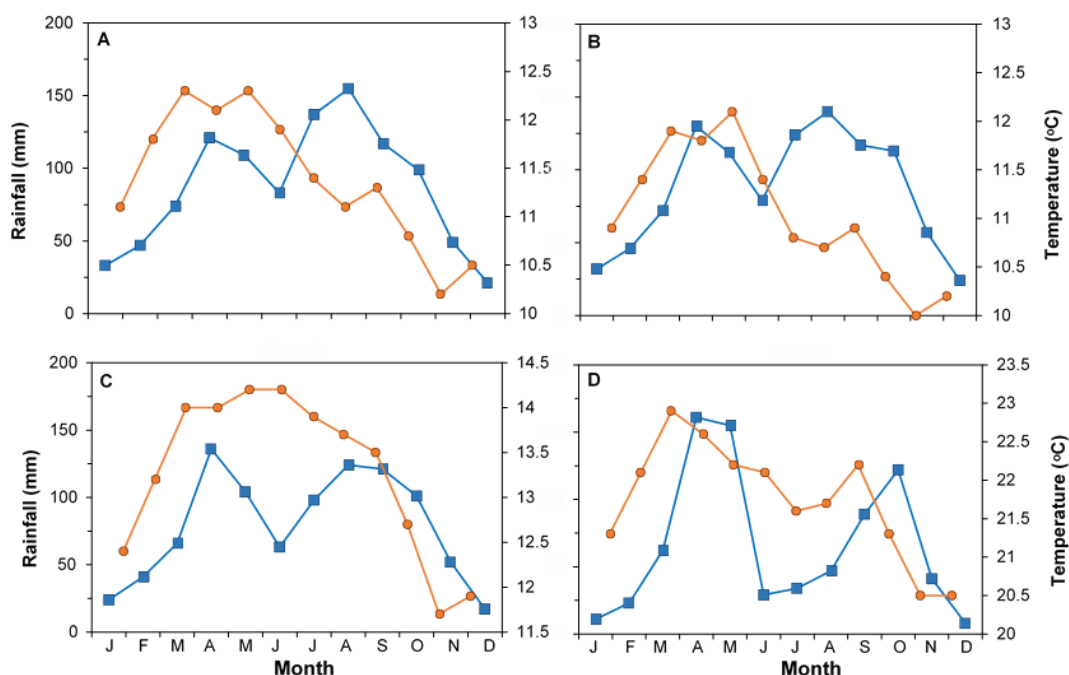


Figure 3.10: Rainfall (blue) and temperature (orange) of areas in, and around, the Bale Mountains. A – Dinsho, B – Rira (6°46.3'N, 39°43.5'E), C – Goba and D – Dola-Mena (for settlement locations see Figure 3.8). Created using weather data from 1982 to 2012 and the Climate-Model available at Climate-data.org (2017). Note the different secondary Y-axis values for each graph.

Palaeoenvironmental studies by Umer *et al.* (2007) and Tiercelin *et al.* (2008), and a single sample point for the East African diatom database presented in Gasse *et al.* (1983), providing the only further insights. This glacial cirque is bounded to the south by up to 140 m high cliffs and steep slopes, formed by basaltic lavas, overlying a thick trachytic tuff unit which forms a large part of the cirque base, and outcrops on the southern and southeastern slopes of the cirque (Tiercelin *et al.*, 2008). As a result of these steep cliffs, the lake watershed is small (0.15 km²) with a lake/watershed ratio of 2. During periods of maximum lake level, a small outlet stream flows out over a partially boulder-covered rock bar on the northern-most edge of the lake which feeds the Togona River at an estimated few litres per second (Tiercelin *et al.*, 2008). However, during the 2017 dry season (fieldwork) this outlet was dry (Figure 3.12).

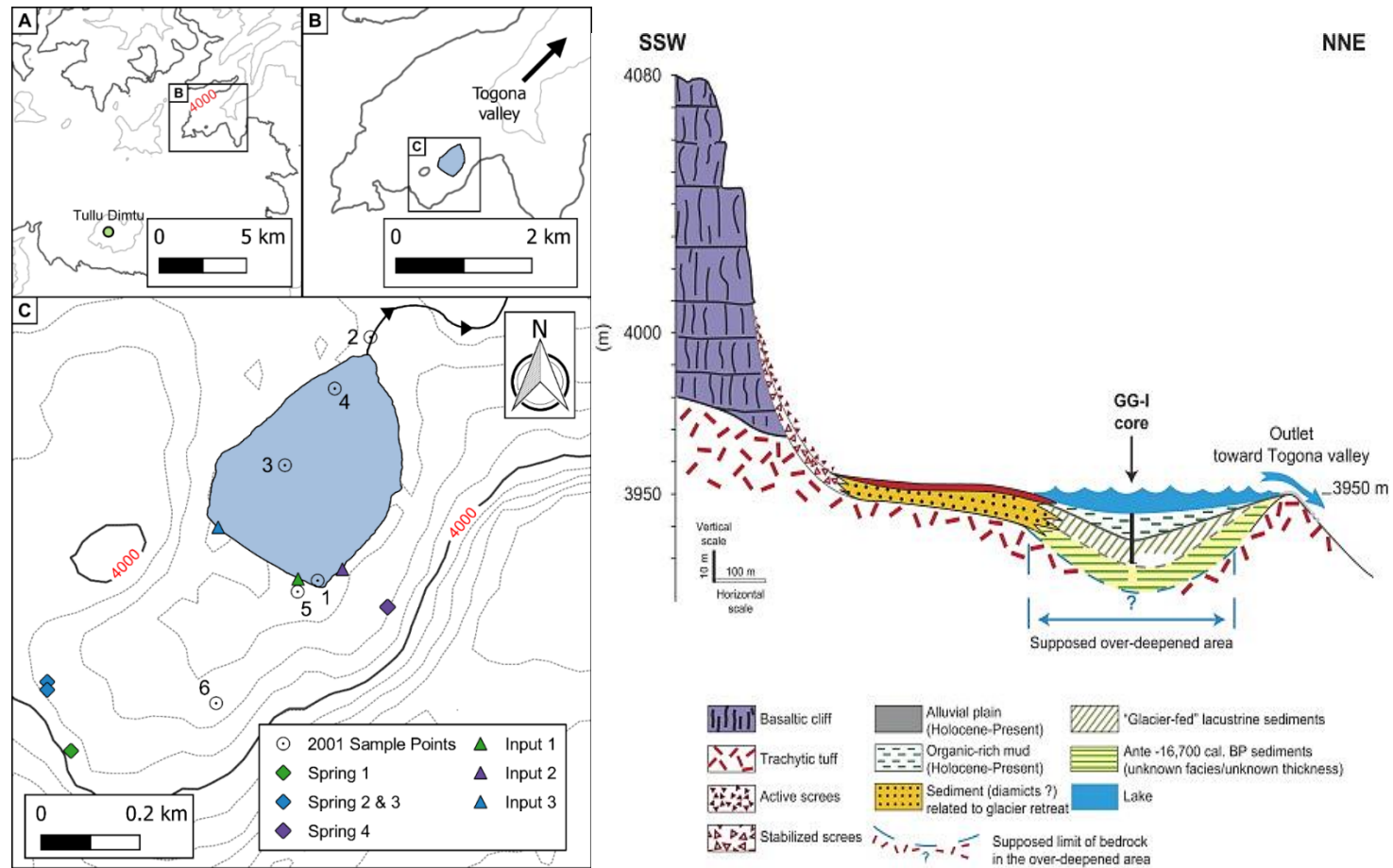


Figure 3.11: Garba Guracha location within the Bale mountains (left) and cross-sectional view of basin characteristics (right; Tiercelin *et al.*, 2008). Sample locations in Tiercelin *et al.* (2008) are shown. The locations of springs and inputs/outlet around the edges of the lake in February 2017, and the outlet stream to the Togona valley on the northern tip of the lake (arrows) are also shown. Thick label contour lines indicate changes of elevation of 1000 m, with faded lines denoting a 500 m change (in A and B). Dotted contours (in C) indicate 20 m changes in elevation.

From an ecological perspective, the lake is situated on the boundary between the Ericaceous and Afroalpine vegetation belts (Figure 3.8), with the surrounding land dominated by *Alchemilla haumannii* and *Helichrysum splendidum* scrub. The adjacent slopes are frequently burned to improve livestock pasturage, with these livestock also grazing in the marsh area adjacent to the lake. Additionally, *Carex monostachya* and *Luzula johnstonii* communities form a lake-shore marsh community (Umer *et al.*, 2007).

Multiple small streams and springs from the southern slopes around the lake merge to feed the lake and form a small meandering fluvial system through a 0.5 km long marshy alluvial plain (Figure 3.11; 3.12). Coarse clastic material is adjacent to the steep western shoreline, likely related to the nearby scree slopes, with some of this material mixed in with well-sorted clean sands that characterise the lake shoreline. Wave action, generated by the strong northerly winds blowing into the cirque, is observable in the lake and is responsible for the sandy, rectilinear southern shoreline (Figure 3.11). Offshore lake sediments are composed of dark, organic-rich muds (total organic carbon (TOC) up to 11%; Tiercelin *et al.*, 2008).

Gasse *et al.* (1983) document that Garba Guracha's water balance is predominantly determined by precipitation and lake inflow and outflow, however Umer *et al.* (2007) presume groundwater is an input to the lake, but this is yet to be determined. Lake water at the time of sampling by Tiercelin *et al.* (2008) was fresh, circum neutral (6.81-6.95 pH) and bicarbonate dominated (Table 3.4), slightly fresher and more acidic conditions to that in the 1970s presented in Gasse *et al.* (1983; 7.4 pH).

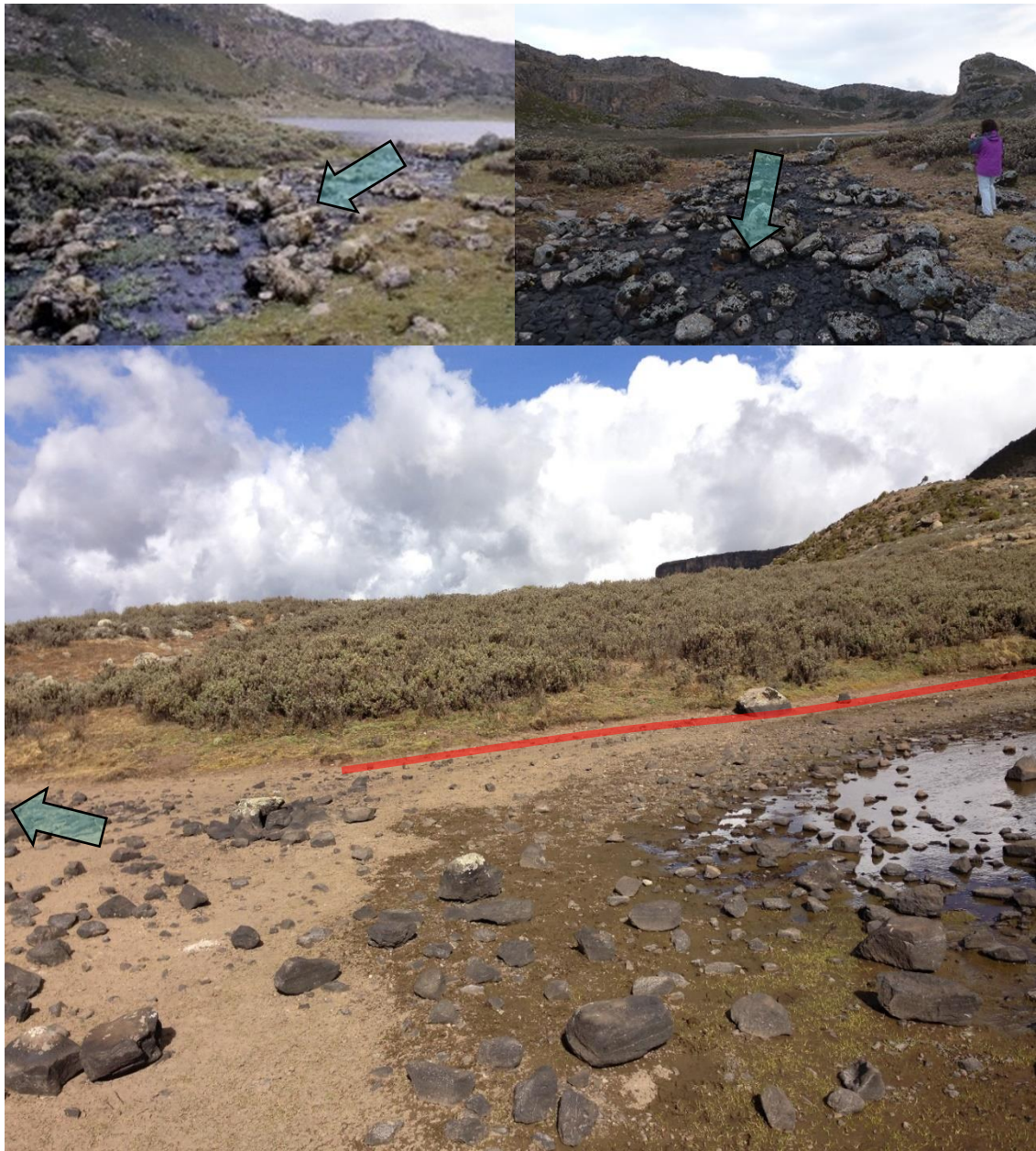


Figure 3.12: Outlet point from Garba Guracha into the Togona valley (arrow) overflowing in 2001 (Tiercelin *et al.*, 2008; left) and desiccated in 2017 (right), with the lake level considerably lower than during overflow periods (red line indicates overflow shoreline level) and far from the outlet point (bottom). Sand is evident on the very outer lake edge, with organic-rich muds towards the centre.

Tiercelin *et al.* (2008) found stable oxygen isotope values from the inflow stream (5 in Figure 3.11) of -2.2‰ (vs. SMOW) are similar to the modern water samples of the rift floor lakes, and the mean annual rainfall isotope contents recorded from the meteorological stations in Awassa and Addis Ababa (-2‰ vs. SMOW). The

ecology of Garba Guracha's waters, however, remains relatively unclear. Umer *et al.* (2007) and Tiercelin *et al.* (2008) identify that much of their core contained some diatoms (abundance corresponding largely to the organic content of each lithostratigraphic unit), but no further identification was undertaken. Furthermore, one mud sample from the lake was included in the East African diatom dataset presented in Gasse *et al.* (1983), Gasse (1986) and Gasse *et al.* (1995). However, the usefulness of this is limited as the only information reported is that the sampled diatoms belong to the East African diatom assemblage II B (typically associated with low conductivity, medium pH and low-medium alkaline waters).

3.4.1.1 | Environmental change at Garba Guracha since the Late Pleistocene

Magnetic susceptibility, organic matter content and rates of sedimentation in a core retrieved from Garba Guracha allow Tiercelin *et al.* (2008) to interpret the glacial development of the lake environment (Figure 3.13) since 16,700 BP. They interpret high rates of large (>100 µm), inorganic sediment input between 16,700 and 13,400 BP as the result of discharges of meltwater and glaciogenic sediment progressively filling the accommodation space (now Garba Guracha) created as the glacier retreated. During this period, pollen in the same core (Figure 3.13) shows that local vegetation was predominantly herbaceous, consisting of predominantly Poaceae, Amaranthaceae / Chenopodiaceae and Cyperaceae, with similar patterns of *Artemisia* pollen influx despite being present at a lower percentage in the core.

Table 3.4: Lake Garba Guracha hydrochemistry in May 2001 from Tiercelin *et al.* (2008). Sampling locations in relation to Lake Garba Guracha are shown in Figure 3.8. Trace concentrations are represented by a '+’.

	Conductivity ($\mu\text{S/cm}$)	pH	HCO_3^- (mg/L)	Cl^- (mg/L)	SO_4^{2-} (mg/L)	F^- (mg/L)	NO_3^- (mg/L)	K^+ (mg/L)	Na^+ (mg/L)	Ca^{2+} (mg/L)	Mg^{2+} (mg/L)
1 (river mouth)	57.8	6.77	29	1.63	1.64	+	+	1.21	7.08	3.04	0.69
2 (output)	56.7	6.95	27	0.49	0.45	+	+	1.19	6.79	2.83	0.63
3 (core site)	58.0	6.91	28	1.68	1.63	+	+	1.21	6.92	3.09	0.67
4 (south shore)	56.7	6.90	28	1.67	1.55	+	+	1.15	7.07	2.90	0.62
5 (input)	53.0	6.81	28	1.10	0.95	0.06	0.09	1.05	8.31	1.95	0.35
6 (swamp)	62.2	6.84	27	1.84	2.48	0.10	3.41	0.87	8.06	2.88	0.59

The presence of this vegetation indicates the local environment was steppe-like, grass-dominated vegetation with dwarf shrubs (Chenopodiaceae, Artemisia) in a dry climate. However, pollen influx through this zone is low, indicative of a sparse vegetation cover (Umer *et al.*, 2007).

A sharp decrease in the abundance of Amaranthaceae / Chenopodiaceae pollen is observed at 13,400 to ~12,500 BP, with an increase in Cyperaceae. Additionally, pollen influx, TOC and the sedimentation rate rise, with a corresponding decrease in magnetic susceptibility, inferred to represent the increase of vegetation cover and acceleration of ice melting, and related meltwater/sediment discharge, in response to wetter climatic conditions. During this period, Ericaceae, Podocarpus and Juniperus pollen also increases slightly, which may indicate a rise in the altitude of the forest limit on the lower slopes of the surrounding Bale Mountains. This interval is short-lived however with a return to drier conditions from 12,550 BP to the start of the Holocene, potentially corresponding to the Younger Dryas (12,700-11,800 BP), represented by reduced Cyperaceae and equivalent large increases in the dry, steppe-like vegetation, with Poaceae dominating this period (~45-60% abundance). At this time, sedimentation becomes fine-grained without a major change in lithological/geochemical characteristics. This suggests a decrease in the influx of melt-water, which can be explained by the colder, arid conditions at the time slowing glacier retreat or the persistence of a lobe of dead ice restricted to the sheltered, southern end of the cirque, with outwash streams transporting smaller quantities of water and finer-grained sediment to Garba Guracha.

From the start of the Holocene (11,800 BP) the Garba Guracha core records the establishment of the contemporary, post-glacial lake environment with an abrupt reduction and disappearance of clastic input, which is replaced by organic-rich

sediments. Local vegetation was dominated by Poaceae (~50-65%) and Cyperaceae (10-20%), with the highest abundance of Ericaceae (10-20%). Taxa such as Podocarpus and Juniperus remain low throughout the zone, indicating that dry Afromontane forests at lower altitudes were not extensive during the early to mid-Holocene, being restricted to lower altitudes. Increased TOC and HI values, as a result of a greater abundance of *Botryococcus braunii* and high OM preservation under a permanent water body suggests wetter, more productive conditions. Furthermore, Tiercelin *et al.* (2008) suggest that, based on higher abundances of *Botryococcus braunii*, the lake was oligohaline during this period. After 4,500 BP drier conditions, characteristic of the late Holocene (see chapter 2), are represented by decreases in lake and vegetation organic matter production (5-10% decrease in TOC).

The pollen records also suggests a reduction in rainfall with an expansion of dry Afromontane forest from 4,500 BP with large, correlated increases in Juniperus (+10-35%), Podocarpus (+15-25%) and Olea (+2-3%), with Juniperus dominating after 2,500 BP. Podocarpus declined from 2,000 BP (-10%), while Juniperus increases to maximum abundance in the core (~40%) following a brief interval of decreased abundance. This may reflect continued climate drying, or the preferential use and selective clearance of Podocarpus by an increasing human population. Anthropogenic disturbance of the natural, local vegetation is also inferred from increases in Plantago and Dodonaea over the last 1,500-2,000 years, with anthropogenic burning potentially represented in the last ~500 years by increases in *Hagenia abyssinica*.

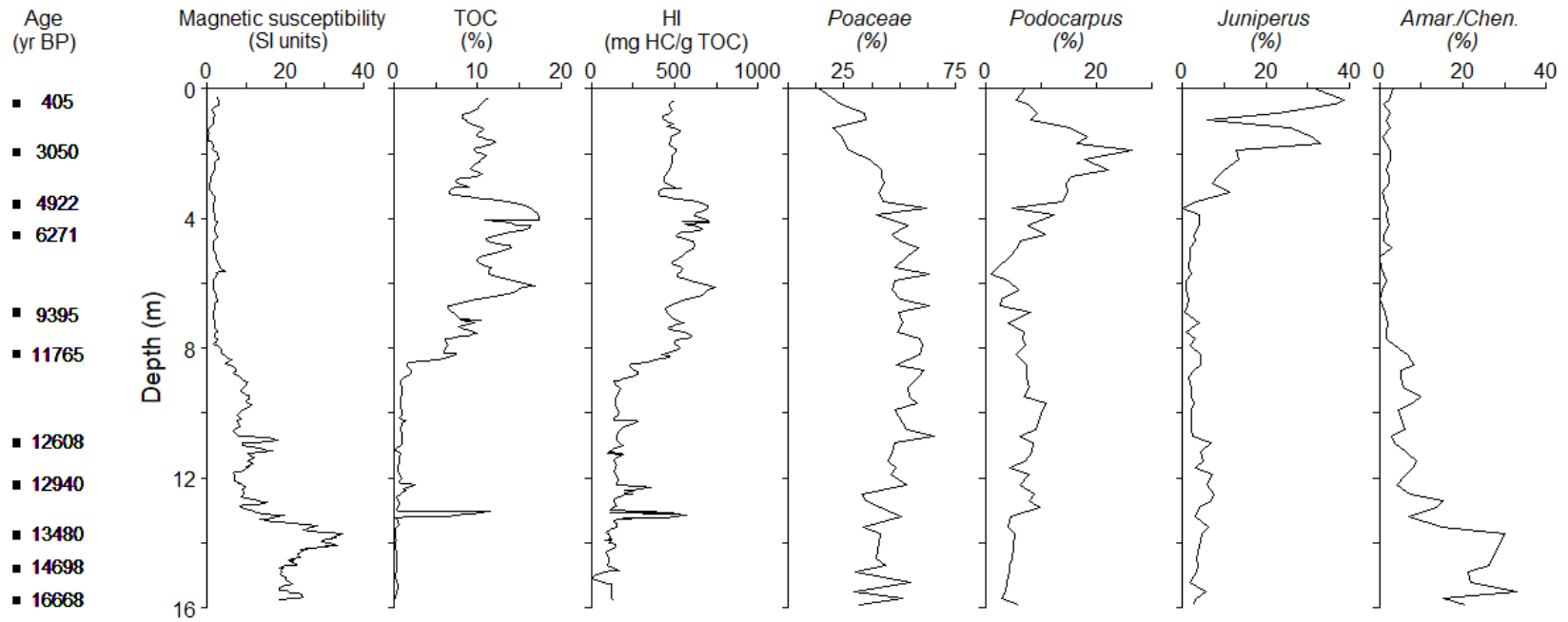


Figure 3.13: Environmental proxies from Garba Guracha in Umer *et al.* (2007) and Tiercelin *et al.* (2008).

Chapter 4 :

Study methods

This chapter outlines the field sampling strategies during the 2017 field campaign at Garba Guracha (as part of the DFG Mountain Exile Hypothesis (MEH) project) and in 2011 at Lake Babogaya. Cores from these locations represent a higher and lower altitude site. The aim of this study was to compare these records to further understand the dynamics of past climatic change between altitudinal scales as well as through time in eastern Africa. It was anticipated that the basal dates of both sites would be broadly similar to allow comparisons to be made for the last ~16,000 years. However, following the chronological controls outlined in this chapter it was revealed that this is not the case thus comparisons are made later in this thesis where possible between the two sites as well as the wider literature as a whole.

The procedures for core analysis, including sampling/analysis of proxies and chronological controls, are presented together with any differences outlined where appropriate. An introduction to the methods applied is also provided where appropriate, with focus placed on diatoms as they are the main proxy of this study. A detailed description of the process to correlate the overlapping sections extracted from Lake Babogaya is provided following this chapter. Plotting of data was performed in *R* (v. 3.5.1; R Core Team, 2018) with the *rioja* (v. 0.9-14.1; Juggins, 2017), *ggpaleo* (Telford, 2018), *ggplot2* (Wickham, 2016) and *cowplot* (v. 0.9.3; Wilke, 2018) packages. *R* was also utilised for the statistical analyses of data, with the packages used in this study stated where appropriate in this chapter.

4.1 | Field sampling

Samples were collected from the field at the end of the dry season (mid-February 2017). Two water samples from each sample location around the Garba Guracha area (Figure 4.1) were collected in Nalgene bottles to determine the anion, cation and trace element concentrations. Field measurements of water conductivity and pH were also made using a Hanna HI98129 meter, with care taken to calibrate before each sample was taken with known standards. However, due to meter malfunctions (infinite increasing of measurements) these data were discarded, and were acquired in the lab upon return (see section 4.2.2).

In conjunction with these water samples, diatom samples were taken from sediment from sites around the lake basin. A total of 9 diatom samples were taken from the shoreline (mud, sand and rock), spring 4 (mix of mud/vegetation), the lake outlet (mud), the swamp (mix of mud/vegetation) and inputs 1, 2 and 3 (mud) in Figure 4.1. To ensure diatom remains were preserved, a few drops of alcohol were added to each sample. All water and diatom samples were stored in cool environments wherever possible while in the field and returning from the field, and stored in a cold store maintained at 4°C upon returning to Aberystwyth.

4.1.1 | Core retrieval

The Lake Babogaya core was extracted in October 2011 by a team led by Prof. Frank Schäbitz, and the Garba Guracha core taken on the February 2017 field campaign. Core sampling reached depths of ~16 m (below sediment surface) in both lakes, with a surface core taken at Garba Guracha and several overlapping sections extracted from Lake Babogaya.

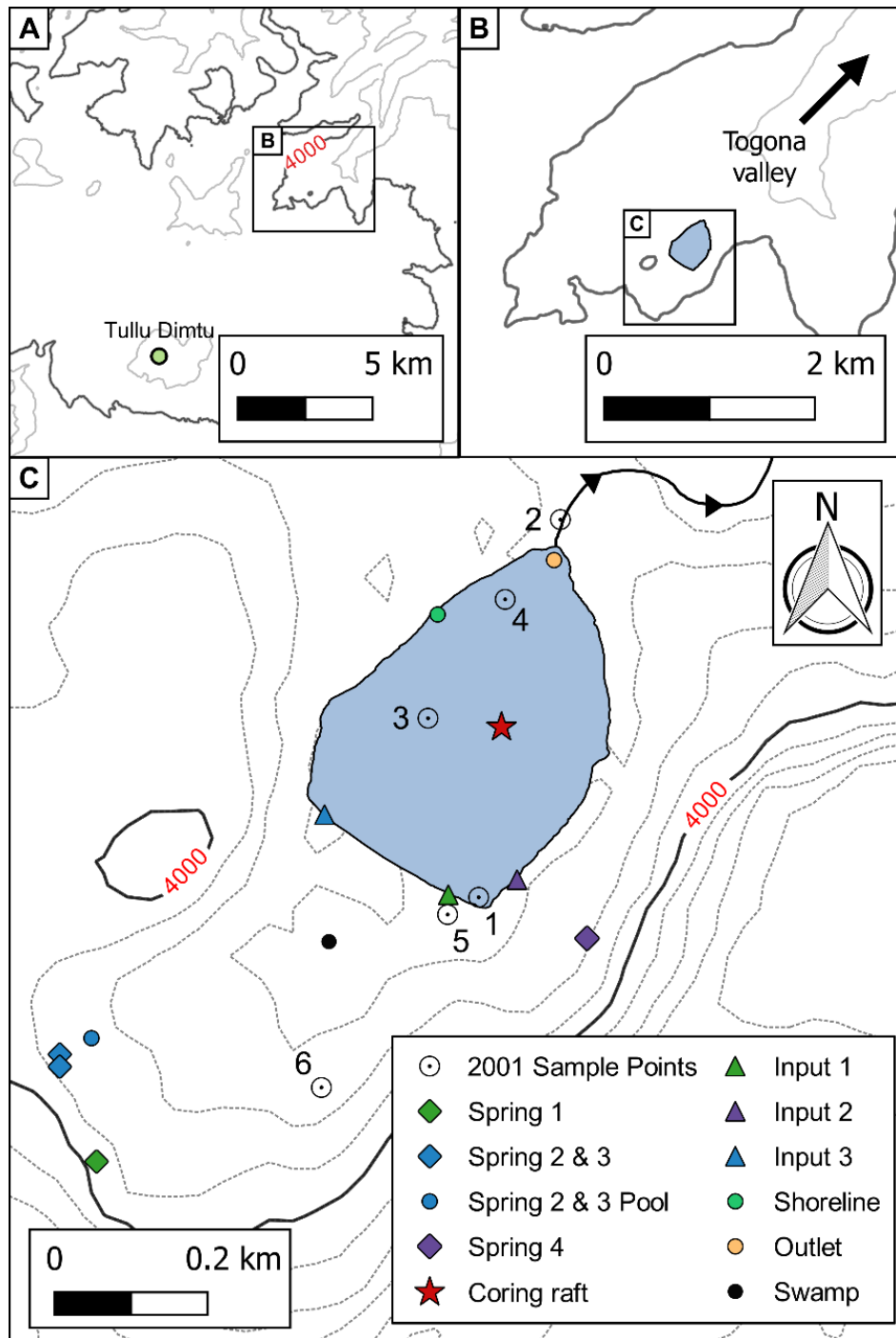


Figure 4.1: Sample locations around Garba Guracha in the 2001 field campaign (in Tiercelin *et al.*, 2008), with sample and spring locations in 2017 also shown (this study). Due to the small size of springs 2 and 3, possibly due to the dry conditions, a small pool where both streams merged downstream was sampled. The location of the coring raft (star) indicates the point at which surface water and sediment samples were taken.

A single long core, comprised of multiple overlapping 1 m drives, was collected from Lake Babogaya (BA-LC-2011) using a UWITEC piston corer between the

28th and 31st of October 2011. Each section was extracted in a 2 m liner, and cut into an upper and lower half (labelled A and B, respectively) following coring (Figure 4.2). However, issues with depth control and estimation were encountered during fieldwork, especially in the upper half of the core. Despite the best efforts to estimate the depth of each section in the field, the position of sections within the overall lake stratigraphy was uncertain (Schäbitz pers comm.; see Chapter 5 for discussion of core correlation in this study).

Numerous short cores were also collected from within Lake Babogaya using the UWITEC corer (Figure 4.2), ranging from 52 to 114 cm in length. However, these cores were not sub-sampled in the field, and due to their high water content and unconsolidated nature, the sediment of these cores was highly disturbed and rendered unreliable following coring/during transit. Consequently, these cores were not considered for analysis in this study.

At Garba Guracha, coring was undertaken on a specifically designed raft, anchored from each corner by heavy weights, and supported by two securely fastened dinghies. The sediment-water interface was sampled to a depth of ~50 cm using a piston equipped plastic tube (Wright *et al.*, 1984) with a 4.5 cm diameter and 1 m long barrel. This was sampled in the field by pushing the core from the bottom and sampling in 1 cm intervals. Additionally, from this sediment-water interface core, a water sample was taken to represent deeper lake water (estimated 5 m depth). Two overlapping cores of 15 and 16 m length were taken in successive 1 m drives of this Livingstone piston corer. These 1 m sections were transferred to labelled plastic tubing and wrapped in cling-film on-site.

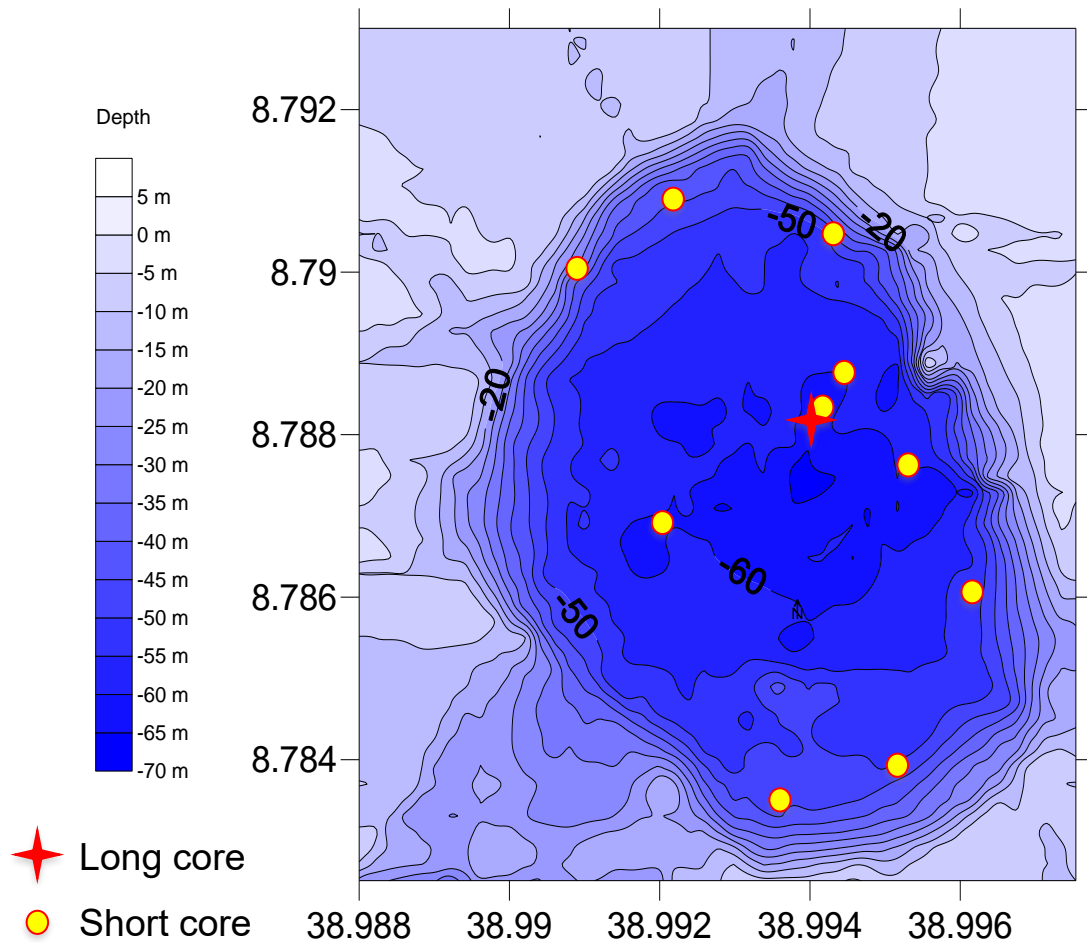


Figure 4.2: Bathymetry of Lake Babogaya, with core sample locations during the 2011 coring campaign (Schäbitz, unpublished data.).

4.2 | Laboratory methods

4.2.1 | Core lithology and chronology

(i) Sediment preparation and storage

After being transported to Aberystwyth University, Wales (Lake Babogaya cores) and the Instituto Pirenaico de Ecología (IPE), Zaragoza, Spain (Garba Guracha cores), the cores were kept chilled in a cold store maintained at 4°C. The Lake Babogaya cores were opened from the thick plastic tubing using a mechanical core splitter and a circular saw. After being opened, these sediment cores were split in half lengthways, using wire and metal wedge plates. As the Garba

Guracha cores were kept in two separate halves of plastic tubing, only metal wedge plates were used to split these cores in half lengthways. All care was taken to avoid contamination during core opening and splitting. After being split, one half of each section was kept as an archive half and the other to be sampled as the replicate working half. These cores were returned to the cold store wrapped in cling-film and were only taken out of this chilled environment to be sampled.

In the summer of 2016, prior to the start of this PhD, the working half of the Babogaya core was sub-sampled by S. Grunhut at Aberystwyth University using a brass sub-sampler to take a 1 cm³ sample of sediment at ~4 cm intervals. These samples, and others taken later by the author, were used in this study. Similarly, sub-samples of sediment (1 cm³) to use in this study were extracted at ~10 cm intervals in the Garba Guracha core, using a cut syringe, by the author at the IPE. These sub-samples for further analyses (diatoms/bulk organic matter analysis; see below) were stored in sealed plastic tubes kept in sealed clip bags in the cold store with the original sediment cores.

(ii) Sediment description

The core sections were initially divided into sub-units depending on visual changes in sediment type. The composition of these units in the Lake Babogaya composite core were then recorded using smear slides, prepared according to Myrbo (2007), and a James Swift polarizing microscope. To accurately characterise and identify the sedimentary units the Limnological Research Centre (LRC) classification framework (Schnurrenberger *et al.*, 2003) was used. The sedimentary sequence was then divided into lithostratigraphic units based on these smear slides and visual changes in sediment type. These preliminary

analyses also provided a first insight into the structure of the core (e.g. volcanic glasses, microfossil occurrences and laminae composition). The composition of the Garba Guracha core was described in a similar way to the Babogaya core, conducted by G. Gil-Romera and A. Moreno at the IPE, with further investigation by D. Grady and G. Gil-Romera at Aberystwyth University. Core lithologies were plotted in *SedLog* (v.3.1; Zervas *et al.*, 2009).

(iib) Thin section preparation and analysis

Thin sections were prepared from laminated sections, and diatoms counted from individual lamina (see below), in the Babogaya core to further understand their formation through time. Samples were taken in a kubiena tin, transferred to fine mesh 'boats' and freeze dried following the methods outlined in LacCore (2015). It was intended to acquire backscatter electron imagery (BSEI) for this study as can be useful for determining differences in discrete layers of predominantly organic/minerogenic components (Kemp *et al.*, 1999). However, following resin impregnation, blocks could not be reduced to an adequately thin sample to use with the SEM at Aberystwyth University without destroying the sample, therefore this avenue of research was abandoned for this PhD study.

(iii) Babogaya ¹⁴C chronology

As discussed in chapter 3, terrestrial macrofossils of plants are considered the most reliable material for radiocarbon dating compared to bulk samples (Zimmerman & Myrbo, 2015). This is especially true for constructing a reliable chronology at Lake Babogaya; crater lakes may experience contamination from groundwater and geothermal sources introducing 'old' ¹⁴C at different stages. The utility of charcoal in radiocarbon dating sedimentary sequences, especially in

African crater lakes, is evident (e.g. Telford, 1998; Blauuw *et al.*, 2011). However, it is important to note that wood charcoal may provide less accurate dates due to the longevity of trees (Oswald *et al.*, 2005; Grimm, 2011), in contrast to charred cuticles from grasses which have a comparatively shorter lifespan. Deposition of 'old' carbon stored in catchment soils can also lead to inaccurate dates. To minimise the likelihood of eroded material being dated, samples were selected where possible from sections of core with comparatively lower rates of terrigenous input (as identified from XRF-derived Ti data) where possible.

Previous smear slide analyses identified potential macrofossil layers in one section of the core and that micro- and macro-charcoal was present throughout the core in varying quantities. Prior to sending bulk samples for analysis, sediments were sampled for dating using terrestrial macrofossils (e.g. twigs, leaves of deciduous trees and insect remains) or charcoal. Multiple 1 cm thick sediment samples were taken from various depths from the working core halves, with care taken to avoid contamination by potentially younger material from the outer edges of the core, and transferred to individual, labelled sample bags. These sub-samples were then individually sieved through a 150 µm mesh with distilled water. Sieving residues were transferred to petri-dishes and observed under a Meiji Techno RZ dissecting microscope (x7.5-75 magnification) to accurately identify potential plant macrofossils and charcoal fragments to be used for obtaining radiocarbon dates. Charcoal fragments were identified based on optical properties (Enache & Cumming, 2006): black colour, opacity, light reflective surface, visible cell lumina and brittle texture. Any relevant material was handpicked from these residues and transferred to sealed glass vials filled with distilled water.

In total, 9 accelerator mass spectrometry (AMS) ^{14}C dates were obtained from the Lake Babogaya core. These were analysed at the Oxford Radiocarbon Accelerator Unit (ORAU). Chemical pre-treatment, target preparation and AMS measurements follow Bronk Ramsey *et al.* (2004) and Brock *et al.* (2010). All ^{14}C dates were calibrated using CALIB 7.1 (Stuiver & Reimer, 1993), using the IntCal13 calibration curve (Reimer *et al.*, 2013). For each date obtained the conventional radiocarbon age, the calibrated age range at the 2- σ level, and the calibrated age (central point estimate; rounded to the nearest 10) are presented in this thesis. When estimates of the sediment accumulation rate are made, the central point estimate of the calibrated age is used and the reader is referred to the table of dates (for the respective cores in those sections) for the full range of associated errors. Bayesian modelling of radiocarbon dates was performed with the *rbacon* (Blauuw & Christen, 2018) R package.

(iv) Garba Guracha chronological controls

A chronology for the surface core of Garba Guracha was produced by analysing these sediments for ^{210}Pb , ^{226}Ra , ^{137}Cs and ^{241}Am . The 1 cm samples extracted in the field were dried and sent for analysis by direct gamma assay in the Environmental Radiometric Facility at University College London, using an ORTEC HPGe GWL series well-type coaxial low background intrinsic germanium detector. The long core, GGU-17-1AB was dated by AMS dating bulk sediments and charcoal fragments at Bern which were used as a control for replicate ^{14}C dating of bulk n-alkane samples at Halle. Dating techniques were applied by L. Bittner, as part of the MEH project.

4.2.2 | Water chemistry

Water samples from Garba Guracha were chilled in the cold store at 4°C upon arrival at Aberystwyth University. Before analysis, these samples were filtered by forcing them through 0.45 µm thick filter paper with a syringe, as particles larger than this may damage the analytical instruments. Samples were transferred to standard 5 ml polypropylene vials and analysed for chloride (Cl⁻), sulphate (SO₄²⁻), fluoride (F⁻), nitrate (NO₃⁻) and phosphate (PO₄³⁻) using a Dionex DX 120 ion chromatograph. Bicarbonate (HCO₃⁻) content was determined through simple acid-based titrimetric analysis, using sodium tetraborate (Na₂B₄O₇) to determine the normality of the hydrochloric acid (HCl) to be used in the titrimetry.

Water samples for cation analysis were acidified with 70% HNO₃, mixed and left for 24 hours, to re-solubilise carbonates and bicarbonates that may have formed during storage. Following this process, samples were transferred to 10 ml plastic test tubes and analysed for sodium (Na⁺), potassium (K⁺), calcium (Ca⁺²) and magnesium (Mg⁺²) using a Perkin Elmer AAnalyst 400 atomic absorption spectrometer. The analytical precision of the equipment used to determine both anion and cation concentration was 3%.

4.2.3 | X-ray fluorescence (XRF) scanning

Unlike more traditional methods (e.g. wet chemical digestion), XRF scanning is a non-destructive method of providing high-resolution, geochemical data. Due to the high-resolution of XRF scanning, and the ability to perform subsequent, additional analyses as the sediment remains intact, its use in understanding past changes archived in sediment cores has significantly increased since its development (Rothwell & Croudace, 2015).

XRF analysis for both cores was performed at Aberystwyth University using the Itrax™ core scanner. Scanning for the Babogaya core was performed by the author, with the Garba Guracha cores scanned by G. Gil-Romera and H. Lamb. Standard scanning procedure for an Itrax scanner was undertaken (Itrax scanner specifications and procedures outlined in Croudace *et al.* (2006)). Scan settings were calibrated to 30 kV, 45 mA, with a stepsize of 200 µm for each scan of the Babogaya core and 30 kV, 45 mA and a stepsize of 500 µm for the Garba Guracha cores. XRF and X-ray exposure times were set to 15 seconds and 200 milliseconds, respectively, for both cores. Fine tuning of the detector parameters was performed before each scan to match the actual and fitted spectra and minimise the mean square error (MSE) value. As a result, MSE values were maintained below 2 for both the Babogaya (mean = 1.62 ± 0.16 MSE) and Garba Guracha (mean = 1.56 ± 0.27 MSE) master cores. Following the calibration of scanner settings, a layer of 1.5 µm thick film was used to cover the core to minimise moisture loss during scanning.

Significant changes in water and organic content may lead to inaccurate detection of some elements, resulting in down core changes in raw element profiles unrelated to sediment geochemistry (Tjallingii *et al.*, 2007; Löwemark *et al.*, 2011). Consequently, to minimise the effects of sediment water and organic content, normalisation of raw element data by the total scatter (both the incoherent and coherent data, equivalent to Compton and Rayleigh scattering, respectively) is commonly used (e.g. Kylander *et al.*, 2011; Chawchai *et al.*, 2013). The raw XRF-derived element data for both cores in this study was similarly normalised by the total scatter by D. Grady. Correlation matrices were

produced using the *PerformanceAnalytics* (v. 1.5.2; Peterson & Carl, 2018) R package.

4.2.4 | Isotopic analysis of bulk organic material

Sub-samples from the working halves of the Babogaya core were analysed for total organic carbon (TOC), including $\delta^{13}\text{C}_{\text{org}}$, and total nitrogen (TN). The C:N ratio provides information related to the origin of organic matter within lake sediments, related to the protein-rich, lignin poor nature of algal material (C:N ratio of 3-9) and relatively protein poor, lignin rich terrestrial biomass (C:N ratio of >20). Similarly, the $\delta^{13}\text{C}$ is broadly used as an indicator for carbon sources in plants and can be used to differentiate between C_3 ($\delta^{13}\text{C} \approx -22$ to -35‰) and C_4 vegetation ($\delta^{13}\text{C} \approx -6$ to -15‰) (Brodie *et al.*, 2011).

Sediment was placed in individual 250 ml beakers with 100 ml of 5% HCl, to remove any inorganic carbon present. The sample was left to react for 24 hours before the supernatant was decanted and the remaining sample washed with distilled water. This process was repeated 4 times at 24 hour intervals. Following this procedure, samples were dried at 40°C overnight, before being ground to a fine powder in an agate pestle and mortar to homogenise the sample. These powders were then stored in sealed glass vials prior to further use. Samples were analysed using an Elementar Geovision with a vario-PYRO-cube EA (elemental analyser) and vision MS (mass spectrometer).

4.3 | Diatoms

Classified as algae (Division Bacillariophyta), diatoms are unicellular, eukaryotic organisms characterised by their siliceous cell walls and yellow-brown pigmentation. Generally, according to Julius & Theriot (2010), diatoms are

classified as one of two biological orders: the Centrales (commonly referred to as centrics) and the Pennales (also known as the pennates, both raphid and araphid; Figure 4.3). Diatoms vary considerably in cell size (typically 20-200 μm), frustule shape, striae and punctae density/pattern and the form of raphe ends (Mann & Droop, 1996). These multiple distinctive morphological features are key to accurately describing and identifying diatoms to variety, species or sub-species level in palaeoenvironmental research, without the need to extract DNA.

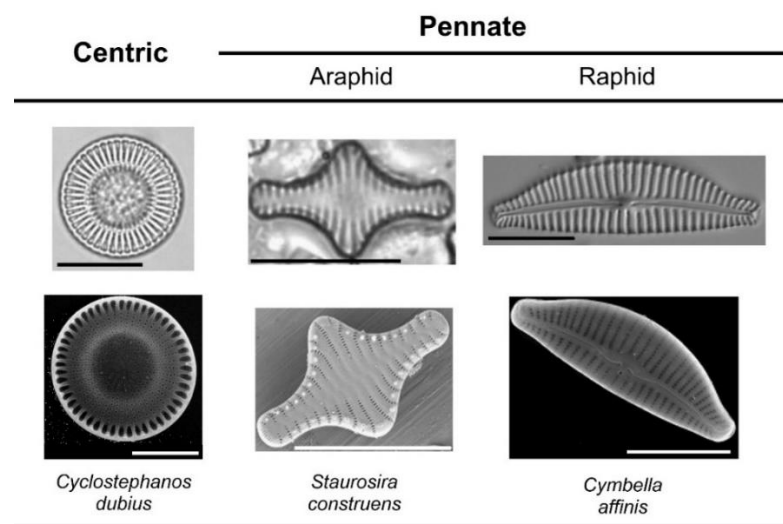


Figure 4.3: Diatom morphology of three example species from the centrics (left) and both araphid (middle) and raphid pennates (right). Diatom images include those taken under a light microscope (top) and a scanning electron microscope (bottom). Scale bars at 10 μm . Created using images from the respective pages on the Diatoms of the United States database (<https://westerndiatoms.colorado.edu/>).

The abundance of diatom cells, even in a small lake body, is considerable; a species occurring at a density of 1 cell m^{-2} of lake surface would be essentially undetectable in most circumstances, yet there would still be 10^4 per hectare (Mann & Droop, 1996). Diatoms are largely restricted to the photic zone, but can occupy a diversity of habitats found within that region where there is sufficient light.

Planktonic diatoms spend their entire life cycle suspended in the water column, whilst benthic diatoms are found attached to some form of substrate around the margins of lakes. Epilithic, epiphytic, epipellic and epipsammic refers to the habitat type of diatoms found on stones, aquatic vegetation, mud and sand, respectively. Diatoms referred to as facultatively planktonic includes taxa which spend part of their life cycle both floating free in the water column or attached to substrates. Similarly, tychoplanktonic diatoms are those that have been detached from their benthic habitat and resuspended into the water column through a disturbance. Species of diatoms often found in subaerial environments, such as bogs and marshes, are referred to as aerophilous. However, the ecology of some species is not known in detail, and so continued monitoring and research is necessary to inform understanding of species' 'optimum' conditions (Battarbee *et al.*, 2001). While the known habitat preferences of taxa can be used to infer habitat distributions in an environment, species can often be found in more than one habitat (Battarbee *et al.* 2001). This can lead to confusion over the habitat preferences of taxa and be problematic in inferring past habitat change through fossil assemblages (e.g. Barker *et al.*, 1994).

4.3.1 | Diatoms and environmental change

Several characteristics of diatoms make them particularly useful palaeoenvironmental proxies and an extensive research effort (e.g. CASPIA project; Juggins *et al.*, 1994), has elucidated their utility in understanding and reconstructing environmental conditions. The amorphous silica frustules of a diatom are usually well preserved in lake sediments, and as discussed above can be identified to a species level (Round *et al.*, 1990; Compton, 2011). Most importantly, their short life-cycles, rapid dispersal and colonisation mean that the

composition of diatom communities changes rapidly in response to environmental change. Numerous studies, from a range of environments, have established that the optima of many taxa fall within a well-defined hydrochemical range for certain species to thrive (e.g. Figure 4.5), making them highly sensitive to fluctuations in their local environment.

After understanding a species' range of optimal conditions within a range of environments (e.g. Figure 4.4), it is possible to begin inferring the characteristics of a specific habitat based upon the composition of the diatom assemblage. This approach has been utilised successfully in, for example, analyses in hydrological, climatological and environmental monitoring applications (Smol & Stoermer, 2010). The analysis of diatom assemblages within sedimentary records facilitates direct and indirect inferences about environmental conditions in specific habitats through time. For example, broad changes in past water depth of a lake can be qualitatively inferred based on the relative abundance of planktonic (deeper-water conditions) vs. benthic diatoms (shallower-water conditions; Wolin & Stone, 2010). Prior to the early work of researchers such as Imbrie & Kipp (1971) environmental reconstructions were primarily qualitative and presented as, for example, 'acid', 'mildly basic', 'cool' or 'dry'. Imbrie & Kipp (1971) modernised Quaternary paleoecology by presenting a procedure for the quantitative reconstruction of past environmental variables from biostratigraphical fossil assemblages involving predictive models or so-called 'transfer functions' (Juggins & Birks, 2012; Figure 4.6).

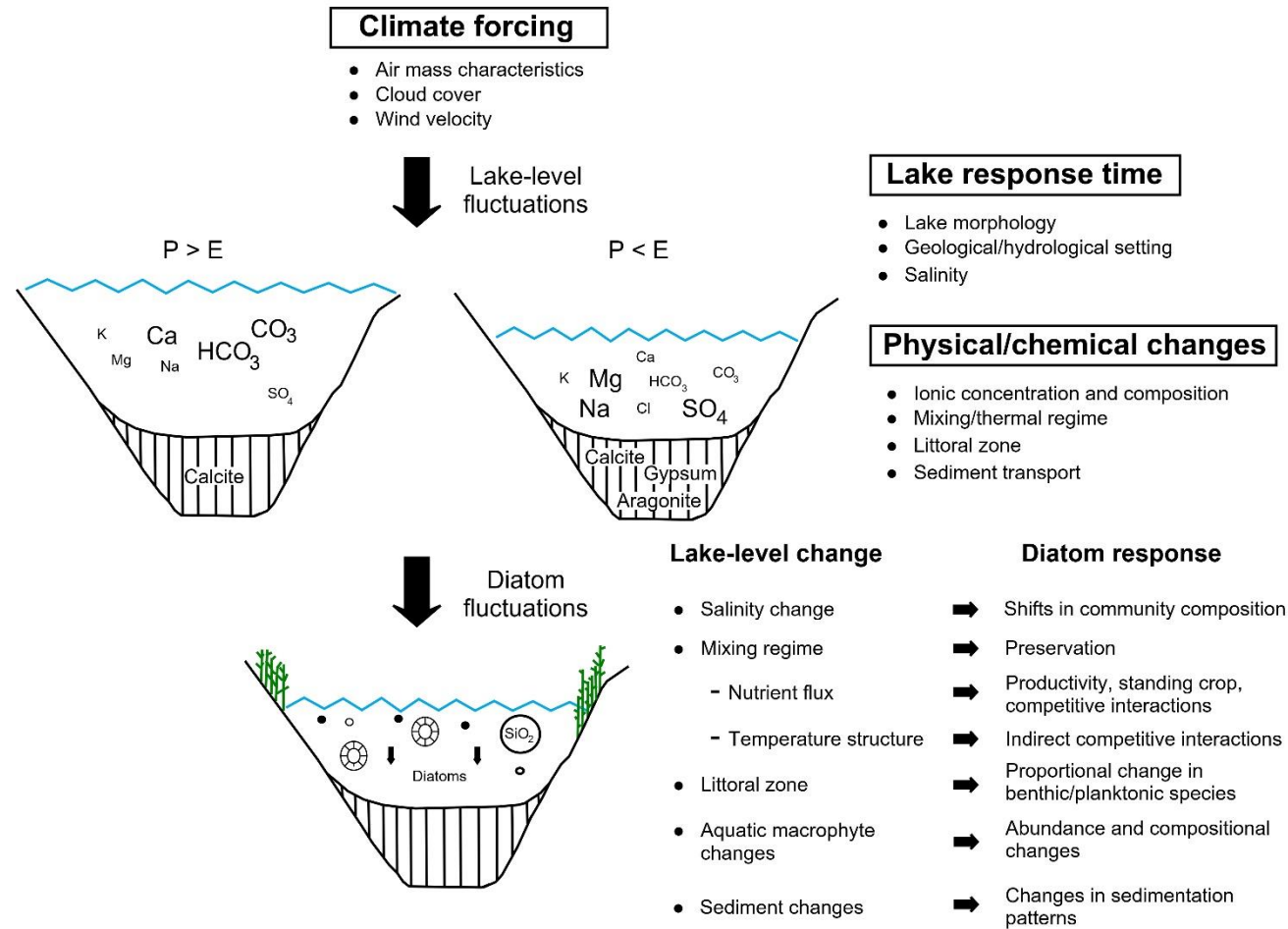


Figure 4.4: Simplified diagram showing the influence of changing precipitation and evaporation on the physical and chemical characteristics of a lake, and the effect this has on the diatom assemblage of that lake. Redrawn from Fritz *et al.* (2010).

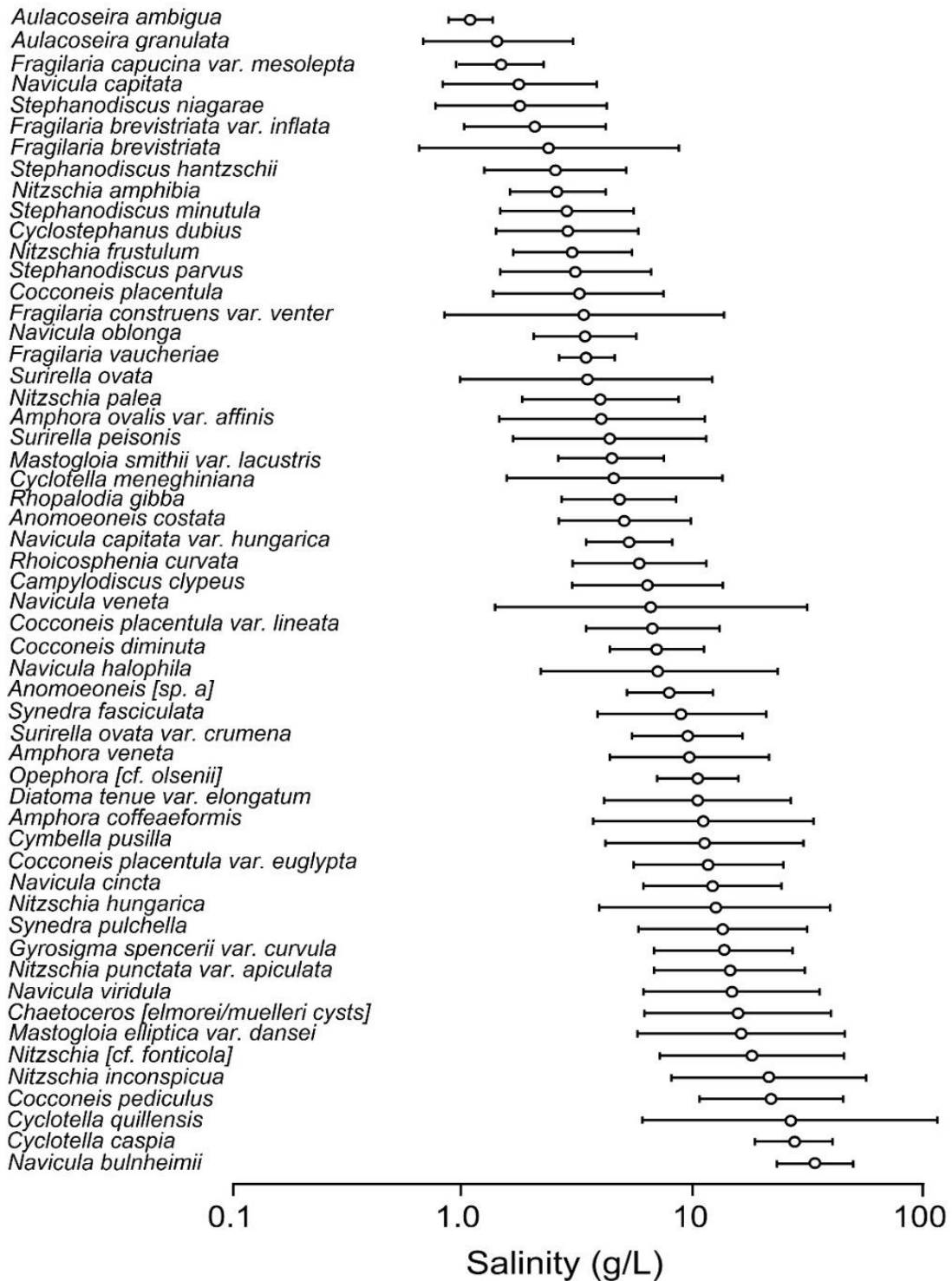


Figure 4.5: The salinity ranges (horizontal line) and salinity optima (circle) of selected diatom species from the Northern Great Plains, North America, generated from a survey of water chemistry and diatoms in the surface sediments of 55 regional lakes. Species are arranged in descending order according to increasing salinity optima. Redrawn from Fritz *et al.* (1993).

An illustrative example of the early use of diatom-based conductivity transfer functions in effectively reconstructing past environments comes from Laird *et al.* (1998). They compare a ~100 year diatom record to a Bhalme-Mooley Drought Index (BMDI) at Moon Lake, Northern Great Plains, USA. They demonstrate a highly significant ($p = < 0.01$) correlation between their diatom log salinity record with a three-year lag and summer (April-September) BMDI ($r = 0.49$; Figure 4.7), with a similarly high correlation between their log salinity record and the annual BMDI based on precipitation ($r = 0.45$, $p = < 0.01$).

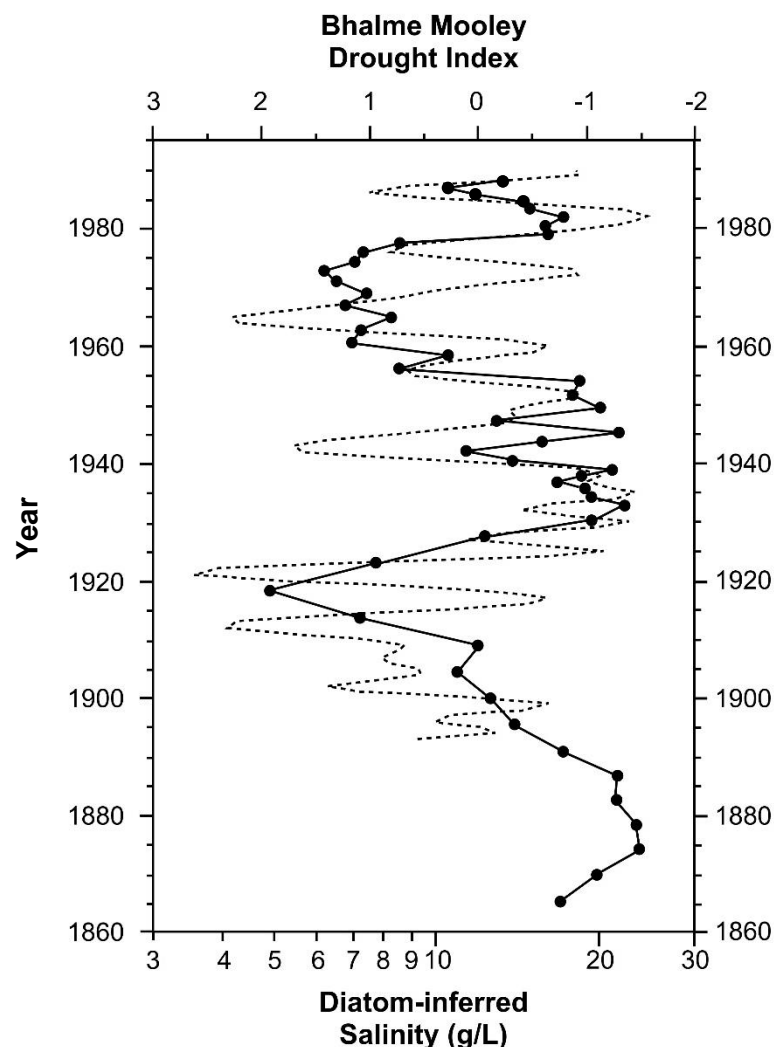


Figure 4.7: Changes in Moon Lake log diatom-inferred salinity estimates (g/L; solid line) redrawn from Laird *et al.* (1998). This diatom-inferred salinity record is compared with a Bhalme-Mooley Drought Index (BMDI; dotted) based on Oladipo (1986) BMDI equation

for the Great Plains region and monthly summer (April–September) precipitation records from nearby climate stations.

4.3.2 | Diatom-based research in eastern Africa

Extensive studies investigating the diatom ecology of water bodies across eastern Africa have been carried out since the start of the 20th Century. The first of these intensive diatom-based studies was carried out at the start of the 20th Century (1900-1925 AD) in African lakes by Otto Müller, G.S. West, A. Forti and Friedrich Hustedt. Furthermore, the first work to characterise eastern African waters according to their diatom flora was undertaken by Hustedt (1949).

Few of the diatom-based works following these early investigations included quantitative analyses regarding the composition of local diatom assemblages in relation to their corresponding environments. The most extensive quantitative survey of the diatom species of eastern Africa, following the early investigations at the start of the 20th Century, was undertaken by Gasse *et al.* (1983) based on 210 diatom samples from 98 different hydrological localities containing a total of 579 taxa. This dataset has since been merged with existing regional datasets from North Africa and Niger (Gasse *et al.*, 1995), increasing the number of diatom sample data to 282 and number of identified taxa to 664. However, the number of taxa used in subsequent analyses reduced to 389 following the removal of species only present in one sample or with a low relative abundance (<1%). By examining the relationships between diatom species distributions and hydrochemistry using Canonical Correspondence Analysis (CCA) and partial CCA, this study developed predictive models using WA (weighted averaging) for conductivity ($r^2=0.87$), pH ($r^2=0.77$), and ratios between alkali and alkaline earth

metals ($r^2=0.81$), and carbonate-bicarbonate and sulphate + chloride ions ($r^2=0.82$).

This transfer function facilitated the quantitative reconstruction of past hydrochemistry from fossil diatom assemblages in Africa. Subsequent diatom-based quantitative reconstructions have been key in inferring long-term (millennial to sub-millennial scale) Quaternary climate-driven changes in hydrology (e.g. Owen *et al.*, 2012), to short-term, abrupt regional climatic perturbations (century to decadal scale). Environmental change associated with anthropogenic activity, as part of these investigations into abrupt, regional change, have also been a focus of research (e.g. Marshall *et al.*, 2009; Mills *et al.*, 2014).

4.3.2.1 | Understanding transfer functions in eastern Africa

Despite their utility, it is important to recognise that, fundamentally like all predictive models, these African transfer functions are based on several assumptions:

- (1) the taxa in the modern training set are related in some way to the conditions of their environment;
- (2) the taxa in the modern calibration set are, biologically, the same taxa present in a fossil assemblage, and that the ecological response of the taxa to environmental variable(s) has not changed over time;
- (3) the environmental variable(s) to be reconstructed is an ecologically important determinant in the system of interest;

- (4) the application of mathematical methods accurately models the biological response of the taxa to the environmental variable(s) of interest, whilst also ensuring unbiased reconstructions;
- (5) that other environmental variables, other than the variable of interest, have a negligible influence, or their joint distribution remains constant over time (Juggins, 2013; Figure 4.5).

Assumptions 3 and 5 are critical to the credibility of environmental reconstructions using transfer functions, but as Juggins (2013) suggests, are rarely appreciated. As discussed above, diatoms are sensitive to changes in their local environment with multiple environmental secondary, or 'nuisance', variables influencing the composition of an assemblage (Figure 4.4; Juggins, 2013), with the relative importance of certain parameters also varying along latitudinal and trophic gradients (Blanco, 2014). Furthermore, changes in the environmental variable over time, in this example conductivity, may not always be climate-driven, especially for lakes in volcanically active regions. For example, Telford *et al.*, (1999) speculate that changes in diatom-inferred conductivity at Lake Awassa, Ethiopia, unlike other local sedimentary records in the mid-Holocene (e.g. Gillespie *et al.*, 1983), indicate that inputs of saline groundwater, via magma degassing events under the Awassa Caldera, were responsible for changes in water salinity and the resulting diatom assemblage, as opposed to climate. It is also important to recognise that many lakes in eastern Africa have experienced significant anthropogenic impacts over the last ~100 years. As a result, anthropogenically-driven changes in nutrient concentration and turbidity, for example, may override conductivity as a key determinant in the diatom ecology of these lakes (Mills & Ryves, 2012).

Telford & Birks (2011) find that uneven sampling of an environmental gradient can considerably bias transfer function performance, as the estimation of a species' optimal conditions will be more precise in the section of the gradient with more observations, in contrast to the part of the gradient with fewer samples. Statistical analyses, such as weighted averaging (WA) or weighted averaging partial least squares (WA-PLS), during the development of a training set introduces bias towards the environmental niches if a few sites have a disproportionately high abundance of species. For example, *Thalassiosira faurii* is comparatively abundant in samples from the Guidimouni salt swamp, Niger in the African training set (8, 14.3 and 26.4% in three samples compared to 0.2-4.4% in the other eighteen), where conductivity measured $13,500 \mu\text{S cm}^{-1}$ (European Diatom Database; EDDI, 2017b). A recent study measuring the growth response rate of *Thalassiosira faurii*, taken from Lake Langano, Ethiopia, to various controlled, laboratory salinity conditions find a conductivity optimum of $\sim 400 \mu\text{S cm}^{-1}$ for the species, with no growth observed, despite the survival of some cells, at $2,000 \mu\text{S cm}^{-1}$ (Roubeix *et al.*, 2014). This highlights a significant discrepancy between the empirical conductivity optimum determined in the African training set ($\sim 9,000 \mu\text{S cm}^{-1}$) by Gasse *et al.* (1995) and the experimental optimum and tolerance range (Roubeix *et al.*, 2014), with the highly saline Guidimouni samples responsible for the overestimation of the optima of *Thalassiosira faurii*. Roubeix *et al.* (2014) suggest that a re-evaluation of sedimentary sequences using *T. faurii* as an indicator of saline, dry periods (Telford *et al.*, 1999; Chalié & Gasse, 2002) may be required. Similarly, *Lindavia ocellata* (formerly *Cyclotella ocellata*) is poorly represented in the African training set (reaching an abundance of $\sim 8.5\%$ in only two, comparatively, hypersaline

samples; EDDI, 2017a). This has also been identified as a potential issue in accurately inferring past conductivity in sedimentary records where *Lindavia ocellata* is abundant (>30% and 40% in some parts of cores analysed by Chalié & Gasse (2002) and Marshall *et al.* (2009), respectively).

It is clear from these selected examples that quantitative reconstructions must be integrated with the qualitative understanding of an individual species' ecological preferences, the fossil diatom assemblage as a whole and the lake system. In Telford (1998), a good understanding of the hydrological system of Lake Awassa, as well as of the fossil assemblage, facilitated a more robust interpretation of ecological changes that seemed out of sync with multiple other local records. This illustrates the need to acknowledge all possible variables and reiterates the discussion in Chapter 3 of the utility of a multi-proxy approach to provide additional independent lines of evidence to support diatoms.

4.3.3 | Diatom sample preparation and analysis

(i) Fossil samples

Diatom analysis was performed on sub-samples taken from each section (see above) at 32 cm intervals from the Babogaya core and at 30 cm intervals from the Garba Guracha core as a preliminary count. Following this initial count, further samples were taken at a higher resolution where appropriate across intervals of interest. Individual lamina were sampled along the same interval covered by thin section analysis (see above) for diatom composition by carefully scraping through them with a needle. These samples were prepared in the same way as other fossil samples.

From the 1 cm³ sub-samples, 0.05-0.1 g (dry weight) of sediment was taken. The known weight of the sample facilitates the concentration of diatoms per gram of dry sediment to be calculated (see Appendix 1 for full equation). These samples were then transferred to Fisherbrand™ 50 ml polypropylene centrifuge tube along with 10 ml of 10% HCl and heated in a water bath to ~80°C to remove any carbonate content. Samples were then centrifuged at 1500 RPM for 15 minutes, decanted and washed three times with distilled water to remove any spent acid and soluble carbonates. Clay rich samples were deflocculated with ~30 ml of 5% sodium pyrophosphate in a water bath at 80°C for 30 minutes, following three water washes to remove any clay particles. After the final wash, 10 ml of H₂O₂ (100 vols.) was added to each sample, until the reaction ceased, in order to remove any organic matter content present. Once the reaction had ceased a final round of three washes was undertaken with distilled water and mixing the samples in a centrifuge at 1500 RPM for 15 minutes. These washed samples were then transferred to a 50 ml stoppered, graduated measuring cylinder to the 30 ml level. With the cylinder stopper securely fastened, the samples were homogenised by shaking the cylinder vigorously and with the sample still in suspension, ~14 ml was transferred into individual small, labelled glass vials with a snap-on plastic closure to safely store the samples for further analyses.

Slide preparation first involved placing a 500 µl aliquot, from each sample glass vial, on to a circular methanol-washed microscope coverslip and allowing it to dry overnight in a dust-free environment. Microscope slides, pre-washed with methanol, were placed on a hotplate set to ~100°C, and once warm, 2-3 drops of Naphrax® was released on to the centre of the slide. Dried coverslips were inverted and placed on to this Naphrax with all care taken to remove trapped air

bubbles. A preliminary analysis of each slide using a HM-Lux 3 microscope at x40 magnification was performed to determine the suitability of the slide for counting and if any dilution was required. Relevant samples were diluted accordingly with the steps above retaken until an adequate level of dilution had been achieved to produce a countable slide. In slides where considerable diatom clumping was observed and dilution was required, a few drops of ammonia were added to the diluted sample. These diluted samples were also used for SEM photography (see below).

(ii) Modern samples

The modern diatom samples from the Garba Guracha basin were large and presumed very organic, therefore samples were transferred to individual 250 ml beakers along with approximately 50 ml of H₂O₂ (100 vols.) and left to stand in a fume cupboard overnight. Sample bottles were washed down thoroughly with distilled water to ensure diatom samples were fully transferred to their individual labelled beakers.

After the samples were reduced to under 50 ml and transferred to individual, labelled centrifuge tubes, the preparation methods used to prepare fossil diatom samples, as described above, was also used in preparing modern diatom samples for counting.

4.3.3.1 | Diatom identification and taxonomy

The identification of diatoms was undertaken with reference to the works of Gasse (1980; 1986), Krammer & Lange-Bertalot (1986, 1988, 1991a, 1991b), and references therein. The online databases: EDDI and Diatoms of the United States were also used for their detailed image catalogues and explanations of

species and their differences. A list of synonyms is included with the full list of diatom taxa identified in this study (Appendix I) to address these taxonomic revisions. Diatom taxonomy has undergone numerous changes through time. Consequently, these changes have led to multiple re-classifications of some species within new genera (Williams & Kociolek, 2007). A full list of diatom names used in this thesis and their other names are available in Appendix 2.

4.3.3.2 | Microscopy and photography

Diatom counting was performed under x1000 magnification with immersion oil using an Olympus BX 51 microscope. Battarbee (1986) illustrated that counting at least 300 valves will provide an accurate representation of the diatom assemblage in the sample in routine analyses. However, Battarbee *et al.* (2001) note that often a greater count is required to fully represent the assemblage should a species dominate. The DARES protocol (2004; Figure 4.8) suggests that if one taxon represents more than one third of the total number of valves, then the sample size should be increased until at least 200 valves of other taxa have been counted. This method may be time consuming, and as illustrated by Loakes (2015) may not significantly impact the representation of species in a sample. Through 21 random samples, Loakes (2015) found that 21.1% of their samples had no change from 300 to 500 valves counted, with only 1 and 2 extra species identified in 26.3 and 47.4% of the samples. Furthermore, increased diversity through the identification of additional taxa accounted for only 0.2-0.8% of a 500 valve count.

In general, during this study, a minimum of 400 valves were counted per sample (modern and fossil) from both sites. A traverse was made of the diameter of a

coverslip and all the diatoms in the field of view were counted in order to estimate changes in diatom abundance. As a known dry weight of core sample was used, and the dilution also known, the number of valves per gram of dry sediment could be calculated. Taxa were grouped according to their habitat preference as; planktonic, facultatively planktonic (incl. tycho planktonic), aerophilous and benthic species (including epiphytic, epilithic, epipelagic, and epipsammic species). The number of other siliceous microfossils present (e.g. phytoliths) was also recorded as their presence/abundance may provide additional ecological information.

Diatom species and other siliceous microfossils were digitally photographed using a CANON EOS 5D camera, with the CANON EOS utility (v. 3) and Digital Photo Professional (v. 4) software. Problematic species to identify under the light microscope were examined further under SEM using a Hitachi S-4700 FESEM in the Advanced Microscopy and Bio-imaging Laboratory in the Institute of Biological, Environmental & Rural Sciences (IBERS) at Aberystwyth University. Samples were diluted and evaporated on to 13 mm diameter coverslips in a dust free environment. These were mounted on to SEM stubs using a carbon coated adhesive, then sputter coated with gold using an Agar high-resolution sputter coater.

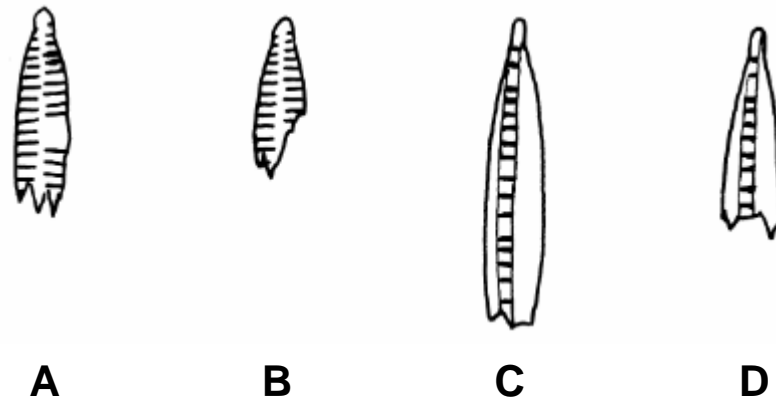


Figure 4.8: DARES protocol for counting broken valves. ‘A’ shows a broken valve with one pole and a central area, which should be included in a count; whilst ‘B’ should not be counted as only one pole is present with no central area. ‘C’ and ‘D’ show an example of specimens with no obvious central area: comparison with intact valves will indicate that ‘C’, and not ‘D’, should be included in the count (DARES, 2004).

4.3.3.3 | Taxonomy of problematic species

4.3.3.3.1 | *Nitzschia* Hassall

Nitzschia Hassall is a widely distributed, diverse genus of diatoms. However, the size of the genus (>1,100 species ‘acceptable’ and ‘unacceptable’ names; Trobajo *et al.*, 2013) and the close similarity in morphological characteristics of species makes them hard to identify accurately under a light microscope (LM). Typically, *Nitzschia* species have finely structured valves with parallel striae, an almost invisible raphe and a limited variation in valve outline. The difficulty in the identification of *Nitzschia* section Lanceolate Grunow has been recognised, especially when considering the diversity of forms within a species (e.g. Coquyt *et al.*, 2012; Trobajo *et al.*, 2013). Most species are characterised as small-medium sized (~5-40 µm length, 2-6 µm width), and finely striated (>20 striae/10 µm). For example, mating tests and morphological and genetic diversity investigations by Trobajo *et al.* (2009) on clones emphasises the taxonomic

difficulties associated with the *Nitzschia palea* (Kützing) W.Smith complex. Their work highlights that *Nitzschia palea* is not a homogenous taxon, and that further splits into up to 3 distinct species is likely necessary.

(i) *Nitzschia lancettula* O.Müller

Such an issue was encountered when trying to identify the species recognised in this research as *Nitzschia lancettula*, which is dominant in much of the core. In an attempt to establish the taxonomy of the species, 50 valves were measured from a sample where the taxon in its many observed forms was abundant. Valves varied from 10-19 µm in length, with a width of 4-6 µm. Striae and fibulae density were 17-22 and 7-11 in 10 µm, respectively (Table 4.1). Less common, *Nitzschia* sp. 'type 1 long' (20-25 µm) have been counted separately, although are likely a larger form of the *Nitzschia lancettula*, as their width, fibulae/striae density are similar.

Based on the width of valves, lack of a central gap in fibulae and the coarseness of striae, *Nitzschia lancettula* is unlikely to be *Nitzschia frustulum* (Kützing) Grunow or *Nitzschia fonticola* (Grunow) Grunow. Similarly, *Nitzschia lancettula* cannot be classified as *Nitzschia amphibia* f. *rostrata* Hustedt, despite a similar morphology, due to the incompatibility of the two species' striae density (Table 4.1). Furthermore, the information for *Nitzschia amphibia* f. *rostrata* in Krammer & Lange-Bertalot (1988) comes from observations made at two lakes in Austria by Hustedt (1959), and Krammer & Lange-Bertalot (1988:108) do highlight that the species "remains to be clarified more precisely".

Gasse (1986) notes that *Nitzschia vanoyei* Cholnoky was only found in one sample (Lake Edward) in association with *Nitzschia lancettula*. Due to this close

association, and the rarity of data for *Nitzschia vanoyei* in the EDDI database, it was merged under *Nitzschia lancettula* for the reconstructions of Stager *et al.* (2011). These species are morphologically similar to the forms of *Nitzschia lancettula* and *Nitzschia* sp. 'type 1 long', leading to the tentative classification of these species as *Nitzschia lancettula* and *Nitzschia vanoyei*. However, further work is required to accurately determine the exact taxonomy of *Nitzschia lancettula*.

The difficulty in the identification of valves morphologically similar to *Nitzschia lancettula* is also evident in other eastern African lakes. For example, a pictured valve with similar visual characteristics to *Nitzschia lancettula* in Telford (1998: pl. 3.5, fig. 19) was identified as *Nitzschia amphibia* Grunow, with the longer form (similar to longer *Nitzschia lancettula* valves) noted as *Nitzschia lancettula* (pl. 3.5, fig. 14). However, Loakes (2015: pl. 6, fig. 2) and Mills (2009: pl. 4. fig. F) identifies a species very similar in morphology to *Nitzschia lancettula*, and *Nitzschia amphibia* in Telford (1998), as *Nitzschia lancettula*. Gasse (1986) notes that *Nitzschia vanoyei* was only found in one sample (Lake Edward) in association with *Nitzschia lancettula*. Due to this close association, and the rarity of data for *Nitzschia vanoyei* in the EDDI database, it was merged under *Nitzschia lancettula* for the reconstructions of Stager *et al.* (2011). The same approach has been applied here.

(ii) *Nitzschia fenestralis* sp. nov. Grady, Mann & Trobajo

To establish the taxonomy of this problematic taxon with precision, metrics such as valve length, width at mid-valve and fibulae density were taken from LM digitised images calibrated against a slide micrometer using the public domain Fiji (ImageJ distribution package) software (Schindelin *et al.* 2012; Rueden *et al.*

2017). 200 valves were imaged and measured in total from 4 samples spread ~1-1.5 m apart through parts of the core where the taxon was abundant (57.9-62.6%). Following further investigation it was established that this taxon is new to science, was described and named (*Nitzschia fenestralis*). Full details are available in Grady *et al.* (2020; see Appendix 1), with some information from this paper given below.

Valves are linear-lanceolate with parallel sides and acutely rounded ends with sometimes small, pimple-like subrostrate poles. Fibulae are rounded-square shaped and irregularly spaced along the keel, but the central pair of fibulae are no more widely spaced than the others. The keel can often be seen to curve slightly towards the valve apices and appear to give a slightly hooked shape to the valve ends. Transapical striae are very fine to irresolvable under LM, with SEM analysis revealing a fine striation of small round areolae. A small helictoglossa is present at the inside of poles (n= 20).

Nitzschia fenestralis are comparable in valve outline to *Nitzschia abonuenensis* Foged and *Nitzschia etoshensis* Cholnoky. An illustration of a specimen with a similar morphology to *Nitzschia fenestralis* has also been placed in the broad *Nitzschia palea* complex by Gasse (1986; Fig. 13, Pl. XXXV), despite the taxa of this complex normally associated with rostrate apices (e.g. Krammer & Lange-Bertalot, 1988; Morales & Hamilton, 2002; Taylor *et al.*, 2007; Figure 4.11). The specimens encountered during this study fit the lower end of the broad measurements of the *Nitzschia palea* complex described from Europe and Africa (Table 4.2).

Table 4.1: Range (mean \pm s.d) of *Nitzschia lancettula* measurements (under LM; in μm) of 50 valves in a sample dominated by the species compared to similar looking species. * - Measurements of *Nitzschia amphibia* used, as source: Hustedt (1959) is currently unavailable. ** - Based on his own observations, Hustedt (1949) argues this is not the full size range of the species and that *Nitzschia lancettula* forma minor (bracketed measurements) described by Müller (1905) are incorrect. Numbers next to species names correspond to the images in Figure 4.9.

	Length	Width	Striae (/10 μm)	Fibulae (/10 μm)	Source
<i>Nitzschia amphibia</i> f. <i>rostrata</i> * (A)	6-50	4-6	13-18	7-9	Krammer & Lange- Bertalot (1988)
<i>Nitzschia lancettula</i> (B)	36-48 (15-20)	6-7 (5-6)	12-13	6-7	Müller (1905)**
	Smallest observed: 7	Smallest observed: 4.5	16-20	-	Hustedt (1949)
	10-36	3-10	12-15 (larger) 18-20 (smaller specimens)	7-10	
<i>Nitzschia vanoyei</i> (C)	10-25	4.5-4.5	18-20	7-9	Cholnoky (1954)
	11-13	4-5	20-21	9	Gasse (1986)
<i>Nitzschia</i> sp (Plate)	10-19 (12.92 \pm 2.54)	4-6 (4.68 \pm 0.5)	17-22 (19.9 \pm 1.42)	7-11 (8.82 \pm 1.04)	This study

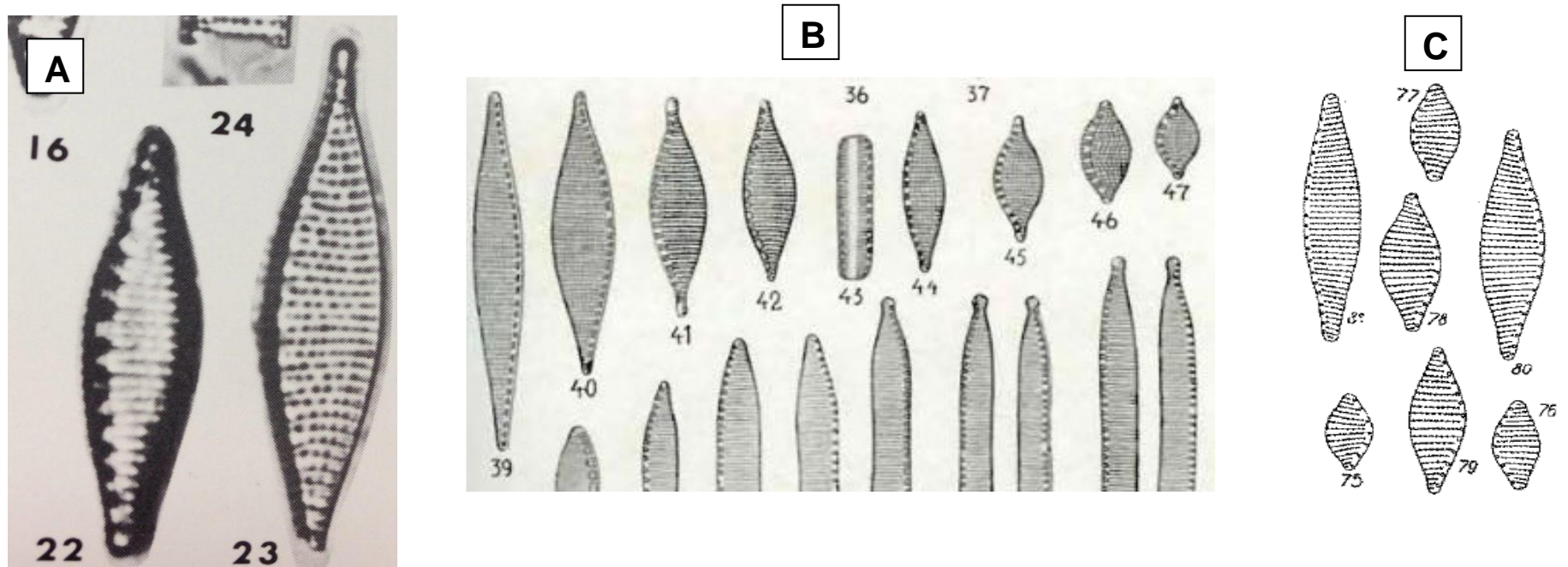


Figure 4.9: Images of similar diatoms in the literature. *Nitzschia amphibia f. rostrata* (left; A), *Nitzschia lancettula* (middle; B) and *Nitzschia vanoyei* (right; C). Images taken from Krammer & Lange-Bertalot (1988: 373, pl. 78, figs. 22-23), Hustedt (1949: pl. 13, figs. 39-47) and Cholnoky (1954: 421, pl. 2, figs. 75-81), respectively.

However, *Nitzschia fenestralis* are starkly different in valve outline, notably when comparing valve ends. Conversely, while the slender outline and ends of *Nitzschia fenestralis* valves broadly resemble that of *Nitzschia abonuenensis* and *Nitzschia etoshensis*, also to some degree *Nitzschia mediocris* Hustedt although the ends of this taxa are described more as “spiky” (Hustedt, 1949), these taxa differ from *Nitzschia fenestralis*, however, with respect to size range and density of fibulae. To the authors’ knowledge, descriptions of the latter two taxa are rare, with SEM analyses not recorded making it difficult (if not impossible in the case of *Nitzschia abonuenensis*) to further differentiate *Nitzschia fenestralis* from these two taxa based on density of striae.

4.3.3.3.2 | *Fragilaria* Lyngbye

The Fragilarioids are a large, taxonomically complex and morphologically variable group of benthic and tycho planktonic diatoms incorporating multiple genera. Taxa of this genus are normally small (<20 µm) and occur in similar times/places due to their similar ecological preferences (e.g. Schmidt *et al.*, 2004; Karst-Riddoch *et al.*, 2009), as is the case with the problematic species below. SEM analyses was originally required to revise the *Fragilaria* genus initially by Williams & Round (1987). The morphology of small Fragilarioid taxa remains notoriously similar and difficult to distinguish from each other (e.g. Edlund *et al.*, 2006), especially in LM, with Morales *et al.* (2001) noting the necessity of SEM in the identification of Fragilarioid taxa.

Table 4.2: Range (1 d.p; mean \pm s.d: 2 d.p) of *Nitzschia fenestralis* measurements (under LM and SEM; in μm) of 200 valves (10 in SEM) in samples dominated by the species, compared to morphologically similar species. All measurements are given in μm . * n = the 10 samples measured under SEM. *nd* = not determined/documentated. Images of each species can be found in Figure 5.11 and 5.12.

Taxon	<i>Nitzschia abonuensis</i>	<i>Nitzschia mediocris</i>	<i>Nitzschia etoshensis</i>	<i>Nitzschia fabiennejansseniana</i>	<i>Nitzschia palea</i>	<i>Nitzschia paleacea</i>	<i>Nitzschia aequalis</i>	<i>Nitzschia fenestralis</i>		
Length	25-30	40-50	20-60	32-88	24-48.5	15-70	25-60	8-55(80)	80-130	20-70.2 (40.65 \pm 9.38)
Width	2.5-3	1.5-2	4-5.5	4-4.5	2.1-2.8	2.5-5	3-4	1.5-3(3.5)	3	1.9-3.3 (2.46 \pm 0.29)
Striae (/10 μm)	Nd	<i>nd</i>	>40	<i>nd</i>	32-35	28-40	34-40	44-55	34-40	32-36* (34 \pm 1.15)
Fibulae (/10 μm)	9-10	14-17 (mostly 16)	15-18	15-19	11-13 (commonly 12)	9-17	10-14	(12)14-19	12-14 (mostly 12)	10-14 (12.09 \pm 0.72)
Central fibulae gap?	No	no	No	yes	no	yes	no	no	no	
Source	Foged (1966)	Hustedt (1949)	Taylor <i>et al.</i> (2007)	Gasse (1986)	Cocquyt & Ryken (2017)	Lange- Bertalot & Krammer (1988)	Gasse (1986)	Lange- Bertalot & Krammer (1988)	Hustedt (1949)	This study

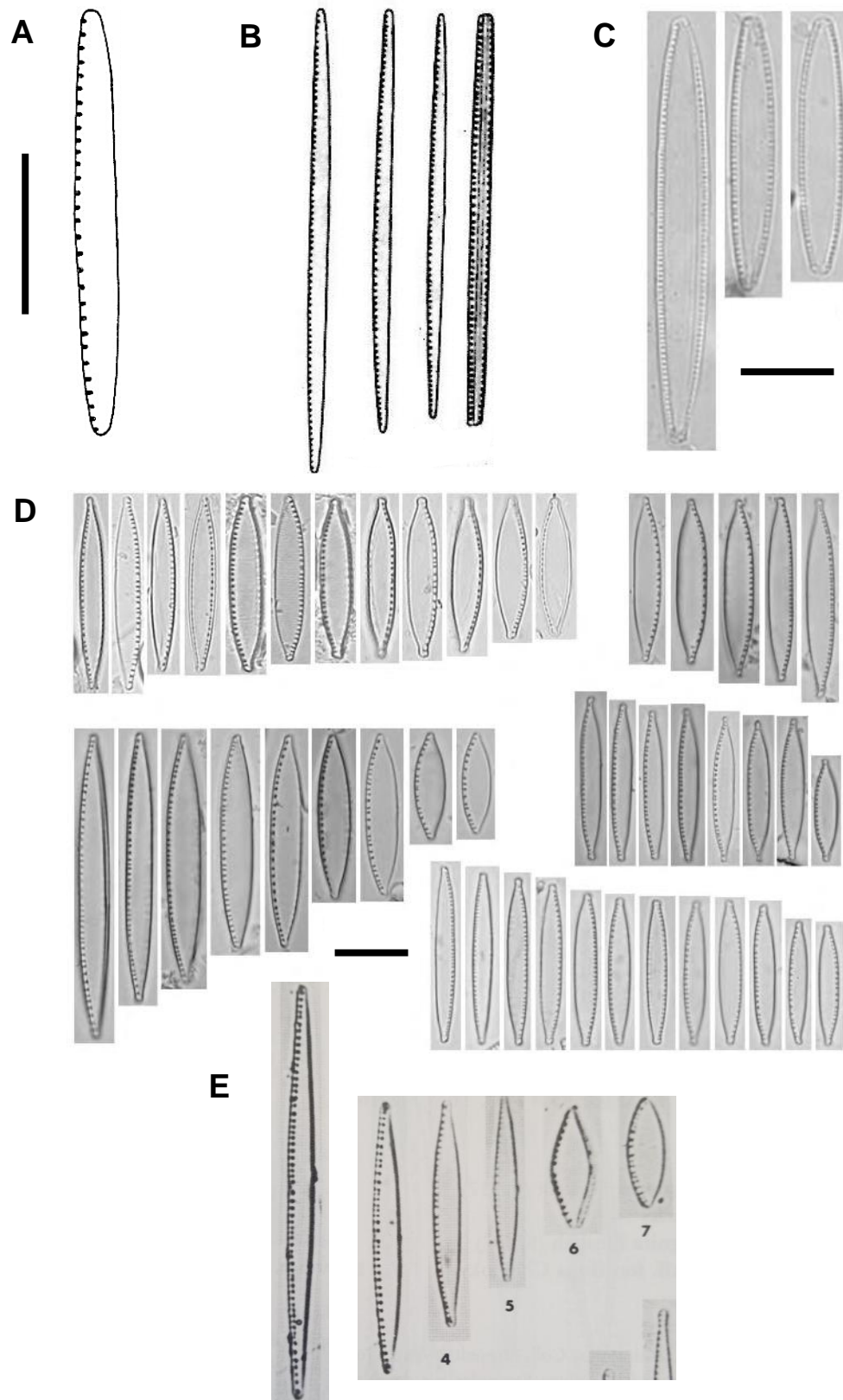


Figure 4.10: Common forms of *Nitzschia abouensis* (A), *Nitzschia mediocris* (B), *Nitzschia etoshensis* (C), *Nitzschia palea* (D) and *Nitzschia paleacea* (E). Images from sources cited in Table 4.2. Scale bars = 10 μm . No scale given in Hustedt (1949) and Krammer & Lange-Bertalot (1988) for B and E.

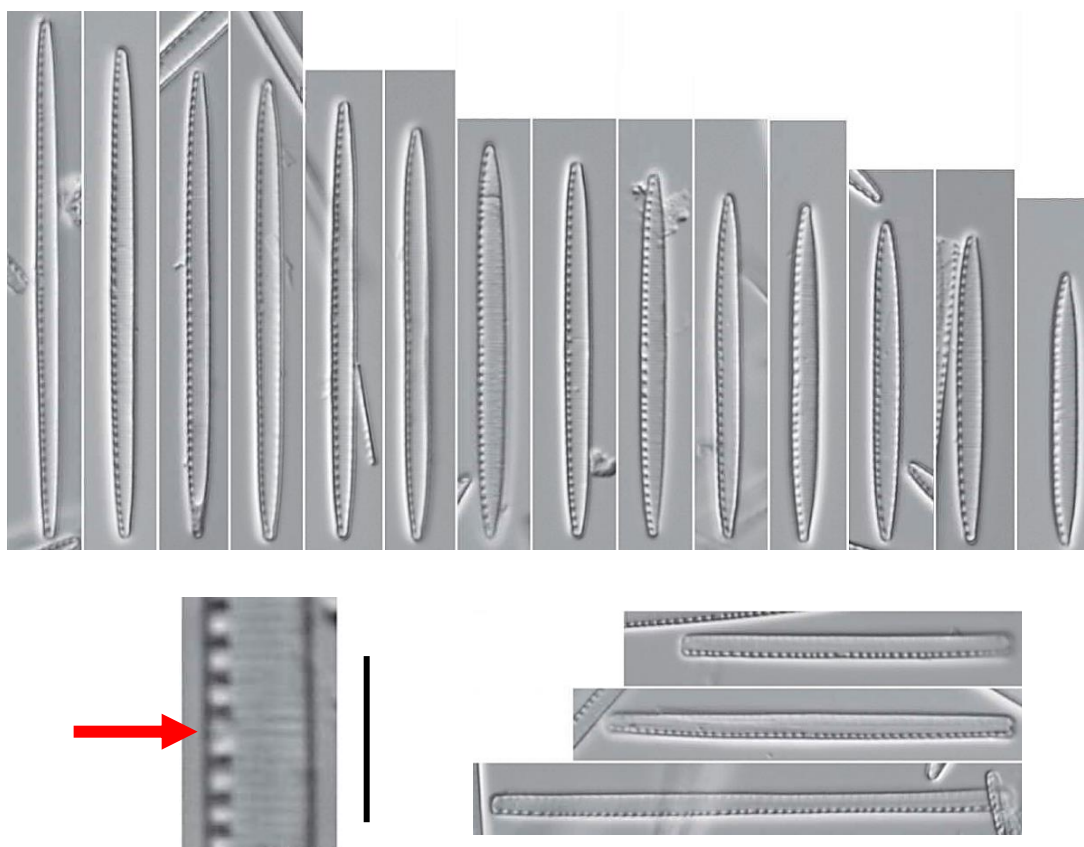


Figure 4.11: *Nitzschia fabiennejansseniana* under LM. 2-15 = valve view, 16-18 = girdle view. 27a = zoomed view of the valve (accompanying scale bar for this figure is 5 μm) to illustrate the central gap between fibulae (arrow). From Cocquyt & Ryken (2017).

(i) Small (<10 μm) Fragilarioid taxa

Staurosira construens var. *venter* (Ehrenberg) P.B.Hamilton, *Staurosirella pinnata* (Ehrenberg) D.M.Williams & Round and *Fragilaria elliptica* (Schumann *sensu* Lange-Bertalot) are similar in appearance under LM, often making it difficult to distinguish between these taxa (Morales *et al.*, 2001; Paull *et al.*, 2008), especially when lying in girdle view. For example, ongoing debate continues as to the exact taxonomy of such small *Fragilaria* (e.g. *Pseudostaurosira elliptica* (Schumann) Edlund, Morales & Spaulding; Edlund *et al.*, 2006; Morales *et al.*, 2010). This issue was encountered during parts of this study at Garba Guracha

where both *Staurosira construens* var. *venter* and *Staurosirella pinnata* co-occurred at high abundances.

Furthermore, exploratory SEM revealed some morphs of *Staurosira construes* var. *venter* with small, rounder areolae resembling those of *Fragilaria elliptica*; a common issue in diagnosis even under SEM (Morales *et al.*, 2001; Morales, 2001; Plate IV-V). Consequently, it is assumed that at least some *Fragilaria elliptica* morphs have been counted under LM as *Staurosira construes* var. *venter*. Every effort was made by the author to correctly differentiate species based on their distinguishing features (e.g. number and shape of striae) under LM during counting. However, due to their similarities, especially in girdle view, there may be some overlap between these taxa.

During SEM analysis, species of the genus *Punctastriata* were also identified alongside the taxa mentioned above (for example, all taxa are present to some degree at 740 cm in GGU-1B under SEM; Plate IV-V). The most common *Punctastriata* taxon (hereafter *Punctastriata* sp. 1) encountered are similar in valve outline and striae structure to *Punctastriata discoidea* Flower (Flower, 2005) and *Punctastriata glubokoensis* D.M.Williams, Chudaev & Gololobova (Williams *et al.*, 2009), with a 'transitional', mallet-shaped spine structure between the more simple spines of *Punctastriata glubokoensis* and complex, cruciate spine structure of *Punctastriata discoidea*. It is important to note that Williams *et al.* (2009) highlight the possibility that *Punctastriata glubokoensis* and *Punctastriata discoidea* may be the same species, with only spine structure used to differentiate these taxa. Less commonly identified was (only 2 observations in SEM) *Punctastriata cf. lancettula*.

With no obvious diagnostic features under LM, SEM is required to differentiate *Staurosira/Staurosirella* and *Punctastriata* based on striae structure (areolae lineolate in the striae of *Staurosirella pinnata* and 'net-like', striae composed of rows of small, round areolae in *Punctastriata*; Williams & Round, 1987). As a result, studies describing new species of *Punctastriata* have noted that it is **highly** likely that the taxa have been previously counted as other small *Fragilaria* such as *Staurosirella pinnata* under LM (e.g. *Punctastriata discoidea*; Flower, 2005 and *Punctastriata glubokoensis*; Williams *et al.*, 2009; Vélez-Agudelo *et al.*, 2017), with Morales (2005) noting such an occurrence in National Water-Quality Assessment (NAWQA) with *Punctastriata mimetica* E.A.Morales. Consequently, due to this likely inadvertent 'lumping' of taxa over time, the ecological information of *Punctastriata* spp. has also been 'lumped' with that of *Staurosirella pinnata* and other small *Fragilaria*.

Currently, due to the difficulty in observing *Punctastriata* spp. little is known of their individual autoecology, with only their common co-occurrence with small other small *Fragilaria* taxa (e.g. Schmidt *et al.*, 2004; Morales, 2005; Panizzo *et al.*, 2013; Vélez-Agudelo *et al.*, 2017), still providing one of the only insights. An isolated example includes Morales (2005) speculating that *Punctastriata mimetica*, at least, grows optimally in fresh, alkaline waters (179 $\mu\text{S}/\text{cm}$ and 8.2 pH) with low to moderate nutrient content (orthophosphate = 0.129 mg/L and total N = 0.437 mg/L), based on their samples from Dismal River, Nebraska, USA (where a fair amount of the taxon was located; 5-22%). Vélez-Agudelo *et al.* (2017) report similar autoecological affinities (estimated by WA and weighted standard deviation) for *Punctastriata glubokoensis* and *Punctastriata lancettula* from 15 samples along the Colorado River, Patagonia, Argentina.

In this study, the *Punctastriata* spp. observed under SEM for the Garba Guracha core were merged with *Staurosirella pinnata* for the purposes of environmental interpretations due to difficulties in reliably identifying *Punctastriata* spp. under LM and the currently limited usefulness of ecological information gained from separating both taxa. However, further work would be useful in describing the taxonomy and autoecology of these taxa in the Bale Mountains for future work in the region and abroad.

(ii) *Staurosira construens* & *Pseudostaurosira pseudoconstruens*

As Krammer & Lange-Bertalot (1986) note, these taxa are similar in their distinctive cruciform outline. Despite this, some small differences are identifiable: *Pseudostaurosira pseudoconstruens* (Marciniak) D.M. Williams & Round has visible punctae (~2/μm; Marciniak, 1982) and a larger gap in the valve central area between striae than *Staurosira construens* Ehrenberg (Finkelstein & Gajewski, 2008). SEM imagery was used confirm that striae are composed of large, rounded areolae, restricted to the margins, that can sometimes be seen in LM. However, these distinguishing features are of limited use with valves lying in girdle view. Due to these difficulties there may some overlap between these taxa in this study, thus have been merged under *Staurosira construens* for quantitative reconstructions.

4.4 | Numerical methods

Diatom species were transformed into percentage abundances and taxa with <3% relative abundance in the record were omitted for further analyses. Diatom assemblage zones were generated in *rioja* (v. 0.9-14.1; Juggins, 2017) using stratigraphically constrained incremental sum-of-squares cluster analysis

(CONISS; Grimm, 1987), applied to the stratigraphic distribution of all taxa included in plots. A broken stick model (Bennett, 1996) was used to determine the number of significant groups and inform the optimal number of zones to include. Hill's N2 (a measure of species diversity used to calculate the "effective" number of species) and rates of ecological change (RoC; Ureggio *et al.*, 2009) were also calculated using the *rioja* and *paleoMAS* (v. 2.0.1; Correa-Metrio *et al.*, 2012) packages in R to estimate magnitude, rate and timing of ecological change.

(i) Ordination techniques

Ordination techniques are commonly used to summarise fossil data obtained from sedimentary records. By reducing the multidimensionality of these data, these techniques offer the possibility of easier interpretation and inference of potential environmental changes reflected in the assemblage (Birks & Gordon, 1985; Legendre & Legendre, 1998; Orlóci *et al.*, 2006). Correspondence analysis (CA) and principal components analysis (PCA) are multidimensional-rescaling techniques that have been routinely applied in paleoecological studies (Birks & Gordon, 1985).

The first axis scores of a PCA or a CA (including detrended correspondence analysis (DCA): a technique used to suppress arch effect of the latter two; Hill & Gauch, 1980) have often been utilised to summarise spatial and/or temporal ecological change. However, the first axis of a PCA or CA often struggles to fully capture a long or dominant gradient, such as might be expected in temporally-ordered data with progressive change in abundance or composition of organisms. Consequently, scores of the first axis through time may be a poor summary of compositional change (Simpson & Birks, 2012).

Principal curves (PrC; Hastie & Stuetzle, 1989) are a non/semi-parametric alternative to the multivariate analyses above for (palaeo)ecological data (De'eath, 1999; Simpson & Birks, 2012), that is particularly suited to the identification of single or dominant gradients within a sequence. Principal curves are particularly useful as compositional change in time is combined into a single measure as opposed to interpreting variance across multiple axes of a CA or PCA (Figure 4.12). For example, in the Abernethy pollen dataset only interpreting the first PCA axis would represent the change in data between A and B in Figure 4.12 well, but would struggle with B to C, and *vice versa* for the second PCA axis. However, a principal curve reveals a gradient through the data to effectively represent the compositional change through the dataset (Figure 4.12). Recent palaeoecological applications of a PrC has proven their ability to perform well in summarising change through time as well as outperforming more traditional multivariate analyses (e.g. PCA) in terms of variance of data explained (Simpson & Birks, 2012; Bennion *et al.*, 2015a & 2015b, Wiik *et al.*, 2015).

Principal curves were determined for this study using the *analogue* (v. 0.17-0; Simpson, 2007; Simpson & Okansen, 2016) R package. The complexity of smoothing splines were allowed to vary between species, with a penalty (argument controlling *df* in GCV calculations) of 1.4 assigned, following Simpson & Birks (2012). The *vegan* (v. 2.5-2; Okansen *et al.*, 2018) package was utilised for comparative PCA and CA analyses. All ordinations were fitted with square-root transformed assemblage data. The data were merged from the floating and composite cores for the purposes of fitting ordinations on the Babogaya diatom data.

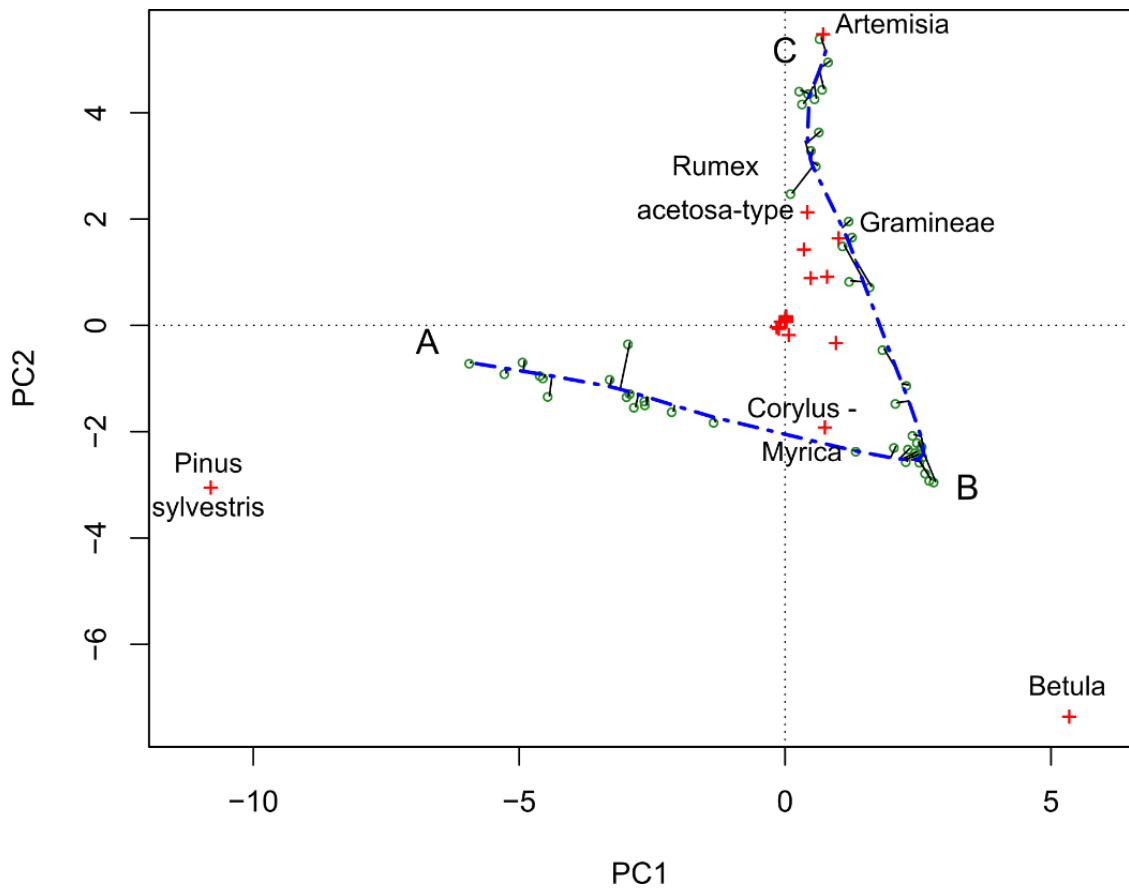


Figure 4.12: Example principal curve through the Abernethy pollen dataset (Birks & Mathewes, 1978), as in Simpson & Birks (2012), created in R.

For both datasets the first CA axis was used as a starting curve to fit the principal curve. The PrC converged after five iterations for Lake Babogaya and ten for Garba Guracha. As in Bennion *et al.* (2015b), the PrC method utilised in this study explains more than both ordination axes which may normally be employed. This gain is marginal for the Garba Guracha dataset. However, for the Babogaya dataset three PCA axes would have to be used to explain a similar variance to distance along the PrC (Table 4.3).

Table 4.3: Variance explained by the PrC compared with PCA/CA axes 1 and 2 for both Lake Babogaya and Garba Guracha. All data have been rounded to 3 decimal places.

	Lake Babogaya	Garba Guracha
PrC	0.548	0.671
PCA Axis 1 / 2 (cumulative)	0.286 / 0.152 (0.439)	0.485 / 0.145 (0.630)
CA Axis 1 / 2 (cumulative)	0.193 / 0.142 (0.335)	0.279 / 0.151 (0.430)

(ii) Quantitative reconstructions using diatoms

In order to quantitatively interpret the diatom record from Garba Guracha the EDDI combined African dataset (East Africa, Niger and North Africa; Gasse *et al.*, 1995) was used in the R package *rioja* (Juggins, 2017) to reconstruct past conductivity. Reconstructions were not performed for the Lake Babogaya fossil dataset due to the abundance (>50% relative abundance in multiple samples) of the newly discovered (thus currently lacking modern analogue data) taxon *Nitzschia fenestralis*.

Classical and inverse deshrinking WA (both with tolerance downweighting also applied) and WA-PLS models (cross-validated with 10,000 bootstrap samples) were created to compare and evaluate their performance. Although the WA model with the greatest predictive power (inverse deshrinking) performed well ($r^2 = 0.792$ and $RMSEP = 0.410$; Table 4.4), the WA-PLS model increased this predictive power with an additional component (p value after randomisation t test = 0.003), and was applied to the Garba Guracha fossil dataset to reconstruct past

conductivity. The standard error for bootstrap estimates for each new sample in the WA-PLS model was low between 1.180 and 1.714 $\mu\text{S}/\text{cm}$.

Further reconstruction diagnostics were performed to evaluate fit of the model to the Garba Guracha fossil data. The minimum distance to the closest modern analogue averaged 31.981 $\mu\text{S}/\text{cm}$, with the maximum sum of taxa in the fossil data not present in the modern data low at 5.21 $\mu\text{S}/\text{cm}$, indicating a good degree of matching between the fossil and modern datasets. If the minimum distance between the fossil assemblage and the modern assemblages is typical of distances between similar assemblages in the calibration set, then the analogue match is considered good.

Although only the usual 'rule of thumb' (see Simpson, 2012 for minor issues when distributions are strongly skewed), the distances shorter than the 5th percentile, and longer than the 10th percentile, of all distances between calibration set assemblages, defines the thresholds between good analogue and no analogue assemblages, respectively (Juggins & Birks, 2012). Similarly, fossil assemblages with a squared residual length compared with the distribution of those of the calibration set against the environmental variable of interest of >90% and >95% may be poorly or very poorly fitted, respectively (Juggins & Birks, 2012).

Table 4.4: Performance statistics for WA and WA-PLS models for conductivity transfer functions using the Garba Guracha fossil diatom data. Units of error/bias are $\mu\text{S/cm}$. toldDW = tolerance down-weighted.

	RMSE	r^2	Average bias	Maximum bias	r^2 (bootstrap)	Average bias (bootstrap)	Maximum bias (bootstrap)	RMSEP	P-value
WA (inverse)	0.352	0.846	-1.110	0.381	0.791	0.016	1.082	0.410	-
WA (classical)	0.382	0.846	-1.074	0.254	0.791	0.019	0.821	0.428	-
WA (toldDW, inverse)	0.320	0.872	-4.193	0.692	0.742	0.035	1.258	0.456	0.920
WA (toldDW, classical)	0.343	0.872	-2.220	0.429	0.743	0.040	1.075	0.473	0.852
WA-PLS 1 Component	0.353	0.846	0.011	0.324	0.791	0.277	1.045	0.411	0.001
WA-PLS 2 Component	0.264	0.913	-0.012	0.179	0.828	0.014	1.150	0.372	0.003
WA-PLS 3 Component	0.214	0.943	0.002	0.136	0.810	0.020	1.080	0.394	0.973
WA-PLS 4 Component	0.182	0.959	-0.004	0.108	0.790	0.180	1.105	0.418	0.997

For this study, the squared residual lengths of the fossil data suggest that only six samples may be poorly fitted to conductivity, with only one considered to be very poorly fitted (Figure 4.13). However, the squared chord distance between fossil and calibration samples suggests multiple samples between 1,000 to 750 cm and 400 cm to 0 cm may lack ‘good’ modern analogues in the African calibration set, with one no analogue situation observable (Figure 4.14). Therefore, additional caution (on top of caution that should be taken with transfer function models; Juggins, 2013) should be taken when interpreting the conductivity estimates in these sections of core.

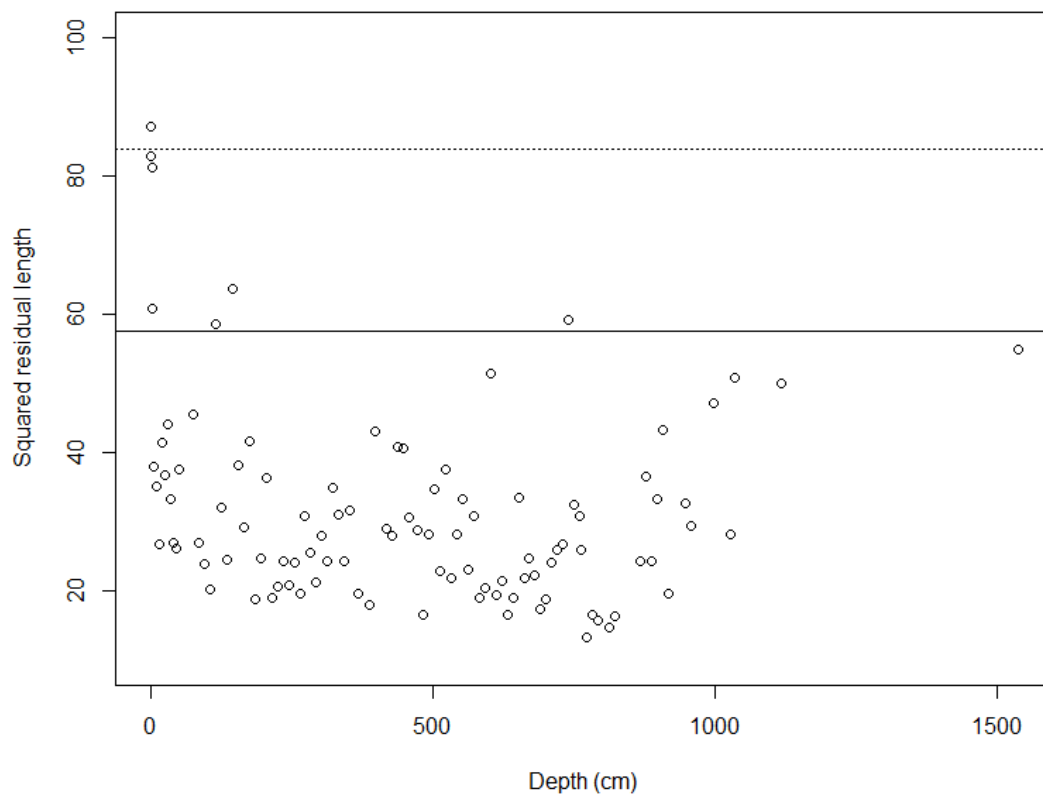


Figure 4.13: Squared residual length for the fossil assemblages down the Garba Guracha core. The solid line marks the 90% limit of the calibration set residual lengths (poorly fitted) and the dotted line marks the 95% limit (very poorly fitted).

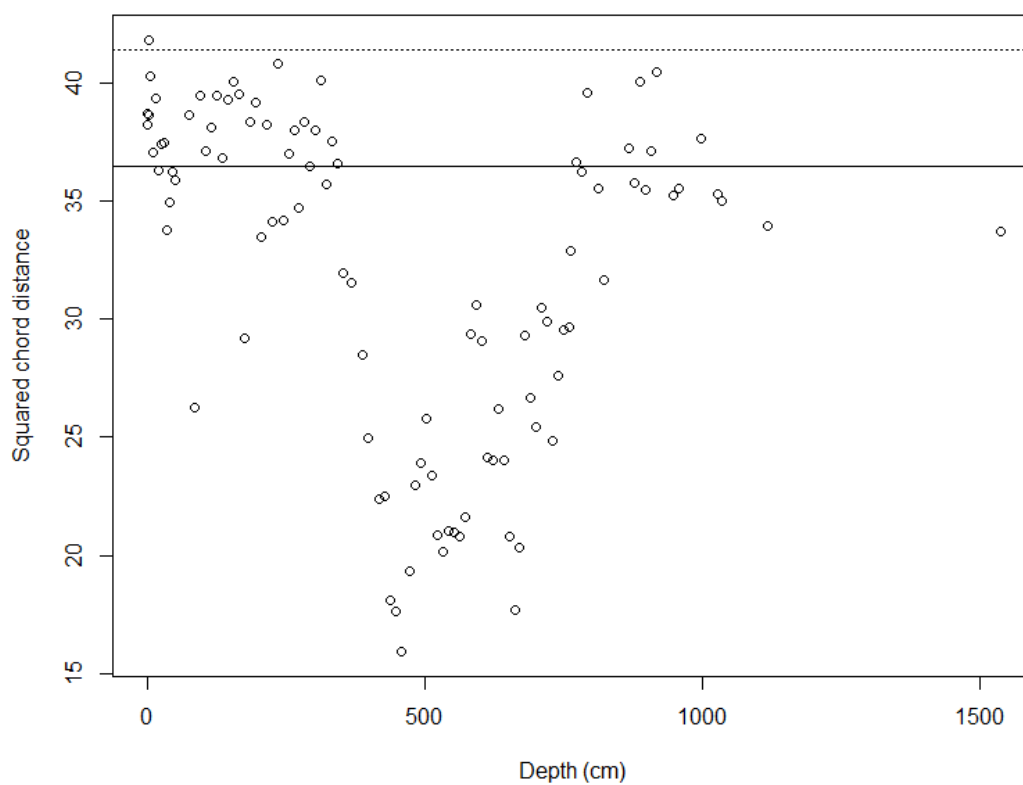


Figure 4.14: Squared chord distance for the fossil assemblages down the Garba Guracha core. The solid line marks the 5th percentile of all distances between calibration set assemblages represent (above this line are poor analogues), and distances greater than the 10th percentile (dotted line) represent no-analogue assemblages.

Chapter 5 :

Constructing the Babogaya composite core depth model

This chapter documents the process of constructing a master splice or composite core from drive sections taken with the UWITEC system (see Chapter 4) by Schäbitz, Lamb *et al.* Due to issues encountered during core retrieval in 2011, the field-estimated depth remained uncertain (see Chapter 4). The author was absent during this field campaign and therefore calculated core depths and descriptions of the issues encountered while coring are based on the field notes of Prof. Schäbitz (University of Cologne). Figure 5.1 summarises the stages in composite correlation. By expanding on the stages of this process, the rationale for the rejection or acceptance of core sections is given in this chapter. Each section of this chapter is divided into the main steps of the procedure and are as follows: (i) initial core description and (ii) XRF-derived geochemistry based on field depths; (iii) using stratigraphic markers and XRF data disregarding field depths; (iv) statistical analyses of XRF data. Through this process field depths were rejected, allowing data from individual core sections to be re-interpreted and overlaps uncovered. This resulted in a composite core stratigraphy, and a floating composite core. As a result, as opposed to field depths, composite depths or meters composite depth (mcd) are given.

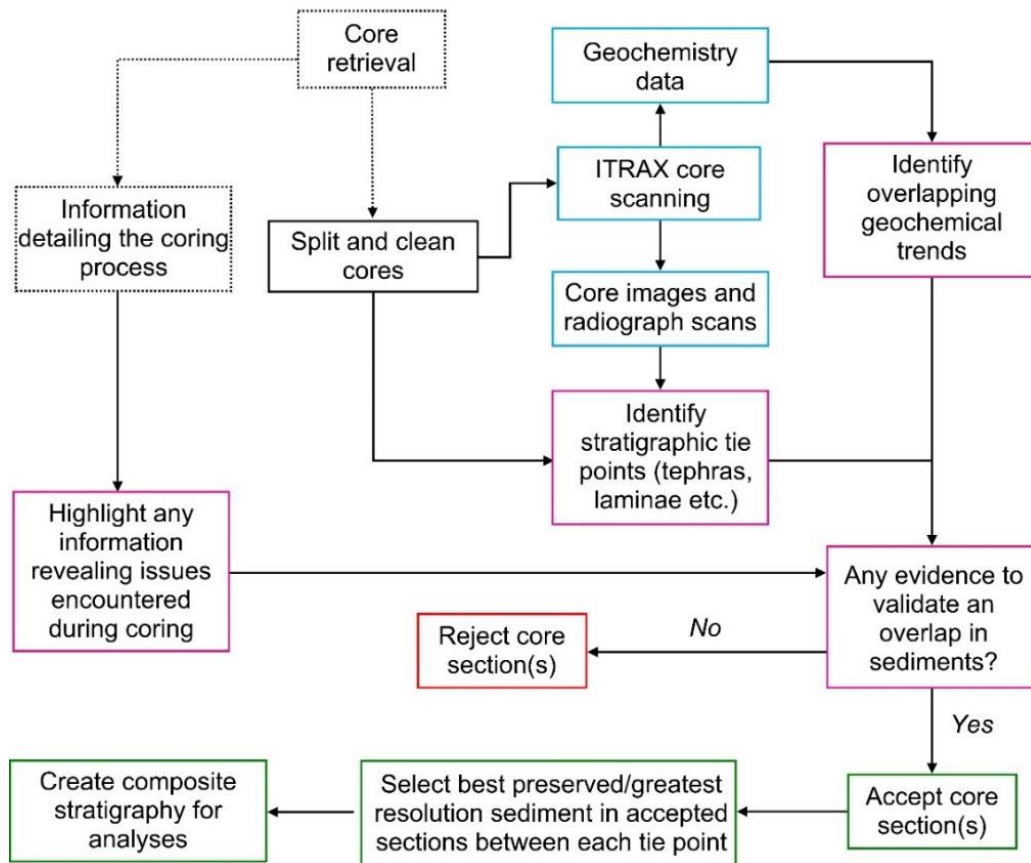


Figure 5.1: Flowchart of determining final core stratigraphy for analysis of the Lake Babogaya core. Dotted boxes/lines represent stages performed during the 2011 fieldwork campaign.

5.1 | Initial core description and section correlation

Cores were first described by changes in colour and through wet smear slide analysis (Aaby & Berglund, 1986) which highlighted stratigraphic markers used to identify section overlaps (e.g. laminae and visible tephra layers). This information was plotted by field depth, to visually display each section within the stratigraphy to aid in correlation (Figure 5.2), and thus to identify potential core overlaps. For example, the patterns of laminated-non-laminated sediments and thick layers of algal matter in sections 1B and 2A highlight a possible overlap. However, despite numerous useful stratigraphic markers, such as the laminated

sections of core (Figure 5.2), complete core correlation based on the field measurements at this stage remained challenging.

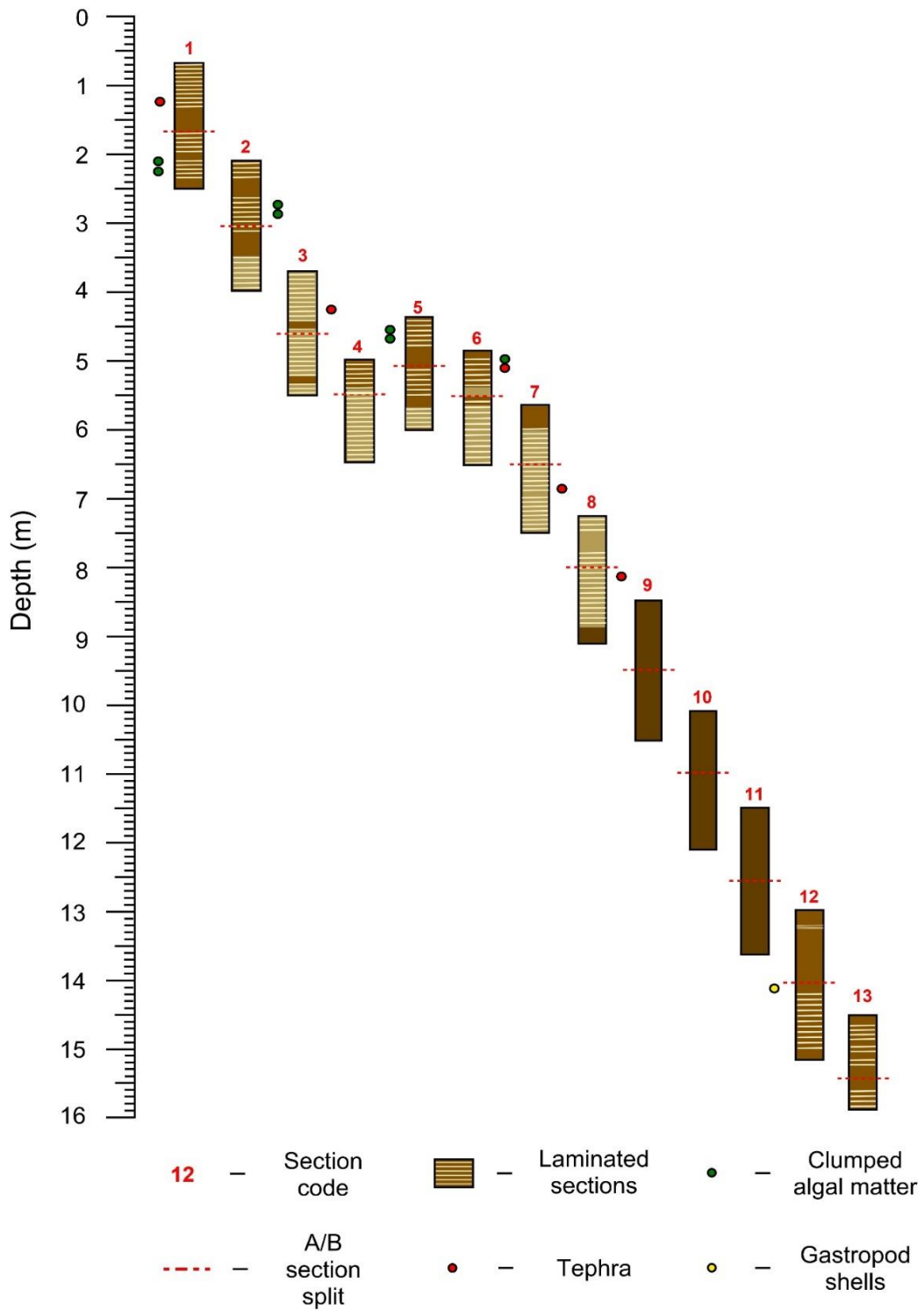


Figure 5.2: Stratigraphy of core BA-LC-2011 plotted against field depth.

5.2 | Section correlation by XRF data

These preliminary attempts at section correlation were aided by XRF-derived geochemical data. Scanning methods can be found in Chapter 4 (Section 4.2.3). An application of a 25-point smoothing of this raw data was used to reduce data noise and to more effectively visualise geochemical trends. Ca and Zr were used at first to visualise changes in the presence of calcium-rich laminae and tephras. Optical and radiograph images were used to identify section overlaps (see below). Magnetic susceptibility measurements, although useful in core correlation, were not obtained, due to malfunctions of the magnetic sensor in the Itrax scanner.

5.3 | Section correlation using visual stratigraphic markers

The CoreWall software suite is an invaluable tool for core stratigraphic correlation and visualisation. In particular, Corelyzer (2.0.4) allows images of core sections to be plotted and compared to other sections in the core (for further software information see Grivna, 2012). This software was used to identify possible overlapping areas based on tephra layers, laminae pattern and sediment colour. However, due to issues reading the dpi of individual core images from the Itrax scanner, the software struggled to accurately display the dimensions of each section, and so was limited to a visualisation tool.

5.3.1 | Matching core stratigraphy to XRF data

Issues with depth control during coring of such a deep lake made it possible that field depths were so inaccurate that field-measured sections were entirely out of sequence. To test this, the field depths were temporarily disregarded, and

section overlaps were sought independent of field depth. Potential tie points were identified by physically comparing possible overlaps based on changes in stratigraphy. Multiple tie points were identified from sections 1A to 8B, based on the presence of distinctive patterns in the laminae, tephra and diatom-rich layers. This revealed that numerous sections towards the top of the core (e.g. Sections 5 and 6) were indeed likely to be considerably out of field order. The XRF data were useful in validating these tie points (e.g. Figure 5.3).

Core overlaps were visually determined from the top of the core to the base of section 8B. Sections 9, 10 and 11 are uniformly brown with no distinguishing visual features. The high-resolution XRF data proved to be useful to validate visual tie points (Figure 5.3), and thus to identify section overlaps for the homogenous, brown sediments. Peaks in the XRF-derived Ti data were especially useful in identifying overlaps between section 8B and 9A (Figure 5.4).

Although a composite core sequence (Sections 1 to 9) was made using initial core descriptions and identifying overlaps in the XRF data, no overlaps were uncovered using these methods between the brown, massive sections 9B and 10A. Furthermore, no overlaps could be found between section 10 and 11, or between the composite core and section 11 leaving a 'floating composite' core (sections 11 to 13) below the composite core and a missing section (section 10) between the two.

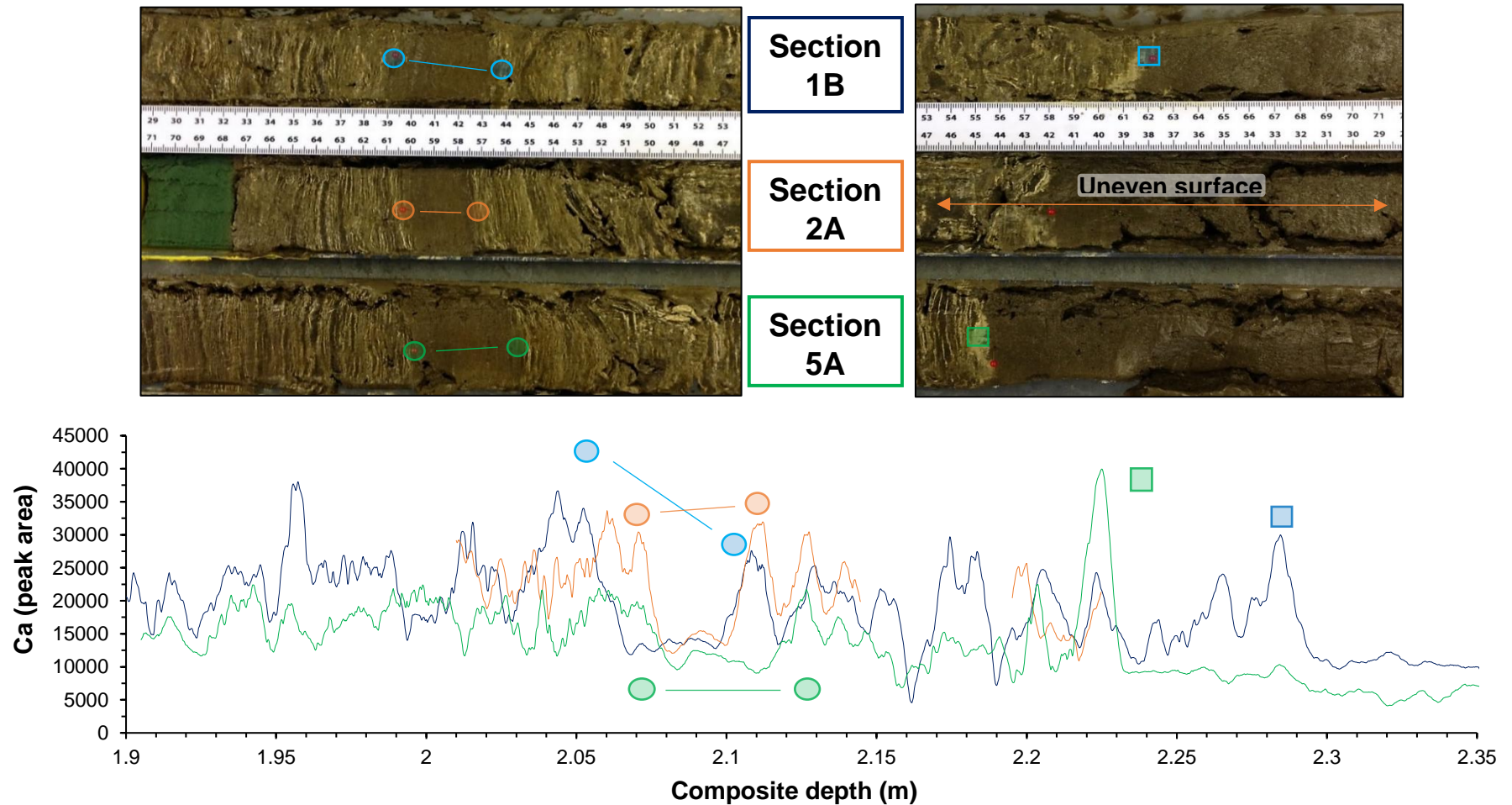


Figure 5.3: Use of XRF in supporting visual core features. Core images (top) and raw, 25-point smoothed XRF-derived trends in Ca (cps; bottom) for section 1B, 2A and 5A. Circles are used to highlight the Ca data associated with the laminated and non-laminated (line) sequences. Squares are used to highlight the abrupt end to laminae. Some data from 2A is unavailable in the XRF record due to an uneven surface.

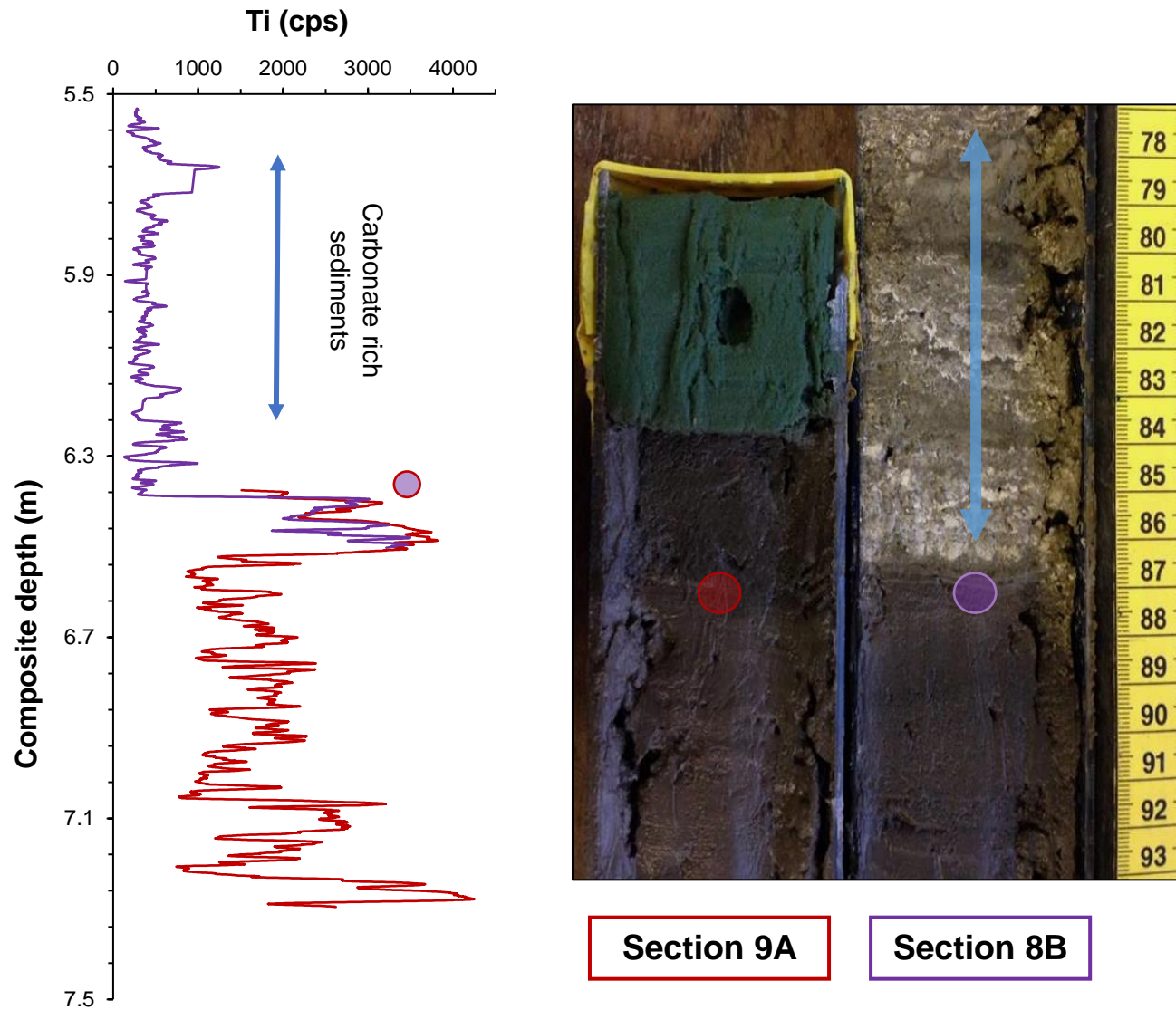


Figure 5.4: Marked peaks in Ti are used to identify an overlap between sections 8B and 9A, following carbonate rich sediments in 8B (blue arrow), in the absence of apparent visual tie points.

5.3.2 | Core section correlation using Dynamic Time Warping

In an attempt to link the composite core, the missing section and the floating core and form a single continuous core Dynamic Time Warping methods (DTW) were used. DTW essentially stretches two time series to determine a common set of points in time such that the sum of the Euclidean distances between corresponding points is as small as possible (Sakoe & Chiba 1978; Müller, 2007). Normally, the DTW function is implemented as a global alignment between time series, i.e. queries the entire series. Sub-sequence matching, also called 'open-begin-end DTW', is achieved by relaxing both the start-point and end-point constraints in a DTW algorithm. As a result, sub-sequence matching determines the contiguous part of a reference time series which optimally fits a query time series, as opposed to assuming all elements must be matched in a global alignment (Sakoe & Chiba 1978; Müller, 2007; Figure 5.5). DTW has been applied in numerous fields (see Giorgino, 2009) including the correlation of multiple overlapping sedimentary sequences to fill gaps in an XRF time series (Trauth *et al.*, 2018).

The implementation of DTW algorithms, including sub-sequence matching, can be achieved in R (R Core Team, 2018) through the dtw package (Giorgino 2009; Tormene *et al.*, 2009). DTW was used to align the normalised Ti records from the base of the composite (section 9B) and the top of the floating core (section 11A) with the missing section of core (section 10) in order to create a full composite BA-LC-2011 core. Potential overlaps between sections 9 and 11 were also tested to explore the possibility that they are contiguous.

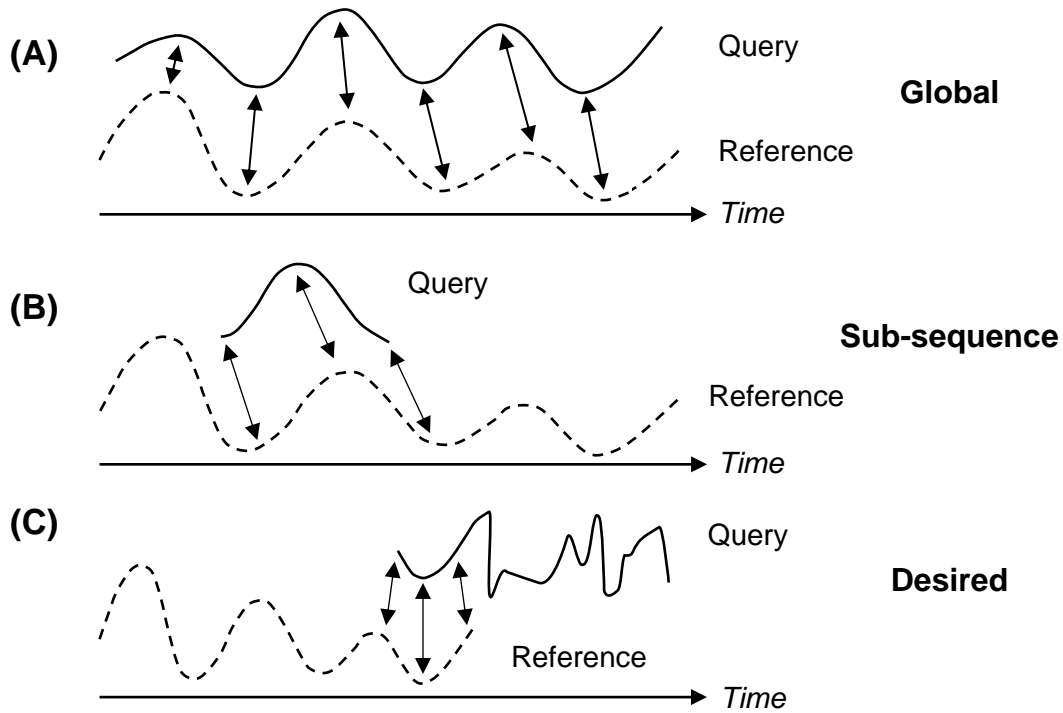


Figure 5.5: Concept of DTW functions for various time series, with dotted and solid lines representing reference and query time series, respectively. (A) Global alignment; (B) sub-sequence DTW between time series. The ideal scenario for this study would be that an overhang of data overlaps with the end of the core can be identified, but without assuming that the entirety of the query must fit a part of the reference series which is generally more uncommon (C). Arrows denote aligned points. Adapted from Müller (2007).

Fundamentally, a sub-sequence DTW will determine the optimal path for the **entire** query sequence within the reference series as shown in Figure 5.5. However, in the context of overlapping core sections it is assumed that some, if not most, of the query time series (section 10) does not overlap with the reference series (sections 9 and 11), similar to Figure 5.5c. To fully test for potential overlapping sections, the query time series was limited to the top of a section. Fundamentally, this method uses a cost-matrix to locate the most efficient path to determine the most similar points between two time series.

The DTW determined some matches between 9B and 10 (Figure 5.6a). The starting point of this match is most likely as a sub-set of the first 750 points of 10A identified the same point as the most optimal match in the sequence (Figure 5.6b). As section 10B immediately follows 10A, the initial DTW was extended to include the entirety of section 10 (Figure 5.6c) and finds a matching path between section 10 and 9B. Under the assumption that section 11A is below sections 9 and 10, and overlaps with one of these sections, a DTW was run for the last 500 points of sections 9B (Figure 5.6d) and 10B (Figure 5.6e) against 11A. However, this shows that any overlap would be in the lower half of section 11A, leaving the upper half of 11A uncorrelated. This leaves the original possibility of a gap between the composite and floating cores. Therefore, despite determining an optimal path and locating some similarities between sections, it is apparent that no meaningful overlaps between the composite and floating cores could be statistically determined with DTW techniques (Figure 5.6).

5.4 | Conclusion: final composites

Through a combination of identifying visual tie points and common geochemical patterns, sections 2 and 4 were omitted from the composite stratigraphy; these sections were badly preserved (e.g. section 2B; Figure 5.3) or damaged by the magnetic susceptibility sensor (section 4B) and were not needed given the evident overlaps in other sections. Sections 1A to 9B are treated in this study as the full composite core (Table 5.1; Figure 5.7). Despite overlaps through sections 11 to 13B (floating core), no overlaps could be identified linking the floating composite with section 9 and thus the rest of the composite to form a single, continuous core.

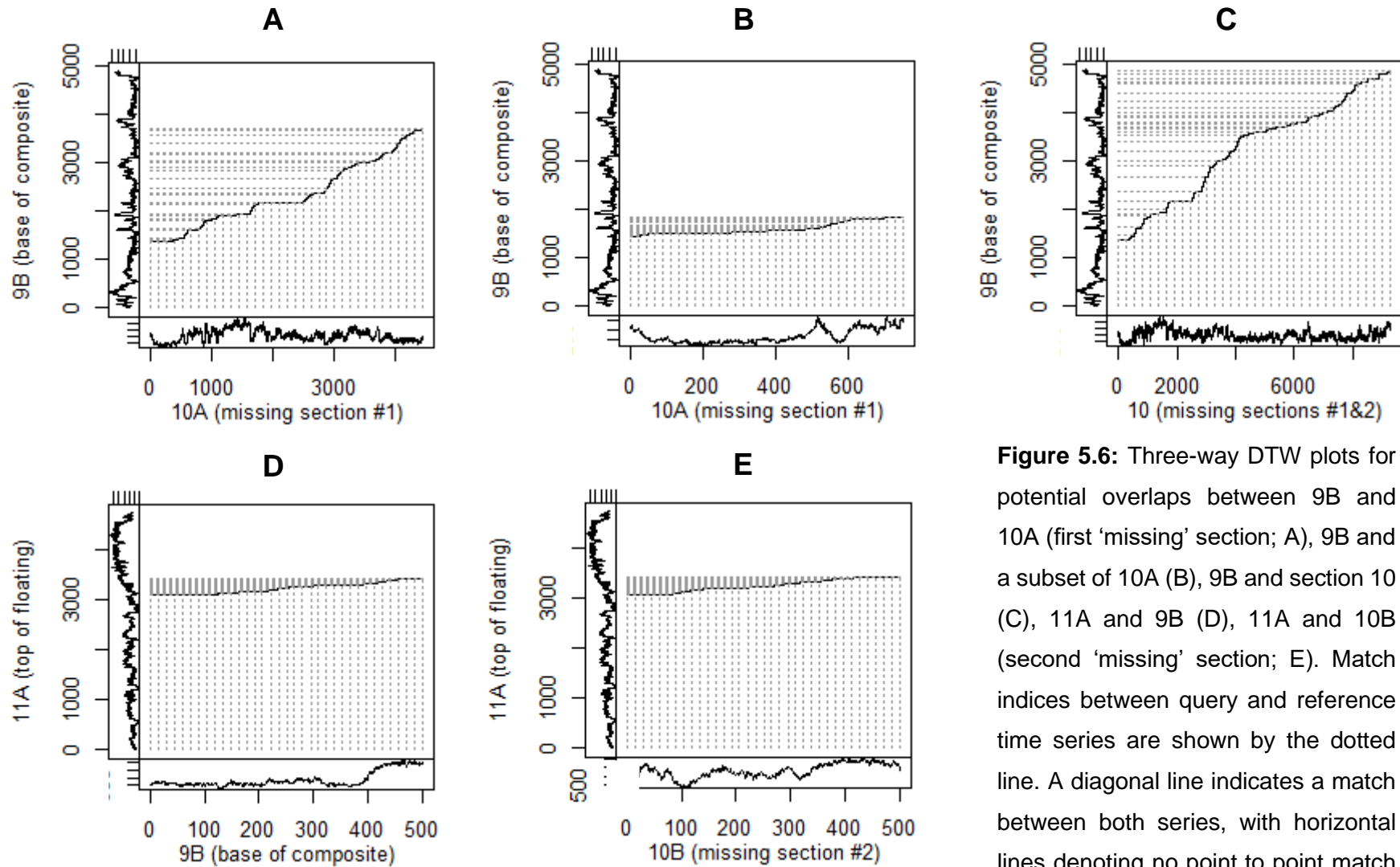


Figure 5.6: Three-way DTW plots for potential overlaps between 9B and 10A (first 'missing' section; A), 9B and a subset of 10A (B), 9B and section 10 (C), 11A and 9B (D), 11A and 10B (second 'missing' section; E). Match indices between query and reference time series are shown by the dotted line. A diagonal line indicates a match between both series, with horizontal lines denoting no point to point match in the query series with the reference.

Table 5.1: Visual and geochemical tie points identified to create a composite.

	Section	Depth in section (cm)	Composite depth (cm)	Visual / stratigraphic marker	Geochemical marker																																																				
<i>Tie point 1</i>	1B	39.16	205.915	Laminated section and beginning of small non-laminated, brown section	Ti																																																				
	5A	21.30				<i>Tie point 2</i>	5B	2.36	252.975	Black band adjacent to a laminated section	Ti	6A	11.52	<i>Tie point 3</i>	6B	60.96	368.815	Black line between yellowy-green oozes	Ti	7A	79.60	<i>Tie point 4</i>	7B	34.98	410.985	Tephra	K and Mn	3A	54.26	<i>Tie point 5</i>	3B	45.54	491.265	Bright white lamina between a dark line and green/orange coloured oozes	Ca	8A	13.88	<i>Tie point 6</i>	8B	87.32	639.025	-	Ti	9A	9.225	<i>Tie point 7</i>	11B	90.66	?	Base of minerogenic unit	Ti	12A	12.82	<i>Tie point 8</i>	12B	92.48	?
<i>Tie point 2</i>	5B	2.36	252.975	Black band adjacent to a laminated section	Ti																																																				
	6A	11.52				<i>Tie point 3</i>	6B	60.96	368.815	Black line between yellowy-green oozes	Ti	7A	79.60	<i>Tie point 4</i>	7B	34.98	410.985	Tephra	K and Mn	3A	54.26	<i>Tie point 5</i>	3B	45.54	491.265	Bright white lamina between a dark line and green/orange coloured oozes	Ca	8A	13.88	<i>Tie point 6</i>	8B	87.32	639.025	-	Ti	9A	9.225	<i>Tie point 7</i>	11B	90.66	?	Base of minerogenic unit	Ti	12A	12.82	<i>Tie point 8</i>	12B	92.48	?	End of laminated section to brown sediments	Ca	13A	17.18				
<i>Tie point 3</i>	6B	60.96	368.815	Black line between yellowy-green oozes	Ti																																																				
	7A	79.60				<i>Tie point 4</i>	7B	34.98	410.985	Tephra	K and Mn	3A	54.26	<i>Tie point 5</i>	3B	45.54	491.265	Bright white lamina between a dark line and green/orange coloured oozes	Ca	8A	13.88	<i>Tie point 6</i>	8B	87.32	639.025	-	Ti	9A	9.225	<i>Tie point 7</i>	11B	90.66	?	Base of minerogenic unit	Ti	12A	12.82	<i>Tie point 8</i>	12B	92.48	?	End of laminated section to brown sediments	Ca	13A	17.18												
<i>Tie point 4</i>	7B	34.98	410.985	Tephra	K and Mn																																																				
	3A	54.26				<i>Tie point 5</i>	3B	45.54	491.265	Bright white lamina between a dark line and green/orange coloured oozes	Ca	8A	13.88	<i>Tie point 6</i>	8B	87.32	639.025	-	Ti	9A	9.225	<i>Tie point 7</i>	11B	90.66	?	Base of minerogenic unit	Ti	12A	12.82	<i>Tie point 8</i>	12B	92.48	?	End of laminated section to brown sediments	Ca	13A	17.18																				
<i>Tie point 5</i>	3B	45.54	491.265	Bright white lamina between a dark line and green/orange coloured oozes	Ca																																																				
	8A	13.88				<i>Tie point 6</i>	8B	87.32	639.025	-	Ti	9A	9.225	<i>Tie point 7</i>	11B	90.66	?	Base of minerogenic unit	Ti	12A	12.82	<i>Tie point 8</i>	12B	92.48	?	End of laminated section to brown sediments	Ca	13A	17.18																												
<i>Tie point 6</i>	8B	87.32	639.025	-	Ti																																																				
	9A	9.225				<i>Tie point 7</i>	11B	90.66	?	Base of minerogenic unit	Ti	12A	12.82	<i>Tie point 8</i>	12B	92.48	?	End of laminated section to brown sediments	Ca	13A	17.18																																				
<i>Tie point 7</i>	11B	90.66	?	Base of minerogenic unit	Ti																																																				
	12A	12.82				<i>Tie point 8</i>	12B	92.48	?	End of laminated section to brown sediments	Ca	13A	17.18																																												
<i>Tie point 8</i>	12B	92.48	?	End of laminated section to brown sediments	Ca																																																				
	13A	17.18																																																							

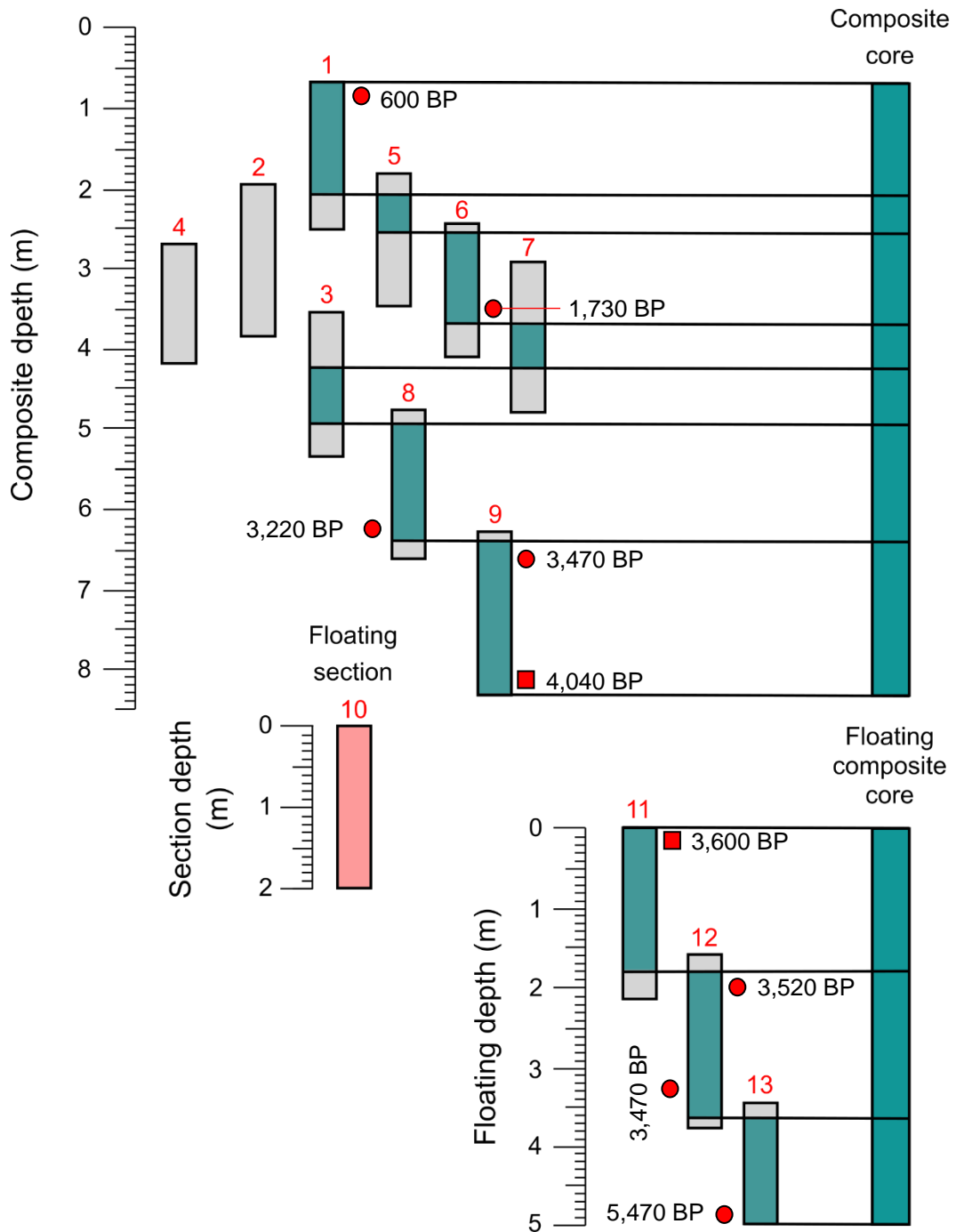


Figure 5.7: BA-LC-2011 sections (numbered in red) plotted by composite depth. Section overlaps are highlighted (blue) which led to the formation of the composite core, with sediment unused in the composite shown as grey. Section 10 is shown in red highlighting the uncertainty associated with the position of this section within the stratigraphy. Radiocarbon sample locations (and the calibrated results) are denoted by red circles (accepted dates in the age-depth model) and squares (dates omitted from the age-depth model).

Chapter 6 :

Results - Lake Babogaya

This chapter focuses on the palaeolimnological record from Lake Babogaya. All data are presented from the composite and floating composite cores (outlined in Chapter 5) separately. The lithological and chronological framework is presented, which facilitates the detailed description of the results of geochemical and diatom analyses. As discussed in Chapter 5, it is assumed that the floating composite continues below the composite core. Thus, the records from both these cores are then interpreted together to reconstruct changes at Lake Babogaya through the Holocene.

6.1 | Core lithology

Three main lithostratigraphical units are identified in BA-LC-2011 based on variations in composition and physical properties of the sediment layers (Figs. 6.1 and 6.2).

6.1.1 | Composite core (0.68 – 8.30 m)

Unit I (830 cm – 650 cm) at the base of the composite core is characterised by minerogenic brown sediments comprising of predominantly clay (<4 µm)-silt (4-62.5 µm) sized siliciclastic material. Carbonate material is also common in this unit mainly in the form of aragonite. Occasional circular, yellowish sediment clusters (~0.5 cm diameter), rich in diatoms, are present within this unit.

Following an abrupt (~5 mm) transition from Unit I, the sediments of Unit II are diatom-rich, carbonate muds with pulpy laminae. Laminae consist of alternating

light white and darker, brown layers, with some pulpy. Lighter sediments are composed of microscopic (~5-10 µm), rice-grain shaped aragonite crystals, with diatoms common and calcite present but rare. Darker layers are more diverse in composition, with less aragonite and greater organic matter content and diatoms. However, it is important to note that non-laminated sections, similar in both colour and composition to the darker lamina described above, are present throughout the unit, varying in size with the largest non-laminated section ~50 cm thick towards the top of the core. The light-dark laminae of sub-unit IIa (650 – 330 cm) are frequently coupled with pulpy, yellow/green laminae, and are predominantly composed of *Synedra*.

Between 3.30 m and the core top (0.68 m; Unit IIb), the white laminae are comparatively thinner and lack any obvious, accompanying pulpy laminae as are present in Unit IIa. Furthermore, the laminated sections are more fragmented by large non-laminated, brown sections of sediment than below (Figure 6.1). Silt-sized siliciclastic material is observable throughout this unit but is rare, and only common in the darker coloured sediments, and composed of predominantly quartz. Indeterminate clay sized particles are present throughout, and are likely micro-carbonates based on the surrounding content and high birefringence properties.

Multiple light grey tephra layers are present within this unit of predominantly silt (2.72-2.722 m; BAT-2), and silt to sand sized grains (5.735-5.745 m, 4.18-4.19 m, 1.265-1.275 m; BAT-4, BAT-3 and BAT-1, respectively). Based on preliminary geochemical analyses by C. Martin-Jones at Cambridge University (unpub data.), the source of BAT-1, BAT-2 and BAT-4 can be tentatively correlated to the Boset volcanic complex, east of Bishoftu, with the BAT-1 tephra likely

associated with a large eruption leaving a deposit (known as the “Boset pumice”) as much as 20 cm thick in nearby Adama (Fontijn *et al.*, 2018; Martin-Jones unpub. data). The provenance of BAT-2 remains unknown but with Corbetti as the likely source due to similar (in terms of colour, texture and geochemistry) tephra layers dated from lakes Chamo and Tilo (Martin-Jones *et al.*, 2017; Martin-Jones pers. comm.).

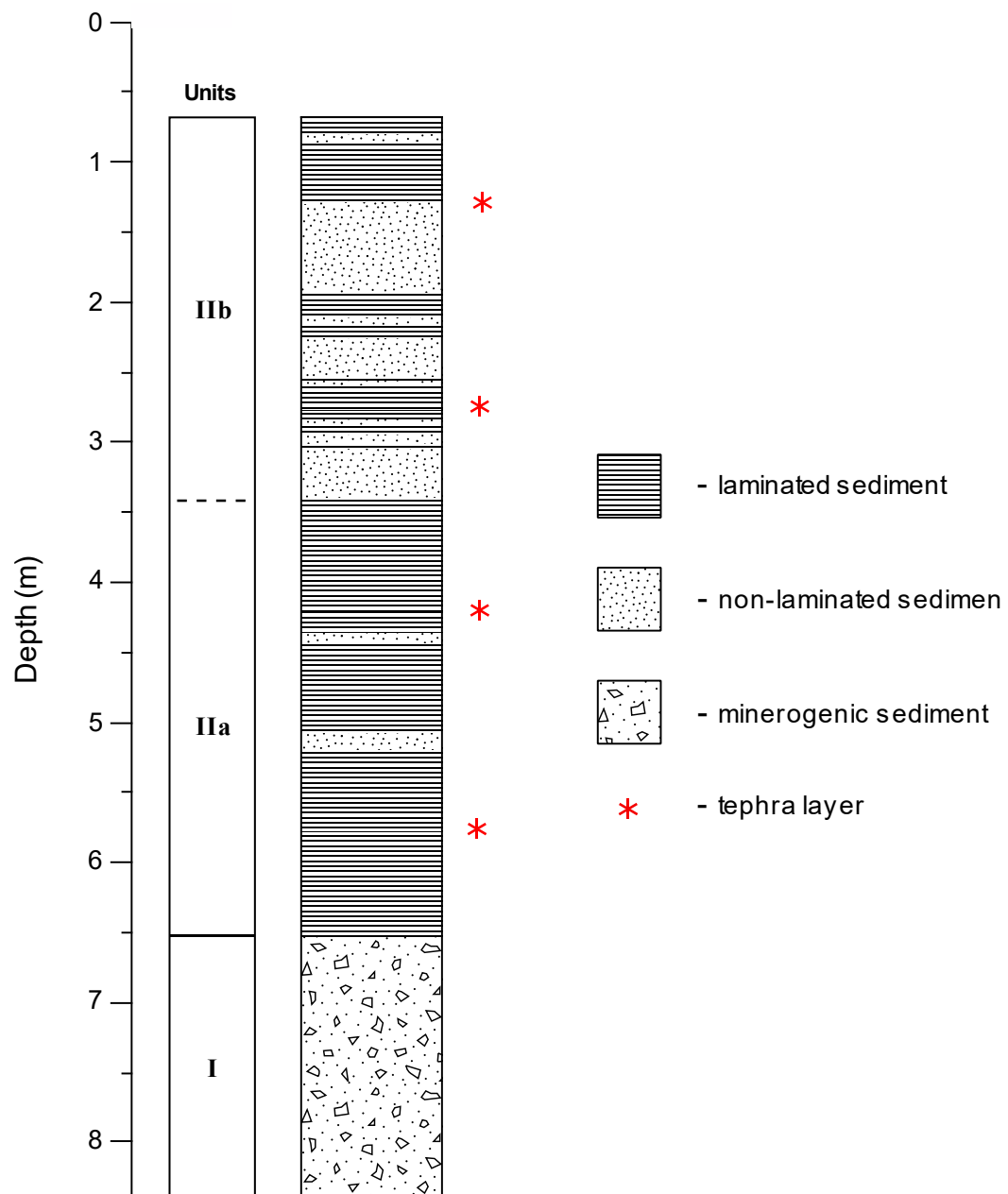


Figure 6.1: Lake Babogaya composite core lithology.

6.1.2 | Floating core

Unit A (470–199 cm) is composed of stiff, partially laminated sediments (Laminae Type 3), similar to the light-dark laminae in Unit II of the composite core with carbonates and diatoms abundant throughout. Occasionally light-dark layers are accompanied by pulpy, green-blue layers. In lighter layers, aragonite is the main form of carbonate, with sub-rounded, ellipsoid calcite grains and calcified loricae of the green algae *Phacotus* abundant, the laminae of the composite core, especially in greyer sediments where these forms of carbonates are common. Like the sediments of the composite core, indeterminate clay sized material are present throughout, and is also likely formed of micro-carbonates based on the surrounding high carbonate content and high birefringence properties. At a depth of 2.7 m, there is a gradual transition from laminated to non-laminated sediments. A distinct heliciform gastropod shell layer is present ~1-2 cm above this transition. Laminated sediments for 6 cm, similar in composition to laminae to Unit IIb of the composite core, mark the top of this unit. At the base of this laminated section (~185 cm) is a 6 cm light grey band rich in diatoms, *Phacotus* loricae and carbonates. One discrete tephra layer (<2 mm) was detected with the aid of XRF-derived Rb and Y data (see below) at ~366 cm depth. As this layer was only discovered following interrogation of the XRF data and could not be sampled along with the tephtras in the composite core, the geochemistry of this layer is now currently being determined by C. Martin-Jones of Ghent University and Cambridge University.

The brown minerogenic sediment described in Unit A of the composite core continues through the top ~2 m of the floating section (Unit B; Figure 6.2), following a sharp transition from Unit A (<1 mm). Small sections of sediment differ

from this with three small (1-3 cm) layers of yellow-brown and orange carbonate and diatom-rich sediment in BA-LC-2011 11A.

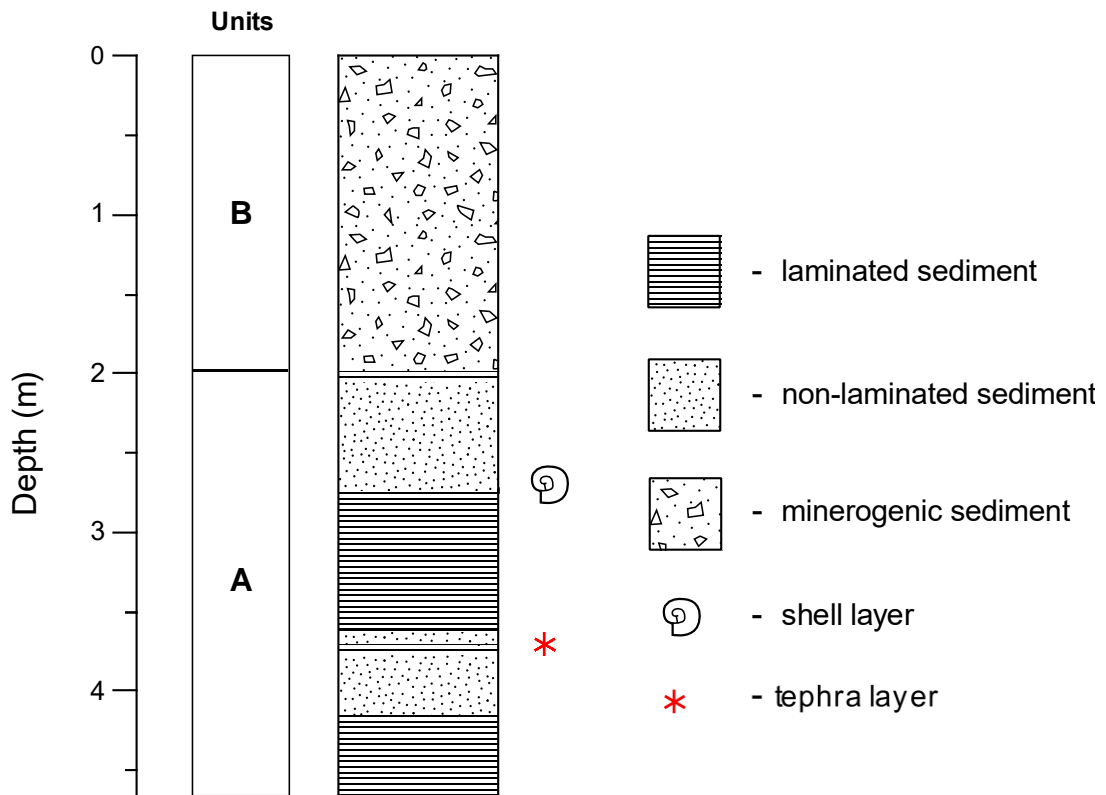


Figure 6.2: Lake Babogaya floating composite core lithology.

6.2 | Chronology

Nine AMS ^{14}C dates were obtained on micro-charcoal from the Babogaya core (Table 6.1). The stratigraphically conformable dates show that the core (including both composite and floating cores) covers the period from ~5,500-600 cal yr BP. P-45150 and P-45149 were omitted from the chronology as these dates are thought to be out of sequence. The alternative would be to reject P-46195, from the top of the floating composite core. However, P-46195 was sampled from laminated sediments which are assumed to be more reliable than the non-laminated, minerogenic sediments at the base of the composite core and top of the floating core (see interpretations of XRF data below) which may be

disturbed/reworked. The age/depth diagram using these dates for the composite and floating cores are show in Figure 6.3 and Figure 6.4, respectively.

Table 6.1: AMS radiocarbon chronology for Lake Babogaya composite and floating cores (* omitted dates). Radiocarbon ages were calibrated in CALIB (v. 7.1; Stuiver & Reimer, 1993) using the IntCal13 calibration curve (Reimer *et al.*, 2013).

	Samples			¹⁴ C age	Calibrated age (cal. BP)	
	Depth in core (cm)	Lab. Code	¹³ C/ ¹² C ratio (‰)	Conventional age (¹⁴ C yrs BP)	Calibrated age 2-σ range (relative area under probability distribution)	Calibrated age median probability (nearest 10 years)
Composite	68-73	P-44532	-16.25	620 ± 40	545 – 662 (100%)	600
	358.9-366.9	P-46194	-13.95	1799 ± 27	1692 – 1818 (84%)	1730
	632.7-637.7	P-44533	-14.70	3025 ± 70	3020 – 3376 (99.2%)	3220
	652.8-658.8	P-44534	-23.89	3240 ± 180	2985 – 3901 (100%)	3470
	814-824*	P-45149	-17.9	3699 ± 33	3964 – 4102 (86%)	4040*
Floating	7-17*	P-45150	-14.73	3356 ± 27	3556 – 3646 (87%)	3600*
	197-202	P-46195	-14.11	3287 ± 28	3542 – 3573 (100%)	3520
	329.5-334.5	P-46196	-15.12	4295 ± 60	4802 – 5044 (84.6%)	4870
	462-467	P-44536	-14.19	4725 ± 50	5441 – 5584 (61.4%)	5470

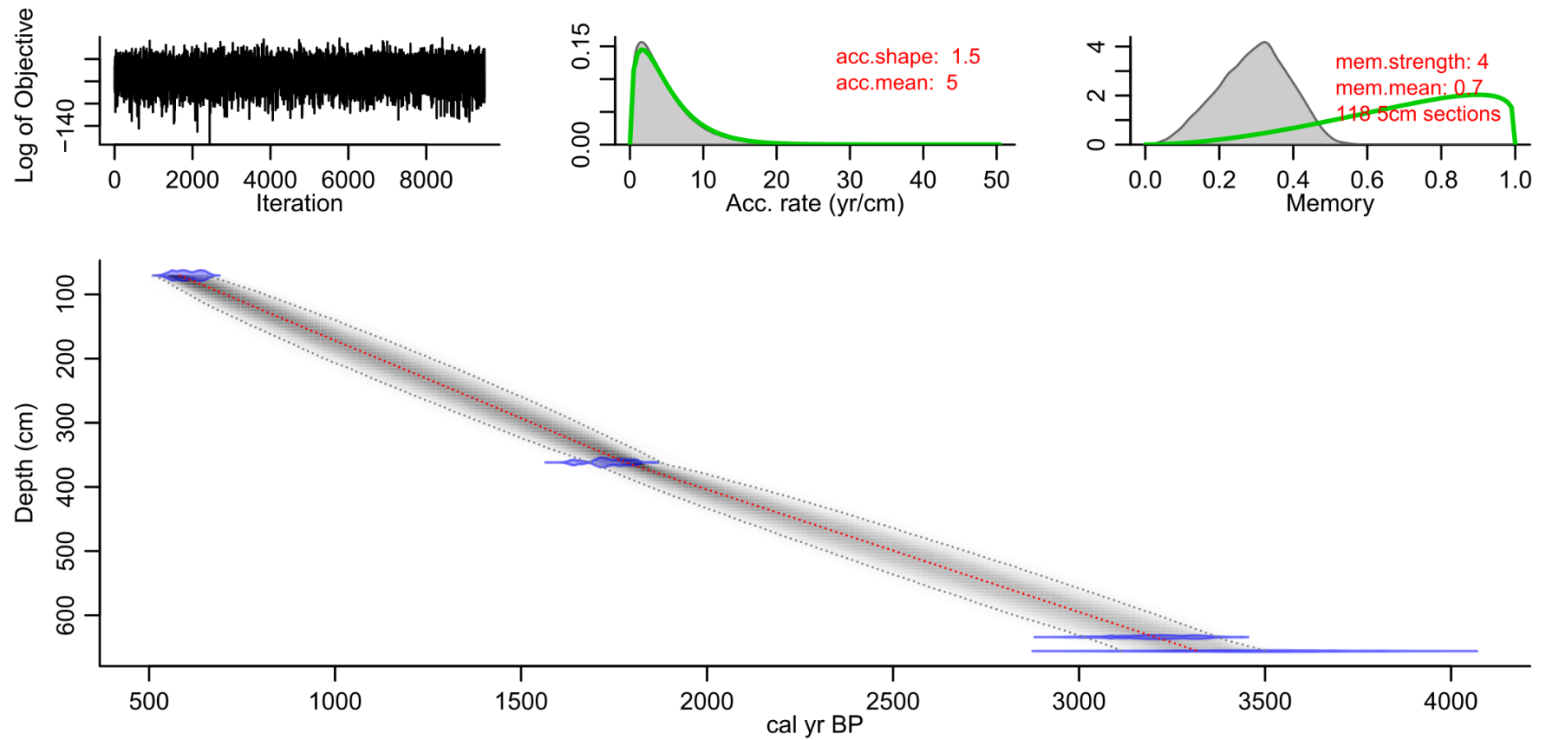


Figure 6.3: Bayesian age-depth model of four micro-charcoal AMS ^{14}C dates from composite Babogaya core, constructed in BACON for R. Depth refers to depth below the start of the composite sequence. The individual age distribution for each date, as relative area under probability distribution, is shown in blue. The red dotted line shows the most likely age-depth distribution, whilst the grey envelope denotes the chronological uncertainty of the model. The upper panel shows the stability of the Markov Chain Monte Carlo runs (3500 iterations); the prior (thick line) and posterior (thin line) distribution for the accumulation rate (yr/cm), and; the prior (thick line) and posterior (thin line) for the dependence of accumulation rate between sections.

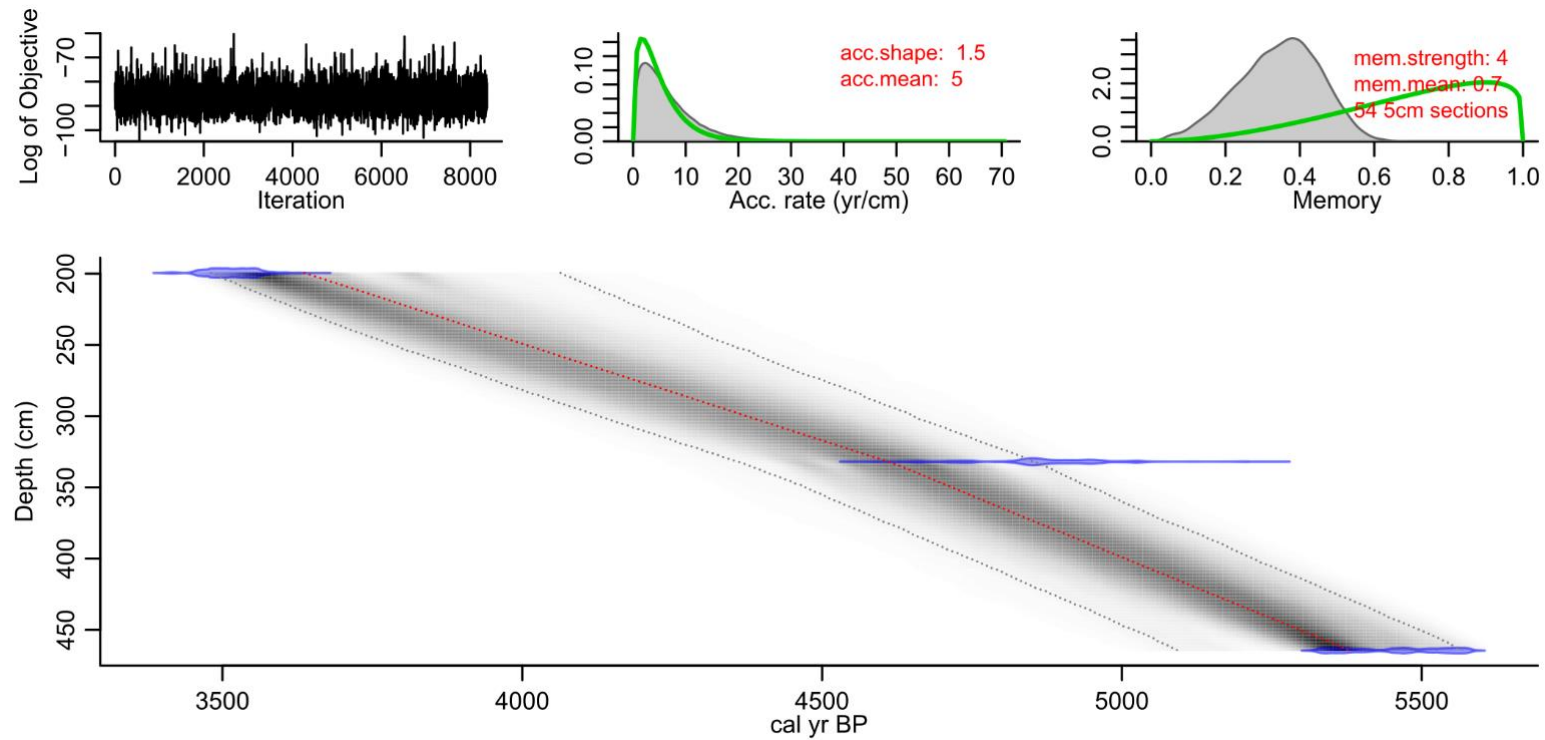


Figure 6.4: Bayesian age-depth model of three micro-charcoal AMS ^{14}C dates from the floating composite Babogaya core, constructed in BACON for R. Depth refers to depth below the start of the floating composite sequence. The individual age distribution for each date, as relative area under probability distribution, is shown in blue. The red dotted line shows the most likely age-depth distribution, whilst the grey envelope denotes the chronological uncertainty of the model. The upper panel shows the stability of the Markov Chain Monte Carlo runs (3500 iterations); the prior (thick line) and posterior (thin line) distribution for the accumulation rate (yr/cm), and; the prior (thick line) and posterior (thin line) for the dependence of accumulation rate between sections.

6.3 | Core chemistry

High-resolution plots of selected XRF-derived geochemistry and organic isotope data are shown in Figure 6.5 for the composite core and Figure 6.7 for the floating composite core. The plots are divided into 2 major zones in the composite core (BAXC-1, BAXC-2) and 2 major zones in the floating core (BAXF-1, BAXF-2) based on large changes in at least two elements. All units for XRF data are given as normalised peak area (hereafter simply peak area; /Mo Inc+Coh see Chapter 4 for details on normalisation process), with the ratio plots dimensionless. The solid black line represents a 500-point smoothing of the data to highlight more general trends.

Correlation matrices for the composite (Figure 6.6) and floating composite (Figure 6.8) cores show that lithogenic elements (Fe, Zr, K, Rb, Ti, Si) mostly correlate strongly, positively in both the composite ($r = 0.69$ to 0.99) and floating core ($r = 0.76$ to 1) and can be seen to covary in Figure 6.5 and Figure 6.6. The elements on the lower range of these correlations include Zr to Fe, Si, and Ti in the composite core and Si to Zr and Rb in the floating core (Figure 6.7; Figure 6.8). This positive correlation amongst lithogenic elements also extends to Mn with r -values of >0.65 (up to $r = 0.95$; Figure 6.7; Figure 6.8). However, Ca is weakly, positively correlated to other lithogenic elements in the composite core ($r = -0.01$ to 0.25) and weakly, negatively correlated to these elements in the floating core ($r = -0.24$ to 0.02). Values of elements such as Rb (0-0.049 peak area across both cores) are low in comparison to elements such as Fe (0.011-8.822 peak area). However, the high correlation of these lower value elements with other lithogenic elements indicate that the data are 'real'. Distinct peaks of

elements such as Rb and to some extent Fe (others such as Y not shown in Figure 6.5 and Figure 6.7) correlate with visible tephra layers.

Total organic carbon (TOC) through the entire core varies from 0.18 to 19.28 %. Low TOC (0.18-3.37 % in the composite core and 0.27-6.78 % in the floating core) occurs within the minerogenic sedimentary unit spanning from the base of the composite core through to 2 m depth into the floating core. The C:N ratios are generally around 13 to 14, but fall as low as a minimum of 5.13 and increase up to a maximum of 21.25, through the core. Similarly, $\delta^{13}\text{C}_{\text{org}}$ varies between –29.60 and –13.94 ‰. However, the higher end of this range is represented by the only sample above –20 ‰, with values generally between –23 to –26 ‰ through the core (Figure 6.5; Figure 6.7).

6.3.1 | Composite core data

BAXC-1: 828 – 646 cm (<3500 – 3260 cal. BP)

As the high r^2 values would suggest (Figure 6.7), Fe, Ti and Rb covary and are variable through this zone, with these elements on average at their highest throughout this zone (3.00, 0.09 and 0.02 respectively) with multiple peaks in peak area. This is especially true at the zone boundary where maximum values are reached for Fe (7.78) and Ti (0.26). Conversely, TOC is low BAXC-1 at an average of $1.72\% \pm 0.86$, reaching the lowest TOC at the upper zone boundary (0.18%). However, the values of $\delta^{13}\text{C}_{\text{org}}$ and C:N remain stable at $-20\text{‰} \pm 0.83$ and 11.99 ± 1.90 , respectively, for the entire zone. Similarly, logged ratio values remain low and stable in comparison to values up core in BAXC-2 for Fe:Mn (1.89 ± 9.52), Ca:Ti (0.69 ± 2.40), Zr:Rb (0.24 ± 0.56) and Si:Ti (-1.09 ± 0.02) for the entire zone. Interestingly, Ca also remains consistent and as a result, while

this zone does not have maximum Ca values for the composite core, Ca on average is higher in zone 1 (0.41 ± 0.15 peak area) than in zone 2 (see below).

BAXC-2: 644 – 68 cm (3260 – 580 cal. BP)

Terrigenous element content decreases sharply at the lower zone boundary. Fe, Ti and Rb continue to visibly covary but are now mostly low on average (Fe = 1.505 ± 0.419 , Ti = 0.011 ± 0.015 , Rb = 0.004 ± 0.004) in comparison to the values in zone 1, with a few peaks covarying with visual tephra layers (127 cm, 272 cm, 418 cm and 575 cm) which contain the highest Rb (and some of the highest values of Fe for example) in this zone, and the maximum peak area in the core (0.050 peak area).

At the zone boundary, TOC sharply increases from 0.18% to 4.10% within 8 cm. TOC increases slightly to ~10%, and except for between 187 and 111 cm where TOC sharply decreases to low TOC (<7.5%, as low as 3.47%), the TOC fluctuates for the rest of the zone between around 16% to around 8%, normally within one or two samples. Similarly, $\delta^{13}\text{C}_{\text{org}}$ fluctuates between -30‰ and -20‰ , with consistently higher values between 187 and 111 cm ($-22.4\text{‰} \pm 0.87$ on average) one sample above -20‰ (-13.94‰) at 572 cm. Conversely, after decreasing to minimum values (5.13) on the zone boundary, C:N rapidly increases to 13.75 and then fluctuates minimally with the zone average value at 15.18 ± 1.68 , slightly higher than the C:N values in zone 1 (13.36 ± 1.78).

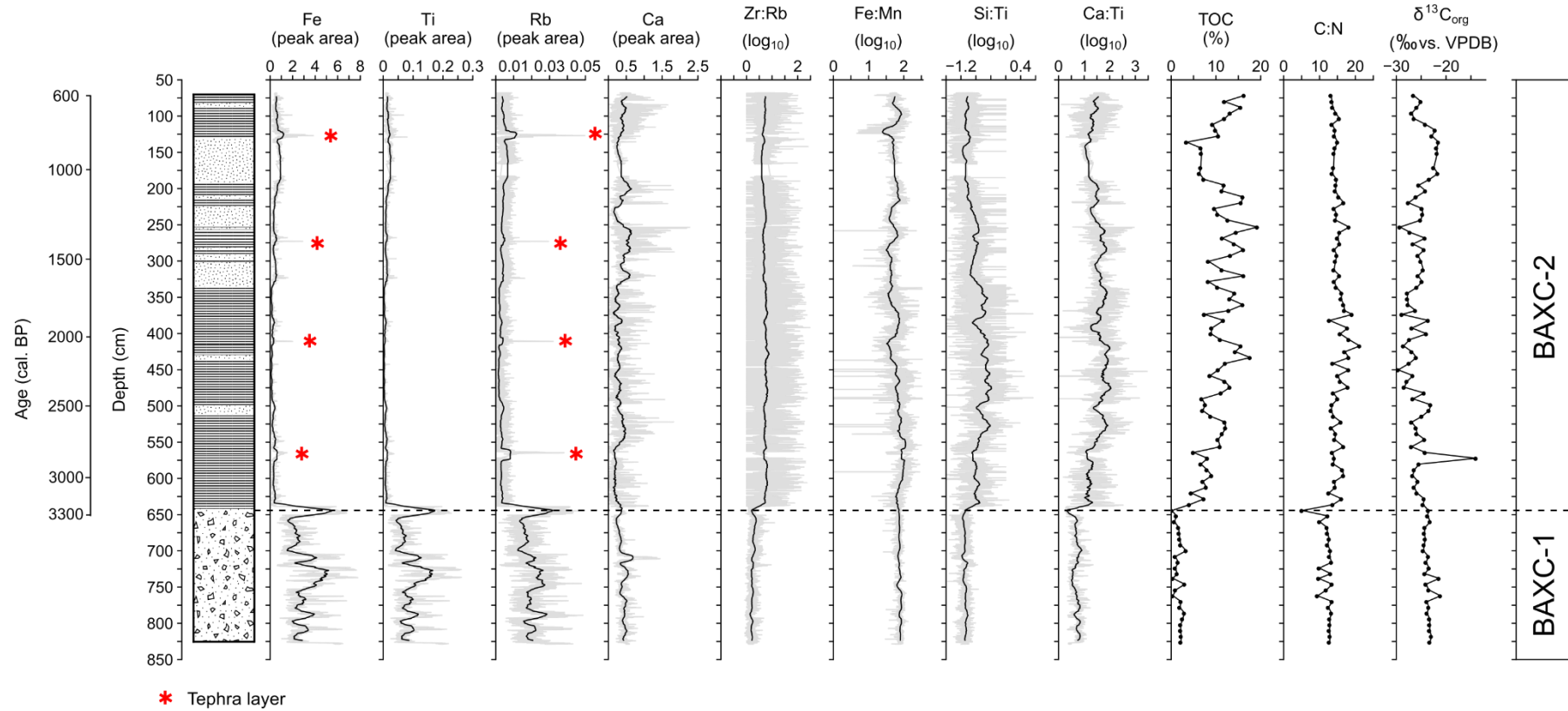


Figure 6.5: Organic carbon and XRF-derived peak area geochemical data for the Babogaya composite core. Solid black line denotes a 500 point running mean.

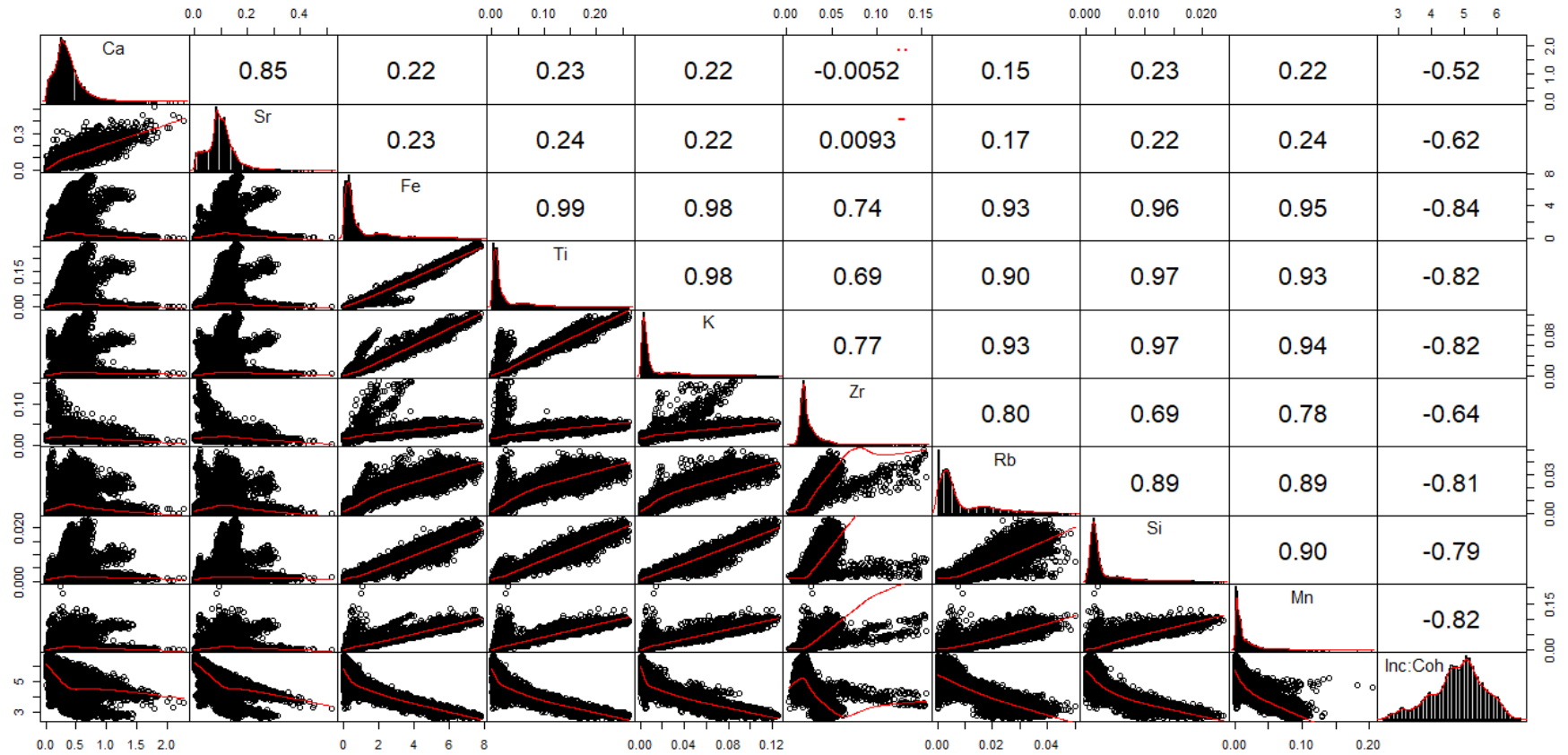


Figure 6.6: Pearson's correlation matrix of selected elements in the Babogaya composite core derived from XRF scanning. Elements are selected based on those exhibiting clear trends in initial interrogation of the data and that are indicative of changing environmental conditions as discussed in Davies *et al.* (2015). The matrices of scatterplots (below histograms) indicate the association and correlation of each comparison (r-values above histograms; $p=0.000$ for each correlation except for “-“ where $p=0.1$ and “..” where $p=1$).

Despite highly variable log ratio values (between 0 and 2), after increasing from 0.185 at the zone boundary to average values of ~ 7 by ~ 625 cm, Zr:Rb is stable at 0.717 ± 0.376 on average throughout the entire zone. Similarly, Si:Ti increases from -1 at the zone boundary to -0.8 at ~ 625 cm. These values return to those similar to zone BAXC-1. Despite some large isolated, sharp decreases in the log ratio values of Fe:Mn, these values remain largely stable only deviating from the mean (1.765) by ± 0.196 . A small decrease in Fe:Mn is evident at ~ 127 cm following the tephra layer. As discussed above, although Ca is slightly lower than in zone 1, Ca is highly variable for much of the zone reaching high values (maximum = 2.273 peak area). Ca values are generally more stable in non-laminated sections of core, with increased variability in the laminated sections.

6.3.2 | Floating core data

BAFX-1: 470 – 202 cm (5400 – 3360 cal. BP)

As in zone 2 of the composite core, while Ca is highly variable during laminated sections, Ca in non-laminated sediments are generally more stable. For example, average Ca between 360 cm and 275 cm is 0.512 ± 0.240 peak area (maximum values of ~ 2.5 peak area), with the adjacent non-laminated sediments nearer the top of the zone (250-225 cm) exhibiting average Ca of 0.796 ± 0.134 . After ~ 260 cm, both Ca and Ca:Ti values decline steadily through to the end of the zone. Lithogenic elements are very low through the entire zone with a few isolated peaks (e.g. four times higher Rb at ~ 366 cm depth corresponding to a discrete tephra layer previously unidentified during smear slide analyses).

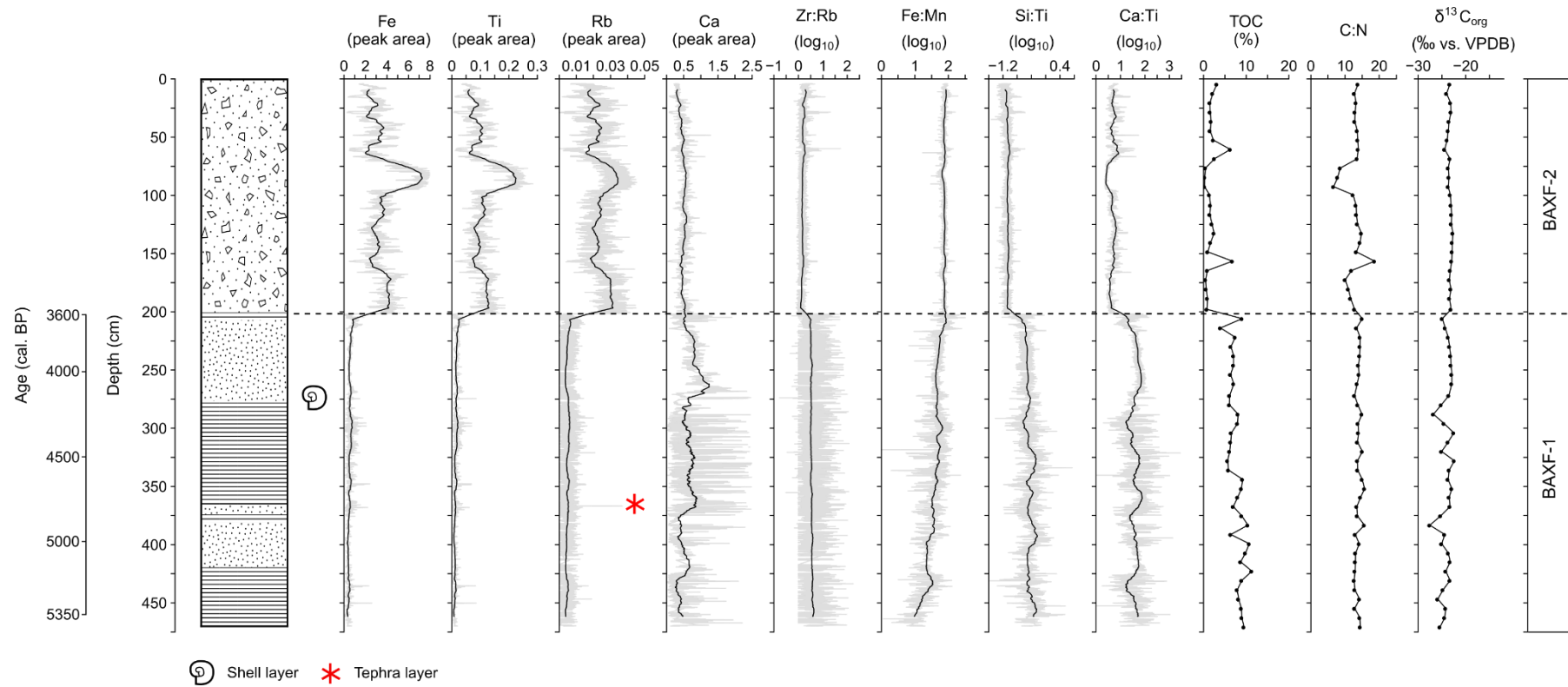


Figure 6.7: Organic carbon and XRF-derived peak area geochemical data for the Babogaya floating core. Solid black line denotes a 500 point running mean.

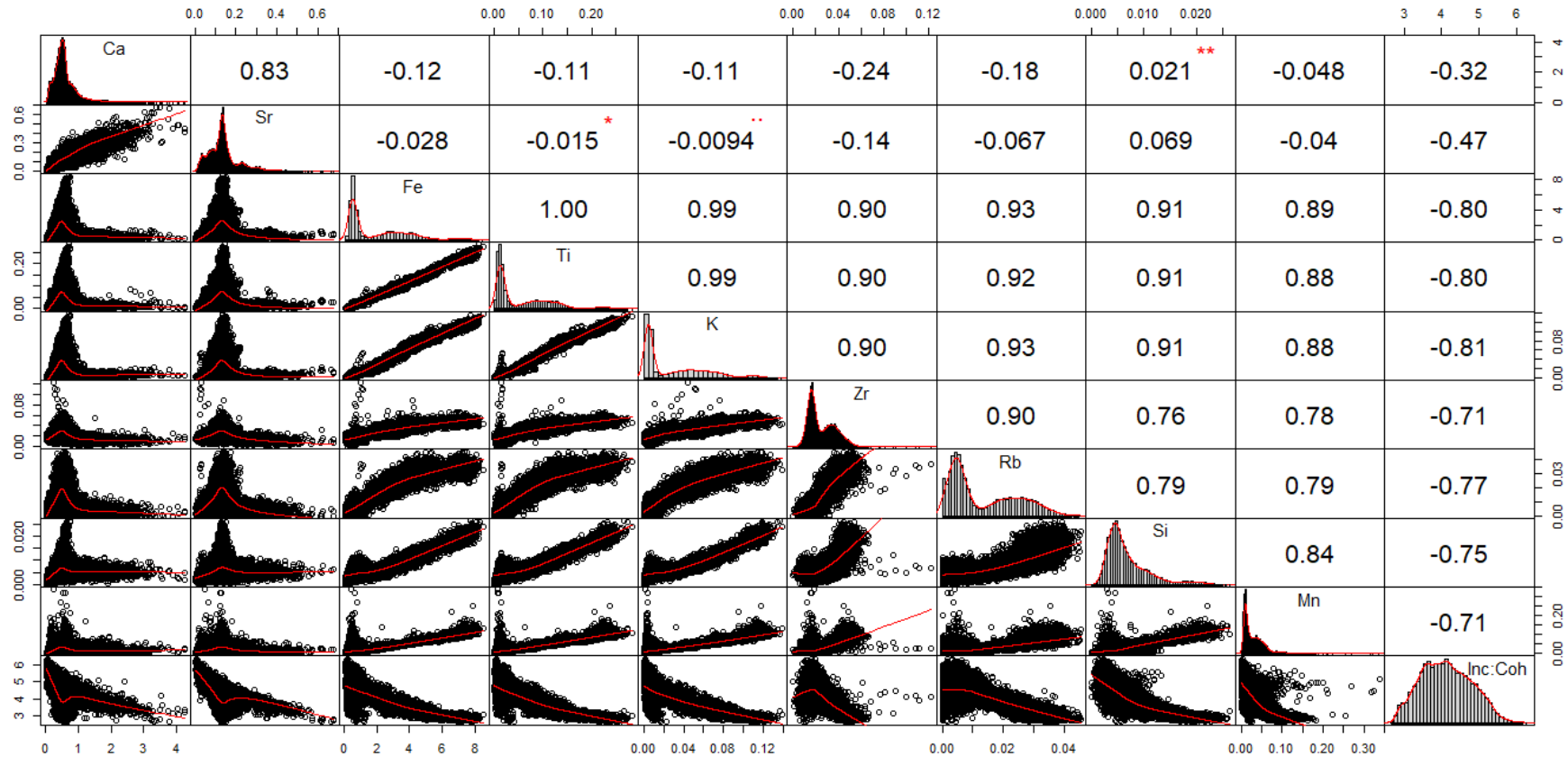


Figure 6.8: Pearson's correlation matrix of selected elements in the Babogaya composite core derived from XRF scanning. Elements are selected based on those exhibiting clear trends in initial interrogation of the data and that are indicative of changing environmental conditions as discussed in Davies *et al.* (2015). The matrices of scatterplots (below histograms) indicate the association and correlation of each comparison (r-values above histograms; $p=0.000$ for each correlation except for “**”, “*” and “..” where $p=0.001$, 0.01 and 1 , respectively).

Fe:Mn increases from the base of the core up to ~2 at around 430 cm, then remains stable at around this value for the remainder of the zone. Zr:Rb despite highly variable raw data (0 to 2), the running mean through this zone is also stable around 0.5. The C:N ratio values and $\delta^{13}\text{C}_{\text{org}}$ values through this zone are also consistent, whilst TOC shows a little more variation (values between 5 and 10%). From ~340 to 202 cm TOC varies around 7% with only a small increase to higher values (~10%) at the upper zone boundary.

BAFX-2: 202 – 0 cm (3360 – >3260 cal. BP)

The beginning of this zone is marked by rapid change (up to 5 times increase in average peak area values within 10 cm) in Fe, Ti and Rb. Lithogenic elements are highly variable through much of this zone, similar to trends in zone 1 of the composite core. Average peak area of Fe, Ti and Rb are high and relatively stable between 200 and 170 cm before decreasing and fluctuating between 170 and 100 cm. At 100 cm, Fe, Ti and Rb increase sharply to peak value for the floating core (8.522, 0.284 and 0.045, respectively) before sharply decreasing at ~65 cm to comparatively lower peak area for the remainder of the zone. Corresponding to this increase in lithogenic element peak area, average TOC decreases by around 4 times that than in zone 1 ($1.85\% \pm 1.60$ compared to $7.80\% \pm 1.65$) with only two small, isolated increases to ~6% at 157 cm and 66 cm.

Additionally, at the zone boundary Ca:Ti, Zr:Rb and Si:Ti also exhibit sharp changes in values, with each decreasing by over half in value over ~10 cm, but then remain fairly consistent for the rest of the zone. Similarly, $\delta^{13}\text{C}_{\text{org}}$ values exhibit minor fluctuations ($-23.33\% \pm 0.41$), with C:N only deviating from around

13-14 at 157 cm (increase to 18.66) and from 100 to 76 cm (decrease to as low as 6.66). Contrasting this trend at the lower zone boundary is Ca which simply continues to gradually decrease between zones 1 and 2 and for the remainder of the core.

6.4 | The diatom record

The detailed diatom record from the composite and floating cores, including valve concentration (valves x 10³/g dry sediment) and diatom habitat group data (taxa <3% relative abundance in the core omitted), is shown in Figure 6.9 and Figure 6.10, respectively. CONISS (Grimm, 1987) analysis, in the R package *rioja* (v. 0.9-14.1; Juggins, 2017), divided the composite core diatom data into 3 major biozones, and 2 major biozones for the floating core, which are shown in Figures 6.9-6.12.

6.4.1 | Composite core data

BACD-1: 828 – 650 cm (<3500 BP)

This zone is populated primarily by *Nitzschia fenestralis* (sp. nov.) at relative abundances of between ~20% and 60%. *Nitzschia lancettula* O.Müller and *Nitzschia paleacea* are also present throughout the zone but at comparatively lower abundances (maximum abundances of up to 30-40% for both taxa). *Nitzschia* “groups latens” (*sensu* Gasse, 1986) increase in abundance up core from negligible abundances at 750 cm to 41% at 671 cm and above 3% until 640 cm, before gradually disappearing in the record above this.

Pseudostaurosira brevistriata (Grunow) D.M.Williams & Round is present throughout this zone but below 20%. Other taxa are present, but in small

amounts through the zone such as *Nitzschia epiphytica* O.Müller, *Encyonema muelleri* (Hustedt) D.G.Mann, *Cymbella leptoceros* (Ehrenberg) Kützing, *Nitzschia amphibia* Grunow and *Sellaphora pupula* (Kützing) Mereschkovsky. The unassigned *Gomphonitzschia* taxon (“sp 1.”) is also present through much of this zone, although at low abundances with only 3 samples where it forms >5% of the assemblage. As a result of numerous taxa being present, despite the low abundances, the Hill’s N2 for this zone is variable, but moderately high for the core (N2 = 10-20).

Adjacent to the upper zone boundary, *Ulnaria acus* (Kützing) Aboal is co-dominant with *Nitzschia fenestralis*, with *Nitzschia gracilis* (*sensu* Gasse, 1986) and *Aulacoseira granulata* var. *angustissima* (O.Müller) Simonsen also appearing in the record (~5%). At 638 cm *Ulnaria acus* almost exclusively populates the assemblage (81%) which is responsible for the sharp increase in rate of change (ROC) and decrease in species diversity. Valve concentrations are negligible values similar to valve concentration in the previous zone.

BACD-2: 616 – 344 cm (3110-1710 BP)

Aulacoseira granulata var. *angustissima* appears in the record and stays quite high for the first ~60 cm of the zone with *Nitzschia fenestralis* continuing to be abundant (>20 to around 60%). This abundance of *Nitzschia fenestralis* continues for the entire zone, and after around 550 cm the abundance of *Aulacoseira granulata* var. *angustissima* gradually declines to lower abundances by 538 cm (0-8.8%). *Nitzschia lancettula* returns at this time with occasional relatively high abundances (>40%).

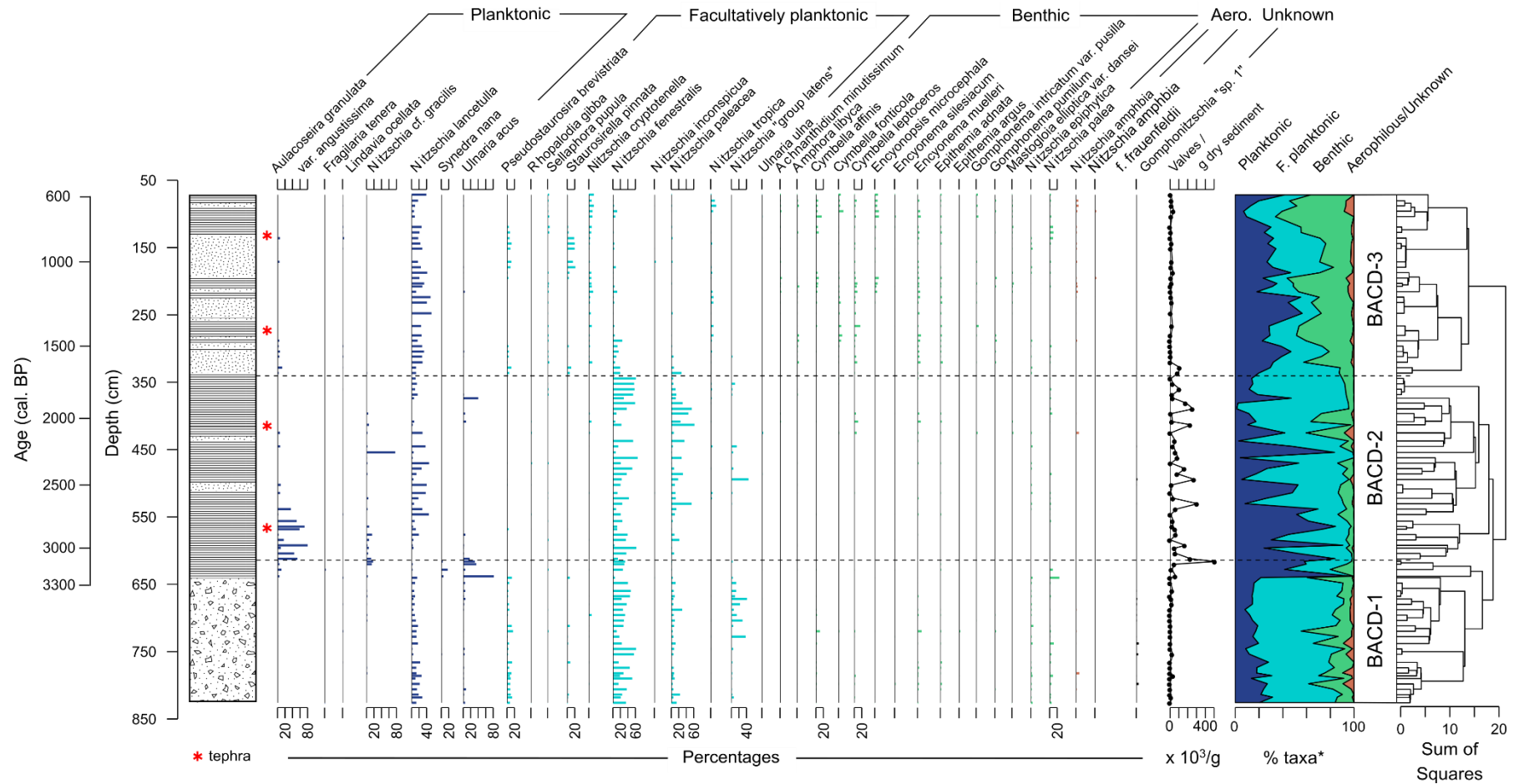


Figure 6.9: Diatom diagram for the Lake Babogaya composite core by depth (age as secondary axis). Included are habitat groupings (*for taxa >3% relative abundance) and valve concentration data. Zones as determined by CONISS are also shown (BACD-1, BACD-2 and BACD-3).

Unlike *Aulacoseira granulata* var. *angustissima* that increases in abundance through the zone boundary, *Nitzschia gracilis* (*sensu* Gasse) is still present but at lower abundances (5-15%). However, one large peak (up to 76%) of *Nitzschia gracilis* is observable at 454 cm and isolated peaks of similar magnitudes (40-45%) in *Ulnaria acus* at 373 cm and of *Nitzschia* “group latens” at 494 cm. *Nitzschia lancettula* abundances decrease after 425 cm to 0.7 to 7%, with parallel increases in *Nitzschia paleacea*, continued dominance of *Nitzschia fenestralis* and small amounts of *Nitzschia* “group latens”.

Although valve concentration declines from the initial peak at the zone boundary values remain high, but variable, for the core. Conversely, due to the dominance of taxa such as *Aulacoseria granulata* var. *angustissima* and *Nitzschia fenestralis* species diversity is generally low through this zone. Species diversity, despite some small, short-lived increases to Hill’s N2 scores comparable to those in zone 1, is generally lower through this zone than in zone 1 attributable to the dominance of *Aulacoseira granulata* var. *angustissima*, *Nitzschia paleacea* and *Nitzschia fenestralis* at different periods.

BACD-3: 344 – 68 cm (1710-580 BP)

Although at a low abundance at the start of this zone the main planktonic taxon is *Nitzschia lancettula* for this zone, with only small amounts of *Lindavia ocellata* (Pantocsek) T.Nakov *et al.* and *Aulacoseria granulata* var. *angustissima*. *Nitzschia lancettula* fluctuates with it being dominant or abundant through much of the zone, only reaching below 10% around 100 to 80 cm. This is normally due to increases in facultatively planktonic and benthic taxa. Although all at low abundances (~1-15%), this zone is diverse in the number of benthic taxa,

especially Cymbelloid lifeforms, including: *Amphora libyca* Ehrenberg, *Cymbella fonticola* Hustedt, *Encyonema muelleri*, *Epithemia adnata* (Kützing) Brébisson, *Achnantheidium minutissimum* (Kützing) Czarnecki, *Cymbella affinis* Kützing, *Encyonopsis microcephala* (Grunow) Krammer and *Gomphonema pumilum* (Grunow) E.Reichardt & Lange-Bertalot. Similarly, the aerophilous taxon *Nitzschia amphibia* (including at times the *forma fraudenlii* variety) continues to be present at a low relative abundance (up to 7%). However, despite this diversity, small increase at the start of the zone valve concentration decreases and remains low (comparable to valve concentration in zone 1) for the remainder of the zone. The increase in benthic taxa is accompanied by a decrease in *Nitzschia fenestralis* and *Nitzschia paleacea*.

6.4.2 | Floating core data

BAFD-1: 470 – 375 cm (5400 – 4865 BP)

The base of the core is dominated by *Staurosirella pinnata* (Ehrenberg) D.M.Williams & Round and *Pseudostaurosira brevistriata*, which is driving species diversity down. Apart from at 359 cm and 391 cm, *Staurosirella pinnata* is below 10% abundance at around 5%, with values from 28% up to 65%. At the base of the core planktonic taxa are present at 0.5%, but by 414 cm *Nitzschia lancettula* occurs at higher abundances in the record in the record at >5%, reaching 45% at 391 cm. Benthic taxa are moderately abundant in this zone (~20% overall), with a large proportion of this taken up by *Nitzschia epiphytica* (abundance between 10 and 20%), with minor amounts of *Encyonema muelleri* and *Epithemia adnata* through the zone. One large peak of *Nitzschia paleacea* (58% relative abundance; the highest in the core) is observable at 430 cm.

BAFD-2: 300 – 210 cm (4370 – 3670 BP)

Facultatively planktonic taxa are well represented in this zone with *Pseudostaurosira brevistriata* increasing in abundance at the expense of *Staurosirella pinnata*, which is virtually absent in the zone apart from 267 to 210 cm at 5-15%. Interestingly, *Lindavia ocellata* appearances in this zone correspond to increased amounts of *Pseudostaurosira brevistriata*. *Nitzschia lancettula* remains abundant for most of this zone, only decreasing to <20%, but above 10%, with increased abundance of *Pseudostaurosira brevistriata* at around 360 to 315 cm. Generally, the abundance of benthic taxa decreases, but taxa such as *Nitzschia epiphytica* and *Epithemia adnata* are still present.

BAFD-3: 210 – 0 cm (3670 - >3300 BP)

The boundary between the two zones covering the floating composite is marked by a rate of change that is relatively large for the floating composite core. Species diversity also increases sharply at the zone boundary. Despite increased diversity, valve concentration is low at an average of 7.21×10^3 valves/g dry sediment. The general abundance of *Pseudostaurosira brevistriata* is generally lower in this zone than in zone 2, at more comparable abundances to those in zone 1. Generally, however, a high facultatively planktonic population is sustained throughout this zone with reduction in planktonic taxa, although *Nitzschia lancettula* is still fairly common (10-26%). A number of taxa appear at the lower zone boundary and are present, often at high abundances, through much of this zone including *Nitzschia fenestralis* (1-52%), *Nitzschia paleacea* (1-19%), *Nitzschia palea* (Kützing) W.Smith (1-15%), *Ulnaria acus* (0-13%), *Nitzschia epiphytica* (0-10%) and *Nitzschia amphibia* (0-3%).

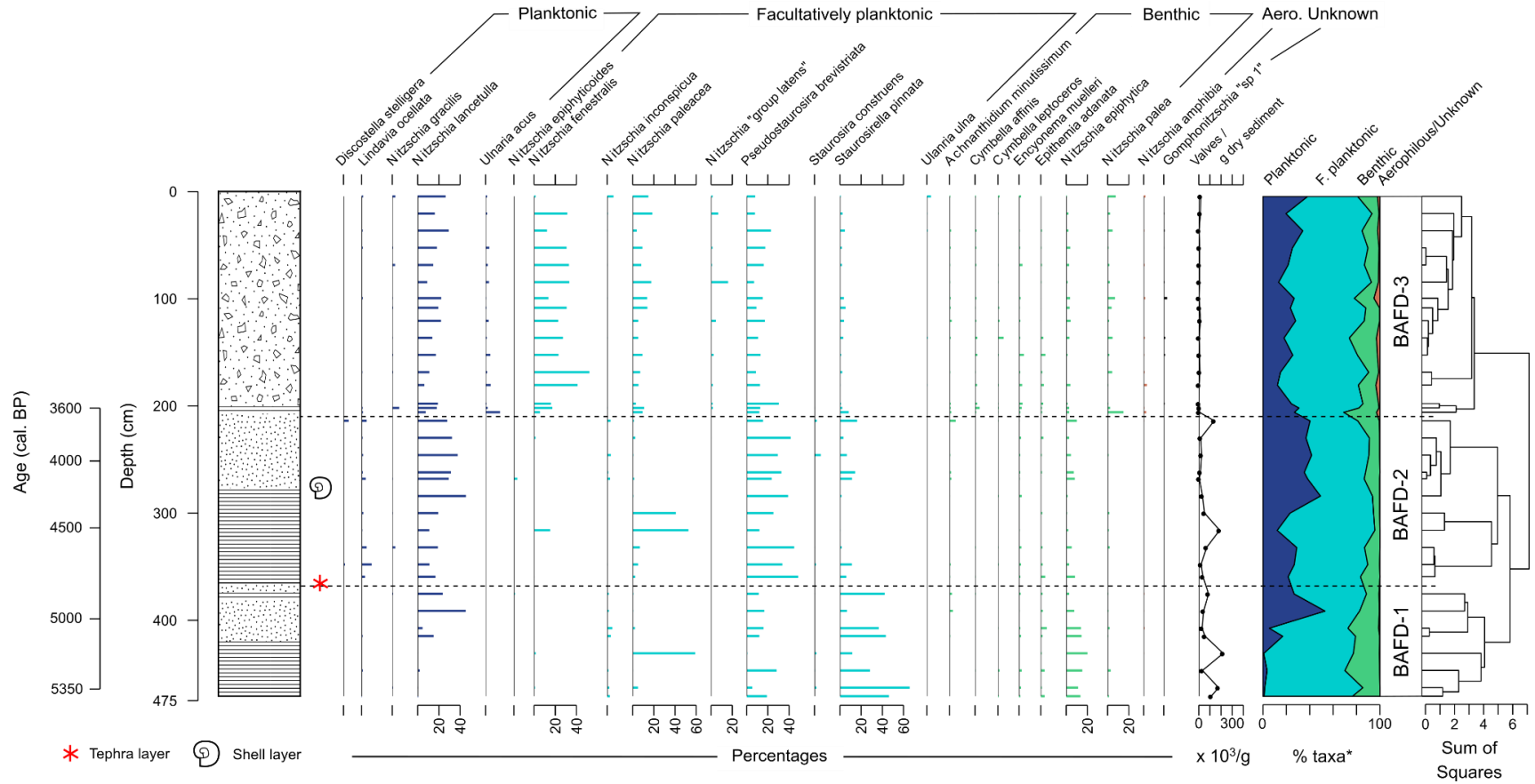


Figure 6.10: Diatom diagram for the Lake Babogaya floating core by depth (age as secondary axis). Included are habitat groupings (*for taxa >3% relative abundance) and valve concentration data. Zones as determined by CONISS are also shown (BAFD-1, BAFD-2 and BAFD-3).

6.4.3 | Laminae diatom counts

The diatom counts of individual laminae from three laminated sections of core (two sections from the composite core and one from the floating composite core), and diatom habitat group data (taxa <3% relative abundance in the core omitted), is shown in figures 6.11, 6.12 and 6.13. The similarity of each lamina within a section is very close in terms of diatom ecology, with very little change between each layer, especially in Figure 6.12 for example. However, it is possible to identify small differences in 6.11 and 6.13. The seasonal lake stratification at Lake Babogaya (see Section 3.3) which presumably leads to the darker, brown layers (Lamb *et al.*, 2002) coincides with slightly increased abundance of the facultatively planktonic *Navicula cryptotenella* Lange-Bertalot, *Nitzschia fenestralis* and *Nitzschia tropica* Hustedt (Figure 6.11). Similarly, *Nitzschia paleacea* and *Nitzschia fenestralis* exhibit a similar pattern in Figure 6.13. In the laminated sections of the floating core some green-blue coloured layers occasionally couple the light-dark lamina and are slightly richer in *Nitzschia lancettula* and *Pseudostaurosira brevistriata* (Figure 6.13).

6.4.4 | Diatom ordination

Ordinations were determined separately for the composite and floating composite cores to explore the potential of different distributions of taxa in both halves of the record. However, the plotted principal curves behaved in similar ways irrespective of this split. Thus, diatom data from the composite and floating cores were plotted and interpreted together.

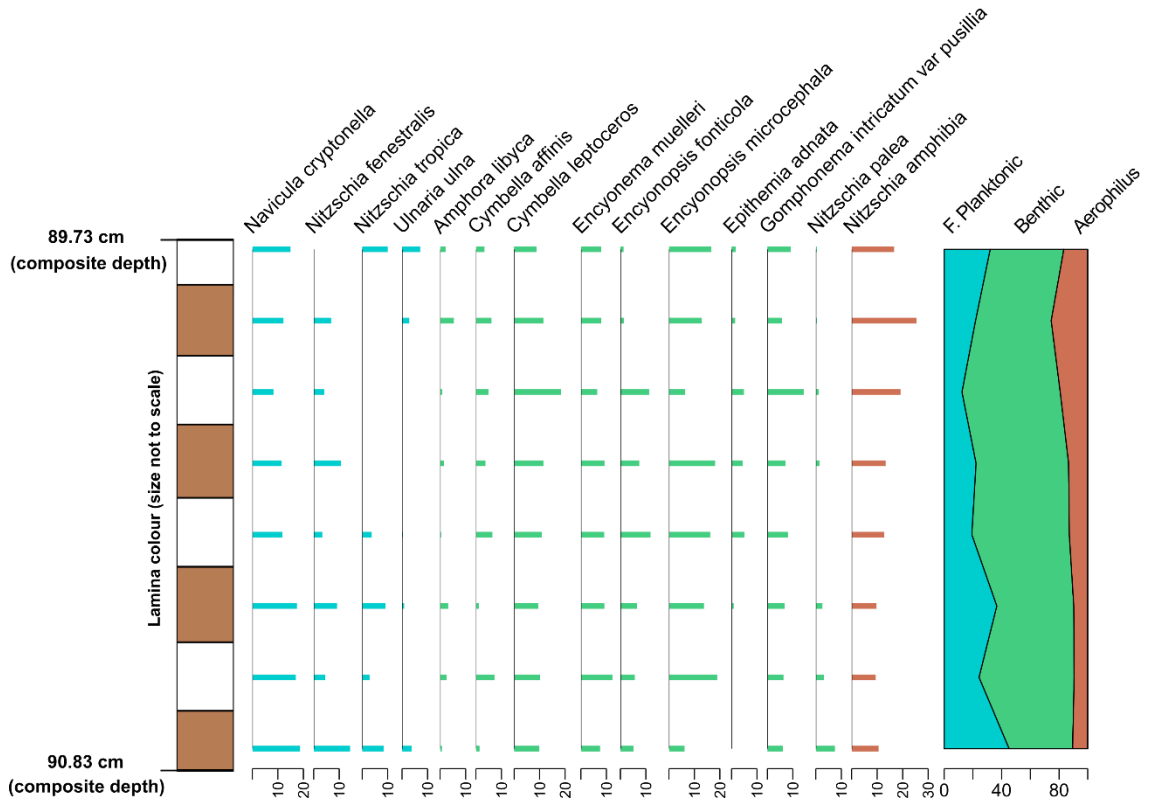


Figure 6.11: Diatom diagram for Lake Babogaya laminated section (89.7-90.8 cm composite depth) counts by depth. Included are habitat grouping data.

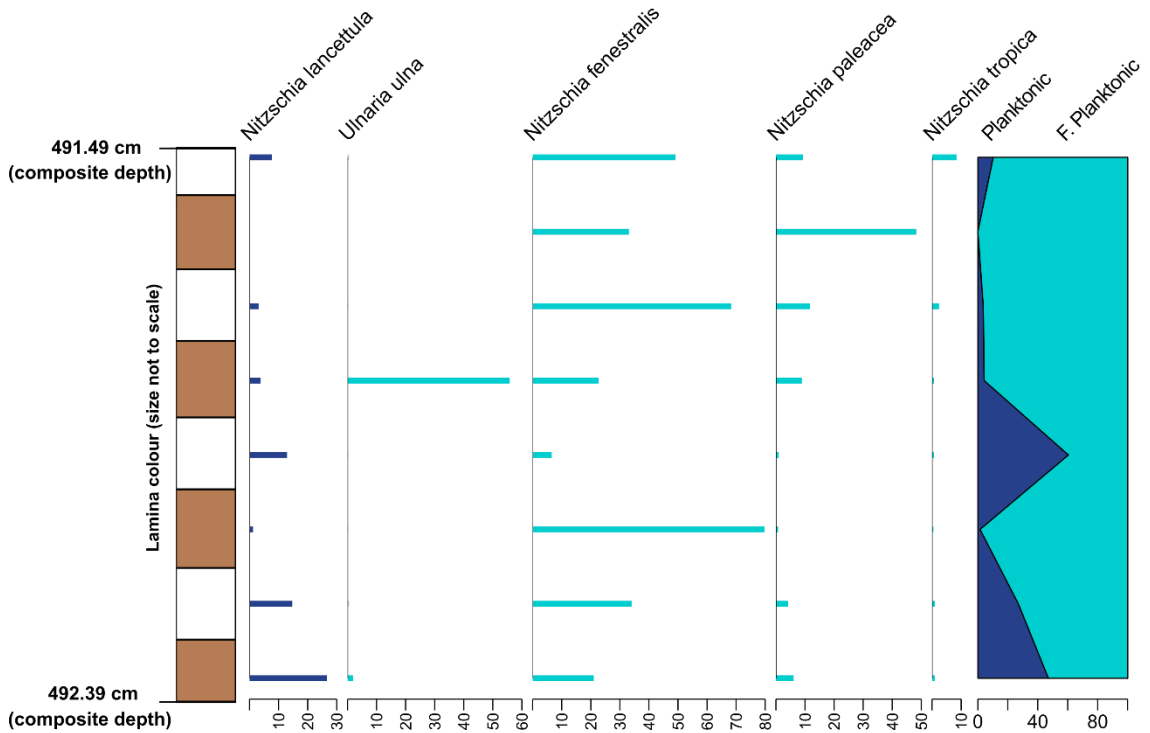


Figure 6.12: Diatom diagram for Lake Babogaya laminated section (491.49-492.39 cm composite depth) counts by depth. Included are habitat grouping data.

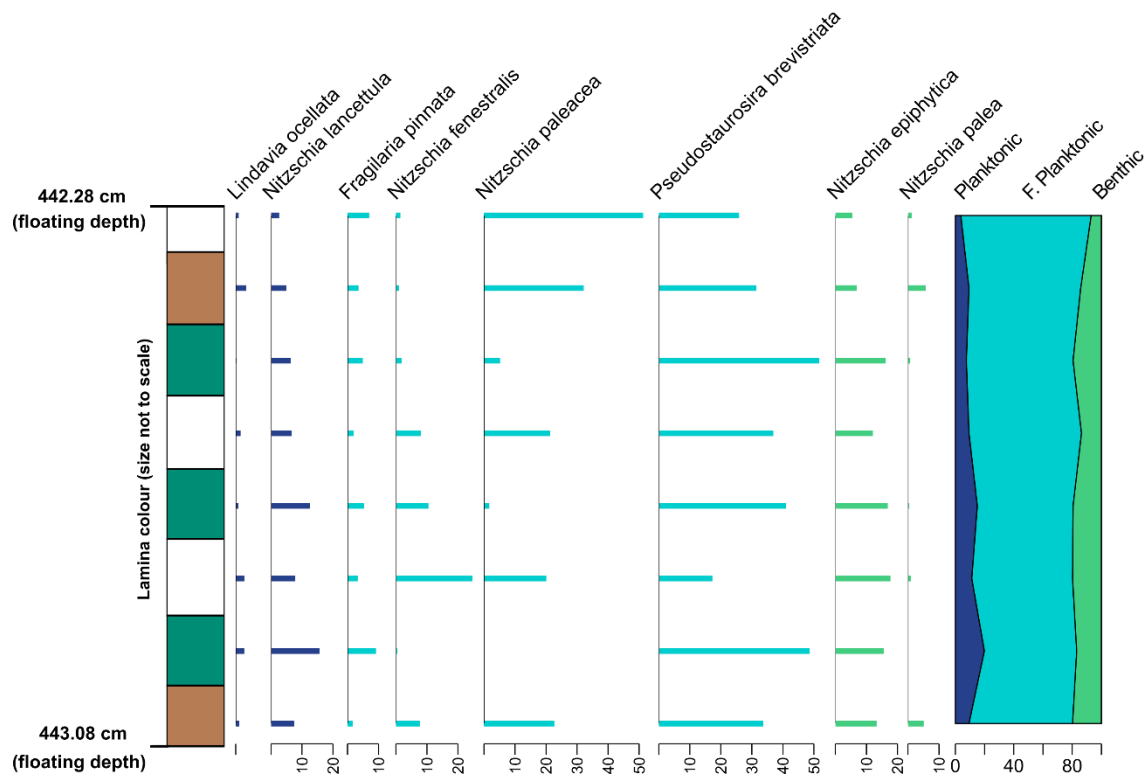


Figure 6.13: Diatom diagram for Lake Babogaya laminated section (442.28-443.08 cm composite depth) counts by depth. Included are habitat grouping data.

The principal curve through the Babogaya diatom data (Figure 6.14) is difficult to interpret however the main driver of change through the data seems to be changing nutrient requirements. The beginning of the curve is populated by *Staurosirella pinnata* and *Pseudostaurosira brevistriata* transitioning from oligotrophic taxa to those associated with more nutrient enriched waters. Towards the end (B in Figure 6.14), the curve is populated by taxa characteristic of meso- to eutrophic waters such as *Ulnaria acus*, *Nitzschia paleacea* and at the apex of the curve *Aulacoseira granulata* var. *angustissima*. However, other factors are likely influencing this ordination. This curve reflects (and simplifies on to one axis) major compositional shifts, the potential drivers of which are interpreted further below in text. PrC scores for each depth, as well as diatom inferred conductivity, rate of change and Hill's N2 (discussed in Chapter 4) are

plotted alongside habitat percentages and core stratigraphy for both the composite (Figure 6.15) and floating (Figure 6.16) cores to more effectively summarise and quantify changes in the diatom record.

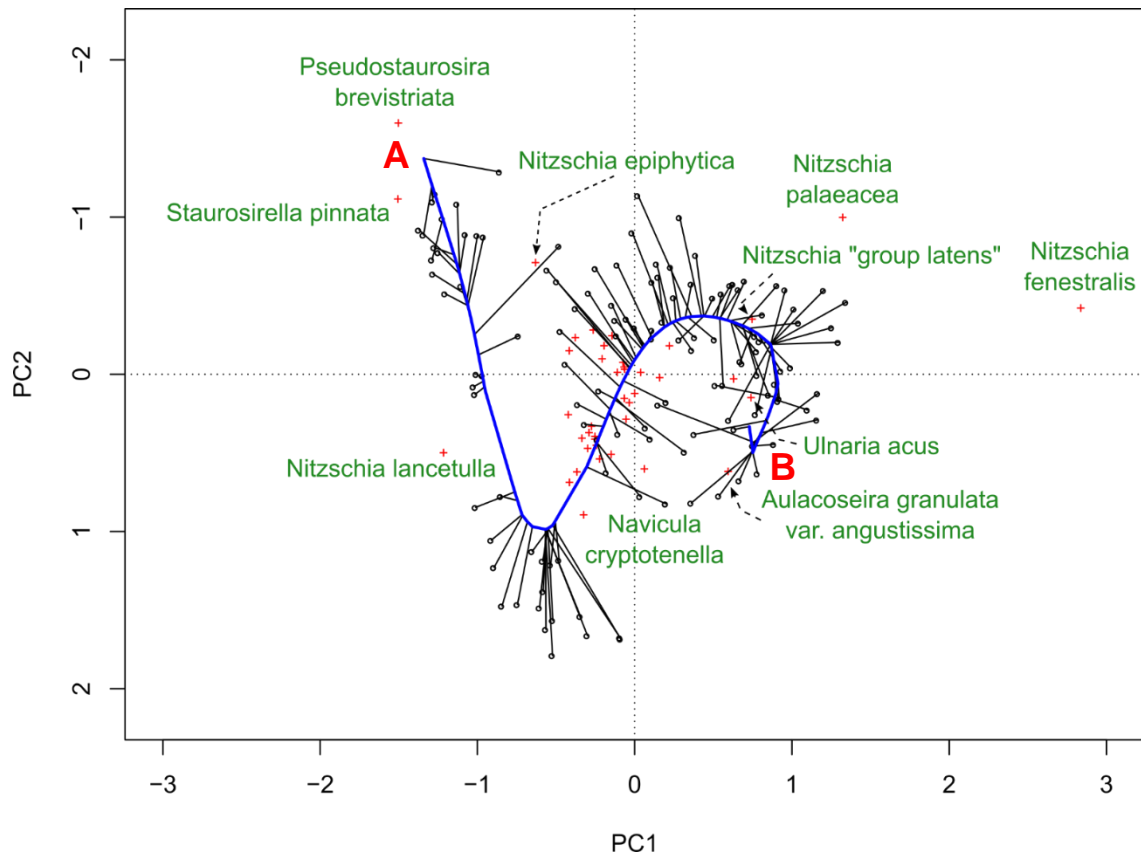


Figure 6.14: Principal curve (blue) of the Babogaya diatom data. Taxa scores in (PCA) ordination space are denoted by red crosses, with the main taxa labelled. The start of the curve (A; 0 PrC score) and end of the curve (B; 1 PrC score) are also shown.

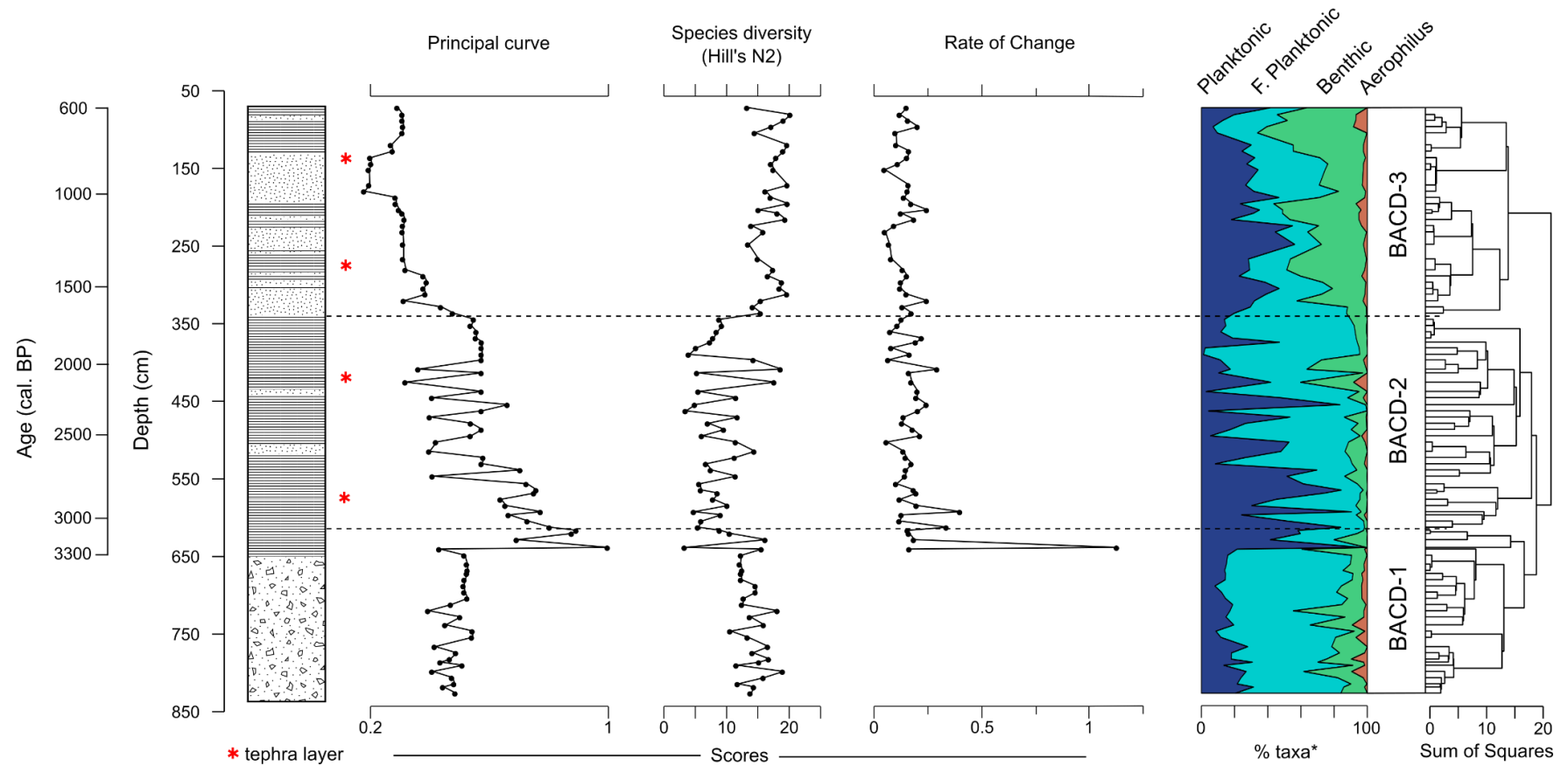


Figure 6.15: Quantitative diatom data for the Lake Babogaya composite core. Principal curve shown in Figure 6.14. Methods and packages used for computing these statistics are detailed in Chapter 4. Zones as determined by CONISS are also shown.

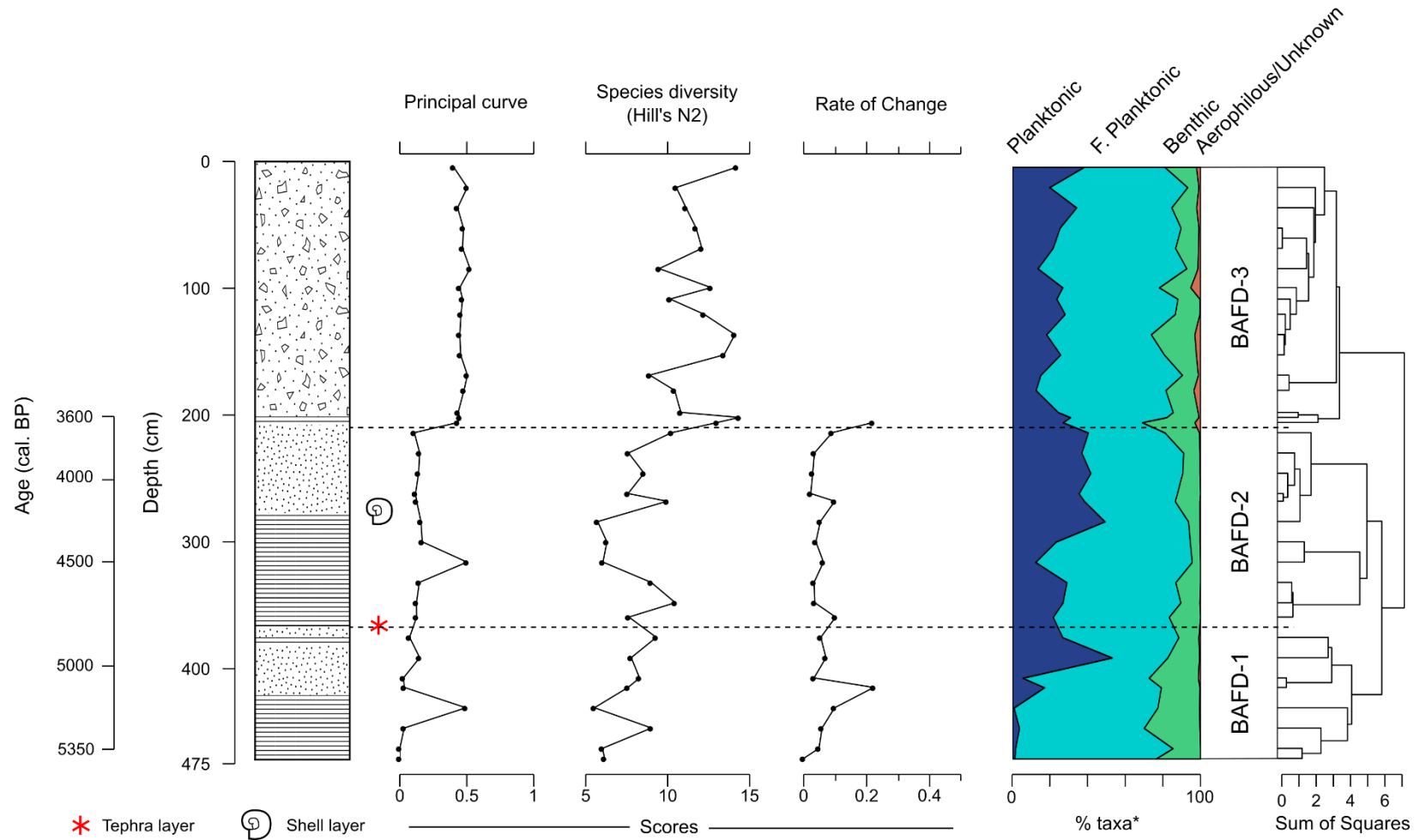


Figure 6.16: Quantitative diatom data for the Lake Babogaya floating core. Principal curve shown in Figure 6.14. Methods and packages used for computing these statistics are detailed in Chapter 4. Zones as determined by CONISS are also shown.

6.5 | Interpretation of the Babogaya sedimentary record

All available data from the independent proxy records analysed from core BA-LC-2011 (including both the composite and floating composite cores) are now interpreted in terms of limnetic and environmental changes that have taken place in the Lake Babogaya basin over the past ~5,400 to 600 cal. BP. For ease of interpretation, the record has been divided into 5 major time periods (BA-1 to BA-5) based on significant changes in the palaeoenvironmental data, primarily in the diatom data, as this is the primary proxy in this research. Furthermore, the non-laminated minerogenic units in both the composite and floating composite cores have been interpreted as one full unit as it is presumed that they are simply missing a section. As only each side of the unit is reliably dated, with mixing and reworking of sediments likely (e.g. old reworked charcoal carbon in radiocarbon dates) as a result of a much faster sedimentation rate of allochthonous material, the data can only be interpreted in general terms for that time period. For ease of interpretation, main environmental changes in both diatom and XRF data have been presented in Figure 6.17. The record has been divided into 5 major time periods (BA-1 to BA-5) based on significant changes in the palaeoenvironmental data.

BA-1: 470 – 375 cm (floating composite depth; 5400 – 4865 BP)

Many small *Fragilaria* are considered r-strategists (Lotter & Bigler, 2000), with low light and very low nutrient (such as N, P and Si) requirements (Michel *et al.*, 2006). *Staurosirella pinnata* and *Pseudostaurosira brevistriata* are known to colonise low-nutrient, cold and shallow waters where growth is inhibited for other taxa (Laird *et al.*, 2010).

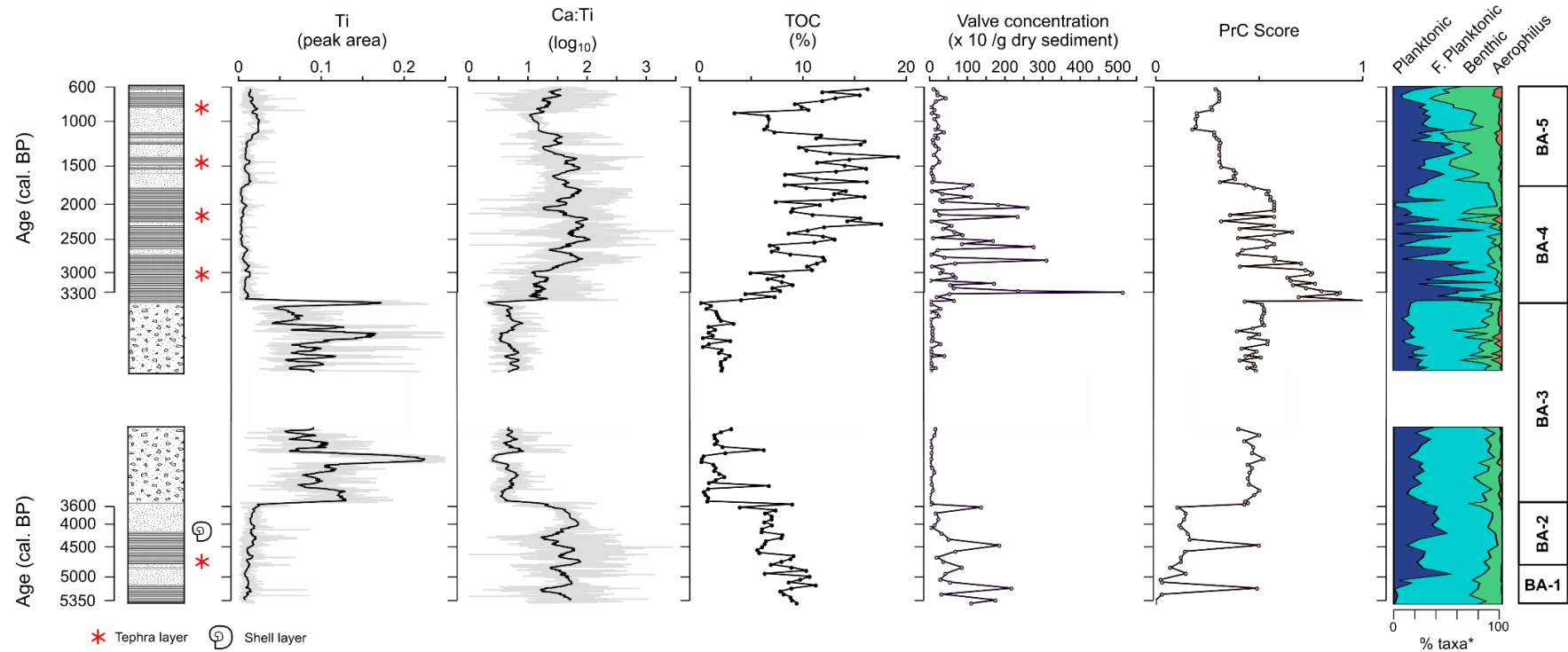


Figure 6.17: Synthesis of diatom, XRF-derived peak area and organic geochemical for the Lake Babogaya core. Interpretation zones referred to in-text are also shown. Solid black line denotes a 500-point running mean through XRF data. *Percentage of taxa included in habitat groupings at a relative abundance of >3%.

However, although small *Fragilaria* (such as *Staurosirella pinnata*) are often associated with benthic habitats in shallower, lower-light waters (e.g. Kingsbury *et al.*, 2012), nutrient supply and light availability is known to be such dominant factors as to limit the expansion of planktonic taxa, even in deeper waters (Lotter & Bigler, 2000; Schmidt *et al.*, 2004). It is also important to note that the term “shallow” in relation to habitat in which small *Fragilaria* (such as *Staurosirella pinnata* and *Pseudostaurosira brevistriata*) thrive can be waters up to 10 m depth (e.g. Lotter & Bigler, 2000; Laird *et al.*, 2010), and even ~20 m in some studies (Cantonati *et al.*, 2009). Waters were likely deep enough to sufficiently mix and stratify seasonally to allow laminae to form during this period.

Periphytic, near-shore habitat was likely abundant during this period with *Nitzschia epiphytica* common in the record. The confusion regarding the precise taxonomy of *Nitzschia epiphytica* makes determining the exact ecology of the species difficult (Cocquyt *et al.*, 2012). However, Gasse (1986) understood the taxon to be epiphytic and has been interpreted by others to favour shallower waters and increased littoral and benthic habitat at Lake Rukwa (Barker *et al.*, 2003) and Hayq (Loakes, 2016).

It should first be noted that the large isolated peaks in *Nitzschia paleacea* may represent blooms of the species that may be ‘swamping’ the record as described by Woodbridge & Roberts (2010): the high abundance of short-lived, blooming diatoms reduces the chances of encountering rarer taxa in a sample, thus artificially reducing species diversity. Nevertheless, their presence (mostly in isolated peaks) likely indicates a period of increased nutrient input (Baier *et al.*, 2004), with moderate Si and P availability also likely key for the taxon to be able to outcompete others (Kilham *et al.*, 1986; Woodbridge & Roberts, 2010).

Normalising Ca against a lithogenic element (e.g. Ti or Al) provides information for the possible source of carbonates to the lake. For example, low Ca:Ti values would indicate higher detrital input (associated with Ti or Al), with higher Ca:Ti values suggesting greater in-lake production of Ca. Autochthonous carbonate production may be associated with increased evaporative concentration, reflecting environmental changes (e.g. Jouve *et al.*, 2013), but also with fluctuating biological productivity in the case of biogenic carbonates (e.g. März *et al.*, 2011; Olsen *et al.*, 2013), associated with lamina formation.

At around ~5,150 BP average Fe:Mn values increase (Figure 6.7) which may be linked to changing redox conditions. The solubility of Fe and Mn are increased under reducing conditions, and as Mn is more readily affected under such conditions, increased Fe:Mn could indicate a reduction in water oxygen content during periods of stratification (Davies *et al.*, 2015). This increase in Fe:Mn is also mirrored by an increased abundance in the planktonic *Nitzschia lancettula* (Figure 6.10). However, the autoecology of *Nitzschia lancettula* is unclear other than it is known to be a plankton optimally growing in the big lakes of Africa (lakes Victoria and Edward; Gasse, 1986). Based on the findings of Stager *et al.* (2005) that find the taxon in interpreted highstands of Lake Victoria, and with trends identified in their data, Mills *et al.* (2014; 2018), Loakes (2016) and Pasche *et al.* (2010) consider the increased abundance of *Nitzschia lancettula* to represent a deepening of lake waters. Furthermore, stratified conditions are optimal for *Nitzschia*, and *Microcystis aeruginosa* (a dominant algae in the modern-day lake) which *Nitzschia* are often associated with (Kilham *et al.*, 1986). Therefore, their presence may also indicate waters became increasingly stratified at this time (Mills *et al.*, 2014).

pH for this zone remains moderately high despite a shift from littoral/benthic to planktonic taxa. Based on their eastern African diatom dataset, Gasse & Tekaia (1983) suggest that *Pseudostaurosira brevistriata* and *Nitzschia lancettula* are indicator taxa for a lake pH of around 8 to 8.6. Indeed, the pH optima for these taxa in the combined African dataset are 7.82 ± 1.02 and 8.51 ± 0.76 pH for *Pseudostaurosira brevistriata* and *Nitzschia lancettula*, respectively (Gasse *et al.*, 1995). Similarly, the other abundant taxa for this period are *Nitzschia epiphytica* and *Staurosirella pinnata* which also have high pH optima (8.19 ± 1.80 and 8.17 ± 0.83 , respectively; Gasse *et al.*, 1995).

The presence of the pelagic *Phacotus* through this zone is difficult to interpret in term of past environmental conditions such as nutrient availability or water depth as they are reportedly flexible with a broad tolerance (Gruenert & Raeder, 2014 and references therein). However, fundamentally, *Phacotus* do require an accessible carbon source to build their thick loricae. Padišák *et al.* (2003) argue the dominant carbon source for *Phacotus* to build their lorica is HCO_3^- , with supersaturation of CaCO_3 also shown to promote their growth (Gruenert & Raeder, 2014), both of which are predominant in alkaline waters.

Assuming pH remained high during this period (and at other periods in the record) rates of valve dissolution may have been elevated due to the disassociation of silicic acid at elevated pH (Barker *et al.*, 1994). This would influence the counts and interpretations presented in this study as more slender, delicately structured valves (e.g. *Nitzschia palea* and *Nitzschia dissipata*; Barker *et al.*, 1994) are lost in the record to dissolution rather than to changing environmental conditions. The F-index can be used to try and quantify the amount of dissolution present in samples (see Ryves *et al.*, 2001). However the F-index relies on visual inspection

and qualitative assessments of dissolution (Ryves *et al.*, 2001). As no significant valve breakage or dissolution could be observed in samples (even in species such as *Nitzschia fenestralis*, *Nitzschia palea* and *Nitzschia paleacea*) it was decided not to employ the F-index method and assume dissolution rates were minimal and not significantly impacting the record.

Based on the African dataset conductivity optima for *Staurosirella pinnata*, *Pseudostaurosira brevistriata* and *Nitzschia epiphytica*, however, is very fresh in terms of conductivity (optima of 145, 580 and 275 $\mu\text{S}/\text{cm}$, respectively). Different optima have been determined from 76 Ugandan crater lakes by Mills & Ryves (2012) with a slightly higher optima calculated for *Pseudostaurosira brevistriata* (389 $\mu\text{S}/\text{cm}$ optimum), a much higher optima for *Nitzschia epiphytica* (2630 ± 2 $\mu\text{S}/\text{cm}$), but broadly a similar optimum for *Staurosirella pinnata* (166 ± 6 $\mu\text{S}/\text{cm}$). The optimum calculated for *Nitzschia epiphytica* is higher than in Gasse *et al.* (1995), however the low occurrences and abundance of this taxon in the dataset may imply the optimum of this taxon may be poorly defined (Mills & Ryves, 2012). Comparatively, *Nitzschia lancettula*, although indicative of deeper water, tends to prefer slightly more solute rich waters with an optimum of 1,905 $\mu\text{S}/\text{cm}$ (Gasse *et al.*, 1995). However, similarly, the conductivity optima determined from the Ugandan dataset for *Nitzschia lancettula* suggests a preference for fresher conditions of 512.86 $\mu\text{S}/\text{cm}$ as opposed to 1,905 $\mu\text{S}/\text{cm}$ (Gasse *et al.*, 1995). This increase in *Nitzschia lancettula* at Lake Babogaya may represent a period of transition to slightly more concentrated (if comparing either the optima determined by Gasse *et al.*, 1995 or by Mills & Ryves, 2012) but deeper, stratified waters, especially with the reduction of the fresher and shallow tolerant *Staurosirella pinnata* and periphytic *Nitzschia epiphytica*. One explanation for this

apparently contradictory scenario (a slightly higher conductivity would normally be related to increased evaporation and reduced lake level; Chapter 4) is overall deeper lake waters, but with increased seasonality and a more established period of stratification with drier or warmer conditions.

BA-2: 375 – 202 cm (floating composite depth; 4865 – 3670 BP)

Increased abundance of the deeper water taxon *Nitzschia lancettula* at the expense of benthic taxa and especially *Staurosirella pinnata* suggests a period of deeper, open waters at Lake Babogaya after 4,600 BP (Figure 6.10). However, shallower, marginal lake areas were still important with a vegetated littoral zone likely persisting indicated by the continued presence of *Nitzschia epiphytica*, *Epithemia adnata*, *Encyonema muelleri* and *Pseudostaurosira brevistriata*. The latter taxon is highly abundant to dominant through some parts of this record and as discussed above is known to proliferate in shallower, oligotrophic waters (Bigler *et al.*, 2000; Laird *et al.*, 2010). Furthermore, *Pseudostaurosira brevistriata* has a broad tolerance to increased conductivity ($2.76 \pm 0.80 \mu\text{S/cm}$ in Gasse *et al.*, 1995 and $2.59 \pm 0.45 \mu\text{S/cm}$ in Mills & Ryves, 2012), especially compared to *Staurosirella pinnata* abundant in BA-1, that may be associated with increased seasonality. Lake waters likely remained alkaline, with the presence of the above taxa and *Phacotus lorica* as in the previous zone.

Often associated with littoral taxa such as *Pseudostaurosira brevistriata* is *Lindavia ocellata* (Chalié & Gasse, 2002; Marshall *et al.*, 2009). This can be seen in the Babogaya record with the large increase in *Pseudostaurosira brevistriata* and appearance of *Lindavia ocellata* (e.g. between 4,700 and 4,500 BP; Figure 6.10). Much of the autoecological affinities of the cosmopolitan and adaptable

Lindavia ocellata are uncertain (Malik & Saros, 2016). However, some useful palaeoenvironmental inferences can be made: the taxon has been shown to adapt well to lake stratification (Winder *et al.*, 2009; Edlund *et al.*, 2017) and is considered by some to be a ‘littoral plankton’. Studies have reported *Lindavia ocellata*, in Africa at least, in shallower waters in association with littoral taxa such as *Pseudostaurosira brevistriata* (Gasse, 1986; Chalié & Gasse, 2002; Marshall *et al.*, 2009), with Stone *et al.* (2011) interpreting their presence to indicate shallower planktonic environments with increased proximity to the littoral zone in their record at Lake Malawi. Their presence, although at low abundances, together with increased abundance of *Pseudostaurosira brevistriata* (Figure 6.10), present during this period further supports the inference of stratified, but slightly shallower, waters at Babogaya during this period. Similar peaks in *Nitzschia paleacea* abundance as in zone BA-1, and the newly described taxon *Nitzschia fenestralis* (Grady *et al.* 2020), may indicate brief intervals of nutrient-rich waters.

With a C:N value of ~14 the sources of organic carbon remained largely mixed between terrestrial and aquatic material (Figure 6.7). However, a small reduction to lower TOC can be observed after 4,800 BP, with a gradual decrease until ~3,790 BP where a second decrease observable (also seen in Si:Ti; a proxy for biogenic silica; Davies *et al.*, 2015) before the transition to the minerogenic sediments of the next unit (Figure 6.7). This may represent gradually reducing productivity for the area with increasingly poorer, drier conditions which may be represented by slightly increased terrigenous input at around 4,800 BP.

Increased average Fe:Mn (Figure 6.7), although fluctuating considerably, indicates lake waters were oxygen-poor, likely as a result of stratification at least

seasonally which would be required for lamina formation. This would also continue to support the increased abundances of *Nitzschia lancettula* which, as discussed earlier, thrives in deeper, stratified waters (Mills *et al.*, 2014; 2018).

The presence of a heliciform gastropod shell layer at ~4,150 BP may indicate a lowering of lake level which was preceded by the step down in TOC. This shell layer is also accompanied by a decrease in diatom productivity with decreased valve concentration and Si:Ti (Figure 6.7). This period also sees the reappearance and increased abundance of *Staurosirella pinnata* and increased abundance of benthic and littoral taxa such as *Nitzschia epiphytica*, *Epithemia adnata* and *Achnanthydium minutissimum* attesting to a lowering of the lake level. However, the consistently high abundance of planktonic taxa during this period (>40%) with littoral and benthic water taxa could point to a fragmenting of the lake as opposed to complete desiccation. While this unlikely scenario is difficult to reconcile with such steep sides to most of the lake, the gradient on southern and northern edges of the basin are far more gradual, with more varied lake bed topography in comparison (Figure 6.18), and may have facilitated areas of shallower waters, but deeper in the central area of the lake.

BA-3: 202 – 0 cm (floating composite core depth) and 828 – 616 cm (composite core depth; 3670 – 3110 BP)

A rapid increase to high Ti, Fe and Rb (as well as other covarying lithogenic elements not shown in Figures 6.5 and 6.6) with consistently high peak area through this zone marks a period of considerable terrigenous input. Furthermore, lower Zr:Rb suggests that much of this is fine-grained material (Kylander *et al.*, 2011). Although changes within the unit could not be dated accurately, the overall

sedimentation rate must have been significantly high in order to supply >4 m worth of minerogenic sediment to the lake within the ages bracketing this lithological unit: 3,600 to 3,300 BP.

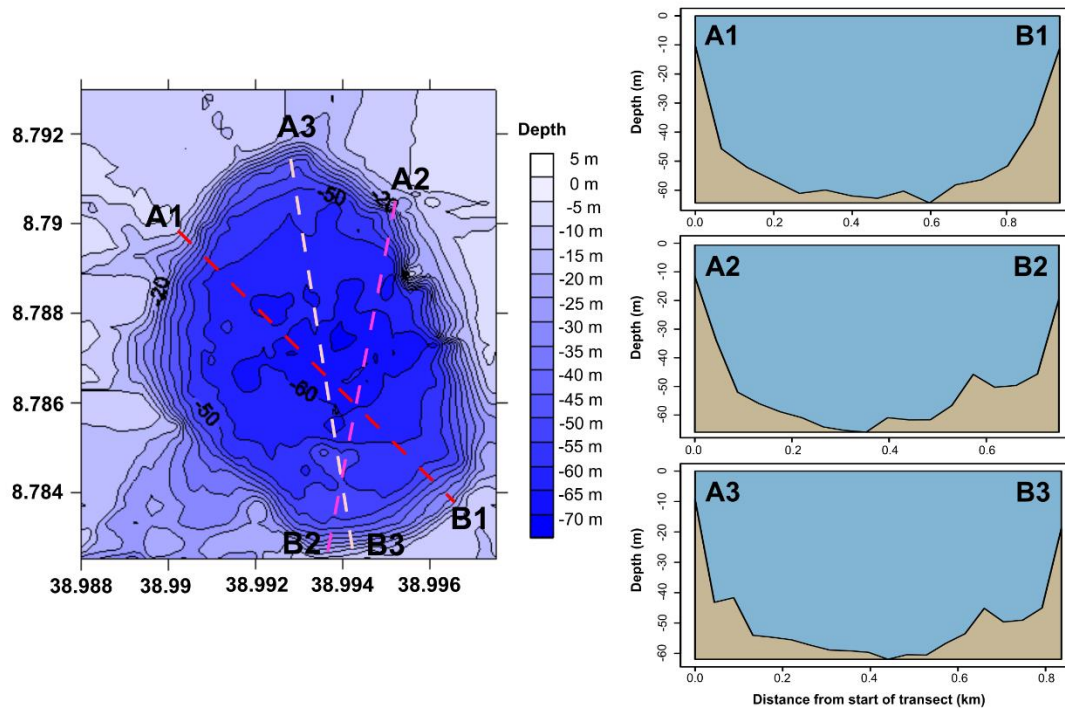


Figure 6.18: Lake Babogaya bathymetry (left) and cross sections of three transects across this data (cross sections shown on the right). Created in the R package *marmap* (Pante & Simon-Bouhet, 2013) using unpublished data from Professor Frank Schäbitz taken in 2011.

This increased terrigenous input may be associated with destabilisation of the local catchment caused by decreased vegetation cover (Davies *et al.*, 2015), which may have been indicated earlier in the record by a reduction in TOC since 4,800 BP in zone BA-2. It is highly likely that mass flow(s) of sediment from the steep crater lake sides are responsible for such a large volume of minerogenic material being deposited in a short space of time. Other than this period between 3,600 BP to 3,300 BP, no clear evidence of turbidites could be observed through the core (e.g. sediment colour change or significant change in TOC, diatom or

grain size which may suggest turbidites (e.g. Moernaut *et al.*, 2014) between laminated and non-laminated sections of core.

Low TOC throughout BA-3 may represent lower overall productivity with similarly decreased with valve concentration, biogenic silica (Si:Ti) and presumably biogenic carbonate production (low Ca:Ti). However, this decrease in TOC, biogenic silica and carbonates, may also be attributed to dilution effects from increased catchment inputs. Interestingly, low C:N throughout this zone suggests that sources of the albeit decreased TOC remained mixed, but with low allochthonous input. Furthermore, with a few samples a C:N ratio <10 organic at some points matter was primarily autochthonous algal material (Leng *et al.*, 2010; Figure 6.5 and Figure 6.7).

The abundance of *Nitzschia paleacea* and *Ulnaria acus* during this period suggest that nutrient input (Si and P at least) must have been sufficiently high to support these taxa. Furthermore, the availability of these nutrients must have varied, at least seasonally, with differing Si:P requirements for these taxa (Kilham *et al.*, 1986). Nutrient input during this period may be an inorganic fraction. P increases slightly (not shown in Figures 6.5-6.8), but only weakly, positively correlated with terrigenous elements such as Fe and Ti ($r^2 = 0.17-0.22$, $p = <0.001$) during this zone. Therefore, some of these nutrients may be explained by in-washed material as in Corella *et al.* (2012) and Ma *et al.* (2016). However, with lower correlation indices than in those studies P may also be sourced from elsewhere. For example, anoxic conditions are related to releasing available P from the bottom sediments and with high Fe:Mn at Babogaya periods of anoxia may contribute to P availability in the lake (Burley *et al.*, 2001; Selig & Schlungbaum, 2003). The consistent, increased abundance of *Nitzschia palea* in

this zone supports increasingly nutrient rich and turbid waters in which they can thrive (Tuchman *et al.*, 2006; Salomoni *et al.*, 2006) likely associated with increased minerogenic input at Babogaya at this time.

The continued presence of deeper water taxon *Nitzschia lancettula*, as well other freshwater taxa, throughout this zone (Figure 6.9 and Figure 6.10) suggests that water levels remained at a high level and likely stratified to some degree. The decrease in the abundance of *Nitzschia lancettula* however through this zone may suggest a slight lowering from the previous zones, although this may also be attributed to the increased abundance of taxa such as *Nitzschia paleacea* and presumably *Nitzschia fenestralis* (see taxonomy and possible ecology of this taxon in Appendix 2) during this period of increased minerogenic and nutrient input.

Shallow water and littoral taxa such as *Staurosirella pinnata*, *Pseudostaurosira brevistriata* and *Nitzschia epiphytica* attest to shallower waters persisting through this period (Figure 6.9 and Figure 6.10). Furthermore, the high abundance of the meso-hypersaline *Nitzschia* “group latens” (optimum of 5259.60 $\mu\text{S}/\text{cm}$; Gasse *et al.*, 1995), despite the potentially ill-defined optima of this taxon (Barker, 1990), may suggest increasingly negative precipitation to evaporation ratios as lake level lowered and became increasingly saline. An explanation for this scenario is that the lake may have experienced some drying out. This period of drying was not sufficiently severe for the loss of habitat for deeper water taxa towards the middle of the lake, but sufficient to create other habitats of shallower water in other areas of the basin, potentially through fragmentation of habitat as before in zone BA-2. Although comparatively less abundant than other taxa, benthic and aerophilous taxa such as *Nitzschia epiphytica*, *Encyonema muelleri* and

Nitzschia amphibia are consistently present through this zone indicating at least some shallow, marshy, likely vegetated, areas persisted.

Towards the top of the zone between 3,300 BP and 3,100 BP the assemblage becomes plankton dominated (up to almost 100% of included taxa in one isolated sample responsible for a sharp increase in ROC; Figure 6.15) primarily by *Ulnaria acus*, *Synedra nana*, *Nitzschia gracilis*, the presumed facultatively planktonic *Nitzschia fenestralis* and *Nitzschia palea*. *Ulnaria acus* and *Synedra nana*, like all *Synedra* (now split into *Synedra* and *Ulnaria*), are some of the best competitors for P, but are poor competitors for Si, thus requiring a high Si:P in comparison to *Nitzschia* for optimal growth (Kilham *et al.*, 1986; Wang *et al.*, 2012). Similarly, *Aulacoseria granulata* var. *angustissima* like all *Aulacoseira* (formerly *Melosira*) are characterised by heavily silicified frustules, often forming long, filamentous colonies which requires high Si content for maximum growth and some degree of mixing to maintain suspension in the water column (Kilham, 1971; Kilham *et al.*, 1986). Furthermore, similar to *Ulnaria acus*, *Aulacoseria granulata* var. *angustissima* has been found to thrive in shallow waters across Africa (Gasse *et al.*, 1983).

The appearance of *Aulacoseira granulata* var. *angustissima* with high abundances of *Ulnaria acus* and increased *Synedra nana* abundance at the expense of taxa such as *Nitzschia lancettula* (Figure 6.9) suggests a niche environment of high Si content in mixed, turbid and shallower waters. During this period *Nitzschia gracilis* and *Nitzschia palea*, nitrogen heterotrophs (Gasse, 1986), are present with *Nitzschia fenestralis* (co-dominant with *Ulnaria acus*), supporting an environment characterised by increased turbidity and nutrient input, at least seasonally, for these taxa to thrive.

BA-4: 616 – 344 cm (composite core depth; 3110 – 1710 BP)

After 3110 BP the record is characterised by a moderately rapid rate of change (Figure 6.15) to an increased abundance of planktonic taxa, primarily *Aulacoseira granulata* var. *angustissima*, and subsequently reduced diversity (Figure 6.9). The shift from *Synedra/Ulnaria* to *Aulacoseira* dominated waters indicates continued fresh and nutrient rich conditions, but with a slight change that benefitted *Aulacoseira*. This taxon is normally associated with fresh, shallow, alkaline and productive waters (e.g. Bennion & Simpson, 2011) and in this case may represent a shift in the Si:P ratio of Lake Babogaya towards more P enriched waters with a higher requirement for this nutrient by *Aulacoseira granulata* and its varieties (Kilham *et al.*, 1986; Cumming *et al.*, 2015). Well-mixed waters, which as discussed above are conditions *Aulacoseira* species require, in shallower lakes is known to be good for nutrient recycling previously buried nutrients such as P (Bennion & Simpson, 2011). Despite the presence of *Nitzschia lancettula*, which indicates stratification may have occurred at least seasonally (required for the formation of lamina), the decreased abundance of this taxon may represent a reduction in lake level and increased mixing which would promote the proliferation of *Aulacoseira granulata* var. *angustissima*.

This zone is also marked by a rapid and considerable increase in local productivity with increased TOC (from mostly mixed sources with a C:N ratio around 15), biogenic silica (increased Si:Ti and valve concentration) and presumably biogenic carbonates (increased Ca:Ti) following the sharp transition from minerogenic to partially laminated sediments (Figure 6.5). A combination of well-mixed, shallower lake waters and increased organic input likely created the optimal conditions for *Aulacoseira granulata* var. *angustissima* to thrive. The

sustained high abundance of *Nitzschia fenestralis* during this period strengthens the interpretation that this newly identified taxon prefers nutrient enriched lake waters (see Appendix 2 for discussion of taxonomy and ecology from Grady *et al.* 2020).

After 2,750 BP the abundance of *Nitzschia lancettula*, *Nitzschia fenestralis* and *Nitzschia paleacea* increases, with the dominant taxa/taxon fluctuating between the latter two and *Nitzschia lancettula*, at the expense of *Aulacoseira granulata* var. *angustissima* (Figure 6.9). This may represent increased stratification which reduces the competitiveness of *Aulacoseira granulata* var. *angustissima* which need to remain buoyant in the water column, despite increased nutrient input as inferred from the abundance of *Nitzschia paleacea* (Woodbridge & Roberts, 2010), attributable to increasingly stratified, deeper waters (at least seasonally – required in the formation of lamina) associated with *Nitzschia lancettula* (Mills & Ryves, 2012). The continued presence (although low) of periphytic taxa such as *Nitzschia epiphytica*, with occasional reappearance of the meso-hypersaline *Nitzschia* “group latens”, suggests small areas of littoral habitat and shallower waters were still present in the lake basin during this period.

After 2,100 BP a decrease to negligible amounts of *Nitzschia lancettula* (<1% to ~14%), together with an increase in benthic (e.g. *Encyonema muelleri* and *Cymbella leptoceros*) and the aerophilous *Nitzschia amphibia* (Figure 6.9), may represent a period of lake level regression. Interpreting change through this period is challenging due to the indirect inferences of the ecology of *Nitzschia fenestralis* and with little change in other proxies analysed. While terrigenous input gradually increases at this point, which may point to increased catchment instability, TOC remains relatively high despite being variable with only a small

decrease in inferred biogenic carbonates (Ca:Ti) and silica (Si:Ti; Figure 6.5). One scenario is, as possible in previous zones, the increased abundance of *Nitzschia fenestralis* and *Nitzschia paleacea* (Figure 6.9) suggests a period of enhanced nutrient availability which may be masking other chemical or physical changes. Another possibility is the immediate influence of a tephra fall on the diatom community. However, it is unlikely that any possible deposition of material had a significant impact on the alkalinity and nutrient availability within the lake with the dominance of *Nitzschia paleacea* and *Nitzschia fenestralis*. Although Telford *et al.* (2004) find that the effects of tephra deposition can last several decades in a lake system, any potential benefits of this small layer in the Lake Babogaya record (~1 cm) such as direct nutrient input are highly unlikely to last for the full length of this period (Harper *et al.*, 1986; Urrutia *et al.*, 2007).

BA-5: 344 – 68 cm (composite core depth; 1710 – 580 BP)

As in previous zones, the reappearance of small Fragilarioid taxa, with similar parallel minor reappearances (~2-3%) of *Lindavia ocellata*, corresponding to decreased *Nitzschia lancettula* (Figure 6.9) abundance may indicate a slight lowering of lake level and expansion of fresh but shallower, littoral areas. This is further supported by a small reappearance of *Aulacoseira granulata* var. *angustissima* indicating sufficiently regular mixing of waters. Furthermore, the abundance of *Nitzschia paleacea* and *Nitzschia fenestralis* typical of nutrient-enriched water decreases considerably to negligible relative abundance by 1,400 BP (Figure 6.9). In their place, a benthic community establishes, especially the appearance and proliferation of a more diverse Cymbelloid community. By their nature of living on the end of mucilage stalks (e.g. *Cymbella* and *Gomphonema*), or within mucilage tubes (e.g. *Encyonema*), taxa belonging to the Cymbellales

order are generally periphytic. Taxa of this order abundant during this period at Babogaya are predominantly characteristic of fresh, well-lit, but shallower, nutrient-poor, marginal water bodies that are often vegetated (Gasse, 1986; Krammer & Lange-Bertlaot, 1988; Rimet & Bouchez, 2012).

After ~1,600 BP, and for the remainder of the zone, *Nitzschia lancettula* recovers and increases again to higher abundances indicating deeper, stratified waters re-established (Mills *et al.*, 2014; Figure 6.9). However, the abundance of benthic, predominantly Cymbelloid, taxa remains high, with sustained presence of a small *Nitzschia amphibia* population as well through this zone attests to the continuation of shallower waters in the basin (Figure 6.9).

This mixture of deeper-water taxa (*Nitzschia lancettula*) and shallower, periphytic taxa indicate lake waters were likely deep, but with a sufficiently large and potentially vegetated littoral zone. However, inferred algal productivity through this zone is poor with reduced deposition of diatom valves (low valve concentration), biogenic silica (Si:Ti) and carbonates (Ca:Ti) despite relatively high TOC from mixed sources (C:N ratio of ~15; Figure 6.5).

These conditions, however, are punctuated by a repeated interval of *Staurosirella pinnata*, *Pseudostaurosira brevistriata* and corresponding abundance of *Lindavia ocellata* (although at a low abundance of ~4%), but at the expense of benthic taxa with the disappearance of *Cymbella affinis* and *Encyonopsis microcephala*, as opposed to *Nitzschia lancettula* as before (Figure 6.9). Sediments are non-laminated with low inferred productivity: TOC decreases to values just higher than those recorded in zone BA-3 and similarly, deposition of biogenic silica and carbonates decreases to lowest average values since zone BA-3 (Figure 6.5).

Terrigenous input also increases during this period which may be attributed to instability of the surrounding, less-vegetated environment caused by drier conditions. Drier conditions may also explain the presence of shallower-water taxa with conditions such as these leading to a slight lowering in the lake level.

6.6 | Summary of the palaeolimnological Lake Baboagaya record

The interpretation of these limnetic and environmental changes inferred from the available data are summarised below. Discussion of these environmental and climatic inferences, and their implications within the wider context of this study, together with the equivalent for Garba Guracha (Chapter 7), can be found in Chapter 8.

BA-1: 470 – 375 cm (floating composite depth; 5400 – 4865 BP)

- Laminae formation evident despite presumably shallower waters indicated by small *Fragilarioid* taxa.
- Extensive habitat for epiphytic taxa.
- Gradual establishment of deeper waters.

BA-2: 375 – 202 cm (floating composite depth; 4865 – 3670 BP)

- Decrease and disappearance in *Staurosirella pinnata* and *Nitzschia epiphytica* suggest continued gradual increase in lake depth.
- Littoral habitat still important with the abundance of *Pseudostaurosira brevistriata* and associated *Lindavia ocellata*.
- Stratified conditions develop in parallel with deeper waters with the abundance of *Nitzschia lancettula*.
- Reduced lake level and re-expansion of littoral habitat after 4,200 BP.

- Possible catchment instability following a decrease in productivity after 4,200 BP with a decrease in TOC.
- However, Ca remains high with laminae continuing to form in the lake.

BA-3: 202 – 0 cm (floating composite core depth) and 828 – 616 cm (composite core depth; 3670 – 3110 BP)

- High rates of terrigenous deposition (enhanced Fe and Ti), likely representing mass flow(s) of sediment from the crater lake sides, following drying and catchment instability after 4,200 BP.
- Despite high Ca content (inferred from high Ca peak area) laminae did not form, presumably due to unstable lake waters.
- Corresponding decrease in productivity with values of TOC, diatom valve concentration, biogenic silica and carbonates reduced.
- Increasingly turbid and nutrient-rich waters with increased abundance of *Nitzschia paleacea* and *Nitzschia palea*.
- Areas of deeper waters in the basin still present with the presence of *Nitzschia lancettula*, but also shallower waters especially with the appearance of the meso-hypersaline *Nitzschia* “group latens”
- Periods of nutrient-rich waters.

BA-4: 616 – 344 cm (composite core depth; 3110 – 1710 BP)

- Increased overall productivity with higher TOC, biogenic silica, carbonates and greater concentration of diatom valves.
- Lake waters were mixed and nutrient-rich between 3,300 and 2,700 BP with the abundance of *Aulacoseira granulata* var. *angustissima*, *Nitzschia*

gracilis and *Nitzschia fenestralis*. Accompanied by return of laminated sediments.

- Presumed lower lake level with decreased *Nitzschia lancettula* population, but this signal may be obscured by other taxa thriving with increased nutrient input.
- Interval of higher, stratified lake levels after 2,700 BP with increase of *Nitzschia lancettula*.
- Return to lower lake level with decrease of *Nitzschia lancettula*, but nutrient input remains high with *Nitzschia fenestralis* and *Nitzschia paleacea* abundant.

BA-5: 344 – 68 cm (composite core depth; 1710 – 580 BP)

- Despite higher TOC, algal productivity is reduced (low valve concentration, biogenic silica and carbonates).
- Increased abundance of benthic taxa, predominantly of the Cymbellales order suggestive of shallower, fresh marginal areas in the lake basin.
- Continued lower levels between 1,250 and 750 BP and decreased nutrient input with re-appearance of small Fragilarioid taxa as in BA-1, replacing *Nitzschia paleacea* and *Nitzschia fenestralis*.
- Gradual increase in lake level with increased abundance of *Nitzschia lancettula* after 750 BP.

Chapter 7 :

Results - Garba Guracha

In this chapter, the modern limnology and environment of Garba Guracha is outlined, then the palaeolimnological record of past environmental change over the past ~16,000 years is discussed. The lithological and chronological framework is presented (as in Bittner *et al.* submitted), which provides the context for the results of detailed geochemical and diatom analyses. The results from this thesis are then also interpreted and synthesised with data produced by other members of the Bale Mountains research group including: biomarkers (Bittner *et al.*, submitted) and pollen (Gil-Romera *et al.*, 2019), facilitating a more detailed reconstruction of environmental change at Garba Guracha for the past 16,000 years.

7.1 | Modern aquatic environment

The waters of the Garba Guracha catchment are largely similar in chemical composition, with few minor differences between sample points (Table 7.1). Water pH is circumneutral with a low conductivity (6.92-7.37 pH and 50-98 $\mu\text{S}/\text{cm}$). The ionic composition is also largely uniform across each sampling site, with HCO_3^- the dominant anionic component and little change with depth in the lake centre. Despite low concentrations across every sample point, anions such as NO_3^- and HCO_3^- are comparatively more concentrated at Input 1. Spring samples typically exhibit lower concentrations of ions, except for nitrate, in comparison with other samples (Table 7.1).

Table 7.1: Garba Guracha hydrochemistry in February 2017. Sampling locations around the lake are shown in Figure 4.1.

	Conductivity ($\mu\text{S/cm}$)	pH	HCO_3^- (mg/L)	Cl^- (mg/L)	SO_4^{2-} (mg/L)	F^- (mg/L)	NO_3^- (mg/L)	K^+ (mg/L)	Na^+ (mg/L)	Ca^{2+} (mg/L)	Mg^{2+} (mg/L)
Spring 1	75	7.37	36.12	3.30	13.81	0	9.20	1.27	12.05	3.06	0.27
Spring 2 & 3 (Pool)	73	7.02	38.90	3.47	14.11	0	8.87	1.78	10.63	3.59	0.43
Spring 4	50	7.13	30.56	2.87	13.84	+	6.56	0.84	5.98	2.88	0.47
Outlet	71	7.04	50.01	3.53	13.66	0	+	1.58	8.86	6.50	0.75
Lake waters (Surface)	75	6.98	39.73	3.60	13.65	0	+	1.87	9.36	5.88	0.78
Lake waters (5 m depth)	88	7.00	44.45	3.75	14.34	0	+	2.65	9.49	6.44	0.83
Shoreline	71	7.08	52.79	3.75	13.64	0	+	1.59	8.91	4.45	0.75
Input 1	83	7.27	77.79	3.05	15.50	0.25	7.12	1.91	13.40	4.25	0.21
Input 2	70	7.29	41.68	3.52	13.89	0	+	1.55	8.94	5.16	0.71
Input 3	98	6.92	50.57	4.79	13.09	0	+	3.14	13.57	4.89	0.71
Swamp	85	7.07	50.01	4.31	13.45	0	+	3.12	13.74	4.91	0.66

7.2 | Modern diatom ecology

The results of each sample and total site abundance are presented in Figure 7.1, with the abundance values written here expressed as a percentage of all samples taken, unless stated otherwise. Small, pennate Fragilarioid taxa are the most dominant (71.4%; Figure 7.1), with *Staurosirella pinnata* and *Staurosira construens* var. *venter* varieties making up >87% of this. This dominance of Fragilarioid taxa is illustrated by the composition of a littoral sample taken at Input 2, with >97% being Fragilarioid taxa. Naviculoid and Cymbelloid species were uncommon across the site (9.3%, 5.6%, 4.5% and 3.1%, respectively). However, the total abundance of these taxa are biased by the relatively high abundance of *Encyonopsis microcephala* and *Cymbella gracilis* in a single epiphytic sample (Spring 4; 23.4%), and *Navicula minima* in the swamp sample (18.8%). Without these samples the relative total abundance of these taxa would be <0.5% and <2.5%, respectively.

Comparatively, epiphytic samples are the most diverse, despite still being dominated by Fragilarioid taxa, with a greater abundance of other taxa. For example, *Achnantheidium* (predominantly *Achnantheidium minutissima*) are the second most common taxa encountered across all samples, but most abundant in 3 samples 2 of which contain vegetation, highest in the swamp (21%). Similarly, *Gomphonema* (predominantly *Gomphonema parvulum*) are most common in epiphytic samples. *Amphora pediculus* (the only *Amphora* species observed) is only present in a few samples, with a relatively high abundance in the shoreline littoral sample (11.2%). Multiple, small *Nitzschia* species (mainly *Nitzschia palea* and *Nitzschia epiphytica*) are rare across the site (0.3-6.2% across samples; 2% total).

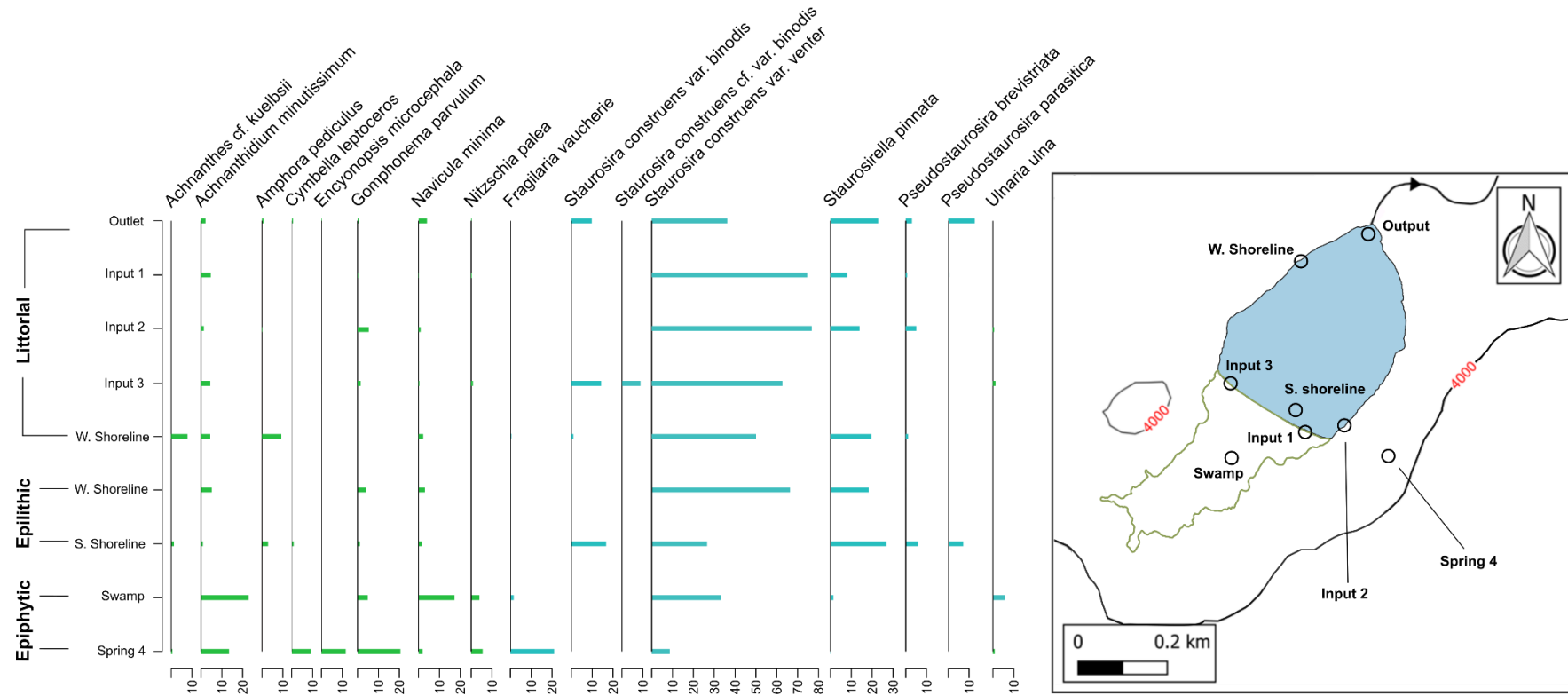


Figure 7.1: Composition of the Garba Guracha diatom flora around the lake (left), with sample locations also shown (right). Taxa above 3% relative abundance are included.

7.3 | Master core creation and lithology

A master core (BAL-GGU17-1AB) of the overlapping BAL-GGU17-1A and 1B cores (included material shown in Figure 7.2) was created by visual correlation of core lithology and several XRF elements (Ti, Fe, Rb, and K) using the Excel software Stratfit (Sagnotti & Caricchi, 2018). Master core creation was performed by L. Bittner, the author of this thesis and G. Gil-Romera.

Four major lithostratigraphic units in BAL-GGU17-1AB are defined based on variations in colour, texture and composition as identified by smear slide analysis (Figure 7.2). The sedimentary sequence of BAL-GGU17-1AB consists of green banded siliciclastic fine material interbedded with layers of coarser material and even gravel in the lower part (Figure 7.2). It can be divided into 4 lithostratigraphic units:

Unit 1 (1552-1476 cm) contains greenish banded siliciclastic coarse sand.

Unit 2 (1476 – 1276 cm) is composed of two meters of highly coarse silt and gravel.

Unit 3 (1276-838 cm) consists predominantly of green banded siliciclastic material mostly coarse silt with amorphous organic matter (OM) intersected by one layer of fine silt between 1219-1166 cm and a layer of coarse sand at 1031-966 cm.

Unit 4 (838-70 cm) consists of nearly 8 m of dark brown massive organic mud with varying diatom content. This unit is intersected by a small layer of green-greyish massive siliciclastic fine silt at 828 cm and two layers of organic poor, finer sediments at 496 cm and 505 cm.

Three tephra layers have been identified at 129 cm (GGT-1), 604 cm (GGT-2), and 1198 cm (GGT-3) depth, respectively. The latter through XRF-derived trends (see below for detail). Geochemical analyses of tephra glass shards by C. Martin-Jones (Cambridge University; as part of Bittner *et al.* in prep) finds that GGT-1 correlates best with tephras TT-2 from Lake Tilo and CHT-1 from Lake Chamo and GGT-2 with Tilo tephra TT-13 (see Martin-Jones *et al.*, 2017), which have been linked to Corbetti (Fontijn *et al.*, 2018). Analyses are ongoing for GGT-3.

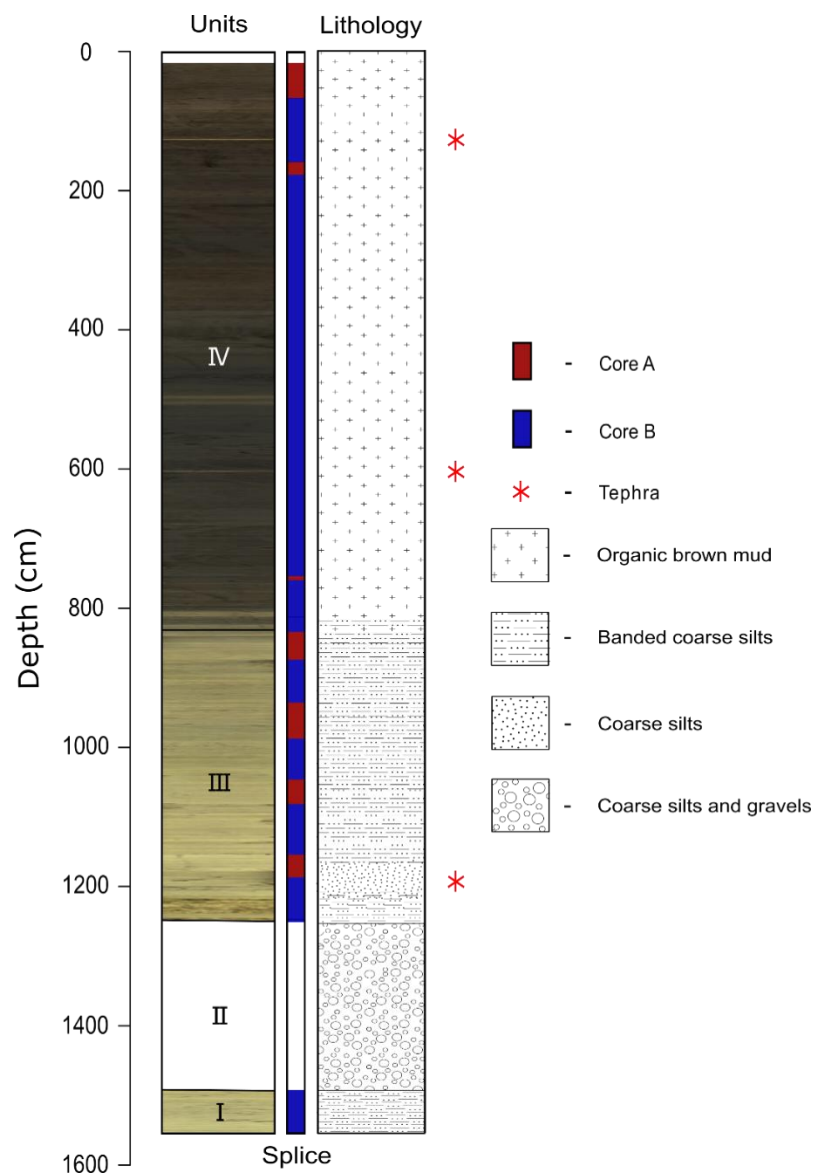


Figure 7.2: Garba Guracha master core (BAL-GGU17-1AB) lithostratigraphy (Bittner *et al.*, submitted.).

7.4 | Core chronology

7.4.1 | Sediment-water interface

Total ^{210}Pb activity reaches equilibrium depth with supported ^{210}Pb at ~52 cm of the core. Unsupported ^{210}Pb activities, calculated by subtracting ^{226}Ra activity (as supported ^{210}Pb) from total ^{210}Pb activity, decline overall irregularly with depth (Figure 7.3b). The unsupported ^{210}Pb activity profile shows two different sections: the top 19 cm and the rest of the core. Within each individual section, unsupported ^{210}Pb activities decline more or less exponentially with depth, suggesting relatively uniform sedimentation rate within the sections. However, sedimentation rates might have changed at 19 cm (Yang, pers. comm.).

The ^{137}Cs activity versus depth profile (Figure 7.3c) shows a well-resolved peak at 7.5 cm. This peak is most likely derived from the 1963 AD fallout maximum of the atmospheric testing of nuclear weapons. The anthropogenic radionuclide Americium-241 is considered rare (~0.5% of the ^{137}Cs inventory) in the environment, but stable in lake sediments (Appleby *et al.*, 1991; Appleby, 2001). Although one data point is insufficient for dating, ^{241}Am activity of any kind at 7.5 cm supports the 1963 fallout of nuclear weapon testing represented by ^{137}Cs trends.

Use of the CIC (constant initial concentration) dating model was precluded by the variability in the unsupported ^{210}Pb profile. ^{210}Pb dates were calculated using the CRS (constant rate of ^{210}Pb supply) dating model (Appleby & Oldfield, 1978). The CRS dating model places 1963 depth at 14.5 cm, which is considerably deeper than the depth suggested by the ^{137}Cs and ^{241}Am records. The corrected CRS chronologies and sediment accumulation rates were calculated by using the

sediments at 7.5 cm as formed in 1963. ^{210}Pb sedimentation rates show similar levels before 1963, while there is a small peak in the 1930s (~19 cm; Table 7.2; Figure 7.3).

Table 7.2: ^{210}Pb chronology of Garba Guracha sediment-water interface core.

Depth (cm)	Drymass (g cm ⁻²)	Chronology		Sedimentation Rate		
		Date (AD)	Age (yr)	g cm ⁻² yr ⁻¹	cm yr ⁻¹	± %
0	0	2017	0	-	-	-
1.5	0.0661	2014	3 ± 2	0.0242	0.248	3.3
4.5	0.4389	1997	20 ± 2	0.0181	0.129	4.3
6.5	0.7642	1976	41 ± 3	0.0138	0.086	5.4
7.5	0.9188	1963	54 ± 5	0.0096	0.062	5.7
8.5	1.0774	1960	57 ± 5	0.066	0.4	6.8
9.5	1.2495	1958	59 ± 5	0.086	0.5	6.3
10.5	1.4216	1956	61 ± 5	0.0799	0.429	9
12.5	1.8091	1951	66 ± 5	0.0762	0.4	8.3
14.5	2.184	1946	71 ± 5	0.0768	0.444	10.7
16.5	2.5007	1942	75 ± 6	0.0782	0.444	12.8
18.5	2.8881	1937	80 ± 6	0.0984	0.444	19
20.5	3.3863	1933	84 ± 6	0.1255	0.5	16.2
22.5	3.8918	1929	88 ± 7	0.108	0.444	21.3
24.5	4.3597	1924	93 ± 7	0.084	0.4	24.8
26.5	4.7295	1919	98 ± 8	0.082	0.5	28.9
28.5	5.017	1916	101 ± 9	0.089	0.556	26
31.5	5.5316	1910	107 ± 10	0.085	0.5	40.8
34.5	6.0403	1904	113 ± 11	0.076	0.437	30.7
38.5	6.742	1894	123 ± 13	0.064	0.364	71.8
42.5	7.4532	1882	135 ± 14	0.0655	0.364	51.4
46.5	8.1826	1872	145 ± 15	0.064	0.346	76.2
51.5	9.1197	1856	161 ± 18	0.058	0.313	86.6

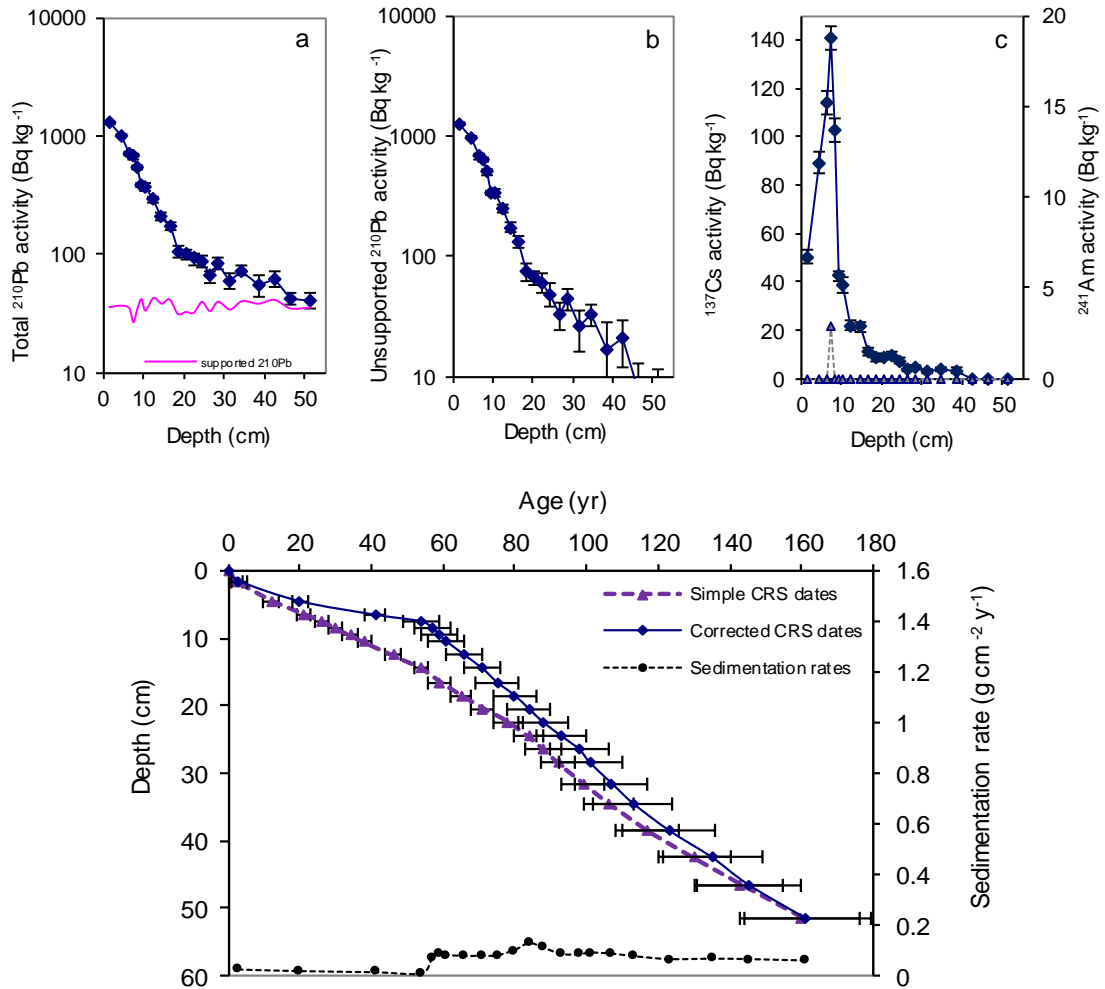


Figure 7.3: Fallout radionuclide concentrations in short core taken from Garba Guracha showing (a) total ^{210}Pb , (b) unsupported ^{210}Pb , and (c) ^{137}Cs and ^{241}Am concentrations versus depth (top). Radiometric chronology showing the CRS model ^{210}Pb dates and sedimentation rates for the Garba Guracha short core (bottom).

7.4.2 | Main core

A total of 25 ^{14}C dates from three different materials (Table 7.3) was merged with data from the surface core to give a full composite chronology created using a Bayesian age-depth model (Figure 7.4). The stratigraphically consistent radiocarbon dates indicate the long core covers from 15930 to 325 cal yr BP, with the surface core extending to the present based on the ^{210}Pb chronology with a small gap of ~70 years between the long core and surface core.

The mean sedimentation rate (MSR) for the BAL-GGU17-AB core is 1.25 mm per year. The sedimentation rate of the core is relatively constant. The highest average values of 2.90 mm per year are recorded between 1,110-990 cm with maximum values of 5 mm per year. A second maximum is present from 900 to 720 cm with a sedimentation rate of 1.26 mm per year. In between these maxima, a marked sedimentation minimum with decreased rates by up to 80% characterizes the time period from 12,800 BP to 11,300 BP. From 720 cm the sedimentation rate decreases constantly until the present day with a mean sedimentation rate of 0.70 mm per year.

7.5 | Core geochemistry

Selected high-resolution geochemical elements plots are shown in Figure 7.5, which is divided into zones based on large changes in at least two elements plots. All units are given as normalised (/Mo Inc+Coh see Chapter 4 for details on normalisation process) peak area, with the ratio plots dimensionless. The solid black line represents a 500-point smoothing of the data to highlight more general trends. Lithogenic elements strongly, positively correlate ($r = 0.89$ to 0.97 ; Figure 7.6) and can be seen to covary in Figure 7.5. This positive correlation amongst lithogenic elements also extends to Mn, Ca and Y with r -values of >0.8 , 0.93 - 0.97 and >0.75 , respectively (Figure 7.6). Values of elements such as Rb (0-0.076 peak area) are low in comparison to elements such as Fe (0.126-2.712 peak area) but co-vary with the more common lithogenic elements indicating that the trends are reliable.

Table 7.3: AMS radiocarbon dates in order of depth for the Garba Guracha core.

	Samples			¹⁴ C age (yrs BP)	Calibrated age (cal. BP)
	Code	Depth (cm)	Material		2-σ range (relative area under probability distribution)
Universität Bern	7931.1.1	105	Bulk	935 ± 118	662-1081 (99.6%)
	8273.1.1	105	n-alkane	1076 ± 79	796-875 (87.2%)
	8282.1.1	185	Charcoal	2124 ± 129	1779-2366 (99.5%)
	7930.1.1	205	Bulk	2323 ± 111	2110-2722 (99.4%)
	8272.1.1	205	n-alkane	2399 ± 101	2302-2743 (95.4%)
	8271.1.1	303	n-alkane	3476 ± 89	3556-3979 (98.5%)
	7929.1.1	303	Bulk	3517 ± 111	3555-4091 (98.2%)
	8270.1.1	503	n-alkane	5789 ± 109	6391-6804 (94.5%)
	7928.1.1	503	Bulk	5794 ± 135	6305-6903 (100%)
	8269.1.1	602	n-alkane	6967 ± 123	6391-6804 (100%)
	7927.1.1	602	Bulk	7320 ± 144	7922-8404 (98.0%)
	8268.1.1	700	n-alkane	8753 ± 156	9516-10201 (99.7%)
	7926.1.1	705	Bulk	8753 ± 162	9496-10206 (100%)
	8279.1.1	794	Charcoal	10214 ± 203	11267-12531 (100%)
	7925.1.1	794	Bulk	9301 ± 273	9740-11235 (100%)
	8267.1.1	898	n-alkane	9650 ± 155	10545-11368 (99.2%)
	8266.1.1	898	n-alkane	9706 ± 175	10563-11640 (99.4%)
7924.1.1	998	Bulk	11110 ± 48	12828- 13082 (100%)	
Direct AMS	D-AMS 029493	1108	Bulk	11377 ± 50	13102- 13313 (100%)
	D-AMS 029494	1218	Bulk	12181 ± 51	1390-14230 (98.7%)
	D-AMS 029495	1493	Bulk	12977 ± 53	15291-15740 (100%)
	D-AMS 027899	1528	Bulk	12997 ± 57	15304-15772 (100%)
	D-AMS 029496	1548	Bulk	13294 ± 59	15772-16193 (100%)

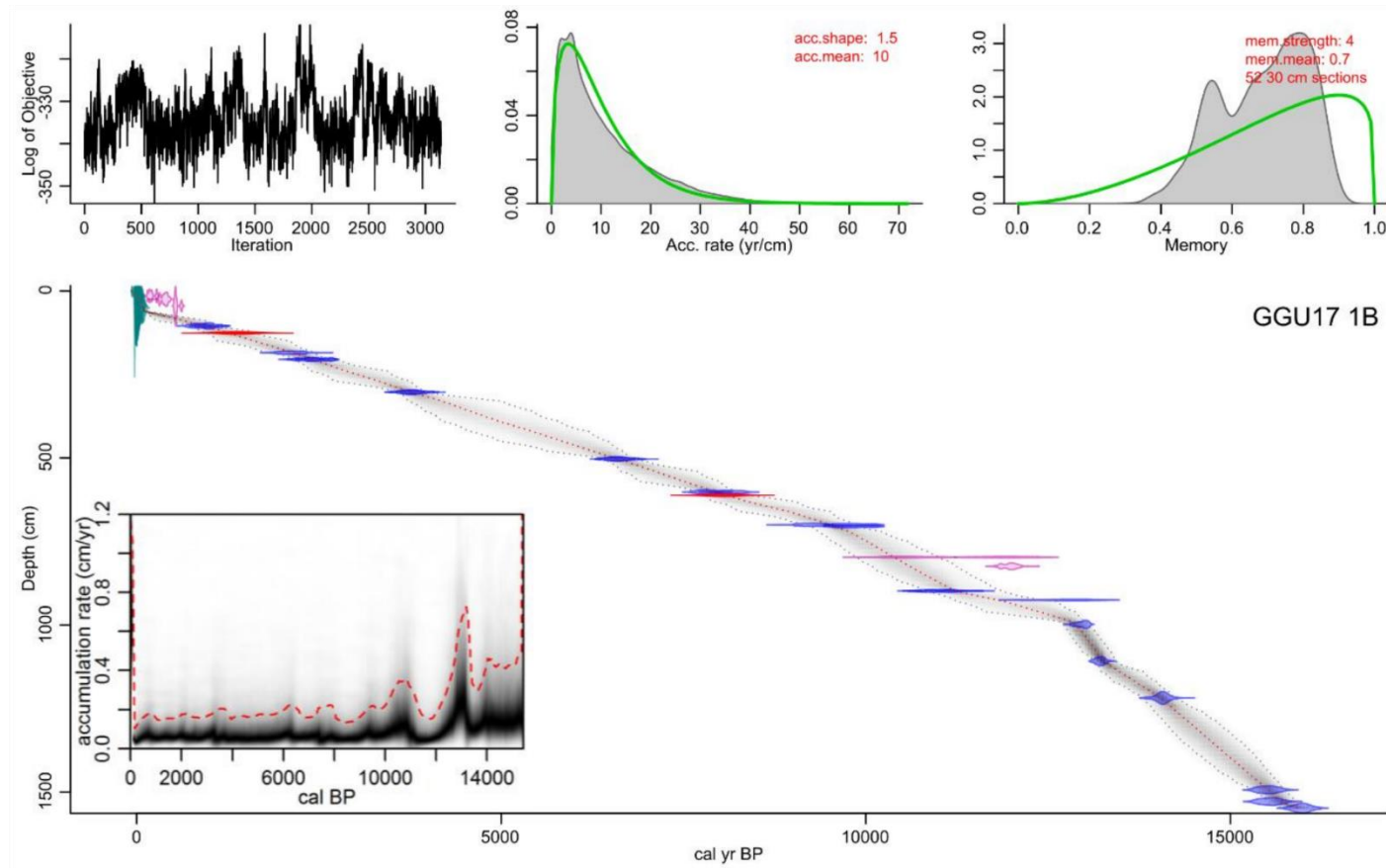


Figure 7.4: Bayesian age-depth model of fourteen bulk AMS ^{14}C dates from core BAL-GGU17, constructed in Bittner *et al.* (submitted) using BACON for R. Depth refers to depth below the sediment surface. The individual age distribution for each date, as relative area under probability distribution, is shown in blue. The red dotted line shows the most likely age-depth distribution, whilst the grey envelope denotes the chronological uncertainty of the model. The upper panel shows the stability of the Markov Chain Monte Carlo runs (3500 iterations); the prior (thick line) and posterior (thin line) distribution for the accumulation rate (yr/cm), and; the prior (thick line) and posterior (thin line) for the dependence of accumulation rate between sections.

The ratio of the incoherent scatter against the coherent scatter (Inc:Coh) can be used as an approximation of the atomic number of the average matrix composition. The number of incoherent scattering between electrons is theorised to be higher for elements with a low atomic mass (Guyard *et al.*, 2007). Since organic carbon has a lower average atomic number than inorganic materials (i.e. silica, carbonates or any clastic materials), increased Inc:Coh ratio values have been used successfully qualitatively to infer higher sediment organic content (e.g. Guyard *et al.*, 2007; Burnett *et al.*, 2011; Chawchai *et al.*, 2013). Strong negative correlation of Inc:Coh with major lithogenic elements ($r = -0.90$ to -0.97) confirms Inc:Coh is a useful proxy for increased organic content. Distinct and co-varying peaks of Fe, Y (not shown), Rb, K and Zr shown in Figure 7.5 also correlate with the location of visible tephra layers, and were thus useful in identifying a tephra horizon not detected in the lithological analyses.

GGX-1: 1,548 – 1,200 cm (15,950 – 13,950 cal BP)

Iron, Zr, Rb, K covary and are variable, but peak area values are on average at their highest throughout this zone (around 1.5, 0.15, 0.075 and 0.045, respectively) especially at the zone boundary between 1,211 and 1,240 cm. At this point, maximum peak area is reached in Zr (0.31), K (0.14) and Rb (0.07). Similarly, Mn is relatively stable at around 0.05 peak area, before reaching peak values (0.227 peak area) at the zone boundary with an average peak area of 0.102 ± 0.041 between 1,211 and 1,240 cm. In a negative correlation with lithogenic elements (Figure 7.5), ratio values of Inc:Coh, and Fe:Mn, are low (~4 and ~30, respectively) with a decrease to three times lower Fe:Mn values at the zone boundary over 30 cm. Zr:Rb values are consistently low at around 3 throughout this zone. The gap in data in this zone (1,237-1,540 cm) corresponds

to the lithostratigraphic unit II (Figure 7.3), composed of coarse sands and gravel, as the uneven surface of this unit could not be accurately scanned by the XRF.

GGX-2: 1,200 – 793 cm (13,950 – 10,630 cal BP)

This zone is characterised by decreased lithogenic element (including Mn) values following the highs of zone boundary, that slowly decreases with depth (e.g. K = ~0.050 peak area at 1,200 cm to ~0.025 peak area at 800 cm), despite some brief, moderate increases (e.g. around 1,200-1,100 cm and 1,000-900 cm) to slightly higher peak area values. The decrease throughout the zone, with moderate fluctuations, are more pronounced in K peak area, with this also true of Rb and Mn at ~1,000-900 cm, in comparison to other lithogenic elements.

Conversely, following the sharp increase at the boundary of zones 1 and 2, comparatively higher and constant values Fe:Mn are evident through this zone (average = 32.14 ± 5.38), with Inc:Coh steadily increasing from ~4 at 1,200 cm to 5.5-6 by 800 cm. Zr:Rb remains negligible at ~3. A previously unidentified tephra horizon was observed in the XRF at 1,199 cm depth by the highest Fe values in the core (2.71 peak area), and confirmed with high, covarying Y (not shown in Figure 7.4), Zr, K and Rb peak area (Figure 7.4).

GGX-3: 793 – 20 cm (10,630 – 80 cal BP)

Two distinct and co-varying peaks in Zr, Fe, Rb and K (with a corresponding sharp decrease in Inc:Coh) correlate with the visible tephra layers identified in lithological analyses at 604 cm and 129 cm. Apart from at these tephras, lithogenic elements are at their lowest throughout this zone after declining from the GGX-2. Despite some small increases (e.g. 500 cm), lithogenic elements continue to slowly decline from 793 to 20 cm. Similarly, Mn steadily decreases

throughout the zone, despite small, isolated peaks in peak area (e.g. 720 m and 530 cm), to reach the lowest values in the core after 180 cm with an average peak area of 0.006 to the top of the core. Inc:Coh continue to steadily rise in this zone, with average values not falling below 5.5, to peak values of around 6 towards the top of the core. In comparison to zones GGX-1 and GGX-2, Zr:Rb values increase through GGX-3 (~4-5 on average) with multiple large peaks in Zr:Rb (>40-88, but with two peaks of 147 and 224 not shown in Figure 7.5) after 350 cm.

Values of Fe:Mn are the most variable throughout this zone after 740 cm with values between 10 and 80 until 375 cm. After a comparatively large decrease starting at 375 cm (with average values from ~50 to ~30 at 325 cm) Fe:Mn continues to fluctuate at higher values, with a sharp increase at 175 cm to average values of >50 after 140 cm, with values of >100 reached toward the top of the core.

7.6 | The diatom record

GGD-1: 1547.5-774.5 cm (15,930-10,460 BP)

Diatom abundance throughout this zone is very low ($6.5\text{-}30 \times 10^3/\text{g}$; average $17.5 \times 10^3/\text{g}$), with the lowest concentrations in the core ($0.8\text{-}4.9 \times 10^3/\text{g}$) leading to incomplete counts, and thus a lack of data, between 1540 and 1120 cm (15,850-13,040 BP). It is important to note however, that a large portion of this gap in data also corresponds to the lithostratigraphic unit II (1,237-1,540 cm; Figure 7.7) composed of coarse sands and gravels, and thus could not be properly sampled for diatom analyses.

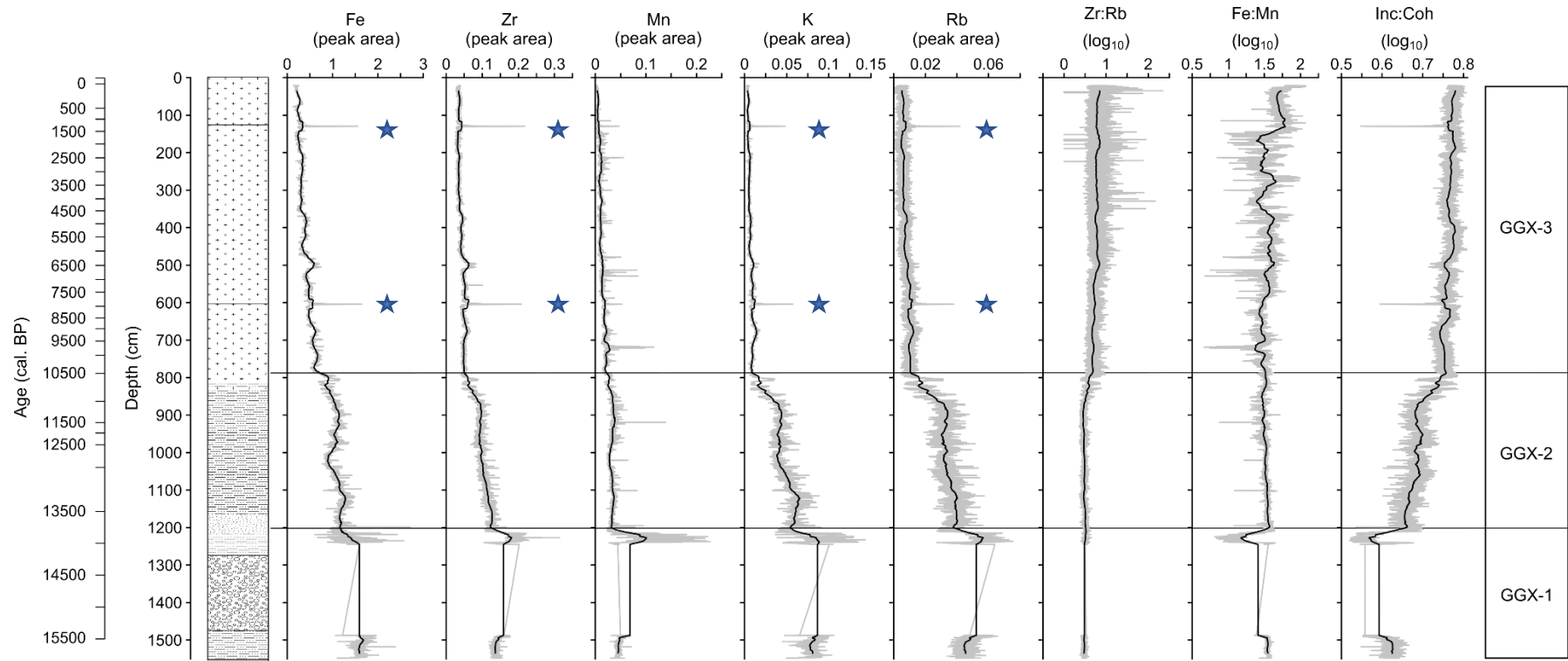


Figure 7.5: XRF-derived peak area geochemical data for the Garba Guracha core. Solid black line denotes a 500-point running mean. Stars denote position of tephra layers.

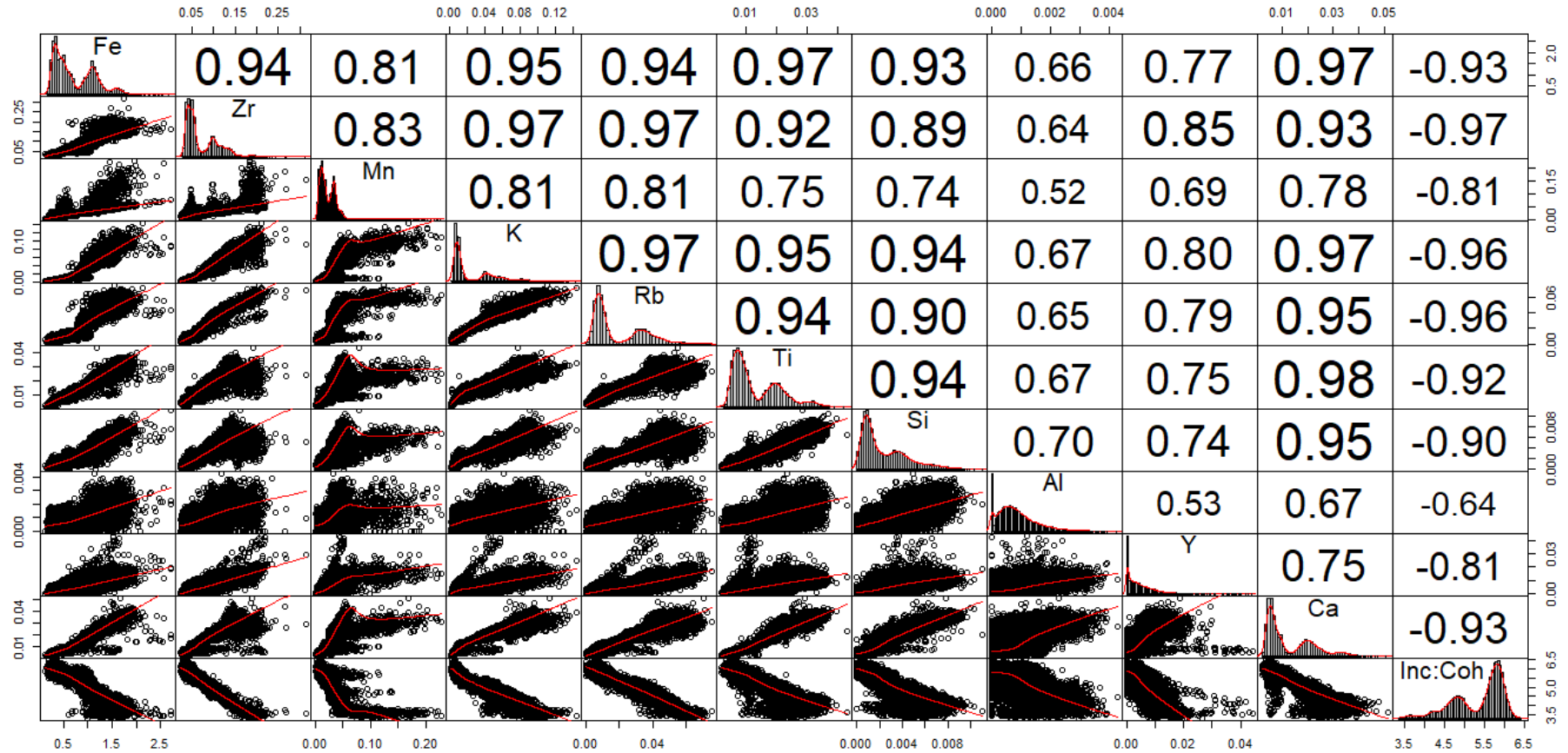


Figure 7.6: Pearson's correlation matrix of selected elements in the Garba Guracha core derived from XRF scanning. The first five elements, and all ratios, are shown in Figure 7.5. The matrices of scatterplots (below histograms) indicate the association and correlation of each comparison (r -values above histograms; $p=0.000$ for each correlation).

Facultatively planktonic Fragilarioid taxa are abundant through this zone. *Stausirella pinnata* (Ehrenberg) D.M.Williams & Round constitute up 20-40% of the assemblage in this zone, with *Pseudostaurosira pseudoconstruens* (Marciniak) D.M.Williams & Round abundance also relatively high, especially toward the base of the core (~40% relative abundance). Benthic taxa also represent up 30-40% of the assemblage in GGD-1, with low abundances of multiple taxa, mostly the epiphytic *Achnantheidium minutissimum* (Kützing) Czarnecki and *Gomphonema parvulum* (Kützing) Kützing. Taxa that are sometimes considered aerophilous (e.g. *Nitzschia amphibia* Grunow) also present at low abundances (<10%) in this zone after 1120 cm. The planktonic *Discostella stelligera* (Cleve & Grunow) Houk & Klee occurs between 918-867 cm, peaking at a relative abundance of 42.1% at 877.5 cm.

GGD-2: 764.5-680.5 cm (10,360-9,200 BP)

Fragilarioid taxa dominate this zone with the relative abundance of facultatively planktonic taxa consistently above 80% and reaching as high as 95% at ~740 cm. *Stausirella pinnata* increase from ~20 to 40% relative abundance from the previous zone to 43.7 at the base of this zone (764.5 cm), varying above 43% with a peak as high as 89.4% relative abundance (highest abundance through the core) at ~740 cm. Interestingly, valve concentration also rapidly increases at the start of the zone to reach high concentrations ($201 \pm 111 \times 10^3/\text{g}$ average between 764 and 680 cm).

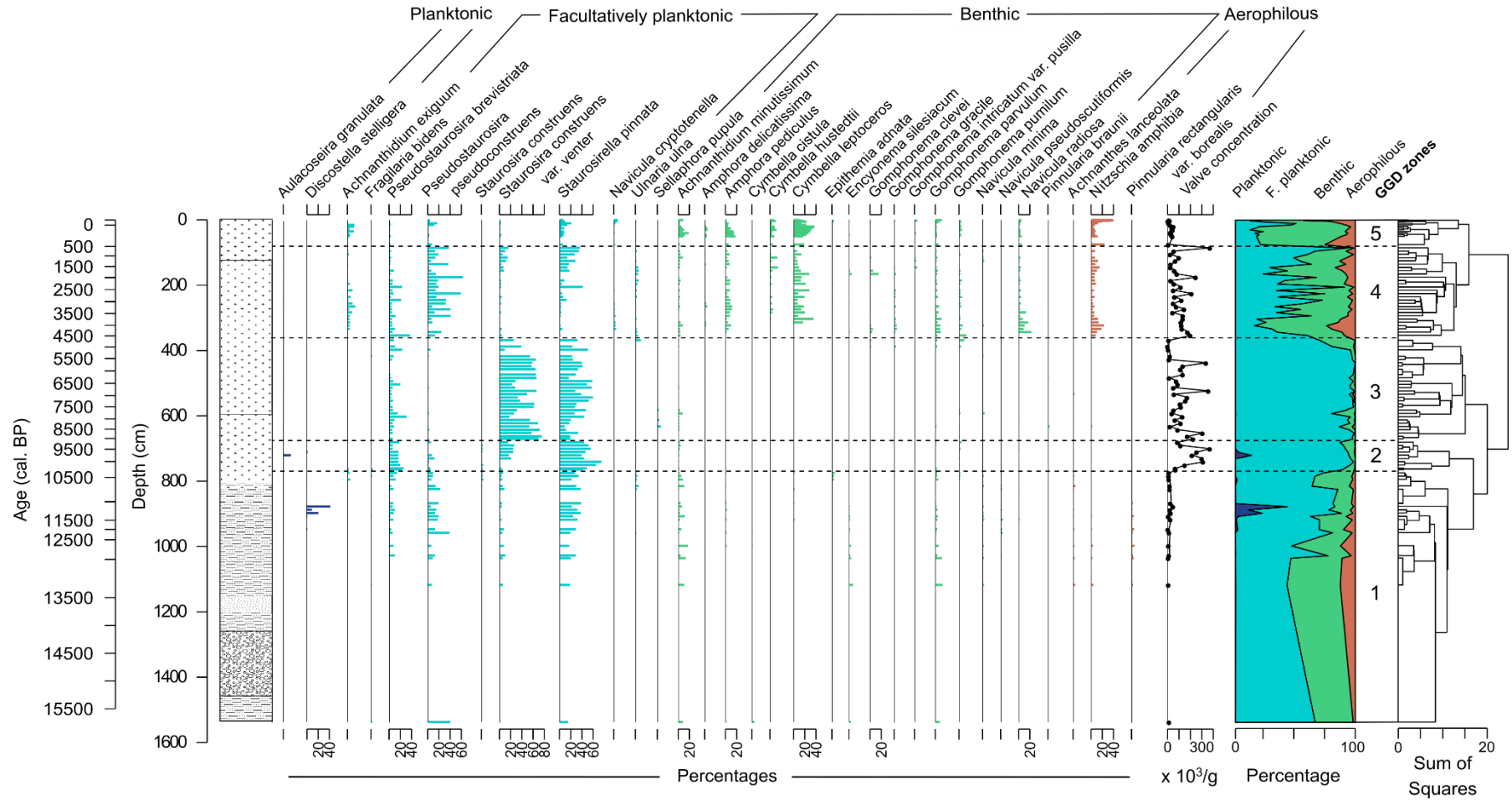


Figure 7.7: Diatom diagram for the Garba Guracha core by depth (age as secondary axis). Included are habitat groupings and valve concentration data. Zones as determined by CONISS are also shown (GGD-1, GGD-2, GGD-3, GGD-4, GGD-5).

After the peak abundance at 740 cm *Staurosirella pinnata* remains dominant at slightly lower abundances (50.5% on average), with a small secondary peak of ~65% at 690.5 cm, for the remainder of the zone. Similarly, valve concentration decreases slightly after ~740 cm, before rising in a similar trend to *Staurosirella pinnata* abundance.

After this small decrease in valve concentration/*S. pinnata* abundance at ~740 cm, *Staurosira construens* var. *venter* (Ehrenberg) P.B.Hamilton reaches an average abundance of 23.17% from 730 to 680 cm. Furthermore, a small, isolated increase in *Pseudostaurosira pseudoconstruens* abundance occurs (3-12% between 740 and 720 cm). *Pseudostaurosira brevistriata* (Grunow) D.M.Williams & Round comprises on average 17.97% of the assemblage throughout most of GGD-2, except for a small reduction to ~7% around 700 cm. Benthic taxa are present in GGD-2, but at considerably low relative abundances (<2%) for multiple individual taxa, with only isolated samples with taxa such as *Achnanthis minutissimum* and *Gomphonema pumilum* (Grunow) E.Reichardt & Lange-Bertalot reaching relative abundances of >5%. A small isolated peak of *Aulacoseira granulata* (Ehrenberg) Simonsen (~15.56% relative abundance) is present at 720 cm.

GGD-3: 680.5-368.5 cm (9,200-4,700 BP)

The relative abundance of facultatively planktonic taxa remains >90% throughout this zone, reaching their highest relative abundance (99.7%) at 437.5 cm. However, despite this high relative abundance, species diversity is low with *Staurosirella pinnata* and *Staurosira construens* var. *venter*, along with

comparatively small amounts of *Pseudostaurosira brevistriata*, are the only taxa present (Figure 7.7).

The relative abundance of *Staurosira construens* var. *venter* increases sharply at the zone boundary (15.6% at the upper boundary of GGD-2 to 73.7% at the lower boundary of GGD-3) and remains high (average 53.8% between 670.5 and 437.5 cm), with small decreases (by ~25%) at 602.5 and 503.5 cm. It is important to note that decreases such as these of *Staurosira construens* var. *venter* are largely mirrored by corresponding increases in *Staurosirella pinnata* and vice versa. Valve concentration remains relatively high between 670.5 and 437.5 cm, at an average of $137.1 \pm 93.6 \times 10^3/\text{g}$, with peaks almost triple the average at 652.5 and 437.5 cm. However, between 437.5 and 368.5 cm (5,730-4,700 BP) valve concentration drastically decreases to an average of $14.4 \pm 9 \times 10^3/\text{g}$, reaching as low as $2.4 \times 10^3/\text{g}$ at 407.5 cm. However, *Staurosira construens* var. *venter*/*Staurosirella pinnata* relative abundance remains high. Isolated peaks of *Pseudostaurosira brevistriata*, namely at 602.5, 503.5 and 397.5 cm of 45.2%, 20.6% and 24% relative abundance, respectively, can also be observed in GGD-3.

GGD-4: 368.5-85.5 cm (4,700-590 BP)

Valve concentration sharply increases from the upper boundary of GGD-3 to the lower boundary of GGD-4 by $189 \times 10^3/\text{g}$. Furthermore, this transition from zone GGD-3 to GGD-4 is also marked by a sudden, decline in *Staurosira construens* var. *venter* (4.1%) and *S. pinnata* (1.4%), a roughly 20 and 30% reduction, respectively. The dominance of facultatively planktonic Fragilarioid taxa is gradually reduced by increases in the abundance of benthic/aerophilous taxa.

Amphora pediculus (Kützing) Grunow and *Gomphonema parvulum* and *Gomphonema pumilum* are present throughout most of zone, but at low abundances (6%, 4% and 2.7% on average). Similarly, *Nitzschia amphibia* is observable throughout this zone with small peaks of ~25% and 15% at 323.5 and 145.5 cm, respectively. *Navicula radiosa* Kützing appears in the assemblage and reaches an average abundance of 10.68% between 353.5 and 283.5.5 cm. After 303.5 cm, the abundance of *Navicula radiosa* declines and remains negligible throughout GGD-4. Interestingly, at this point the abundance of *Cymbella leptoceros* (Ehrenberg) Kützing increases and the taxon remains abundant (16.1% relative abundance on average) between 303.5 and 185.5 cm, despite some isolated troughs (e.g. ~8% relative abundance between 255.5 and 245.5 cm).

However, it is important to note that facultatively planktonic taxa still represent a large percentage of the assemblage throughout parts of this zone this zone (9.8-92.7% through GGD-4). *Pseudostaurosira pseudoconstruens* is the most common facultatively planktonic taxon in GGD-4, with its relative abundance fluctuating multiple times between 0.5 and 64% through the zone (20.1 ± 15.9 % on average through GGD-4). *Pseudostaurosira brevistriata* is also sporadically present with a large peak at the lower zone boundary. Facultatively planktonic Fragilarioid taxa re-establish dominance after 155 cm with a gradual increase in the abundance of *Staurosirella pinnata*, small increases in *Staurosira construens* var. *venter* abundance. These increases correspond with gradual decreases in the abundance of taxa such as *Cymbella leptoceros* and *Nitzschia amphibia*. A large increase in valve concentration (61 to 378×10^3 /g; peak valve concentration for the core) marks the upper boundary of this zone.

GGD-5: 85.5-0.5 cm (590 BP-present day)

Following the peak in valve concentration at 85.5 cm GGD-5 begins with a sharp decrease to $\sim 13 \times 10^3/\text{g}$ and remains comparatively low ($31.2 \pm 15.3 \times 10^3/\text{g}$ on average) with valve concentration only reaching $>50 \times 10^3/\text{g}$ once (20.5 cm). The abundance of facultatively planktonic also decreases to $\sim 20\%$ at this point, with a corresponding rise in benthic/aerophilous taxa. *Cymbella leptoceros* is abundant during this period, with *Amphora pediculus* (4.3-19%), *Nitzschia amphibia* (3.8-12.4; max 24.2% at 75.5 cm), *Achnanthydium Minutissimum* (2.6-12.9%) also common. the relative abundance of *Cymbella leptoceros* (with similar trends in *Cymbella hustedtii* Krasske abundance) gradually increases and dominates the total counts ($>38\%$; $>46\%$ when including *Cymbella hustedtii*) by 20.5 cm. Numerous other benthic species are present during this interval (e.g. *Navicula radiosa* and *Gomphonema parvulum*) but are rarer ($<5\%$ each).

A decrease in the relative abundance of *Nitzschia amphibia* corresponding to the gradual increase in *Cymbella leptoceros* abundance is observable. However, after 20.5 cm the relative abundance of *Nitzschia amphibia* beings to rapidly increase to $\sim 40\%$ at the top of the core. This rise is coupled with a corresponding decrease in the abundance of epiphytic taxa such as *Cymbella leptoceros*. Additionally, small increases in *Staurosirella pinnata* and *Pseudostaurosira pseudoconstruens* ($\sim 20\%$ for each) are evident at ~ 20 cm, although the relative dominance of *Nitzschia amphibia* also replaces these toward the top of the core.

7.6.1 | Garba Guracha diatom principal curve and quantitative data

The principal curve through the Garba Guracha diatom data is shown in Figure 7.8. The start of the gradient is populated by facultatively planktonic species,

mirrored by largely benthic/aerophilous taxa towards the end. The main trend along the gradient follows *Staurosira construens* var. *venter* through to *Staurosirella pinnata* (dominant to largely exclusive in GGD-5 and GGD-4). This is followed by an area populated by *Pseudostaurosira brevistriata* and *Pseudostaurosira pseudoconstruens* (common in many zones, but most prevalent through GGD-4 to GGD-2 and GGD-2, respectively), with a gradual transition to a large cluster of the remaining taxa which are benthic/aerophilous that are common in GGD-2, and dominate GGD-1, such as *Cymbella leptoceros*, *Amphora pediculus* and *Nitzschia amphibia*. This curve reflects (and simplifies on to one axis) major compositional shifts, the potential drivers of which are interpreted further below in text. PrC scores for each depth, as well as diatom inferred conductivity, rate of change and Hill's N2 (discussed in Chapter 4) are plotted alongside habitat percentages and core stratigraphy from Figure 7.9 to more effectively summarise and quantify changes in the diatom record.

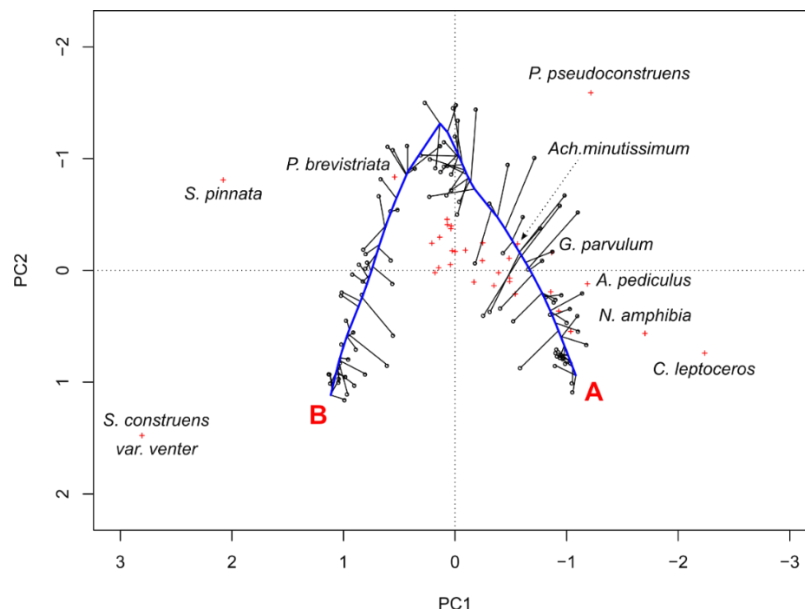


Figure 7.8: Principal curve (blue) of the Garba Guracha diatom data. Taxa scores in (PCA) ordination space are denoted by red crosses, with the main taxa labelled. 'A' denotes the beginning of the curve (i.e. lowest principal curve scores) and 'B' representing the end of the curve (i.e. highest principal curve scores).

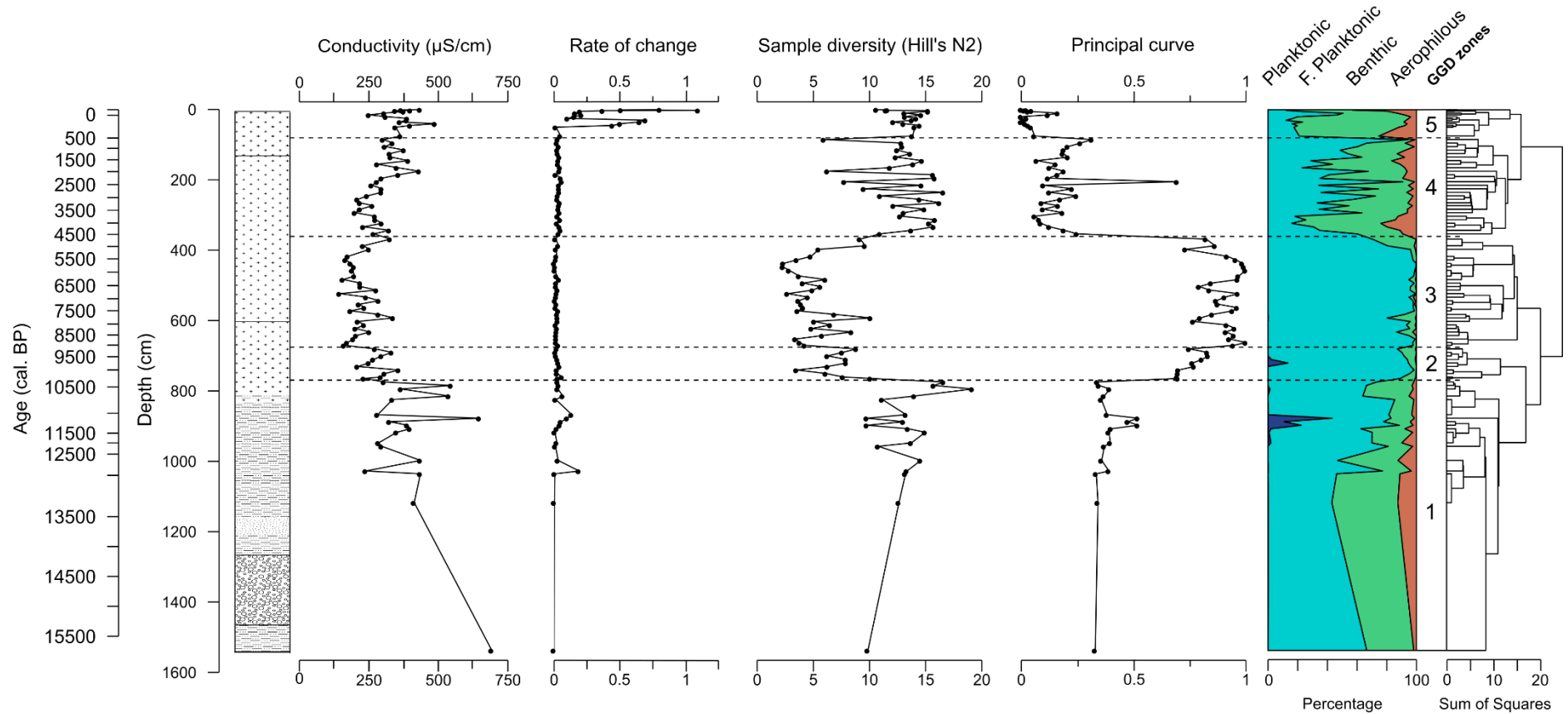


Figure 7.9: Quantitative diatom data for the Garba Guracha core. Principal curve shown in Figure 7.8. Methods and packages used for computing these statistics are detailed in Chapter 4. Zones as determined by CONISS are also shown (GGD-1, GGD-2, GGD-3, GGD-4 and GGD-5).

7.7 | Interpretation of the Garba Guracha sedimentary record

All data from the Garba Guracha core presented in this study are now interpreted in terms of environmental changes in the lake basin over the past ~16,000 years. Additionally, pollen and stable isotope data produced by other members of the research team (Gil-Romera *et al.*, in prep; Bittner *et al.*, in prep) are also referred to in this section, to aid interpretation of specific trends. For ease of interpretation, main environmental changes in both diatom and XRF data are summarised in Figure 7.10. The record has been divided into 4 major time periods (GGU-1 to GGU-4) based on significant changes in the palaeoenvironmental data.

GGU-1 (15,930-10,430 BP; 1548-774 cm)

The duration and extent of ice cover exerts an overriding influence on habitat availability, amongst other things; it is a key factor in determining the development and diversity of a diatom community (Smol & Douglas 2010). For example, sediment trap experiments in the Swiss Alps and ten High Arctic lakes demonstrate that longer periods of colder water and ice-cover inhibit the development of a planktonic community and more complex growth forms (e.g. motile, stalked or tube dwelling), known to favour the proliferation of Fragilarioid species (Lotter & Bigler, 2000; Griffiths *et al.*, 2017). Many small Fragilarioid are considered r-strategists (Lotter & Bigler, 2000), with low light and very low nutrient (such as N, P and Si) requirements (Michel *et al.* 2006). As a result, Fragilarioid taxa can exploit the harsh environments that are characterised by prolonged cold waters and ice cover: low light, low nutrients and a lack of aquatic macrophytes, which might exclude other taxa.

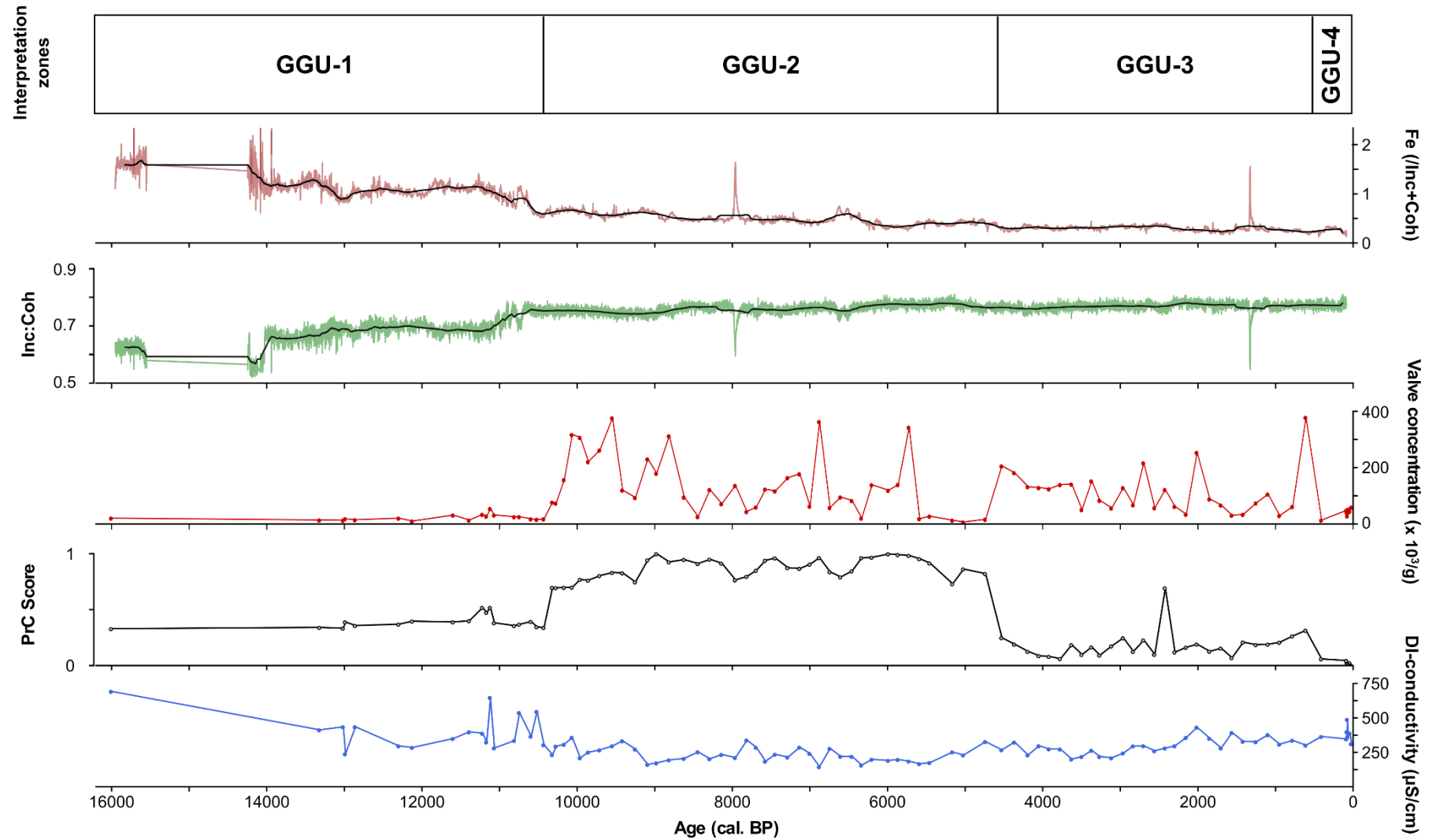


Figure 7.10: Synthesis of both XRF-derived peak area geochemical and diatom data for the Garba Guracha core. Interpretation zones referred to in-text are also shown. Solid black line denotes a 500-point running mean through XRF data.

Thin layers of ice have been observed to form on the modern-day lake surface at night (personal observation by the author), but not to the extent of developing a thick ice cover for extended periods as seen in the European Alps. Nevertheless, the dominance of small, Fragilarioid in the Garba Guracha core between 16,000 and 10,500 BP implies cold, niche conditions where generalists can thrive.

High Poaceae, *Artemisia* and Amaranthaceae/Chenopodiaceae percentages (but with a low pollen influx; Umer *et al.*, 2007; Figure 7.11) indicates a local environment characterised by a sparse cover of steppe-like, grasses and dwarf shrubs under a dry and cold climate. This is further evidenced by relatively high diatom inferred conductivity (Figure 7.10), although this may represent poor representation of the high altitude assemblage in the low altitude dominated African dataset (Gasse *et al.*, 1995). Low valve concentrations suggest that despite the dominance of Fragilarioid (Figure 7.9), unfavourable conditions severely restricted their growth. Although, the large input of minerogenic matter may be 'diluting' the concentration of diatom valves during this period.

Achnanthydium minutissimum is a pioneer taxon that prefers fresh, clean waters, but is tolerant of heavy disturbance/pollution (Peterson & Stevenson, 1992). Consequently, it is dominant in the fresh, glacial streams of the Himalayas, Canada and European Alps (Cantonati *et al.*, 2009; Gesierich & Rott, 2012). The presence of benthic taxa (Figure 7.7), such as *Achnanthydium minutissimum*, suggests that glacial meltwater may have been a key source for Garba Guracha and that these streams may have served as one of the isolated corridors of habitat for more motile diatoms.

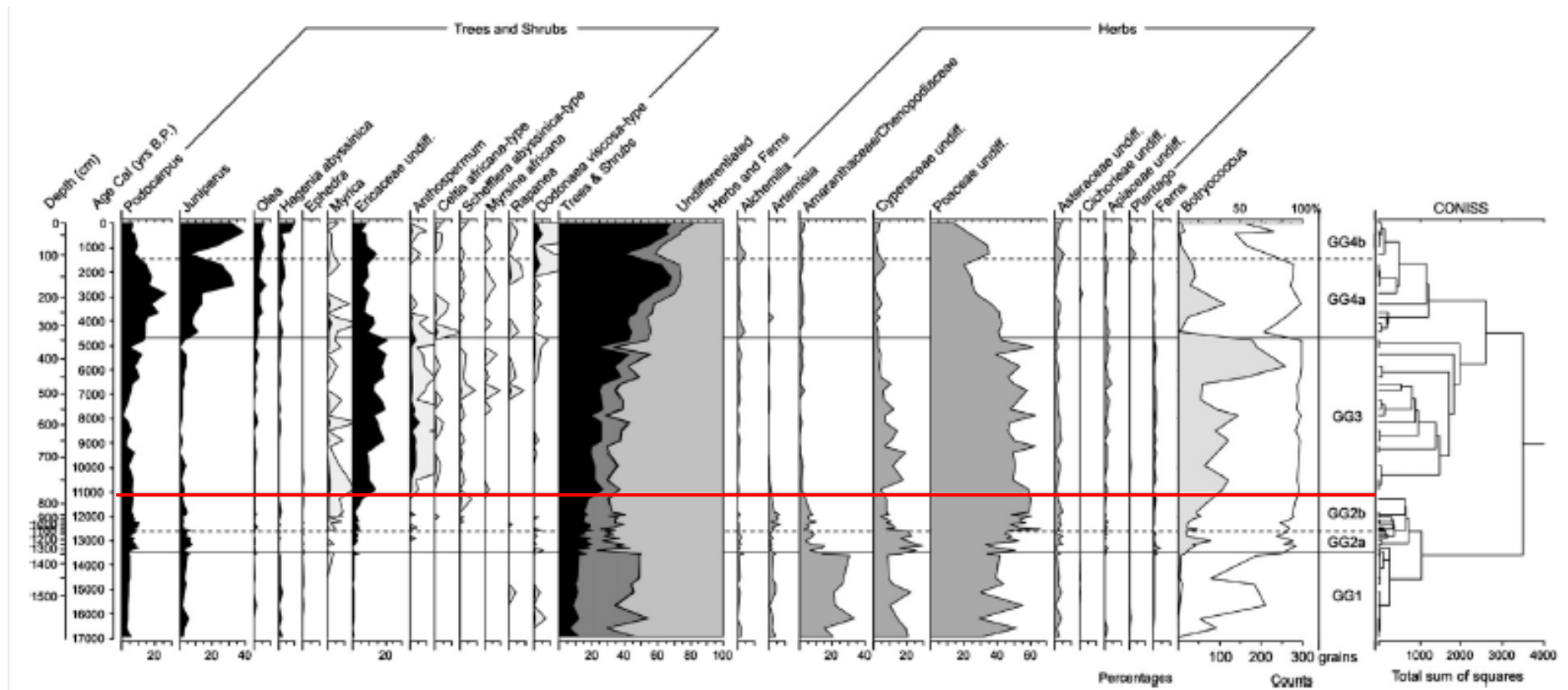


Figure 7.11: Pollen diagram from Garba Guracha from Umer *et al.* (2007). Percentages are calculated from the sum of all pollen grains and fern spores counted. The red line denotes the increase in Ericaceous vegetation cover.

High lithogenic element values (Figure 7.5) are indicative of high allochthonous inputs, likely associated with the adjacent glacier, to the core site and lake during this period. The highly minerogenic sediment that was delivered to the lake was composed of grains of multiple sizes due to the increased peak area of both Zr and Rb, associated with coarser and fine grain fractions, respectively (Davies *et al.*, 2015; Figure 7.5). However, low Zr:Rb suggests that the majority of minerogenic material is fine, likely associated with retreat of the nearby glacier. It is also likely that the retreat of the glacier delivered large volumes of minerogenic matter (such as those cores that could not be split between 1476 to 1276 cm) as sudden mass flows of material. The identification of turbidites through the remainder of the core however is problematic with no significant changes in sediment colour (unlike at Lake Babogaya with clear breaks in laminated sections) or grain size observable. Further, more detailed grain size work may aid in the identification of possible layers, but such analyses were not performed in this study. Consequently, it is not possible to accurately discern the impact, if any, of turbidites on the ecological and geochemical record.

The dominance of Fragilarioid taxa may also be in response to increased turbidity (therefore light availability) and Al content (Tiercelin *et al.*, 2008 and XRF data in this study (not shown in Figure 7.5)), normally associated with glacial flour, the latter influencing P bioavailability availability (see Norton *et al.*, 2011; Burpee *et al.*, 2018). For example, Burpee *et al.* (2018) highlight the higher turbidity in Greenland glacier-fed lakes as one of the key factors influencing the dominance of Fragilarioid taxa in these lakes. Furthermore, they tentatively link increased Al input with reduced mobility of P as a factor in determining ecology of these lakes.

Continued autoecological studies have illustrated some subtle differences exist between Fragilarioid taxa in terms of preferred habitats and environmental optima (e.g. Schmidt *et al.*, 2004; Karst-Riddoch *et al.*, 2009; Griffiths *et al.*, 2017). For example, in comparison to other *Pseudostaurosira brevistriata* and *Pseudostaurosira pseudoconstruens* (more common above 10°C), across 49 Icelandic lakes that *Staurosirella pinnata* and *Staurosira construens* var. *venter* were more common in colder waters (<10°C), with the latter being marginally more competitive in water colder than 8°C (Karst-Riddoch *et al.*, 2009).

Similarly, in sedimentary records from the Arctic, different taxa within the Fragilarioid group exhibit dissimilar responses to Holocene climatic changes (e.g. Cremer *et al.*, 2001; Podritske & Gajewski, 2007; Finkelstein & Gajewski, 2008). At Garba Guracha the dominance of Fragilarioid taxa, especially *Staurosirella pinnata*, reaffirm that cold and oligotrophic waters likely prevailed during zone GGU-1. *Pseudostaurosira brevistriata* and *Pseudostaurosira pseudoconstruens* are also known to be competitive in cold, shallow waters. However, their presence, although in smaller abundances, may represent additional environmental gradients such as changes in seasonal temperatures, as they are known to be more successful in slightly warmer waters (e.g. Schmidt *et al.*, 2004; Karst-Riddoch *et al.*, 2009). These small seasonal differences in temperature may be driving the clear differentiation between *Pseudostaurosira brevistriata*/*Pseudostaurosira pseudoconstruens* and *Staurosirella pinnata*/*Staurosira construens* var. *venter* towards the end of the principal curve (Figure 7.8; Figure 7.9). Between 11,500 and 11,000 BP, the planktonic *Discostella stelligera* briefly appears in the record (Figure 7.7). *Discostella stelligera* require a N-rich environment (especially when P is limited) and thermal stratification of the water

column to proliferate in a system (Saros *et al.* 2014). As this taxon is present in a presumably nutrient limited system (low TOC and high Fragilarioid taxa abundance), it is possible that *Discostella stelligera* during this interval is responding to a change in the mixing regime of the lake. In this case either: (i) larger areas of the lake became completely ice-free for entire diurnal cycles or (ii) waters became deeper and warmer, and as a result experienced a sustained, albeit short-lived period of stratification and thermal stability where *Discostella stelligera* thrived. However, it is important to note that the clearest signals of changing lake stratification patterns inferred from *Discostella stelligera* abundance occurs when N:P supply ratios are at a sustained higher level (Saros *et al.*, 2014). Thus, a brief interval of increased nutrient content cannot be completely ruled out.

GGU-2 (10,430-4,440 BP; 774-353 cm)

After 10,425 BP (774 cm), significantly higher valve concentrations in the core are evident (Figure 7.10). Valve dissolution undoubtedly influences diatom valve concentration in a record, however as this was not observed to a significant degree in this core, increased primary productivity after 10,425 BP is inferred as the cause of increased valve concentration. However, it is important to note that diatom valve concentration as a direct proxy for productivity as concentrations may be heavily influenced by changes in the sediment accumulation rate. Consequently, another explanation for this change may be that previously high rates of allochthonous material deposition may have diluted the concentration of diatom valves per gram of dry sediment, with an increase in concentration following reduced terrigenous input reflecting reduced dilution of the diatom valves.

After ~10,500 BP diatom inferred conductivity decreases slightly suggesting a shift to slightly wetter conditions. Increases in the abundance of woody *Erica*, imply increased terrestrial productivity in the basin and therefore nutrient loading potential, during an expansion of the *Ericaceous* belt in a presumably wetter climate (Umer *et al.*, 2007; Figure 7.11) Continually decreasing lithogenic element peak area through this zone (Figure 7.5) also suggests reduced rates of erosion, likely reflecting the more humid climate and the impact of increased soil stabilisation as a result of expansion of *Erica* forest/shrubland and associated increased leaf litter, herb/bryophyte layer and soil humus content (Umer *et al.*, 2007; Lamb & Gil-Romera, pers comm.).

However, despite increased algal productivity, likely in response to wetter but also warmer environmental conditions, limited diatom diversity reduces further in this zone with only two taxa practically exclusively representing the community (Figure 7.7). This would suggest niche habitats composed of oligotrophic and cold waters, which may have experienced some ice-cover for sustained periods, similar to those present between 16,000 and 10,500 BP. Subtle changes between *Staurosirella pinnata* and *Staurosira construens* var. *venter* abundance (Figure 7.7) may represent slightly fluctuating cold temperatures, although these differences uncovered in other lakes is minor (e.g. Karst-Riddoch *et al.*, 2009). Furthermore, after ~8,500 BP diatom productivity (inferred from valve concentrations) decreases and begins to vary at lower concentrations for ~3000 years. Although after a small increase at ~9,000 diatom inferred conductivity data remains at some of the lowest values observed in the core indicative of fresher waters as a result of increased moisture availability.

At first the interpretation of wetter, deeper lake conditions seems to contradict the diatom data. Small Fragilarioid taxa (such as *Staurosirella pinnata*) are often associated with benthic habitats in shallower waters (e.g. Lotter & Biggler, 2000), water temperature and duration of ice cover, as well as nutrient supply, are known to be such dominant factors as to limit the expansion of planktonic taxa, even in deeper waters (Lotter & Bigler, 2000; Schmidt *et al.*, 2004). Despite possible deeper lake waters, cold waters during this period are likely inhibiting the expansion of a diverse diatom community. It is also important to briefly note that the term “shallow” in relation to habitat in which Fragilarioid taxa thrive can be waters up to 10 m depth (e.g. Lotter & Bigler, 2000; Laird *et al.*, 2010). The morphology of Garba Guracha currently allows for approximately 5 to 6 m of water (at the time of sampling in this study and in 2001; Tiercelin *et al.*, 2008). However, the maximum depth may have extended down to ~12 m prior to sediment in-filling.

Between 5,500 and 4,500 BP (427-368 cm) *Staurosira construens* var. *venter* and *Staurosirella pinnata* continue to dominate the diatom assemblage (Figure 7.7). However, a 5% decrease in TOC and a ~140 $10^3/g$ decrease in average valve concentration reveals that the sustained, higher aquatic and terrestrial productivity at Garba Guracha was temporarily interrupted. Based on these multiple proxies, the environment of the Garba Guracha basin likely returned to habitat and nutrient limited as in GGU-1. Interestingly, lithogenic element content remains consistently low during this interval (Figure 7.5), despite being linked to increased detrital input (Davies *et al.*, 2015), which may be instigated by enhanced catchment instability as a result of drier conditions. However, this may be attributed to soil stabilisation and the vegetation layers discussed above which persisted through this period.

GGU-3 (4,440-560 BP; 353-85 cm)

After ~4,500 BP, these drier conditions continue, but with slightly increased diatom productivity with changes in the terrestrial and aquatic ecology. *Pseudostaurosira pseudoconstruens* is the dominant Fragilarioid taxon (Figure 7.7) with pollen data showing an expansion of the dry Afromontane *Juniperus* and *Podocarpus* forests (Gil-Romera *et al.*, in prep.). Despite similarities to *Staurosirella pinnata* and *Staurosira construens* var. *venter*, *Pseudostaurosira pseudoconstruens* are more common in slightly warmer waters (e.g. Finklestein & Gajewski, 2008; Karst-Riddoch *et al.*, 2009), with Perren *et al.* (2003) placing them on the gradient between colder (*Staurosirella pinnata* dominated) and slightly warmer (more motile/complex, periphytic life forms) conditions.

In addition to slightly warmer waters, an increasingly diverse diatom assemblage, with an increased abundance of more motile, periphytic diatom taxa imply an expansion of favourable habitat, with a developing aquatic macrophyte community. Community shifts such as this are attributed to increased nutrient supply and subsequent increased growing season (Smol *et al.* 2005) and is represented on the opposite side of the principal curve to the small Fragilarioid taxa (Figure 7.8). *Cymbella leptoceros* (and the morphologically similar *Cymbella hustedtii*), which is common throughout this zone, is known in Europe to be abundant in alpine/sub-alpine regions, rarely found at lower altitude sites, but are mainly associated with fresh, oligotrophic waters (Krammer & Lange-Bertalot, 1988).

However, while *Gomphonema parvulum*, *Nitzschia amphibia*, *Amphora pediculus* and *Navicula radiosa* are sometimes associated with fresh, alkaline and

oligotrophic waters, they are also reported as eutradients, especially regarding N, with *Nitzschia amphibia* is known to be a facultatively nitrogen-heterotrophic taxon. (van Dam *et al.*, 1994; Gasse *et al.*, 1995; Potapova & Charles, 2007; Besse-Lototskaya *et al.*, 2011; Pérez *et al.*, 2013), suggesting an increase in nutrient supply to Garba Guracha at this time. Increased vegetation in and around Garba Guracha, likely increased nutrient supply, as well as provided periphytic habitat, for a more diverse community. It is important to note that anthropogenic indicators are evident in the pollen and fungal spore record after 2,300 BP (Gil-Romera *et al.*, in prep.). Initially at the start of the Late Holocene, the influence of anthropogenic activities on environmental conditions, such as nutrient content, is likely to be limited. Nevertheless, with the introduction of livestock and the contemporary increase in atmospheric N, impacting the natural N cycle (Glibert *et al.*, 2006), caution must be taken when interpreting biochemical changes due to disruptions of the natural cycle at Garba Guracha by anthropogenic activities.

Variable environmental conditions (reflected by fluctuating *Pseudostaurosira pseudoconstruens* abundance; Figure 7.7) in a less nutrient limited environment may also play a role in the composition of the diatom community at Garba Guracha. *Nitzschia amphibia* is placed in the midpoint of the 1-5 gradient of moisture conditions by van Dam *et al.* (1994), meaning this taxon mainly occurs in water bodies, but can often be located on “moist/wet places”. Indeed, they can often be found in, but not exclusive to, damp and periodically dry areas characteristic of aerophilous habitats (Grunow, 1862), ie. habitats characterised by low moisture or periodic drying. Furthermore, *Navicula radiosa* (briefly common after 4,500 BP) can also be found on “moist/wet places” according to van Dam’s (1994) moisture scale, and may be a ‘pioneer’ taxon at Garba Guracha

after the dry conditions of the 5,500-4,500 BP interval when lake levels may have decreased and aerophilous habitats expanded.

After ~1,700 BP the gradual increase in *Staurosirella pinnata* (Figure 7.7), peaking at 550 BP, together with the re-appearance of *Staurosira construens* var. *venter* (although in small abundances) and coupled to the decline in periphytic taxon abundance may reflect a decrease in aerophilous habitat in response to increased lake level and wetter conditions.

GGU-4 (560 BP-present day; 85-0 cm)

The relative absence of the ice and cold tolerant Fragilarioid taxa is combined here with the dominance of larger and more complex growth forms (e.g. *Cymbella leptoceros* and *Cymbella hustedtii*), suggestive of continued nutrient input, expansion of habitat and longer growing seasons with a reduced duration of ice-covered water. However, after 560 BP *Nitzschia amphibia* becomes more common in the record, reaching high abundance (>35%) at ~10 BP, with rapid rates of change evident. This may reflect increased N input to the lake as discussed above. However, a caveat highlighted by Arnett *et al.* (2012) is that multiple gradients inevitably persist in this case making it difficult to attribute N enrichment as the primary driver of increased *Nitzschia amphibia* abundance. For example, the potential association with aerophilous habitat (discussed above), thus increased importance of marshy/boggy habitat in response to drier conditions (as discussed above) must also be considered.

7.8 | Summary of the palaeolimnological record of BAL-GGU17-1AB

The interpretation of these limnetic and environmental changes inferred from the available data are summarised below and in Figure 7.10. Discussion of these

environmental and climatic inferences, and their implications within the wider context of this study, together with the record from Lake Babogaya (Chapter 6), follows in Chapter 8.

GGU-1: (15,930-10,430 BP; 1548-774 cm)

- Cold and dry conditions, with high erosion rates following glacier retreat
- Glacier fed oligotrophic, neutral-alkaline waters
- Likely extended periods of ice cover restricting habitat availability
- Negligible lake productivity
- Colonisation of limited habitat by adaptable, pioneer taxa

GGU-2: (10,430-4,440 BP; 774-353 cm)

- Increased terrestrial and aquatic productivity.
- Low diversity indicative of niche conditions.
- Dominance of *Staurosirella pinnata* and *Staurosira construens* var. *venter* suggest cold water temperature, restricting habitat availability and inhibiting a stable stratification regime, despite wetter conditions.
- Brief interval of negligible productivity between 5,500 and 4,500 BP, comparable to that between 16,000 and 10,500 BP.

GGU-3: (4,440-560 BP; 353-85 cm)

- Appearance of *Psuedostaurosira pseudoconstruens* a ‘transition’ taxon between colder and slightly warmer conditions
- Expansion of habitats favourable for multiple taxa, including epiphytic life forms
- Increased nutrient loading due to enhanced productivity around the basin

- Likely increase in water temperature and extended growing season
- Aerophilous taxa common suggestive of moist boggy/marshy environments around the lake shore.
- Brief interval of increased lake level between 1,690 and 560 BP

GGU-4: (560 BP-present day; 85-0 cm)

- Development of the conditions present in GGU-3, increased growing season facilitating the continued expansion of habitat and diversification of the diatom community
- Increased nutrient loading
- Enhanced importance of benthic/aerophilous habitat with drier conditions prevailing.

Chapter 8 :

Discussion

In this chapter the results from the BA-LC-2011 (Lake Babogaya) and GGU-17-1AB (Garba Guracha) sediment cores presented in Chapter 7 and Chapter 8 are synthesised and discussed with reference to the original research questions and objectives outlined in Chapter 1. An evaluation of the methods used forms part of this discussion. Furthermore, where possible (due to the difference in core basal ages), the degree of overlap between the two palaeolimnological records is discussed, while also framing the findings from these sites in the wider palaeoclimatic context of other published records from Ethiopia and eastern Africa as a whole.

8.1 | Consideration of methods and avenues of further research

The proxies used in this study have provided comprehensive palaeolimnological records at both Lake Babogaya and Garba Guracha with wide ranging implications. Significant changes have been identified in the biological and geochemical records, which with the use of quantitative analyses, have been interpreted in terms of past limnological variability in response to climatic change. This has provided a holistic, detailed record of the changes in climate and environment in the areas of both lakes. It is evident that different proxies have diverging responses to climatic variability. It has been noted in this study that the elemental profiles, at Garba Guracha at least, often indicate a climatic transition of different magnitude, duration and timing to the diatom records. For example, much of the Holocene change recorded by the diatom data at Garba Guracha is

virtually indistinguishable in the XRF-derived geochemical record. Such discrepancies between proxies are common in palaeolimnological research owing to varying sensitivity between proxies and the environmental changes that they primarily respond to. In this research, diatoms have been utilised as the primary proxy to interpret environmental change given their power as an ecological indicator (see Section 4.4.3). The multi-proxy approach in this study has provided additional, independent lines of evidence, and thereby has facilitated a more holistic and thorough investigation of the lake-catchment system responses to external perturbations through time. Future work could produce additional palaeo-records from the Bale Mountains and from the nearby Arsi Mountains to add to the small, but growing body of data at high altitude in south-central Ethiopia, and eastern Africa as a whole.

Although the utility of diatoms as a proxy in this research has been hindered by the difficult taxonomy of certain taxa (e.g. Fragilarioid taxa at Garba Guracha and Nitzschioid taxa at Lake Babogaya), this issue is evident in many other studies and has been addressed where possible with uncertainties included in interpretations. Furthermore, the use of SEM in this study has facilitated the identification of certain taxa that would otherwise be 'lumped' into a single, large group (e.g. to identify the presence of *Punctastriata* spp. at Garba Guracha). The occurrence of a new taxon at Lake Babogaya (*Nitzschia fenestralis* nom. prov.) initially limited the palaeoenvironmental interpretation of the diatom assemblage where this taxon was abundant (e.g. 3,300 to 1,750 BP). However, best inferences were made on the ecological tolerances of *Nitzschia fenestralis* based on the known autoecology of co-occurring taxa (e.g. *Nitzschia paleacea*) and by using other proxies, further illustrating the usefulness of a holistic, multi-proxy

approach. Furthermore, at the time of writing, dialogue is ongoing with diatomists working at multiple Ugandan crater lakes (Mills, K. & Driessen, T. at Loughborough University and the BGS) and Lake Challa (Heidi T; Universiteit Gent), two areas with strong modern ecological datasets (e.g. Mills & Ryves, 2012; Wolff *et al.*, 2014), with Lake Challa suspected to have an occurrence of *Nitzschia fenestralis* (H. Tantuu pers comm.), or at least a very similar morphotype, then we can further understand the autoecology of the taxon.

The gap in the BA-LC-2011 core inhibits this study to provide a continuous record of environmental change at this site. However, this missing section is suspected to be a reworked unit of sediments and dating likely to be unreliable, hindering the usefulness of including this section as part of a continuous record in any case. Dates at both the beginning and end of interpretation unit BA-3 facilitate an effective and reliable interpretation of this event, and provides valuable insights into the past dynamics of the lake following climatic perturbations. If possible, a core from Lake Babogaya extending into the Late Pleistocene or further would offer further insights on environmental change in central Ethiopia. However, although the full utility of the individual laminae was not developed in this study as the priority was to examine the full sequence and they were not continually preserved through the entire core, further work could exploit them as a very powerful tool for reconstructing Late Holocene climate at a high resolution.

8.2 | Late Pleistocene/Early Holocene environmental change at Garba Guracha

The base of the palaeolimnological record at Garba Guracha presented in this study reflects the dry post-glacial conditions that must have prevailed after 16,000 BP following the formation of the lake as ice retreated up the Togona valley: considerable erosion (high terrigenous input and deposition of large

grained material), low organic productivity (low organic matter content and negligible diatom valve concentrations) and likely a cold, nutrient-poor lake water environment (e.g. high abundance of r-strategist *Fragilarioid* taxa). However, it is difficult to compare the Garba Guracha record with other regional records due to the nature of the recently glaciated environment, which is rare in eastern Africa.

Although the onset of aridification of eastern African sites in the LGM is linked to a combination of multiple triggers: migration of the ITCZ, changes in Hadley cell strength or in ocean upwelling and circulation (Denton *et al.*, 2010; Stager *et al.*, 2011; Weldeab *et al.*, 2014), drier conditions are evident at multiple sites (with a few exceptions: e.g. Tierney *et al.*, 2011a) during the LGM and Heinrich 1 (H1; ~16,000 BP). Lakes Tana and Victoria, large regional water bodies as the heads of the Nile were desiccated at this time (Lamb *et al.*, 2007; Stager & Johnson, 2008; Marshall *et al.*, 2011). Further evidence of this aridity has been documented by increased $\delta^{13}\text{C}_{\text{diatom}}$ at Lake Challa (Barker *et al.*, 2013), more positive $\delta\text{D}_{\text{leaf wax}}$ values at Lake Tanganyika (Tierney *et al.*, 2008) and by increased Zr:Ti at Lake Malawi (Brown *et al.*, 2007).

Decreased precipitation at Garba Guracha would have undoubtedly impacted local organic productivity, however development of the catchment at this time is likely primarily reliant on deglaciation of the area. While reduced precipitation would have undoubtedly impacted the ablation rate of local ice masses, temperature increase is also likely key in driving local productivity (see below for further discussion related to the beginning of the Holocene).

8.2.1 | Younger Dryas-type hydrological change at Garba Guracha?

High terrigenous input, low organic matter and low diatom valve content continues through the record at Garba Guracha until ~10,500 BP. A trend of increased precipitation and productivity, following the general regional aridity of H1, is associated with the African Humid Period across multiple sites in eastern Africa (e.g. Gasse *et al.*, 2002; Weldeab *et al.*, 2005; Tierney *et al.*, 2008; Foerster *et al.*, 2012; Juninger & Trauth, 2013).

As a consequence of the humid conditions and productivity associated with the AHP, a reversal to more arid conditions during the Younger Dryas interval is particularly prominent in multiple records and proxies across much of Africa (e.g. Stager *et al.*, 2002; Castañeda *et al.*, 2009; Tierney *et al.*, 2008; 2011a; Foerster *et al.*, 2012; Barker *et al.*, 2013). This includes higher altitude sites (>2000 m) with aridity documented at Lake Ashenge (Marshall *et al.*, 2009; albeit drier conditions established ~900 years prior to the YD proper), in the Burundi Highlands (Bonnefille *et al.*, 1995), Aberdare Mountains (Street-Perrott & Perrott, 1990) and possibly at Lake Dendi (Wagner *et al.*, 2018; base of core half-way through YD). However, as the Garba Guracha catchment was likely a poorly developed post-glacial landscape prior to the YD, any dry conditions associated with the YD would have been superimposed on to high soil erosion due to the early development of local vegetation and soils leading to a muted response in the Ti record in contrast to records such as the K record at Chew Bahir (Foerster *et al.*, 2012). Similarly, diatom productivity was low prior to the YD, thus further decreasing productivity would register only a slight signal in the record (in this case insufficient diatom concentrations leading to no counts in the record as opposed to negligible valve counts). YD-like drying is also not a clear, high

magnitude event in the Small Hall Tarn $\delta^{18}\text{O}$ record, a similarly high altitude (>4,000 m) site, however this comparison is limited by a low sampling resolution (Barker *et al.*, 2001).

8.3 | Onset of humid conditions at Garba Guracha – delayed AHP?

At around 10,250 BP diatom preservation and inferred conductivity increased with a corresponding decrease in terrigenous input. Although previous dilution of valves by high rates of allochthonous input may now artificially increase valve concentration as this terrigenous input reduces, isotope, biomarker and pollen data from the research group (L. Bittner and G. Gil-Romera) suggest more humid conditions and an increase in lake level at this time. Increased diatom productivity and the dominance of facultatively planktonic Fragilarioid taxa may be responding to an increased growing season and wetter conditions.

The AHP resumes following the arid interval of the YD and by 9,000 BP increased precipitation and higher lake levels are documented across much of Africa (Figure 8.1). Furthermore, by the start of the Holocene temperature had increased considerably at lakes Tanganyika (Tierney *et al.*, 2008), Victoria (Berke *et al.*, 2012) and Tana (Loomis *et al.*, 2015) compared to those inferred in the Late Pleistocene. Discrepancies in the timing of the start of the AHP reflect local variability in moisture availability over eastern Africa caused by shifts in the position of major convergence zones such as the Congo Air Boundary (Tierney *et al.*, 2011a; Costa *et al.*, 2014).

Costa *et al.* (2014) discuss a time-transgressive change in atmospheric circulation potentially attributed to a north-south migration of the tropical rain belts and an east-west migration of the Congo Air Boundary. Although it is crucial to

recognise that these discrepancies may be as a result of chronological uncertainties, Costa *et al.* (2014) argue that this may be evidence for the gradual onset of the AHP at multiple sites in eastern Africa. However, such a discrepancy of >3,000-4,000 years for the onset of the AHP at 11,000-10,000 BP is unlikely to represent a change that gradual at Garba Guracha, especially since the area is presumably unaffected by migration of the CAB (Tierney *et al.*, 2011a).

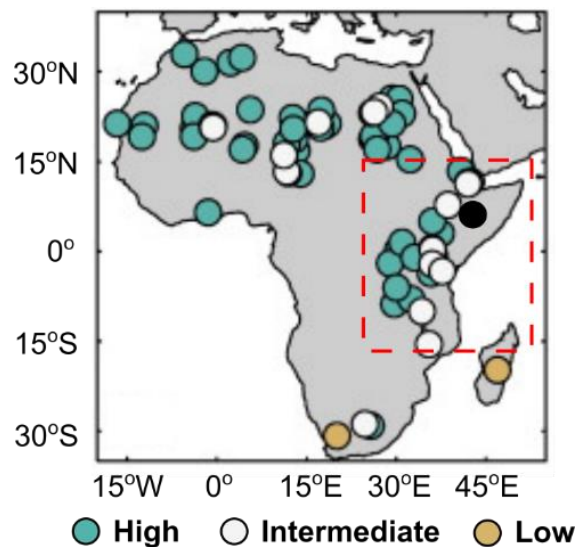


Figure 8.1: Lake levels around Africa at 9,000 BP (redrawn from Tierney *et al.*, 2011b). The red dashed box outlines the region of eastern Africa region as defined in Chapter 2, with the solid black circle the location of Garba Guracha.

Diatom valve concentration, assuming this reflects productivity and not reduced dilution from allochthonous material (lower XRF-derived Ti), does not seem to increase in response to increased moisture availability at around 11,250 BP (brief interval of reduced $\delta^{18}\text{O}$ values; Bittner *et al.*, in prep.), but does correspond to warmer temperatures at 10,250 BP ($\sim 2^\circ\text{C}$ MAT increase; Bittner *et al.*, in prep.). Again, relevant analogues of ecological change during the deglaciation of an alpine environment are limited in eastern Africa. However, Wooller *et al.* (2003), while recognising the importance of precipitation, primarily attribute changing temperatures as well as changing CO_2 concentrations as the main drivers of

increased grass productivity and diversity around Rutundu, Mt. Kenya. In other areas of the world modern-day increases in temperature in alpine areas, alongside increased moisture availability, have been linked with increased terrestrial productivity associated with lengthened and more productive growing seasons (Zha *et al.*, 2005; Winkler *et al.*, 2016). Furthermore, higher lake-water temperature has been linked with a longer aquatic growing season between 1980 and 2009 at Lake George, NY (USA), attributable to increased organic mineralisation and productivity (e.g. Swinton *et al.*, 2015), with warmer waters attributable to increased diatom productivity at Jinshahe Reservoir, Hubei (China) when interspecific interactions are not present (Zhang *et al.*, 2018), which is the case at Garba Guracha with the dominance of Fragilarioid taxa at this time. Therefore, ecological change may be driven in the early Holocene by changes in temperature rather than by changes in moisture availability.

8.4 | Abrupt changes in the Holocene?

As discussed above, the Early Holocene is largely humid and productive at numerous sites in eastern Africa (Figure 8.1; Tierney *et al.*, 2011b), including Garba Guracha in this study. However, potential arid intervals are identifiable in many records. The '8.2 cooling event' as recorded in the Greenland GISP2 core (used for the definition of the Northgrippian stage of the Holocene; Walker *et al.* 2018) is extensively documented as an abrupt event across Europe and North America (Alley, 2004), with aridity documented at some sites at lower latitudes (e.g. Cariaco basin; Haug *et al.*, 2001), even potentially in Africa (e.g. Trauth *et al.*, 2015). There is also some evidence for sites in eastern Africa experiencing some aridity around this time, but with some arguing that an arid 'event' unique to Africa occurred hundreds of years before the 8.2 event (Shanahan *et al.*, 2006;

Tierney *et al.*, 2010). For example, Thompson *et al.* (2002) observe a rapid fluctuation in F^- and Na^+ concentrations from the Kilimanjaro ice core record around 8,400 BP to 8,200 BP, suggesting a brief pulse of aridity, with a lowstand dated to 8,600 BP at Lake Bosumtwi by Shanahan *et al.* (2006).

Such an abrupt, short-lived arid event is not clear in the Garba Guracha record, although this may reflect the sampling resolution used. Diatom valve concentration decreases considerably (Figure 7.7), remaining lower and variable for the next ~2,000 years, but there is no clear evidence for catchment changes in XRF-derived terrigenous content (Figure 7.5). However, the oxygen isotope values in the core do gradually increase from the lowest values recorded at around 8,500 (Bittner in prep.). This increase in $\delta^{18}O$ coincides with a slight increase in diatom inferred conductivity, low diatom concentrations and lower, variable diatom abundance thereafter (Figure 7.10). Gradual drying and reduced productivity such as this have been noted at multiple other sites in eastern Africa after ~8,500 BP. For example, a drought event identified at 8,150 BP in the Chew Bahir K record marks a period of instability (Trauth *et al.*, 2018). This event is one of 19 drought events identified between 8,200 BP and 5,000 BP. Furthermore, a planktic foraminifera Ba/Ca record from the eastern Mediterranean Sea suggests that while Nile runoff was still strong, 8,700 BP marks the onset of a 3,500 year period of progressive decline in runoff (Weldeab *et al.*, 2014), with similarly gradual drying inferred at this time at lakes Tana and Victoria (Marshall *et al.*, 2011; Berke *et al.*, 2012), the headwaters of the Blue Nile and White Nile. This may tentatively suggest a longer-term decline in moisture availability and stability, and therefore variability in lake level and productivity, at Garba Guracha from the

early to mid-Holocene, rather than a well-defined, abrupt shift centred around 8,200 BP.

8.4.1 | Termination of the African Humid Period

Despite very few significant geochemical changes in the Garba Guracha sedimentary record, a significant decrease in diatom productivity occurs from 5,720 to 5,585 BP (Figure 7.7), followed by increased diatom-inferred conductivity thereafter. Similar considerable shifts have been documented by various biological and geochemical proxies at multiple nearby sites (e.g. Marshall *et al.*, 2009; Marshall *et al.*, 2011; Tierney & deMenocal, 2013; Loakes *et al.*, 2018; Roubéix & Chalé, 2018) attributing this change to the end of the AHP. Tierney & deMenocal (2013) suggest an average timing of the termination of the AHP in eastern Africa to be around $4,960 \pm 70$ BP, based on records from Lakes Tanganyika, Challa and P178-15 from the Gulf of Aden. However, the timing of termination of the AHP varies considerably across the continent (Figure 8.2). Nevertheless, the considerable decline in productivity in the Garba Guracha diatom record falls within the broad age range of AHP termination across the continent, and close to the estimated mean age of termination (Figure 8.2). The basal age of the BA-LC-2011 core coincides with the termination of the AHP at some sites, which makes it difficult to interpret the termination of potential AHP-like conditions at Lake Babogaya. No comparisons can be made between more humid conditions in the mid-early Holocene making it virtually impossible to detect a change to more arid conditions. Presumably the AHP had ended at the site, or was ending, at Lake Babogaya at $\sim 5,400$ BP due to the abundance of shallower water taxa such as *Staurosirella pinnata* and *Pseudostaurosira brevistriata* at the base of the core (Figure 6.10). An alternative hypothesis is that

the full termination of AHP-like conditions occurred later at Lake Babogaya similar to other sites in the region around 1,000 years later. However, this cannot be confirmed in this study.

Identifying a geographic pattern in terms of climatic response to the often named 'time-transgressive' termination of the AHP in sites across the continent is notoriously difficult (Shanahan *et al.*, 2015; Figure 8.2), which can be attributed in part to complex interplays between moisture availability, vegetation cover and catchment morphology at each site. The north-south progressive onset of aridity associated with termination of the AHP as monsoon rains gradually reduced in response to decreasing summer insolation, as well as the southward migration of the tropical rain belts, has been discussed (e.g. deMenocal, 2015; Shanahan *et al.*, 2015). However, the inferred termination of the AHP at Garba Guracha in this study may reflect an east-west divide across the region. Moisture from the Congo basin, and migration of the CAB, is important for multiple sites across the region (Costa *et al.*, 2014), but less so for easternmost sites such as Lake Challa and those on the Horn of Africa which are reliant on the Indian Ocean for rainfall (Viste & Sorteberg, 2011; Tierney *et al.*, 2011a; Costa *et al.*, 2014). As well as a proposed southern migration of the rain belts, changes in moisture supply from the Indian Ocean would have impacted these sites further east (such as Garba Guracha; Figure 8.2) more than those further west that would still be supplied with moisture from the Congo basin (Tierney *et al.*, 2011a). Nevertheless, the termination at Garba Guracha is neither significantly early nor late in comparison to other records in the region, but in combination with these other datasets, emphasises the largely heterogeneous pattern of regional response to this climatic event across the African continent. Further studies investigating the

termination of the AHP across these north-south and east-west gradients, with robust chronologies which may also be hindering current interpretations of synchronicity, will aid our understanding of the nature of the termination of the AHP.

The rapidity of the AHP termination is a topic of much research and uncertainty (Tierney & deMenocal, 2013; Shanahan *et al.*, 2015; Collins *et al.*, 2017). However, before interpreting the rate of termination of the AHP at Garba Guracha and comparing to other sites it is first important to consider the uses of ‘abrupt’ and ‘gradual’ in previous palaeoenvironmental studies in Africa. deMenocal *et al.* (2000) describe geologically inferred terminations of the AHP over a millennia (from ~6,000 to 5,000 BP) as “relatively abrupt”, with the termination of the AHP recorded in their 658C core (~500 years transition) as “abrupt” and “very abrupt”.

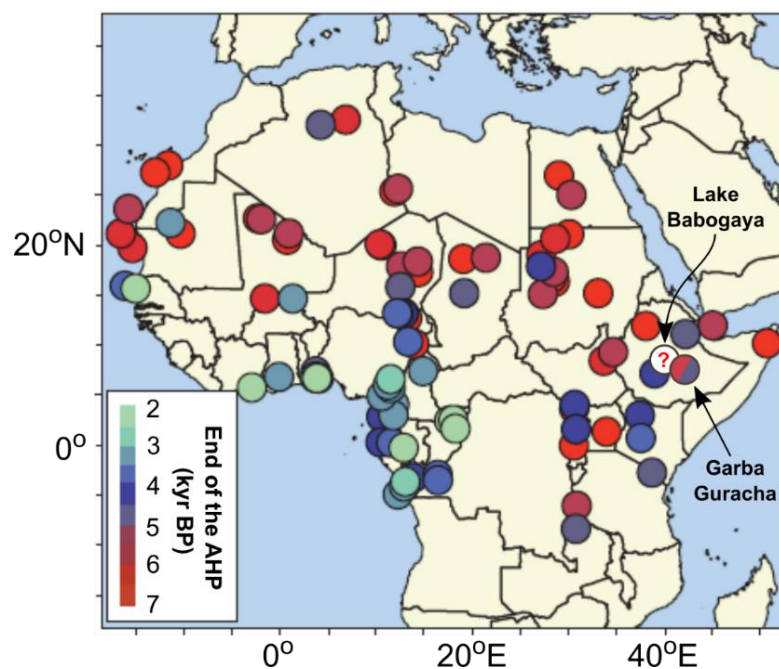


Figure 8.2: Termination of the AHP across multiple sites in much of Africa as determined by Shanahan *et al.* (2015), including the locations and timings of the termination of the AHP at the study sites included in this study. See text for discussion of two possible colours representing the termination at Garba Guracha at either around 5,500 BP or 4,500 BP.

Similarly, Tierney & deMenocal (2013) describe the duration of the AHP termination (280–490 years), based on their δD_{wax} record from the Gulf of Aden, in terms of being ‘abrupt’. Conversely, the 990-year transition (based on change-point analyses) from the AHP recorded in the K record from Chew Bahir is considered ‘gradual’ by Trauth *et al.* (2018).

Under one interpretation the clear change in diatom productivity (Figure 7.7) at Garba Guracha may be considered ‘very abrupt’, based on the broad use of ‘abrupt’, occurring over decades to centuries rather than millennia. However, this event at 5,500 BP may represent the beginning of a transitional phase at Garba Guracha. At this time conditions became unsuitable for Fragilarioid productivity, and the lake gradually shifted to an environment optimal for the growth of a more diverse, periphytic community at 4,500 BP (see below for further discussion). Therefore, this change at 5,500 BP may represent the beginning of a gradual shift rather than an abrupt ‘event’ at Garba Guracha.

Marshall *et al.* (2011) question whether the ‘4,200 BP event’ should mark the end of the AHP at Lake Tana. They argue that increased aridity began in northern Ethiopia around 8,500 BP which may in fact represent the start of a gradual, stepwise drying which reached its climax with an abrupt event around 4,200 BP. If earlier changes in the Garba Guracha record are taken into account then a similar consideration may be invoked: the 5,500 BP decrease in productivity (or even preceding change at 4,500 BP) may simply represent a threshold being exceeded following the gradual decline in moisture availability originating from 8,500 BP.

8.4.2 | The Meghalayan (4,200 BP to present day)

The most recent subdivision of the Holocene: the Meghalayan (Middle–Late Holocene Boundary), is based on the widespread ‘4.2 ka BP event’ (Walker *et al.*, 2012). A period of pronounced aridity from around 4,200 BP is evident across Africa (Gasse, 2000) including in records from lacustrine sites in eastern Africa including: the Ziway-Shala lake basin system (Gillespie *et al.*, 1983; Chalié & Gasse 2002a), Tana (Marshall *et al.*, 2011), Awassa (Telford *et al.*, 1999; Lamb *et al.*, 2002a), Tilo (Telford & Lamb 1999; Lamb *et al.*, 2000), and Victoria (Stanley *et al.*, 2003), with this aridity also reflected in high-altitude sites with enhanced dust influx initiating at around 4,200 BP culminating in a significant peak at ~4,000 BP in the Mt. Kilimanjaro ice core record (Thompson *et al.*, 2002). Despite increased diatom productivity, reorganisation of the diatom assemblage at Garba Guracha at ~4,500 BP likely represents a culmination of increasing aridity (see section 8.3.1) and suitable expansion and establishment of habitat optimal for the growth of a diverse, periphytic community.

However, a change at around this time is less obvious in the Lake Babogaya diatom or geochemical record. It has been noted that the identification of an intense arid event such as the ‘4.2 ka BP event’ is notoriously difficult in lacustrine records as it is superimposed on already drier conditions following the breakdown of the AHP (Marshall *et al.*, 2011). This difficulty in identifying a ‘4.2 ka event’ signature in a record may be apparent at Lake Babogaya. The deposition of a gastropod shell layer at the site implies lower lake levels at this time, with a decrease (albeit small) in TOC suggesting a less productive environment. Furthermore, the abundance of taxa indicative of shallower waters also attests to possible aridity at this time.

Earlier interpretations of potential considerable (>30 m) lake regression to allow shallower waters to pool on potential lake shelves at Lake Babogaya at this time (Section 6.5) are not incompatible with near desiccation of lakes documented elsewhere in the region, albeit at lakes with a significantly larger surface area. Lake lowstands were present by this time at Lake Turkana (Garcin *et al.*, 2012; >100 m lake level decrease), in the Ziway-Shala basin (Gillespie *et al.*, 1983; >100 m lake level decrease) and at palaeo-lake Suguta (Junginger *et al.*, 2014; ~300 m lake level decrease).

At nearby Lake Tilo the 4,200 BP event is recorded by an abrupt 3-4‰ increase in $\delta^{18}\text{O}$, marking a fall in lake level (Lamb *et al.* 2000). However, a wetter period is then interpreted after this dry phase (from 3,700 to 3,400 BP), indicated by an increase in the freshwater *Aulacoseira granulata* and reduction in $\delta^{18}\text{O}$ values (Telford *et al.* 1999; Lamb *et al.*, 2000). Further south, a short-lived humid episode can also be seen at ~3,000 BP in a small peak in the K record at Chew Bahir (Foerster *et al.*, 2012). Diatom productivity briefly increases within a laminated section of the Babogaya core at ~3,600 BP before the large section of minerogenic material between 3,600 and 3,300 BP. A humid period following a period of catchment instability and reduced lake level after 4,200 BP, may have triggered catchment disturbance or slumping at Lake Babogaya. Furthermore, at around 3,300 BP increased abundance of *Aulacoseira granulata* var. *angustissima*, comparable to that at Lake Tilo (Telford *et al.*, 1999), reflects this period of increased rainfall, increased stability and lake infilling. However, it is important to note the possibility of anthropogenic disturbance causing such instability at this time at Lake Babogaya. For example, to the north of Lake Babogaya at Lake Ashenge the first evidence for human induced landscape

change is interpreted in the fossil pollen and geochemical record at around 3,900-3,600 BP (Lamb unpub. data in Marshall, 2006; Marshall *et al.*, 2009).

8.5 | Post-4.2 ka BP event to present

A variable climate following the end of AHP and '4.2 ka event' is evident in many records across the region. Due to the influence of ENSO in eastern Africa, Stager *et al.* (2009), Tierney *et al.* (2011a) and Foerster *et al.* (2012) have speculated this increased variability in the Late Holocene may reflect more frequent ENSO events, as part of a fluctuating cycle, during this period (at least as recorded along the South American coast; Moy *et al.*, 2002; Conroy *et al.*, 2008 and in Mexico; Jones *et al.*, 2015) or increased dominance of ENSO variability as a result of reduced insolation following the mid-Holocene maxima (Lu *et al.* 2018). Such periods of enhanced ENSO activity are evident between 3,000 and 2,500 BP, and around 1,600 BP and 1,300 BP (Figure 8.3).

Invoking a similar interpretation to Foerster *et al.* (2012), enhanced ENSO activity may have aided in the refilling of the lake, or at least the increased rainfall resulted in enhanced lake water mixing, required for the appearance and proliferation of *Aulacoseira granulata* var. *angustissima* between 3,000 and 2,500 BP. Similarly, changes between *Nitzschia lancettula* and a *Nitzschia paleacea*: *Nitzschia fenestralis* complex at Lake Babogaya may reflect a fluctuating hydrological and mixing regime during a more variable ENSO cycle. The abundance of Cymbelloid taxa at Lake Babogaya after ~1,750 BP may represent a shift towards drier conditions during this more variable climate. However, some periods of increased planktonic abundance at around 1,300 BP and 1,600 BP may tentatively be ENSO-type variability associated with more frequent ENSO

activity and increased lake level and humidity (Figure 8.3). Variability in Fe:Mn and the diatom productivity and community composition in the Garba Guracha record is clear following the large scale reorganisation of the diatom community at 4,500 BP.

The clear influence of increased ENSO-type variability is less apparent in the Garba Guracha record (Figure 8.4), despite being an area that receives a large proportion of its moisture from the Indian Ocean (Viste & Sorteberg, 2011). The most noticeable change coinciding with increased ENSO variability is the increased abundance of Fragilarioid taxa (Figure 7.7). This may be in response to their adaptability to wet-dry shifts and the increase in humidity leading to the decrease in aerophilous habitat, although there are no noticeable coincidences between ecological or environmental change at Garba Guracha and increased ENSO activity (Figure 8.4) as may be found at other sites (Figure 8.3). This may be associated with the high altitude of the Bale Mountains effectively blocking moisture transport from an ENSO event to the area. However, this is difficult to reconcile with increased moisture availability evident at another high altitude, albeit lower latitude, site with the Small Hall Tarn Lake, Mt. Kenya $\delta^{18}\text{O}$ record consistent with more frequent ENSO events (Barker *et al.*, 2001).

At Lake Babogaya during this period, a small change may be detectable through the reappearance of *Pseudostaurosira brevistriata* and *Staurosirella pinnata* in the Lake Babogaya record between 780 to 1,115 BP, corresponding to an increase in terrigenous input (Ti XRF data in Figure 8.3) and decrease in TOC, which may indicate a period of aridity and lower lake level.

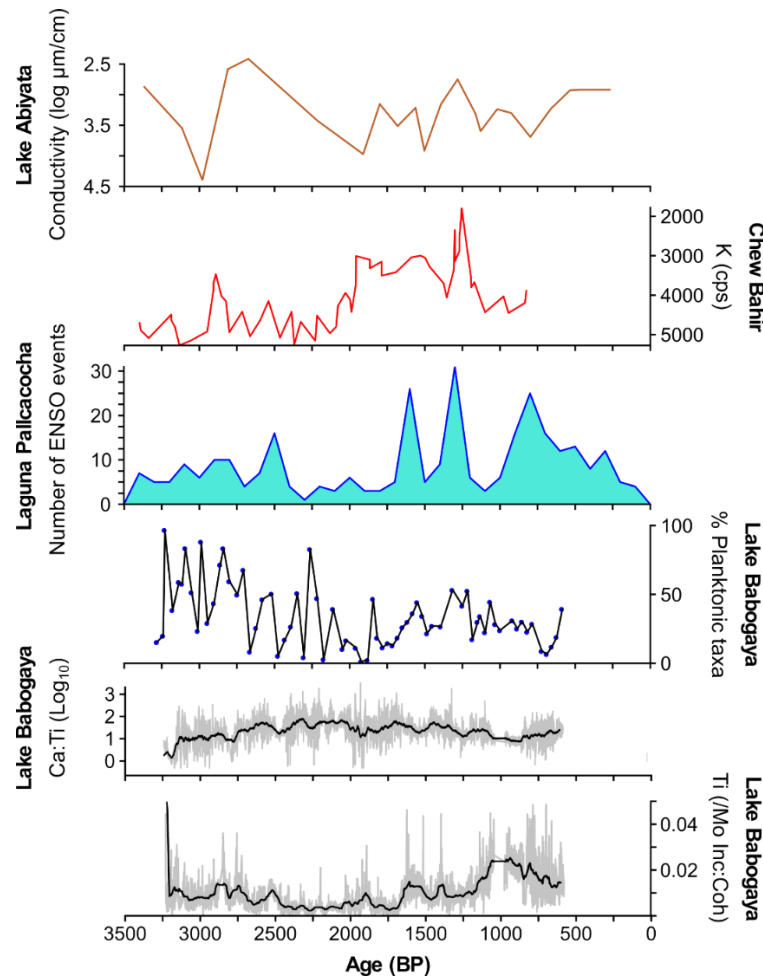


Figure 8.3: Comparison of Lake Babogaya records discussed in text with similar records from relatively nearby Lake Abiyata (Chalie & Gasse, 2018; note reverse scale) and Chew Bahir (Foerster *et al.*, 2012; note reverse scale), with ENSO activity as recorded in the Laguna Pallacocha red colour intensity record (Moy *et al.*, 2002) also shown.

Although wetter conditions may wash in marginal, shallower water taxa consistently low Ti suggests low rates of in-washing. This period of drier conditions broadly corresponds to the Northern Hemisphere ‘Medieval Climate Anomaly’ (MCA) or ‘Medieval Warm Period’ (Mann *et al.*, 2009), which has also been documented in numerous sites across the region (e.g. Mills *et al.*, 2014; Tierney *et al.*, 2015; Buckles *et al.*, 2016), including an intense, short-lived pulse of aridity around ~1,150 BP inferred from increased $\delta^{18}\text{O}$ (average of +6.2 ‰;

Lamb *et al.*, 2007) and lower lake levels (by ~8-9 m) between 950 and 650 BP (Ghinassi *et al.*, 2012) at Lake Hayq to the north.

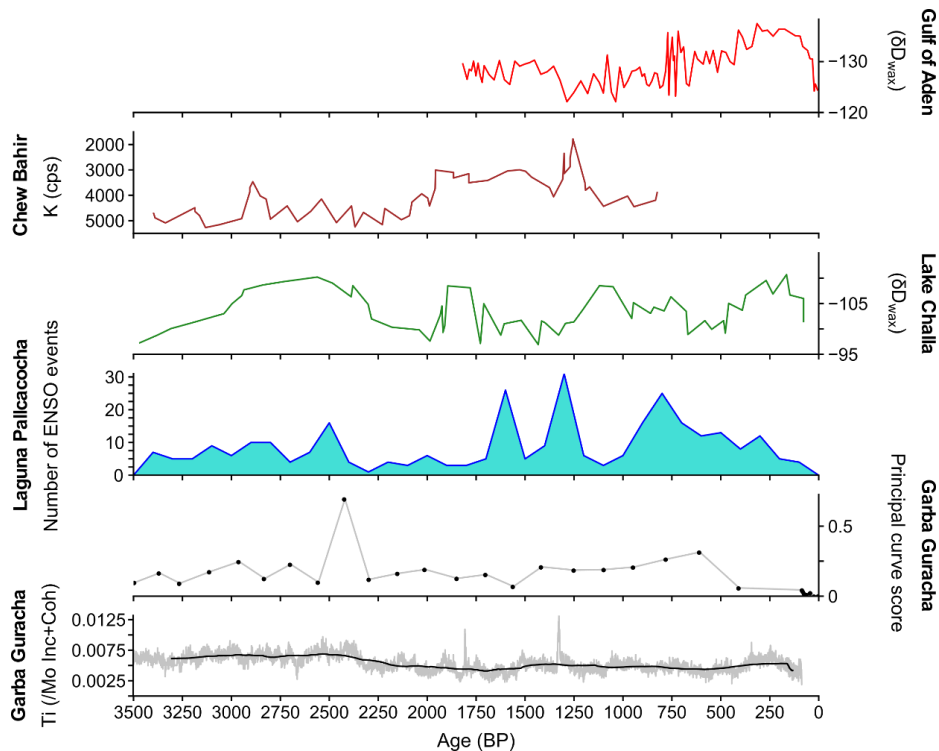


Figure 8.4: Comparison of Garba Guracha records discussed in text with similar records from relatively close sites (the Gulf of Aden (Tierney *et al.*, 2015) Chew Bahir (Foerster *et al.*, 2012; note reverse scale) and Lake Challa (Tierney *et al.*, 2011b) in easternmost areas where moisture from the Indian Ocean is important and ENSO activity as recorded in the Laguna Pallacocha red colour intensity record (Moy *et al.*, 2002).

However, a ‘fingerprint’ of the MCA in the Garba Guracha record is unclear. An increase in Fragilarioid taxa, and reduction in aerophilous taxa, coincides with the broad timing of the MCA, especially the reappearance of *Staurosira construens var. venter* in the record (see higher principal curve scores in Figure 8.4). However, the evidence from Garba Guracha is inconsistent with the drying trend exhibited at other sites in the region, with an increase in Fragilarioid taxa normally associated with, albeit shallower, more dilute waters, with reductions in aerophilous habitat presumably in response to a decrease in available habitat (Figure 8.4).

Unfortunately, the Lake Babogaya record ends shortly after the termination of MCA-like conditions, but the Garba Guracha extends into the present day offering further insights into the impacts of climatic perturbations on high altitude sites. A second perturbation punctuates the last ~1,000 years of eastern African climate in many records across the region: the Little Ice Age (LIA). The LIA in eastern Africa is a focus of debate with a west (dry)-east (wet) dichotomy (Tierney *et al.*, 2013; 2015), and therefore insights from a high altitude, eastern site would be invaluable in this discussion. However, interpretations from the Garba Guracha record are severely limited for the LIA as the gap between the surface core and long core almost exclusively covers this period. XRF data are present through this section of core, but only small increases in minerogenic input (Ti; Figure 8.4) are observable at this time which may indicate wet or dry conditions enhancing soil erosion. Potentially drier conditions are present before the LIA with high abundance of the aerophilous *Nitzschia amphibia*, with an increase in the abundance of periphytic Cymbelloid taxa, and corresponding decrease in conductivity immediately preceding this event suggestive of slightly wetter conditions (~80 BP). It is important to stress that other variables such as nutrient content and habitat availability (as previously discussed) potentially driving ecological change at Garba Guracha (cf. Juggins, 2013), not necessarily climate-induced changes in salinity. Thus, the resolution through this period is simply inadequate to fully understand the dynamics of the diatom ecology and the impact of the LIA at this altitude at Garba Guracha.

8.5.1 | Modern rapid change in eastern Africa

Ecological instability, inferred through high rate of change values (Figure 7.9), is prominent in the Garba Guracha record in the late 19th Century and into the

present day, with the aerophilous *Nitzschia amphibia* dominant in the record after around 1970 CE. This likely reflects high magnitude variability in climate across the region with humid and arid periods, with the dominance of *Nitzschia amphibia* likely reflecting drying out of the environment and opening up aerophilous habitat. The onset of modern aridity has been dated in the δD_{wax} record of P178-15, Gulf of Aden to the start of the 19th Century (Tierney *et al.*, 2015), with arid conditions dated towards the end of the 19th Century at Lake Abiyata (Legesse *et al.*, 2002). Even in a more remote site in Sacred Lake, Mt. Kenya pronounced drying is represented in the δD_{wax} record presented by Konecky *et al.* (2014) at ~1870 CE (although their dating control precludes exact timing of this onset), which broadly corresponds to the timing of this change observed in the Garba Guracha diatom record. A period of high rainfall during the 1960s interrupted this general trend of aridity and led to peak discharges in many waterbodies in the region (Nash *et al.*, 2016). This may be represented by increase in Fragilarioid taxa at Garba Guracha at this time, despite being associated with shallower waters in this case it may be related to reduced aerophilous habitat and slight reduction in conductivity. The dominance of *Nitzschia amphibia* after 1970 CE may represent the considerably drier conditions present across much of the region (Nash *et al.*, 2016), with Tierney *et al.* (2015) suggesting current (late-20th Century-present) is some of the regions driest conditions documented in the last 2,000 years.

8.6 | Anthropogenic impacts

The anthropogenic impact on the Mid-Late Holocene eastern African environment is a known issue that complicates paleoenvironmental reconstructions by providing sometimes overlapping signals that are sometimes difficult to distinguish from the climate signals (Kiage & Liu, 2006). In Ethiopia the

impact of anthropogenic activities is clear in the latter half of the Late Holocene, with forest clearance in the north of the country, for example, dated at around 2,500-2,000 BP (Darbyshire *et al.*, 2003) with ceramics and domestic animals appearing in archaeological records in the Kaffa province in the southwest of the country by ~2,000 BP (Hildebrand *et al.*, 2010). A similar timing of anthropogenic modification of the Bale Mountain environment is recorded with the replacement of forest by *Hagenia abyssinica* and *Dodonaea* after 2,000-2,500 BP and minor abundances of *Plantago* after 1,300 BP (Umer & Bonnefille, 1998; Umer *et al.*, 2007). Recent counting of the dung-fungus sporormiella in the GGU-17-AB core by Gil-Romera (in prep.) suggests that the presence of livestock is only represented in the record through the last few millennia. Although a fire record is now available from Garba Guracha (Gil-Romera *et al.*, 2019), it is difficult to untangle climatic and human factors in the origination of fire events and thus is of limited use to understand possible anthropogenic impacts on the waters and flora of the lake.

Although no distinct indicators of anthropogenic activity are present in the Garba Guracha and Lake Babogaya records, it does not preclude the possibility of such influences being superimposed on climatic trends or *vice versa*. Anthropogenic clearance of forests, for example, destabilises soils in the catchment, thus potentially leading to increased erosion and minerogenic input unrelated to climatic changes. At Lake Babogaya, for example, the increase in Ti at around 1,500 BP (Figure 6.5) may reflect anthropogenic induced catchment destabilisation and soil erosion, although this is not clear in the diatom records.

Chapter 9:

Conclusions

This research aimed to present a high-resolution, detailed reconstruction of palaeoenvironmental changes at two contrasting sites in Ethiopia, by applying a holistic, multi-proxy approach to sedimentary records from Garba Guracha (GGU-17-1AB) and Lake Babogaya (BA-LC-2011). Based on the biological and geochemical proxies used, palaeolimnological evidence has been successfully utilised to infer changes in both complex lake systems. These records have not only provided reliable evidence of local changes to the environment and climate, but have allowed for wider comparison to records from Ethiopia, the Horn of Africa and eastern Africa since the late Pleistocene. The Garba Guracha record, covering the last 16,000 years, represents one of the longest continuous reconstructions of its kind from any site in Africa. Furthermore, the results obtained from Garba Guracha aid in our understanding of how long- and short-term climate trends have been expressed at different sites and altitudes since the Last Glacial Maximum.

9.1 | Palaeolimnological change at Lake Babogaya and Garba Guracha

Garba Guracha was a typical post-glacial environment from 16,000 BP (following the formation of the lake by the retreat of ice masses up valley) to around 10,500 BP, characterised by poorly developed catchment soils and low organic productivity. Because of this poorly productive environment any enhanced aridity associated with the Younger Dryas interval, identified at multiple other sites in the region, is muted in the Garba Guracha record. A distinct increase in the abundance of facultatively

planktonic Fragilarioid taxa (and corresponding decrease in benthic/aerophilous taxa) is observed after 10,500 BP reflecting a fresher, deeper lake environment, presumably representing a lagged response to the AHP. The increase in humidity associated with the AHP did not seem to drive productivity and ecological change at Garba Guracha, with increased temperature in correspondence to peak insolation at 10,500 BP seemingly required, presumably in response to a longer growing season.

Tentative evidence is presented for gradually drier and unstable conditions after 8,500 BP, although this is difficult to identify based solely on diatom productivity in this study as interpreting based on ecological change is limited by factors nutrient availability and temperature leading to a virtually monospecific, Fragilarioid community. The termination of wetter AHP-like conditions is clear in the Garba Guracha diatom record at around 5,500 BP, with further change distinct in the record at around 4,500 BP (associated with the 4.2 ka BP event) with significant re-organisation of the diatom community. The Garba Guracha record corroborates multiple other records from across Africa: there was no distinct geographic trend in the timing of the termination of the AHP, highlighting the heterogeneous pattern of regional response to this climatic event. Whether the change at 5,500 BP is abrupt (occurring over <200 years), or as part of a more gradual regime shift if the change at 4,500 BP is considered (thus occurring over ~1,000 years), is unclear due to the inconsistent use of 'abrupt' or 'gradual' in the wider literature. Unfortunately, it is virtually impossible to detect the termination of the AHP at Lake Babogaya as the base of the core is likely deposited following the end of the AHP or during it.

However, the 4.2 ka BP event is subtle but noticeable in the Lake Babogaya record with the deposition of a shell layer at 4,150 BP and presumably leading to a 300-year, high magnitude deposition of inorganic materials either as a consequence of slumping or as a result of a destabilised catchment in response arid conditions.

Generally drier conditions following the Meghalayan and into the late Holocene (seen at multiple other sites in Africa; Gasse, 2000) is represented at both sites by a clear, gradual increase in the abundance of benthic and aerophilous taxa presumably reflecting reduced lake levels under a drier climate following the AHP. Climatic change associated with the Medieval Climate Anomaly is clear in the Lake Babogaya and Garba Guracha records, although the latter appears to exhibit wetter rather than drier conditions during this period. The Lake Babogaya sediment record ends at ~600 BP. However, the Garba Guracha record continues to the present day and thus offers valuable insights into the Late Holocene climatic changes at high altitude areas in the Ethiopian Highlands. Contemporary post-industrial revolution drying identified in other less remote sites is prominent in the Garba Guracha diatom record. In the late Holocene it is less clear if enhanced ENSO activity is an influence on both of these catchments. Similarly, anthropogenic induced changes may be present and may be contributing to (or vice versa) climate driving ecological and catchment changes, but in these records it is difficult to tease apart these two drivers.

References

- Aaby, B., and B. Berglund. 1986. "Characterization of Peat and Lake Deposits." In *Handbook of Holocene Palaeoecology and Palaeohydrology*, edited by B. Berglund, 231–46. New York: John Wiley & Sons.
- Adhikari, Umesh, A. Pouyan Nejadhashemi, and Sean A. Woznicki. 2015. "Climate Change and Eastern Africa: A Review of Impact on Major Crops." *Food and Energy Security* 4 (2): 110–32. <https://doi.org/10.1002/fes3.61>.
- Ali, A. 1999. "River-Groundwater Interactions in the Sekelo-Akaki Basin". M.Sc thesis, Addis Ababa University.
- Alley, Richard B. 2000. "The Younger Dryas Cold Interval as Viewed from Central Greenland." *Quaternary Science Reviews* 19 (1): 213–26. [https://doi.org/10.1016/S0277-3791\(99\)00062-1](https://doi.org/10.1016/S0277-3791(99)00062-1).
- Amaral, P G C, A Vincens, J Guiot, G Buchet, P Deschamps, J.-C Doumnang, and F Sylvestre. 2013. "Palynological Evidence for Gradual Vegetation and Climate Changes during the African Humid Period Termination at 13 N from a Mega-Lake Chad Sedimentary Sequence." *Clim. Past* 9: 223–41. <https://doi.org/10.5194/cp-9-223-2013>.
- Andersen, K. K., N. Azuma, J.-M. Barnola, M. Bigler, P. Biscaye, N. Caillon, J. Chappellaz, et al. 2004. "High-Resolution Record of Northern Hemisphere Climate Extending into the Last Interglacial Period." *Nature* 431 (7005): 147–51. <https://doi.org/10.1038/nature02805>.
- Anderson, N, H Bugmann, J Dearing, and M Gaillard. 2006. "Linking Palaeoenvironmental Data and Models to Understand the Past and to Predict the Future." *Trends in Ecology & Evolution* 21 (12): 696–704. <https://doi.org/10.1016/j.tree.2006.09.005>.
- Appleby, P. 2001. "Chronostratigraphic Techniques in Recent Sediments." In *Tracking Environmental Change Using Lake Sediments Volume 1: Basin Analysis, Coring, and Chronological Techniques*, edited by W. Last and J. Smol, 171–203. Dordrecht: Kluwer Academic Publishers.
- Appleby, P. G., N. Richardson, and P. J. Nolan. 1991. "241Am Dating of Lake Sediments." *Hydrobiologia* 214 (1): 35–42. <https://doi.org/10.1007/BF00050929>.
- Appleby, P.G., and F. Oldfield. 1978. "The Calculation of Lead-210 Dates Assuming a Constant Rate of Supply of Unsupported 210Pb to the Sediment." *CATENA* 5 (1): 1–8. [https://doi.org/10.1016/S0341-8162\(78\)80002-2](https://doi.org/10.1016/S0341-8162(78)80002-2).

- Arnett, Heather A., Jasmine E. Saros, and M. Alisa Mast. 2012. "A Caveat Regarding Diatom-Inferred Nitrogen Concentrations in Oligotrophic Lakes." *Journal of Paleolimnology* **47** (2): 277–91. <https://doi.org/10.1007/s10933-011-9576-z>.
- Arz, Helge, Frank, Lamy, and Jürgen, Pätzold. 2006. "A pronounced dry event recorded around 4.2 ka in brine sediments from the northern Red Sea". *Quaternary Research* **66** (3): 432-441. <https://doi.org/10.1016/j.yqres.2006.05.006>.
- Asrat, Asfawossen, Andy Baker, Mohammed Umer Mohammed, Melanie J. Leng, Peter Van Calsteren, and Claire Smith. 2007. "A High-Resolution Multi-Proxy Stalagmite Record from Mechara, Southeastern Ethiopia: Palaeohydrological Implications for Speleothem Palaeoclimate Reconstruction." *Journal of Quaternary Science* **22** (1): 53–63. <https://doi.org/10.1002/jqs.1013>.
- Awulachew, Seleshi, Wakena Totoba, Philippe Lempriere, Nigatu Alemayehu, and Kiflu Getahun. 2006. "Assessment of Water Resources and Recommendation to Improve Water Resources Management." Final draft report. Nairobi, Kenya: ILRI and IWMI.
- Baier, J., A. Lücke, J.F.W. Negendank, G.-H. Schleser, and B. Zolitschka. 2004. "Diatom and Geochemical Evidence of Mid- to Late Holocene Climatic Changes at Lake Holzmaar, West-Eifel (Germany)." *Quaternary International* **113** (1): 81–96. [https://doi.org/10.1016/S1040-6182\(03\)00081-8](https://doi.org/10.1016/S1040-6182(03)00081-8).
- Baker, A., A. Asrat, I. J. Fairchild, M. J. Leng, L. Thomas, M. Widmann, C. N. Jex, Buwen Buwen Dong, P. van Calsteren, and C. Bryant. 2010. "Decadal-Scale Rainfall Variability in Ethiopia Recorded in an Annually Laminated, Holocene-Age, Stalagmite." *The Holocene* **20** (6): 827–36. <https://doi.org/10.1177/0959683610365934>.
- Barker, P. A., 1990. "Diatoms as palaeolimnological indicators: A reconstruction of Late Quaternary environments in two East African salt lakes." Ph.D. thesis, Loughborough University of Technology, UK. 267 pp.
- Barker, P. A., F. A. Street-Perrott, M. J. Leng, P. B. Greenwood, D. L. Swain, R. A. Perrott, R. J. Telford, and K. J. Ficken. 2001. "A 14,000-Year Oxygen Isotope Record from Diatom Silica in Two Alpine Lakes on Mt. Kenya." *Science* **292** (5525): 2307–10.
- Barker, P. A., J.-C. Fontes, F. Gasse, and J.-C. Druart. 1994. "Experimental dissolution of diatom silica in concentrated salt solutions and implications for paleoenvironmental reconstruction" *Limnol. Oceanogr.* **39** (1): 99-110. <https://doi.org/10.4319/lo.1994.39.1.0099>.

- Barker, Philip A., Melanie J. Leng, Françoise Gasse, and Yongsong Huang. 2007. "Century-to-Millennial Scale Climatic Variability in Lake Malawi Revealed by Isotope Records." *Earth and Planetary Science Letters* **261** (1–2): 93–103. <https://doi.org/10.1016/j.epsl.2007.06.010>.
- Barker, P.A., Talbot, M.R., Street-Perrott, F.A., Marret, F., Scourse, J.D., Odada, E. 2004 "Late quaternary climatic variability in intertropical Africa." In: "Past climate variability through Europe and Africa". Edited by Battarbee, Richard W., Françoise Gasse, and Catherine, Stickley: 117-138. Netherlands: Springer.
- Barker, Philip, David Williamson, Françoise Gasse, and Elisabeth Gibert. 2003. "Climatic and Volcanic Forcing Revealed in a 50,000-Year Diatom Record from Lake Massoko, Tanzania." *Quaternary Research* **60** (3): 368–76. <https://doi.org/10.1016/J.YQRES.2003.07.001>.
- Battarbee, R. 1986. "Diatom Analysis". In: "Handbook of Holocene Palaeoecology and palaeohydrology". Edited by B. E. Berglund, 527-570. Chichester: John Wiley & Sons Ltd.
- Battarbee, R, V, Jones, R, Flower, N, Cameron, H, Bennion, L, Carvalho, and S, Juggins. 2001. "Diatoms". In: "Tracking environmental change using lake sediments: terrestrial, algal and siliceous indicators". Edited by Smol, J.P., H.J.B., Birks, W.M., Last: 155-202. Dodrecht: Kluwer.
- Baxter, R. M., M. V. Prosser, J. F. Talling, and R. B. Wood. 1965. "Stratification in Tropical African Lakes at Moderate Altitudes (1,500 to 2,000 M)." *Limnology and Oceanography* **10** (4): 510–20. <https://doi.org/10.4319/lo.1965.10.4.0510>.
- Belay, D. 2007. "Temporal and Spatial Dynamics of Zooplankton in Relation to Phytoplankton in Lake Babogaya (Bishoftu Guda) Ethiopia." MSc thesis, Addis Ababa University.
- Bennet, K. 1996. "Determination of the number of zones in a biostratigraphical sequence". *New Phytologist* **132** (1): 155-170. <https://doi.org/10.1111/j.1469-8137.1996.tb04521.x>.
- Bennion, Helen, and Gavin L. Simpson. 2011. "The Use of Diatom Records to Establish Reference Conditions for UK Lakes Subject to Eutrophication." *Journal of Paleolimnology* **45** (4): 469–88. <https://doi.org/10.1007/s10933-010-9422-8>.
- Bennion, H., Davidson, T.A., Sayer, C.D., Simpson, G.L., Rose, N.L., Sadler, J.P. 2015a. "Harnessing the potential of the multi-indicator palaeoecological approach: an assessment of the nature and causes of ecological change in a eutrophic shallow lake". *Freshwater*

Biology **60** (7): 1423-1442. doi:10.1111/fwb.12579

Bennion, H., Simpson, G.L., Goldsmith, B.J. 2015b. "Assessing degradation and recovery pathways in lakes impacted by eutrophication using the sediment record". *Frontiers in Ecology and Evolution* **3**. doi:10.3389/fevo.2015.00094

Berger, A, and Loutre, M. 1991. "Insolation values for the climate of the last 10 million years". *Quaternary Science Reviews* **10** (4): 297-317. [https://doi.org/10.1016/0277-3791\(91\)90033-Q](https://doi.org/10.1016/0277-3791(91)90033-Q).

Berke, Melissa A., Thomas C. Johnson, Josef P. Werne, Kliti Grice, Stefan Schouten, and Jaap S. Sinninghe Damsté. 2012. "Molecular Records of Climate Variability and Vegetation Response since the Late Pleistocene in the Lake Victoria Basin, East Africa." *Quaternary Science Reviews* **55**: 59–74. <https://doi.org/10.1016/j.quascirev.2012.08.014>.

Besse-Lototskaya, Anna, Piet F.M. Verdonchot, Michel Coste, and Bart Van de Vijver. 2011. "Evaluation of European Diatom Trophic Indices." *Ecological Indicators* **11** (2): 456–67. <https://doi.org/10.1016/J.ECOLIND.2010.06.017>.

Beyene, Abebe, Aymere Awoke, and Ludwig Triest. 2014. "Estimation of Environmental Optima and Tolerances of Diatoms Using Multifactor Multiplicative Modeling." *Ecological Informatics* **19**: 53–61. <https://doi.org/10.1016/j.ecoinf.2013.12.007>.

Birks, H.J.B., and A.D, Gordon. 1985. "Numerical methods in quaternary pollen analysis". Orlando: Academic Press. Harcourt Brace Jovanovich.

Birks, Hilary H., and H. John B. Birks. 2006. "Multi-Proxy Studies in Palaeolimnology." *Vegetation History and Archaeobotany* **15** (4): 235–51. <https://doi.org/10.1007/s00334-006-0066-6>.

Björck, Svante, and Barbara Wohlfarth. 2001. "14C Chronostratigraphic Techniques in Paleolimnology." In *Tracking Environmental Change Using Lake Sediments*, 205–45. Dordrecht: Kluwer Academic Publishers. https://doi.org/10.1007/0-306-47669-X_10.

Blanchet, Cécile L., Martin Frank, Stefan Schouten, NA Drake, RM Blench, SJ Armitage, CS Bristow, et al. 2014. "Asynchronous Changes in Vegetation, Runoff and Erosion in the Nile River Watershed during the Holocene." Edited by Cheng–Sen Li. *PLoS ONE* **9** (12): e115958. <https://doi.org/10.1371/journal.pone.0115958>.

Blanchet, Cécile L., Rik Tjallingii, Martin Frank, Janne Lorenzen, Anja Reitz, Kevin Brown, Tomas Feseker, and Warner Brückmann. 2013. "High- and Low-Latitude Forcing of the Nile River Regime during the Holocene Inferred from Laminated Sediments of the Nile Deep-Sea

- Fan." *Earth and Planetary Science Letters*. **364**. <https://doi.org/10.1016/j.epsl.2013.01.009>.
- Blanco, S. 2014. "Environmental Factors Controlling Lake Diatom Communities Environmental Factors Controlling Lake Diatom Communities: A Meta-Analysis of Published Data Environmental Factors Controlling Lake Diatom Communities." *Biogeosciences Discuss* **11**: 15889–909. <https://doi.org/10.5194/bgd-11-15889-2014>.
- Blaauw, M, and J. Christen. 2019. "rbacon: Age-Depth Modelling using Bayesian Statistics". R package version 2.3.7. <https://CRAN.R-project.org/package=rbacon>
- Blauuw, M, B van Geel, I Kristen, B Plessen, A Lyaruu, D Engstrom, J van der Plicht, and D Verschuren. 2011. "High-Resolution 14C Dating of a 25,000-Year Lake-Sediment Record from Equatorial East Africa." *Quaternary Science Reviews* **30** (21–22): 3043–59. <https://doi.org/10.1016/J.QUASCIREV.2011.07.014>.
- Bond, Gerard, Hartmut Heinrich, Wallace Broecker, Laurent Labeyrie, Jerry McManus, John Andrews, Sylvain Huon, et al. 1992. "Evidence for Massive Discharges of Icebergs into the North Atlantic Ocean during the Last Glacial Period." *Nature* **360** (6401): 245–49. <https://doi.org/10.1038/360245a0>.
- Bonnefille, R., G., Riollet, G., Buchet, M., Icole, R., Lafont, M., Arnold, and D., Jolly. 1995. "Glacial interglacial record from intertropical Africa, high resolution pollen and carbon data at Rusaka, Burundi". *Quaternary Science Reviews* **14** (9): 917-936. [https://doi.org/10.1016/0277-3791\(95\)00071-2](https://doi.org/10.1016/0277-3791(95)00071-2).
- Borchardt, Sven, and Martin H. Trauth. 2012. "Remotely-Sensed Evapotranspiration Estimates for an Improved Hydrological Modeling of the Early Holocene Mega-Lake Suguta, Northern Kenya Rift." *Palaeogeography, Palaeoclimatology, Palaeoecology* **361**: 14–20. <https://doi.org/10.1016/j.palaeo.2012.07.009>.
- Bouimetarhan, I., L. Dupont, H. Kuhlmann, J. Pätzold, M. Prange, E. Schefuß, and K. Zonneveld. 2015. "Northern Hemisphere Control of Deglacial Vegetation Changes in the Rufiji Uplands (Tanzania)." *Climate of the Past* **11** (5): 751–64. <https://doi.org/10.5194/cp-11-751-2015>.
- Brock, Fiona, Thomas Higham, Peter Ditchfield, and Christopher Bronk Ramsey. 2010. "Current Pretreatment Methods for AMS Radiocarbon Dating at the Oxford Radiocarbon Accelerator Unit (Orau)." *Radiocarbon* **52** (01): 103–12. <https://doi.org/10.1017/S0033822200045069>.
- Brodie, C, James S.L., Casford, Jeremy M. Lloyd, Melanie J. Leng, Tim. H. E. Heaton,

- Christopher P. Kendrick and Zong Yongqiang. 2011. "Evidence for bias in C/N, $\delta^{13}\text{C}$ and $\delta^{15}\text{N}$ values of bulk organic matter, and on environmental interpretation, from a lake sedimentary sequence by pre-analysis acid treatment methods". *Quaternary Science Reviews* **30** (21–22): 3076-3087. <https://doi.org/10.1016/j.quascirev.2011.07.003>.
- Broecker, Wallace, Gerard Bond, Mieczyslawa Klas, Elizabeth Clark, and Jerry McManus. 1992. "Origin of the Northern Atlantic's Heinrich Events." *Climate Dynamics* **6** (3–4): 265–73. <https://doi.org/10.1007/BF00193540>.
- Bronk Ramsey, Christopher, Thomas Higham, and Philip Leach. 2004. "Towards High-Precision AMS: Progress and Limitations." *Radiocarbon* **46** (01): 17–24. <https://doi.org/10.1017/S0033822200039308>.
- Brooks, Keely, Christopher A. Scholz, John W. King, John Peck, Jonathan T. Overpeck, James M. Russell, and Philip Y.O. Amoako. 2005. "Late-Quaternary Lowstands of Lake Bosumtwi, Ghana: Evidence from High-Resolution Seismic-Reflection and Sediment-Core Data." *Palaeogeography, Palaeoclimatology, Palaeoecology* **216** (3): 235–49. <https://doi.org/10.1016/j.palaeo.2004.10.005>.
- Brown, E. T., T. C. Johnson, C. A. Scholz, A. S. Cohen, and J. W. King. 2007. "Abrupt Change in Tropical African Climate Linked to the Bipolar Seesaw over the Past 55,000 Years." *Geophysical Research Letters* **34** (20): L20702. <https://doi.org/10.1029/2007GL031240>.
- Buckles, Laura K, Dirk Verschuren, Johan W H Weijers, Christine Cocquyt, Maarten Blaauw, and Jaap S Sinninghe Damsté. 2016. "Interannual and (Multi-)Decadal Variability in the Sedimentary BIT Index of Lake Challa, East Africa, over the Past 2200 Years: Assessment of the Precipitation Proxy." *Clim. Past* **12**: 1243–62. <https://doi.org/10.5194/cp-12-1243-2016>.
- Burley, Kim L., Ellie E. Prepas, and Patricia A. Chambers. 2001. "Phosphorus Release from Sediments in Hardwater Eutrophic Lakes: The Effects of Redox-Sensitive and -Insensitive Chemical Treatments." *Freshwater Biology* **46** (8): 1061–74. <https://doi.org/10.1046/j.1365-2427.2001.00789.x>.
- Burnett, Allison P., Michael J. Soreghan, and Erik T. Brown. 2011. "Tropical East African Climate Change and Its Relation to Global Climate: A Record from Lake Tanganyika, Tropical East Africa, over the Past 90+ Kyr." *Palaeogeography, Palaeoclimatology, Palaeoecology* **303** (1–4): 155–67. <https://doi.org/10.1016/J.PALAEO.2010.02.011>.
- Burpee, Benjamin T., Dennis Anderson, and Jasmine E. Saros. 2018. "Assessing Ecological

Effects of Glacial Meltwater on Lakes Fed by the Greenland Ice Sheet: The Role of Nutrient Subsidies and Turbidity." *Arctic, Antarctic, and Alpine Research* **50** (1): S100019. <https://doi.org/10.1080/15230430.2017.1420953>.

Camarero, J., J, Garcia-Ruiz, G, Sanguesa-Barreda, J, Galvan, A, Alla, Y, Sanjuan, S, Begueria, and E, Gutierrez. 2015. "Recent and Intense Dynamics in a Formerly Static Pyrenean Treeline". *Arctic, Antarctic, and Alpine Research* **47** (4): 773-783.

Camberlin, P, S Janicot, and I Pocard. 2001. "Seasonality and Atmospheric Dynamics of the Teleconnection between African Rainfall and Tropical Sea-Surface Temperature: Atlantic vs. ENSO." *International Journal of Climatology* **21**: 973–1005. <https://doi.org/10.1002/joc.673>.

Cantonati, Marco, Silvia Scola, Nicola Angeli, Graziano Guella, and Rita Frassanito. 2009. "Environmental Controls of Epilithic Diatom Depth-Distribution in an Oligotrophic Lake Characterized by Marked Water-Level Fluctuations." *European Journal of Phycology* **44** (1): 15–29. <https://doi.org/10.1080/09670260802079335>.

Castañeda, Isla S., Stefan Schouten, Jürgen Pätzold, Friedrich Lucassen, Simone Kasemann, Holger Kuhlmann, and Enno Schefuß. 2016. "Hydroclimate Variability in the Nile River Basin during the Past 28,000 Years." *Earth and Planetary Science Letters*. **438**. <https://doi.org/10.1016/j.epsl.2015.12.014>.

Castañeda, Isla S., Josef P. Werne, Thomas C. Johnson, and Timothy R. Filley. 2009. "Late Quaternary Vegetation History of Southeast Africa: The Molecular Isotopic Record from Lake Malawi." *Palaeogeography, Palaeoclimatology, Palaeoecology* **275** (1): 100–112. <https://doi.org/10.1016/j.palaeo.2009.02.008>.

Chalié, Françoise, and Françoise Gasse. 2002. "Late Glacial–Holocene Diatom Record of Water Chemistry and Lake Level Change from the Tropical East African Rift Lake Abiyata (Ethiopia)." *Palaeogeography, Palaeoclimatology, Palaeoecology* **187** (3): 259–83. [https://doi.org/10.1016/S0031-0182\(02\)00480-7](https://doi.org/10.1016/S0031-0182(02)00480-7).

Chawchai, S, A Chabangborn, M Kylander, L Löwemark, C-M Mörth, M Blauuw, W Klubseang, P Reimer, S Fritz, and B Wohlfarth. 2013. "Lake Kumphawapi – an Archive of Holocene Palaeoenvironmental and Palaeoclimatic Changes in Northeast Thailand." *Quaternary Science Reviews* **68**: 59–75. <https://doi.org/10.1016/J.QUASCIREV.2013.01.030>.

Chorowicz, Jean. 2005. "The East African Rift System." *Journal of African Earth Sciences* **43**: 379–410. <https://doi.org/10.1016/j.jafrearsci.2005.07.019>.

- Claussen, M., C. Kubatzki, V. Brovkin, A. Ganopolski, P. Hoelzmann, and H-J. Pachur. 1999: "Simulation of an abrupt change in Saharan vegetation in the mid-Holocene". *Geophys. Res. Lett.* **26** (14): 2037–2040. <https://doi.org/10.1029/1999GL900494>.
- Clement, A. C., A. Hall, and A. J. Broccoli. 2004. "The Importance of Precessional Signals in the Tropical Climate." *Climate Dynamics* **22** (4): 327–41. <https://doi.org/10.1007/s00382-003-0375-8>.
- Climate-Data.org. 2017. <https://en.climate-data.org/country/249/>.
- Cobb, Kim M., Niko Westphal, Hussein R. Sayani, Jordan T. Watson, Emanuele Di Lorenzo, H. Cheng, R. L. Edwards, and Christopher D. Charles. 2013. "Highly Variable El Niño–Southern Oscillation Throughout the Holocene." *Science* **339** (6115): 67-70,
- Cocquyt, Christine, and Ryken, Els. 2017. "Two new needle-shaped *Nitzschia* taxa from a deep East African crater lake." *Diatom Research* **32** (4): 465-475. <https://doi.org/10.1080/0269249X.2017.1401009>.
- Cocquyt, Christine, Myriam de Haan, Regine Jahn, and Friedel Hinz. 2012. "Nitzschia Epiphytica, N. Epiphyticoides and N. Pseudepiphytica (Bacillariophyta), Three Small Diatoms from East and Central Africa." *Phycologia* **51** (2): 126–34. <https://doi.org/10.2216/10-61.1>.
- COHMAP Members. "Climatic changes of the last 18,000 years: Observations and model simulations." *Science* **241** (4869): 1043-1052. DOI: 10.1126/science.241.4869.1043.
- Compton, J. 2011. *Diatoms: Ecology and Life Cycle*. New York: Nova Science Publishers, Inc.
- Conroy, Jessica L., Jonathan T. Overpeck, Julia E. Cole, Timothy M. Shanahan, and Miriam Steinitz-Kannan. 2008. "Holocene Changes in Eastern Tropical Pacific Climate Inferred from a Galápagos Lake Sediment Record." *Quaternary Science Reviews* **27** (11): 1166–80. <https://doi.org/10.1016/j.quascirev.2008.02.015>.
- Corella, Juan Pablo, Achim Brauer, Clara Mangili, Valentí Rull, Teresa Vegas-Vilarrúbia, Mario Morellón, and Blas L. Valero-Garcés. 2012. "The 1.5-Ka Varved Record of Lake Montcortès (Southern Pyrenees, NE Spain)." *Quaternary Research* **78** (2): 323–32. <https://doi.org/10.1016/J.YQRES.2012.06.002>.
- Correa-Metrio, Alexander, Dunia H. Urrego, Kenneth R. Cabrera and Mark B. Bush. 2012. "paleoMAS: Paleoecological Analysis". R package version 2.0-1. <https://CRAN.R-project.org/package=paleoMAS>.

- Costa, Cassandra, James Russell, Bronwen Konecky, and Henry Lamb. 2014. "Isotopic Reconstruction of the African Humid Period and Congo Air Boundary Migration at Lake Tana, Ethiopia." *Quaternary Science Reviews* **83**: 58–67. <https://doi.org/10.1016/j.quascirev.2013.10.031>.
- Cremer, Holger, Martin Melles, and Bernd Wagner. 2001. "Holocene Climate Changes Reflected in a Diatom Succession from Basaltsø, East Greenland." *Canadian Journal of Botany* **79** (6): 649–56. <https://doi.org/10.1139/b01-039>.
- Croudace, Ian W., Anders Rindby, and R. Guy Rothwell. 2006. "ITRAX: Description and Evaluation of a New Multi-Function X-Ray Core Scanner." *Geological Society, London, Special Publications* **267** (1): 51–63. <https://doi.org/10.1144/GSL.SP.2006.267.01.04>.
- Cumming, Brian F., Kathleen R. Laird, Irene Gregory-Eaves, Kyle G. Simpson, Michael A. Sokal, Rick N. Nordin, and Ian R. Walker. 2015. "Tracking Past Changes in Lake-Water Phosphorus with a 251-Lake Calibration Dataset in British Columbia: Tool Development and Application in a Multiproxy Assessment of Eutrophication and Recovery in Osoyoos Lake, a Transboundary Lake in Western North America." *Frontiers in Ecology and Evolution* **3** (August): 84. <https://doi.org/10.3389/fevo.2015.00084>.
- Darbyshire, I, Henry, Lamb, and Mohammed, Umer. 2003. "Forest clearance and regrowth in northern Ethiopia during the last 3000 years". *The Holocene* **13** (4): 537-546. <https://doi.org/10.1191/0959683603hl644rp>.
- DARES. 2004. "Enumeration of Diatom Slides. DARES (Diatom Assessment of River Ecological Status)." http://craticula.ncl.ac.uk/Dares/methods/DARES_Protocol_Diatom_Counting.pdf.
- Davies, S.J., S.E. Metcalfe, M.E. Caballero, and S. Juggins. 2002. "Developing Diatom-Based Transfer Functions for Central Mexican Lakes." *Hydrobiologia* **467** (1/3): 199–213. <https://doi.org/10.1023/A:1014971016298>.
- Davies, Sarah J., Henry F. Lamb, and Stephen J. Roberts. 2015. "Micro-XRF Core Scanning in Palaeolimnology: Recent Developments." In *Micro-XRF Studies of Sediment Cores*, edited by R. Croudace, I. & Rothwell, 189–226. Dordrecht: Springer . https://doi.org/10.1007/978-94-017-9849-5_7.
- Dearing, J. A., R. T. Jones, J. Shen, X. Yang, J. F. Boyle, G. C. Foster, D. S. Crook, and M. J. D. Elvin. 2008. "Using Multiple Archives to Understand Past and Present Climate–Human–Environment Interactions: The Lake Erhai Catchment, Yunnan Province, China." *Journal of Paleolimnology* **40** (1): 3–31. <https://doi.org/10.1007/s10933-007-9182-2>.

- Dearing, John A. 2013. "Why Future Earth Needs Lake Sediment Studies." *Journal of Paleolimnology* **49** (3): 537–45. <https://doi.org/10.1007/s10933-013-9690-1>.
- De'eath, G. 1999. "Principal Curves: a new technique for indirect and direct gradient analysis". *Ecology* **80** (7): 2237-2253. [https://doi.org/10.1890/0012-9658\(1999\)080\[2237:PCANTF\]2.0.CO;2](https://doi.org/10.1890/0012-9658(1999)080[2237:PCANTF]2.0.CO;2).
- deMenocal, P., and D. Rind. 1993. "Sensitivity of Asian and African climate to variations in seasonal insolation, glacial ice cover, sea-surface temperature, and Asian orography". *J. Geophys. Res.* **98** (D4): 7265-7287. <https://doi.org/10.1029/92JD02924>.
- deMenocal, Peter, and Jessica E Tierney. 2012. "Green Sahara: African Humid Periods Paced by Earth's Orbital Changes." *Nature Education Knowledge* **3** (10): 1–6. <http://www.nature.com/scitable/knowledge/library/green-sahara-african-humid-periods-paced-by-82884405>.
- deMenocal, Peter, Joseph Ortiz, Tom Guilderson, Jess Adkins, Michael Sarnthein, Linda Baker, and Martha Yarusinsky. 2000. "Abrupt Onset and Termination of the African Humid Period:: Rapid Climate Responses to Gradual Insolation Forcing." *Quaternary Science Reviews* **19** (1): 347–61. [https://doi.org/10.1016/S0277-3791\(99\)00081-5](https://doi.org/10.1016/S0277-3791(99)00081-5).
- di Lernia, and M. Gallinaro. 2010. "The date and context of Neolithic rock art in the Sahara: engravings and ceremonial monuments from Messak Settafet (south-west Libya)". *Antiquity* **84** (326): 954-975. <https://doi.org/10.1017/S0003598X00067016>.
- Ding, Qinghua, John M. Wallace, David S. Battisti, Eric J. Steig, Ailie J. E. Gallant, Hyung-Jin Kim, and Lei Geng. 2014. "Tropical Forcing of the Recent Rapid Arctic Warming in Northeastern Canada and Greenland." *Nature* **509** (7499): 209–12. <https://doi.org/10.1038/nature13260>.
- Diro, G. T., D. I. F. Grimes, and E. Black. 2011. "Teleconnections between Ethiopian Summer Rainfall and Sea Surface Temperature: Part I—Observation and Modelling." *Climate Dynamics* **37** (1–2): 103–19. <https://doi.org/10.1007/s00382-010-0837-8>.
- Donders, Timme H., Friederike Wagner-Cremer, and Henk Visscher. 2008. "Integration of Proxy Data and Model Scenarios for the Mid-Holocene Onset of Modern ENSO Variability." *Quaternary Science Reviews* **27** (5): 571–79. <https://doi.org/10.1016/j.quascirev.2007.11.010>.
- Donders, Timme H, Friederike Wagner, David L Dilcher, and Henk Visscher. 2005. "Mid- to Late-Holocene El Nino-Southern Oscillation Dynamics Reflected in the Subtropical

Terrestrial Realm." *Proceedings of the National Academy of Sciences of the United States of America* **102** (31): 10904–8. <https://doi.org/10.1073/pnas.0505015102>.

Dosio, Alessandro, and Hans-Jürgen Panitz. 2016. "Climate Change Projections for CORDEX-Africa with COSMO-CLM Regional Climate Model and Differences with the Driving Global Climate Models." *Climate Dynamics* **46** (5–6): 1599–1625. <https://doi.org/10.1007/s00382-015-2664-4>.

Dunne, Julie, Richard P. Evershed, Mélanie Salque, Lucy Cramp, Silvia Bruni, Kathleen Ryan, Stefano Biagetti, and Savino di Lernia. 2012. "First Dairying in Green Saharan Africa in the Fifth Millennium Bc." *Nature* **486** (7403): 390–94. <https://doi.org/10.1038/nature11186>.

Dykoski, C, R, Edwards, H, Cheng, D, Yuan, Y, Cai, M, Zhang, Y, Lin, J, Qing, Z, An, and J, Revenaugh. 2005. "A high-resolution, absolute-dated Holocene and deglacial Asian monsoon record from Dongge Cave, China." *Earth and Planetary Science Letters* **233** (1-2): 71-86. <https://doi.org/10.1016/j.epsl.2005.01.036>.

EDDI. 2017a. "African Dataset. List of Samples for: Cyclotella Ocellata (CY009A)." 2017. <http://craticula.ncl.ac.uk/Eddi/jsp/taxonlist.jsp?DatasetId=Africa&TaxonId=CY009A&TaxId=Salinity>.

EDDI. 2017b. "African Dataset. List of Samples for: Thalassiosira Faurii (AF_5701)." 2017. http://craticula.ncl.ac.uk/Eddi/jsp/taxonlist.jsp?DatasetId=Africa&TaxonId=AF_5701&TaxId=Salinity.

Edlund, M.B., E.A. Morales and S.A. Spaulding. 2006. "The type and taxonomy of *Fragilaria elliptica* Schumann, a widely misconstrued taxon". In: "Proceedings of the 18th International Diatom Symposium". Edited by Witkowski, A: 53-59. Biopress Limited, Bristol, England.

Edlund, Mark, James Almendinger, Xing Fang, Joy Hobbs, David VanderMeulen, Rebecca Key, Daniel Engstrom, et al. 2017. "Effects of Climate Change on Lake Thermal Structure and Biotic Response in Northern Wilderness Lakes." *Water* **9** (9): 678. <https://doi.org/10.3390/w9090678>.

Eggermont, Hilde, Oliver Heiri, James Russell, Mathias Vuille, Leen Audenaert, and Dirk Verschuren. 2010. "Paleotemperature Reconstruction in Tropical Africa Using Fossil Chironomidae (Insecta: Diptera)." *Journal of Paleolimnology* **43** (3): 413–35. <https://doi.org/10.1007/s10933-009-9339-2>.

Eggermont, Hilde, Oliver Heiri, and Dirk Verschuren. 2006. "Fossil Chironomidae (Insecta: Diptera) as Quantitative Indicators of Past Salinity in African Lakes." *Quaternary Science*

Reviews 25 (15): 1966–94. <https://doi.org/10.1016/j.quascirev.2005.04.011>.

Enache, M., and B. Cumming. 2006. "Tracking Recorded Fires Using Charcoal Morphology from the Sedimentary Sequence of Prosser Lake, British Columbia (Canada)." *Quaternary Research* **65** (2): 282–92. <https://doi.org/10.1016/J.YQRES.2005.09.003>.

Finkelstein, S. A., and K. Gajewski. 2008. "Responses of Fragilarioid-Dominated Diatom Assemblages in a Small Arctic Lake to Holocene Climatic Changes, Russell Island, Nunavut, Canada." *Journal of Paleolimnology* **40** (4): 1079–95. <https://doi.org/10.1007/s10933-008-9215-5>.

Flower, R. J. 2005. "A taxonomic and ecological study of diatoms from freshwater habitats in the Falkland Islands, South Atlantic." *Diatom Research* **20** (1): 23–96. <https://doi.org/10.1080/0269249X.2005.9705620>.

Foerster, V, A Junginger, A Asrat, H F Lamb, M Weber, J Rethemeyer, U Frank, M C Brown, M H Trauth, and F Schaebitz. 2014. "46 000 Years of Alternating Wet and Dry Phases on Decadal to Orbital Timescales in the Cradle of Modern Humans: The Chew Bahir Project, Southern Ethiopia." *Clim. Past Discuss* **10**: 977–1023. <https://doi.org/10.5194/cpd-10-977-2014>.

Foerster, Verena, Annett Junginger, Oliver Langkamp, Tsige Gebru, Asfawossen Asrat, Mohammed Umer, Henry F Lamb, et al. 2012. "Climatic Change Recorded in the Sediments of the Chew Bahir Basin, Southern Ethiopia, during the Last 45,000 Years." *Quaternary International* **274**: 25–37. <https://doi.org/10.1016/j.quaint.2012.06.028>.

Folk, Robert L. 1974. "The Natural History Of Crystalline Calcium Carbonate: Effect of Magnesium Content And Salinity." *Journal of Sedimentary Research* **44** (1): 40–53.

Fontijn, Karen, Keri McNamara, Amdemichael Zafu Tadesse, David M. Pyle, Firawalin Dessalegn, William Hutchison, Tamsin A. Mather, and Gezahegn Yirgu. 2018. "Contrasting Styles of Post-Caldera Volcanism along the Main Ethiopian Rift: Implications for Contemporary Volcanic Hazards." *Journal of Volcanology and Geothermal Research* **356** (May): 90–113. <https://doi.org/10.1016/J.JVOLGEORES.2018.02.001>.

Fritz, S. C. B. F. Cumming, F. Gasse, and K. R. Laird. 2010. "Diatoms as indicators of hydrologic and climatic change in saline lakes." In: "The diatoms: applications for the environmental and earth sciences.". Edited by Smol, J.P., and E. F. Stoermer.: 186–208. Cambridge: Cambridge University Press.

Fritz, S. C., S. Juggins, and R. W. Battarbee. 1993. "Diatom Assemblages and Ionic

Characterization of Lakes of the Northern Great Plains, North America: A Tool for Reconstructing Past Salinity and Climate Fluctuations.” *Canadian Journal of Fisheries and Aquatic Sciences* **50** (9): 1844–56. <https://doi.org/10.1139/f93-207>.

Garcin, Yannick, Annett Junginger, Daniel Melnick, Daniel O. Olago, Manfred R. Strecker, and Martin H. Trauth. 2009. “Late Pleistocene–Holocene Rise and Collapse of Lake Suguta, Northern Kenya Rift.” *Quaternary Science Reviews* **28** (9): 911–25. <https://doi.org/10.1016/j.quascirev.2008.12.006>.

Garcin, Yannick, Daniel Melnick, Manfred R. Strecker, Daniel Olago, and Jean-Jacques Tiercelin. 2012. “East African Mid-Holocene Wet–Dry Transition Recorded in Palaeo-Shorelines of Lake Turkana, Northern Kenya Rift.” *Earth and Planetary Science Letters*. **331**. <https://doi.org/10.1016/j.epsl.2012.03.016>.

Garcin, Yannick, Annie Vincens, David Williamson, Guillaume Buchet, and Joël Guiot. 2007a. “Abrupt Resumption of the African Monsoon at the Younger Dryas—Holocene Climatic Transition.” *Quaternary Science Reviews* **26** (5): 690–704. <https://doi.org/10.1016/j.quascirev.2006.10.014>.

Garcin, Yannick, David Williamson, Laurent Bergonzini, Olivier Radakovitch, Annie Vincens, Guillaume Buchet, Joël Guiot, Simon Brewer, Pierre-Etienne Mathé, and Amos Majule. 2007b. “Solar and Anthropogenic Imprints on Lake Masoko (Southern Tanzania) during the Last 500 Years.” *Journal of Paleolimnology* **37** (4): 475–90. <https://doi.org/10.1007/s10933-006-9033-6>.

Gasparon, M., F. Innocenti, P. Manetti, A. Peccerillo, and A. Tsegaye. 1993. “Genesis of the Pliocene to Recent Bimodal Mafic-Felsic Volcanism in the Debre Zeyt Area, Central Ethiopia: Volcanological and Geochemical Constraints.” *Journal of African Earth Sciences (and the Middle East)* **17** (2): 145–65. [https://doi.org/10.1016/0899-5362\(93\)90032-L](https://doi.org/10.1016/0899-5362(93)90032-L).

Gasse, F., Barker, P. & Johnson, T. 2002. “A 24,000 Yr Diatom Record from the Northern Basin of Lake Malawi.” In *The East African Great Lakes: Limnology, Palaeolimnology and Biodiversity*, edited by D. Odada, E. & Olago, 393–414. Dordrecht: Kluwer Academic Publishers.

Gasse, E, and F Street. 1978. “Late Quaternary Lake-Level Fluctuations and Environments of the Northern Rift Valley and Afar Region (Ethiopia and Djibouti).” *Palaeogeography, Palaeoclimatology, Palaeoecology* **24** (4): 279–325. [https://doi.org/10.1016/0031-0182\(78\)90011-1](https://doi.org/10.1016/0031-0182(78)90011-1).

Gasse, F. 1980. "Late Quaternary changes in lake levels and diatom assemblages on the

- Southeastern margin of the Sahara". *Paleoecology of Africa* **12**: 333–350. https://doi.org/10.1007/978-94-009-7290-2_14.
- Gasse, F. 1986. "East African diatoms: Taxonomy, ecological distribution". Berlin, Stuttgart: J. Cramer. pp. 201. 44 plates.
- Gasse, F. 2000. "Hydrological Changes in the African Tropics since the Last Glacial Maximum." *Quaternary Science Reviews* **19**: 189–211.
- Gasse, F, P, Barker, P, Gell, S, Fritz, and F, Chalie. 1997. "Diatom-inferred salinity in palaeolakes: An indirect tracer of climate change". *Quaternary Science Review* **16** (6): 547-563. [https://doi.org/10.1016/S0277-3791\(96\)00081-9](https://doi.org/10.1016/S0277-3791(96)00081-9).
- Gasse, F, and E, van Campo. 1994. "Abrupt post-glacial climate events in West Asia and North Africa monsoon domains". *Earth and Planetary Science Letters* **126** (4): 435-456. [https://doi.org/10.1016/0012-821X\(94\)90123-6](https://doi.org/10.1016/0012-821X(94)90123-6).
- Gasse, F, and F. A. Street. 1986. "Late Quaternary lake-level fluctuations and environments of the northern Rift Valley and Afar region (Ethiopia and Djibouti)". *Palaeogeogr. Palaeoclimat. Palaeoecol.* **24**: 279-325. [https://doi.org/10.1016/0031-0182\(78\)90011-1](https://doi.org/10.1016/0031-0182(78)90011-1).
- Gasse, F, and F, Tekaia. 1983. "Transfer functions for estimating paleoecological conditions (pH) from East African diatoms". *Hydrobiologia* **103**: 85–90. <https://doi.org/10.1007/BF00028433>.
- Gasse, F, J, F, Talling, and P, Kilham. 1983. "Diatom assemblages in East Africa: classification, distribution and ecology". *Rev. Hydrobiol. Trop.* **16**: 3-24.
- Gasse, F, S Juggins, and L Ben Khelifa. 1995. "Diatom-Based Transfer Functions for Inferring Past Hydrochemical Characteristics of African Lakes." *Palaeogeography, Palaeoclimatology, Palaeoecology* **117**: 31–54.
- Gesierich, Doris, and Eugen Rott. 2012. "Is Diatom Richness Responding to Catchment Glaciation? A Case Study from Canadian Headwater Streams." *Journal of Limnology* **71** (1): 7. <https://doi.org/10.4081/jlimnol.2012.e7>.
- Ghinassi, M, D'Oriano, F, Benvenuti, M, Awramik, S, Bartolini, C, Fedi, M, Ferrari, G, Papini, M, Sagri, M, and Talbot, M. 2012. "Shoreline fluctuations of Lake Hayk (northern Ethiopia) during the last 3500 years: Geomorphological, sedimentary, and isotope records". *Palaeogeography, Palaeoclimatology, Palaeoecology* **365–366**: 209-226. <https://doi.org/10.1016/j.palaeo.2012.09.029>.

- Giannini, Alessandra, Michela Biasutti, Isaac M. Held, and Adam H. Sobel. 2008. "A Global Perspective on African Climate." *Climatic Change* **90** (4): 359–83. <https://doi.org/10.1007/s10584-008-9396-y>.
- Gillespie, Richard, F. Alayne Street-Perrott, and Roy Switsur. 1983. "Post-Glacial Arid Episodes in Ethiopia Have Implications for Climate Prediction." *Nature* **306** (5944): 680–83. <https://doi.org/10.1038/306680a0>.
- Giorgino, T. 2009. "Computing and Visualizing Dynamic Time Warping Alignments in R: The Dtw Package." *Journal of Statistical Software* **31**: i07.
- Glibert, Patricia M., John Harrison, Cynthia Heil, and Sybil Seitzinger. 2006. "Escalating Worldwide Use of Urea – A Global Change Contributing to Coastal Eutrophication." *Biogeochemistry* **77** (3): 441–63. <https://doi.org/10.1007/s10533-005-3070-5>.
- Gil-Romera, Graciela, Carole Adolf, Blas M. Benito, Lucas Bittner, Maria U. Johansson, David A. Grady, Henry F. Lamb, Bruk Lemma, Mekbib Fekadu, Bruno Glaser, Betelhem Mekonnen, Miguel Sevilla-Callejo, Michael Zech, Wolfgang Zech, and Georg Miehe. 2019. "Long-term fire resilience of the Ericaceous Belt, Bale Mountains, Ethiopia". *Biology Letters* **15** (7). <https://doi.org/10.1098/rsbl.2019.0357>.
- Grady, D, D, Mann, and R, Trobajo. 2020. "Nitzschia fenestralis: A new diatom species abundant in the Holocene sediments of an eastern African crater lake". *Fottea* **20** (1): 36-48. DOI: 10.5507/fot.2019.011.
- Griffiths, Katherine, Neal Michelutti, Madeline Sugar, Marianne S V Douglas, and John P Smol. 2017. "Ice-Cover Is the Principal Driver of Ecological Change in High Arctic Lakes and Ponds." *PloS One* **12** (3): e0172989. <https://doi.org/10.1371/journal.pone.0172989>.
- Grimm, E. 1987. "CONISS: a FORTRAN 77 program for stratigraphically constrained cluster analysis by the method of incremental sum of squares". *Computers & Geosciences* **13** (1): 13-35. [https://doi.org/10.1016/0098-3004\(87\)90022-7](https://doi.org/10.1016/0098-3004(87)90022-7).
- Grimm, E. 2011. "High-Resolution Age Model Based on AMS Radiocarbon Ages for Kettle Lake, North Dakota, USA." *Radiocarbon* **53** (1): 39–53. <https://journals.uair.arizona.edu/index.php/radiocarbon/article/view/3441/3723>.
- Grivna, B. 2012. "Corelyzer User's Manual". Version 5 - 06/21/2012. <http://www.corewall.org/documents/manual/index.html>.
- Grove, A. T., and A. S. Goudie. 1971. "Late Quaternary Lake Levels in the Rift Valley of Southern Ethiopia and Elsewhere in Tropical Africa." *Nature* **234** (5329): 403.

<https://doi.org/10.1038/234403a0>.

Gruenert, Uta, and Uta Raeder. 2014. "Growth Responses of the Calcite-Loricated Freshwater Phytoflagellate *Phacotus Lenticularis* (Chlorophyta) to the CaCO₃ Saturation State and Meteorological Changes." *Journal of Plankton Research* **36** (3): 630–40. <https://doi.org/10.1093/plankt/fbu006>.

Grunow, A. (1862). Die österreichischen Diatomaceen nebst Anschluss einiger neuen Arten von andern Lokalitäten und einer kritischen Uebersicht der bisher bekannten Gattungen und Arten. Erste Folge. Epithemieae, Meridioneae, Diatomeae, Entopyleae, Surirelleae, Amphipleureae. Zweite Folge. Familie Nitzschieae. Verhandlungen der Kaiserlich-Königlichen Zoologisch-Botanischen Gesellschaft in Wien. 12: 315-472, 545-588, 7 pls.

GSE. 1996. "Geological Map of Ethiopia". 1:2,000,000 scale, 2nd edn. <http://www.gse.gov.et>

Guyard, Hervé, Emmanuel Chapron, Guillaume St-Onge, Flavio S. Anselmetti, Fabien Arnaud, Olivier Magand, Pierre Francus, and Marie-Antoinette Mélières. 2007. "High-Altitude Varve Records of Abrupt Environmental Changes and Mining Activity over the Last 4000 Years in the Western French Alps (Lake Bramant, Grandes Rousses Massif)." *Quaternary Science Reviews* **26** (19–21): 2644–60. <https://doi.org/10.1016/J.QUASCIREV.2007.07.007>.

Harper, M, R, Howorth, and M, Mcleod. 1986. "Late Holocene diatoms in Lake Poukawa: Effects of airfall tephra and changes in depth". *New Zealand Journal of Marine and Freshwater Research* **20** (1): 107-118. <https://doi.org/10.1080/00288330.1986.9516135>.

Hastie, T. and W. Stuetzle. 1989. "Principal Curves". *Journal of the American Statistical Association* **84** (406): 502-516.

Haug, G, K, Hughen, D, Sigman, L, Peterson, and U, Röhl. 2001. "Southward migration of the intertropical convergence zone through the Holocene.". *Science* **293** (5533): 1304-1308. DOI: 10.1126/science.1059725.

Heinrich, Hartmut. 1988. "Origin and Consequences of Cyclic Ice Rafting in the Northeast Atlantic Ocean during the Past 130,000 Years." *Quaternary Research* **29** (2): 142–52. [https://doi.org/10.1016/0033-5894\(88\)90057-9](https://doi.org/10.1016/0033-5894(88)90057-9).

Hély, C, P, Braconnot, J, Watrin, and W, Zheng. 2009. "Climate and vegetation: Simulating the African humid period". *Comptes Rendus Geoscience* **341** (8–9): 671-688. <https://doi.org/10.1016/j.crte.2009.07.002>.

Hemming, Sidney R. 2004. "Heinrich Events: Massive Late Pleistocene Detritus Layers of

- the North Atlantic and Their Global Climate Imprint." *Reviews of Geophysics* **42** (1): RG1005. <https://doi.org/10.1029/2003RG000128>.
- Hildebrand, E, S, Brandt, and J, Lesur-Gebremariam. 2010. "The Holocene Archaeology of Southwest Ethiopia: New Insights from the Kafa Archaeological Project". *The African Archaeological Review* **27** (4): 255-289. DOI: 10.1007/s10437-010-9079-8.
- Hill, M. O. and H. G. Gauch Jr. 1980. "Detrended correspondence analysis: An improved ordination technique". *Vegetatio* **42**: 47-58. <https://doi.org/10.1007/BF00048870>.
- Hustedt, F. 1949. Süßwasser-Diatomeen aus dem Albert-Nationalpark in Belgisch-Kongo. Exploration du Parc National Albert, Mission H. Damas (1935-1936), Institut des Parcs Nationaux du Congo Belge, Bruxelles, 8: 199 pp., 16 pls.
- Hustedt, F. 1959. Die Diatomeenflora des Neusiedler Sees im österreichischen Burgenland. *Österreichische Botanische Zeitschrift*, **106** (5): 390-430
- Imbrie, J., and N. Kipp. 1971. "A New Micropaleontological Method for Quantitative Paleoclimatology: Application to a Late Pleistocene Caribbean Core, in The Late Cenozoic Glacial Ages." In *The Late Cenozoic Glacial Ages*, edited by K. Turekian, 71–181. New Haven: Yale University Press.
- IPCC. 2013. "Climate Change 2013: The Physical Science Basis. Contribution of Working Group I to the Fifth Assessment Report of the Intergovernmental Panel on Climate Change" Cambridge: Cambridge University Press. 1535 pp, doi:10.1017/CBO9781107415324.
- Ivory, Sarah J., Anne-Marie Lézine, Annie Vincens, and Andrew S. Cohen. 2012. "Effect of Aridity and Rainfall Seasonality on Vegetation in the Southern Tropics of East Africa during the Pleistocene/Holocene Transition." *Quaternary Research* **77** (1): 77–86. <https://doi.org/10.1016/j.yqres.2011.11.005>.
- Johnson, T, C, S, L, Barry, Y, Chan, and P, Wilkinson. 2001. "A decadal record of climate variability spanning the last 700 years in the southern tropics of East Africa". *Geology* **29**: 83-86. [https://doi.org/10.1130/0091-7613\(2001\)029<0083:DROCVS>2.0.CO;2](https://doi.org/10.1130/0091-7613(2001)029<0083:DROCVS>2.0.CO;2).
- Jones, Matthew D., Sarah E. Metcalfe, Sarah J. Davies, and Anders Noren. 2015. "Late Holocene Climate Reorganisation and the North American Monsoon." *Quaternary Science Reviews* **124** (September): 290–95. <https://doi.org/10.1016/J.QUASCIREV.2015.07.004>.
- Jouve, Guillaume, Scott Lamoureux, Laurence Provencher-Nolet, Annette Hahn, Torsten Haberzettl, David Fortin, Laurence Nuttin, and . The PASADO Science Team. 2013. "Microsedimentological Characterization Using Image Analysis and μ -XRF as Indicators of

Sedimentary Processes and Climate Changes during Lateglacial at Laguna Potrok Aike, Santa Cruz, Argentina." *Quaternary Science Reviews* **71**: 191–204. <https://doi.org/10.1016/J.QUASCIREV.2012.06.003>.

Juggins, S. 2013. "Quantitative reconstructions in palaeolimnology: new paradigm or sick science?". *Quaternary Science Reviews* **64**: 20-32. <https://doi.org/10.1016/j.quascirev.2012.12.014>.

Juggins, S. 2017. "rioja: Analysis of Quaternary Science Data". R package version. (0.9-15.1). (<http://cran.r-project.org/package=rioja>).

Juggins, S., R. W. Battarbee, S. C. Fritz, and F. Gasse. 1994. "The CASPIA Project: Diatoms, Salt Lakes, and Environmental Change." *Journal of Paleolimnology* **12** (3): 191–96. <https://doi.org/10.1007/BF00678020>.

Juggins, S, and J Birks. 2012. "Quantitative Environmental Reconstructions from Biological Data." In *Tracking Environmental Change Using Lake Sediments, Volume 5: Data Handling and Numerical Techniques*, edited by J Birks, A Lotter, S Juggins, and J Smol, 431–95. Dodrecht: Springer.

Julius, M, and E, Theriot. 2010. "The Diatoms: a primer". In: "The diatoms: applications for the environmental and earth sciences.". Edited by Smol, J.P., and E. F. Stoermer.: 8-22. Cambridge: Cambridge University Press.

Kalnay, E., M. Kanamitsu, R. Kistler, W. Collins, D. Deaven, L. Gandin, M. Iredell, et al. 1996. "The NCEP/NCAR 40-Year Reanalysis Project." *Bulletin of the American Meteorological Society* **77** (3): 437–71. [https://doi.org/10.1175/1520-0477\(1996\)077<0437:TNYRP>2.0.CO;2](https://doi.org/10.1175/1520-0477(1996)077<0437:TNYRP>2.0.CO;2).

Karst-Riddoch, Tammy L., Hilmar J. Malmquist, and John P. Smol. 2009. "Relationships between Freshwater Sedimentary Diatoms and Environmental Variables in Subarctic Icelandic Lakes." *Fundamental and Applied Limnology / Archiv Für Hydrobiologie* **175** (1): 1–28. <https://doi.org/10.1127/1863-9135/2009/0175-0001>.

Kebede, Seifu, Henry Lamb, Richard Telford, Melanie Leng, and Mohammed Umer. 2002. "Lake — Groundwater Relationships, Oxygen Isotope Balance and Climate Sensitivity of the Bishoftu Crater Lakes, Ethiopia." In , 261–75. Springer Netherlands. https://doi.org/10.1007/0-306-48201-0_9.

Kelts, K., and K. J. Hsü. 1978. "Freshwater Carbonate Sedimentation." In *Lakes: Chemistry, Geology, Physics*, edited by A Lerman, 295–323. New York: Springer.

https://doi.org/10.1007/978-1-4757-1152-3_9.

Kemp, A. A., Dean, R., Pearce, and J. Pike. 2001. "Recognition and analysis of bedding and sediment fabric features". In: "Tracking Environmental Change Using Lake Sediments: Physical and Geochemical Methods". Edited by Last, W., and J. Smol: 7-22. Dordrecht: Kluwer Academic Publishers.

Kiage, L. M., and K.-b. Liu. 2006. "Late Quaternary Paleoenvironmental Changes in East Africa: A Review of Multiproxy Evidence from Palynology, Lake Sediments, and Associated Records." *Progress in Physical Geography* **30** (5): 633–58. <https://doi.org/10.1177/0309133306071146>.

Kilham, Peter. 1971. "A Hypothesis Concerning Silica and the Freshwater Planktonic Diatoms." *Limnology and Oceanography* **16** (1): 10–18. <https://doi.org/10.4319/lo.1971.16.1.0010>.

Kilham, Peter, Susan S. Kilham, and Robert E. Hecky. 1986. "Hypothesized Resource Relationships among African Planktonic Diatoms." *Limnology and Oceanography* **31** (6): 1169–81. <https://doi.org/10.4319/lo.1986.31.6.1169>.

Kingsbury, Melanie V., Kathleen R. Laird, and Brian F. Cumming. 2012. "Consistent Patterns in Diatom Assemblages and Diversity Measures across Water-Depth Gradients from Eight Boreal Lakes from North-Western Ontario (Canada)." *Freshwater Biology* **57** (6): 1151–65. <https://doi.org/10.1111/j.1365-2427.2012.02781.x>.

Klein, François, Hugues Goosse, Nicholas E. Graham, and Dirk Verschuren. 2016. "Comparison of Simulated and Reconstructed Variations in East African Hydroclimate over the Last Millennium." *Clim. Past* **12**: 1499–1518. <https://doi.org/10.5194/cp-12-1499-2016>.

Konecky, Bronwen, James Russell, Yongsong Huang, Mathias Vuille, Lily Cohen, and F. Alayne Street-Perrott. 2014. "Impact of Monsoons, Temperature, and CO₂ on the Rainfall and Ecosystems of Mt. Kenya during the Common Era." *Palaeogeography, Palaeoclimatology, Palaeoecology* **396**: 17–25. <https://doi.org/10.1016/j.palaeo.2013.12.037>.

Korecha, Diriba, and Anthony G. Barnston. 2007. "Predictability of June–September Rainfall in Ethiopia." *Monthly Weather Review* **135** (2): 628–50. <https://doi.org/10.1175/MWR3304.1>.

Krammer, K., and H. Lange-Bertalot. 1986. "Bacillariophyceae. 1. Teil: Naviculaceae" In: "Süßwasserflora von Mitteleuropa, Band 2/1". Edited by Ettl, H., J. Gerloff, H. Heynig, and D. Mollenhauer. Jena: Gustav Fisher Verlag.

- Krammer, K, and H, Lange-Bertalot. 1988. "Bacillariophyceae. 2. Teil: Bacillariaceae, Epithemiaceae, Surirellaceae". In: "Süßwasserflora von Mitteleuropa, Band 2/2". Edited by Ettl, H, J, Gerloff, H, Heynig, and D, Mollenhauer. Jena: Gustav Fisher Verlag.
- Krammer, K, and H, Lange-Bertalot. 1991a. "Bacillariophyceae. 3. Teil: Centrales, Fragilariaceae, Eunotiaceae" In: "Süßwasserflora von Mitteleuropa, 2 (3)". Edited by Ettl, H, J, Gerloff, H, Heynig, and D, Mollenhauer. Stuttgart: Gustav Fisher Verlag.
- Krammer, K, and H, Lange-Bertalot. 1991b. " Bacillariophyceae. 4, Achnantheaceae ; kritische ergänzungen zu navicula (lineolatae) und Gomphonema ; gesamtliteraturverzeichnis teil 1-4". In: "Süßwasserflora von Mitteleuropa, Bd 2/4". Edited by Ettl, H, J, Gerloff, H, Heynig, and D, Mollenhauer. Stuttgart: Gustav Fisher Verlag.
- Kröpelin, S, D Verschuren, A-M Lézine, H Eggermont, C Cocquyt, P Francus, J-P Cazet, et al. 2008. "Climate-Driven Ecosystem Succession in the Sahara: The Past 6000 Years." *Science* **320** (5877): 765–68. <https://doi.org/10.1126/science.1154913>.
- Kuper, Rudolph, and Stefan Kröpelin. 2006. "Climate-Controlled Holocene Occupation in the Sahara: Motor of Africa's Evolution." *Science* **313** (5788): 803-807
- Kylander, Malin E., Linda Ampel, Barbara Wohlfarth, and Daniel Veres. 2011. "High-Resolution X-Ray Fluorescence Core Scanning Analysis of Les Echets (France) Sedimentary Sequence: New Insights from Chemical Proxies." *Journal of Quaternary Science* **26** (1): 109–17. <https://doi.org/10.1002/jqs.1438>.
- Kutzbach, J, E, and F, A, Street-Perrott. 1985. "Milankovitch forcing of fluctuations in the level of tropical lakes from 18 to 0 kyr BP". *Nature* **317**: 130-134. <https://doi.org/10.1038/317130a0>.
- LacCore. 2015. "Epoxy impregnation of lake sediment slabs for thin sections Standard Operating Procedure". Methods report. Minneapolis: LacCore, National Lacustrine Core Facility. pp. 1-10.
- Laird, Kathleen R., Sherilyn C. Fritz, and Brian F. Cumming. 1998. "A Diatom-Based Reconstruction of Drought Intensity, Duration, and Frequency from Moon Lake, North Dakota: A Sub-Decadal Record of the Last 2300 Years." *Journal of Paleolimnology* **19** (2): 161–79. <https://doi.org/10.1023/A:1007929006001>.
- Laird, Kathleen R., Melanie V. Kingsbury, and Brian F. Cumming. 2010. "Diatom Habitats, Species Diversity and Water-Depth Inference Models across Surface-Sediment Transects in Worth Lake, Northwest Ontario, Canada." *Journal of Paleolimnology* **44** (4): 1009–24.

<https://doi.org/10.1007/s10933-010-9470-0>.

Lamb, Angela L., Melanie J. Leng, Henry F. Lamb, and Mohammed Umer Mohammed. 2000. "A 9000-Year Oxygen and Carbon Isotope Record of Hydrological Change in a Small Ethiopian Crater Lake." *The Holocene* **10** (2): 167–77. <https://doi.org/10.1191/095968300677444611>.

Lamb, Angela L., Melanie J. Leng, Mohammed Umer Mohammed, and Henry F. Lamb. 2004. "Holocene Climate and Vegetation Change in the Main Ethiopian Rift Valley, Inferred from the Composition (C/N and $\Delta^{13}\text{C}$) of Lacustrine Organic Matter." *Quaternary Science Reviews* **23** (7): 881–91. <https://doi.org/10.1016/j.quascirev.2003.06.010>.

Lamb, H., M. J. Leng, R. J. Telford, T. Ayenew, and M. Umer. 2007a. "Oxygen and Carbon Isotope Composition of Authigenic Carbonate from an Ethiopian Lake: A Climate Record of the Last 2000 Years." *The Holocene* **17** (4): 517–26. <https://doi.org/10.1177/0959683607076452>.

Lamb, H, S Kebede, M Leng, D Ricketts, R Telford, and M Umer. 2002. "Origin and Isotopic Composition of Aragonite Laminae in an Ethiopian Crater Lake." In *The East African Great Lakes: Limnology, Palaeolimnology and Biodiversity*, edited by E. Odada and D. Olago, 487–508. Dordrecht: Springer. https://doi.org/10.1007/0-306-48201-0_20.

Lamb, Henry F., C. Richard Bates, Paul V. Coombes, Michael H. Marshall, Mohammed Umer, Sarah J. Davies, and Eshete Dejen. 2007b. "Late Pleistocene Desiccation of Lake Tana, Source of the Blue Nile." *Quaternary Science Reviews* **26** (3): 287–99. <https://doi.org/10.1016/j.quascirev.2006.11.020>.

Legesse, D, F, Gasse, O, Radalovitch, C, Vallet-Coulomb, R, Bonnefille, D, Verschuren, E, Gibert, and P, Barker. 2002. "Environmental changes in a tropical lake (Lake Abiyata, Ethiopia) during recent centuries". *Palaeogeography, Palaeoclimatology, Palaeoecology* **187** (3–4): 233-258. [https://doi.org/10.1016/S0031-0182\(02\)00479-0](https://doi.org/10.1016/S0031-0182(02)00479-0).

Lemma, Brook. 2009. "Observations on the Relations of Some Physico-Chemical Features and DVM of Paradiaptomus Africanus in Lakes Bishoftu-Guda and Hora-Arsedi, Bishoftu, Ethiopia." *Limnologica* **39** (3): 230–43. <https://doi.org/10.1016/j.limno.2008.06.007>.

Leng, M. J., I. Baneschi, G. Zanchetta, C. N. Jex, B. Wagner, and H. Vogel. 2010. "Late Quaternary Palaeoenvironmental Reconstruction from Lakes Ohrid and Prespa (Macedonia/Albania Border) Using Stable Isotopes." *Biogeosciences* **7** (10): 3109–22. <https://doi.org/10.5194/bg-7-3109-2010>.

- Lernia, Savino di, and Marina Gallinaro. 2010. "The Date and Context of Neolithic Rock Art in the Sahara: Engravings and Ceremonial Monuments from Messak Settafet (South-West Libya)." *Antiquity* **84** (326): 954–75. <https://doi.org/10.1017/S0003598X00067016>.
- Levin, Naomi E., Edward J. Zipser, and Thure E. Cerling. 2009. "Isotopic Composition of Waters from Ethiopia and Kenya: Insights into Moisture Sources for Eastern Africa." *Journal of Geophysical Research* **114** (D23): D23306. <https://doi.org/10.1029/2009JD012166>.
- Lézine, Anne-Marie, Jean-Claude Duplessy, and Jean-Pierre Cazet. 2005. "West African Monsoon Variability during the Last Deglaciation and the Holocene: Evidence from Fresh Water Algae, Pollen and Isotope Data from Core KW31, Gulf of Guinea." *Palaeogeography, Palaeoclimatology, Palaeoecology* **219** (3): 225–37. <https://doi.org/10.1016/j.palaeo.2004.12.027>.
- Lézine, Anne-Marie, Christelle Hély, Christophe Grenier, Pascale Braconnot, and Gerhard Krinner. 2011. "Sahara and Sahel Vulnerability to Climate Changes, Lessons from Holocene Hydrological Data." *Quaternary Science Reviews* **30** (21): 3001–12. <https://doi.org/10.1016/j.quascirev.2011.07.006>.
- Liebmann, Brant, Martin P. Hoerling, Chris Funk, Ileana Bladé, Randall M. Dole, Dave Allured, Xiaowei Quan, et al. 2014. "Understanding Recent Eastern Horn of Africa Rainfall Variability and Change." *Journal of Climate* **27** (23): 8630–45. <https://doi.org/10.1175/JCLI-D-13-00714.1>.
- Liu, Xiting, Rebecca Rendle-Bühning, Holger Kuhlmann, and Anchun Li. 2017. "Two Phases of the Holocene East African Humid Period: Inferred from a High-Resolution Geochemical Record off Tanzania." *Earth and Planetary Science Letters*. Vol. **460**: 123-134. <https://doi.org/10.1016/j.epsl.2016.12.016>.
- Livingstone, D. A. 1967. "Postglacial Vegetation of the Ruwenzori Mountains in Equatorial Africa." *Ecological Monographs* **37** (1): 25–52. <https://doi.org/10.2307/1948481>.
- Loakes, K. 2015. "Late Quaternary Palaeolimnology and Environmental Change in the South Wollo Highlands, Ethiopia." PhD Thesis, Loughborough University.
- Loakes, K, D, Ryves, H, Lamb, F, Scabnitz, M, Dee, J, Tyler, K, Mills, S, McGowan. 2018. "Late Quaternary climate change in the north-eastern highlands of Ethiopia: A high resolution 15,600 year diatom and pigment record from Lake Hayk". *Quaternary Science Reviews* **202**: 166-181. <https://doi.org/10.1016/j.quascirev.2018.09.005>.
- Löffler, H. 1978. "Limnology and paleolimnological data on the Bale Mountain Lakes".

Internationale Vereinigung für Theoretische und Angewandte Limnologie: Verhandlungen **20** (2): 1131–1138. <https://doi.org/10.1080/03680770.1977.11896663>.

Loomis, Shannon E., James M. Russell, and Henry F. Lamb. 2015. "Northeast African Temperature Variability since the Late Pleistocene." *Palaeogeography, Palaeoclimatology, Palaeoecology* **423** (April): 80–90. <https://doi.org/10.1016/j.palaeo.2015.02.005>.

Lotter, André F., and Christian Bigler. 2000. "Do Diatoms in the Swiss Alps Reflect the Length of Ice-Cover?" *Aquatic Sciences* **62** (2): 125. <https://doi.org/10.1007/s000270050002>.

Löwemark, L, H-F Chen, T-N Yang, M Kylander, E-F Yu, Y-W Hsu, T-G Lee, S-R Song, and S Jarvis. 2011. "Normalizing XRF-Scanner Data: A Cautionary Note on the Interpretation of High-Resolution Records from Organic-Rich Lakes." *Journal of Asian Earth Sciences* **40** (6): 1250–56. <https://doi.org/10.1016/J.JSEAES.2010.06.002>.

Lu, Zhengyao, Zhengyu Liu, Jiang Zhu, and Kim M. Cobb. 2018. "A Review of Paleo El Niño-Southern Oscillation." *Atmosphere* **9** (4): 130. <https://doi.org/10.3390/atmos9040130>.

Lubbe, H van der, J Kraue-Nehring, A Junginger, Y Garcin, J Joordens, G Davies, C Beck, C Feibel, T Johnson, and H Vonhof. 2017. "Gradual or Abrupt? Changes in Water Source of Lake Turkana (Kenya) during the African Humid Period Inferred from Sr Isotope Ratios." *Quaternary Science Reviews* **174**: 1–12. <https://doi.org/10.1016/J.QUASCIREV.2017.08.010>.

Ma, Long, Jinglu Wu, Jilili Abuduwaili, and Wen Liu. 2016. "Geochemical Responses to Anthropogenic and Natural Influences in Ebinur Lake Sediments of Arid Northwest China." *PloS One* **11** (5): e0155819. <https://doi.org/10.1371/journal.pone.0155819>.

Malik, Heera I., and Jasmine E. Saros. 2016. "Effects of Temperature, Light and Nutrients on Five *Cyclotella Sensu Lato* Taxa Assessed with *in Situ* Experiments in Arctic Lakes." *Journal of Plankton Research* **38** (3): 431–42. <https://doi.org/10.1093/plankt/fbw002>.

Mann, D, and S Droop. 1996. "Biodiversity, Biogeography and Conservation of Diatoms." *Hydrobiologia* **336**: 19–32.

Mann, Michael E., Zhihua Zhang, Scott Rutherford, Raymond S. Bradley, Malcolm K. Hughes, Drew Shindell, Caspar Ammann, Greg Faluvegi, and Fenbiao Ni. 2009. "Global Signatures and Dynamical Origins of the Little Ice Age and Medieval Climate Anomaly." *Science* **326** (5957): 1256–60.

Manning, Katie, and Adrian Timpson. 2014. "The Demographic Response to Holocene

Climate Change in the Sahara." *Quaternary Science Reviews* **101**: 28–35. <https://doi.org/10.1016/j.quascirev.2014.07.003>.

Mapande, Amin T., and C. J. C. Reason. 2005. "Interannual Rainfall Variability over Western Tanzania." *International Journal of Climatology* **25** (10): 1355–68. <https://doi.org/10.1002/joc.1193>.

Marchant, Robert, and Henry Hooghiemstra. 2004. "Rapid Environmental Change in African and South American Tropics around 4000 Years before Present: A Review." *Earth-Science Reviews* **66** (3): 217–60. <https://doi.org/10.1016/j.earscirev.2004.01.003>.

Marciniak, B. 1982. "Late glacial and Holocene new diatoms from a glacial lake Przedni Staw in the Piec Stawów Poliskich Valley, Polish Tatra Mts". In: E. Szádeczky-Kardoss (ed.), Proceedings of the Sixth Symposium on Recent and Fossil Diatoms, Budapest, September 1-6, 1980, Biostratigraphy-Paleoecology-Paleogeography-Paleoclimatology. Acta Geologica, Academiae Scientiarum Hungaricae. 25 (1-2): 161-171.

Marshall, Michael H., Henry F. Lamb, Sarah J. Davies, Melanie J. Leng, Zelalem Kubsa, Mohammed Umer, and Charlotte Bryant. 2009. "Climatic Change in Northern Ethiopia during the Past 17,000 Years: A Diatom and Stable Isotope Record from Lake Ashenge." *Palaeogeography, Palaeoclimatology, Palaeoecology* **279** (1): 114–27. <https://doi.org/10.1016/j.palaeo.2009.05.003>.

Marshall, Michael H., Henry F. Lamb, Dei Huws, Sarah J. Davies, Richard Bates, Jan Bloemendal, John Boyle, Melanie J. Leng, Mohammed Umer, and Charlotte Bryant. 2011. "Late Pleistocene and Holocene Drought Events at Lake Tana, the Source of the Blue Nile." *Global and Planetary Change* **78** (3): 147–61. <https://doi.org/10.1016/j.gloplacha.2011.06.004>.

Martin-Jones, Catherine M., Christine S. Lane, Nicholas J.G. Pearce, Victoria C. Smith, Henry F. Lamb, Frank Schaebitz, Finn Viehberg, Maxwell C. Brown, Ute Frank, and Asfawossen Asrat. 2017. "Recurrent Explosive Eruptions from a High-Risk Main Ethiopian Rift Volcano throughout the Holocene." *Geology* **45** (12): 1127–30. <https://doi.org/10.1130/G39594.1>.

März, C., A. Stratmann, J. Matthiessen, A.-K. Meinhardt, S. Eckert, B. Schnetger, C. Vogt, R. Stein, and H.-J. Brumsack. 2011. "Manganese-Rich Brown Layers in Arctic Ocean Sediments: Composition, Formation Mechanisms, and Diagenetic Overprint." *Geochimica et Cosmochimica Acta* **75** (23): 7668–87. <https://doi.org/10.1016/J.GCA.2011.09.046>.

McGee, D, P, deMenocal, G, Winckler, J, Stuut, and L, Bradtmiller. 2013. "The magnitude,

- timing and abruptness of changes in North African dust deposition over the last 20,000 yr". *Earth and Planetary Science Letters* **371-372**: 163-176. <https://doi.org/10.1016/j.epsl.2013.03.054>.
- McManus, J. F., R. Francois, J.-M. Gherardi, L. D. Keigwin, and S. Brown-Leger. 2004. "Collapse and Rapid Resumption of Atlantic Meridional Circulation Linked to Deglacial Climate Changes." *Nature* **428** (6985): 834–37. <https://doi.org/10.1038/nature02494>.
- Michel, Timothy J., Jasmine E. Saros, Sebastian J. Interlandi, and Alexander P. Wolfe. 2006. "Resource Requirements of Four Freshwater Diatom Taxa Determined by in Situ Growth Bioassays Using Natural Populations from Alpine Lakes." *Hydrobiologia* **568** (1): 235–43. <https://doi.org/10.1007/s10750-006-0109-0>.
- Mills, K. 2009. "Ugandan crater lakes: limnology, palaeolimnology and palaeoenvironmental history". PhD Thesis, Loughborough University. https://repository.lboro.ac.uk/articles/Ugandan_crater_lakes_limnology_palaeolimnology_and_palaeoenvironmental_history/9487238.
- Mills, K, D B Ryves, N J Anderson, C L Bryant, and J J Tyler. 2014. "Expressions of Climate Perturbations in Western Ugandan Crater Lake Sediment Records during the Last 1000 Years." *Clim. Past* **10**: 1581–1601. <https://doi.org/10.5194/cp-10-1581-2014>.
- Mills, Keely, and David B. Ryves. 2012. "Diatom-Based Models for Inferring Past Water Chemistry in Western Ugandan Crater Lakes." *Journal of Paleolimnology* **48** (2): 383–99. <https://doi.org/10.1007/s10933-012-9609-2>.
- Mills, Keely, Christopher H. Vane, Raquel A. Lopes dos Santos, Immaculate Ssemmanda, and David B. Ryves. 2018. "Linking Land and Lake: Using Novel Geochemical Techniques to Understand Biological Response to Environmental Change." *Quaternary Science Reviews* **202**: 122–38. <https://doi.org/10.1016/J.QUASCIREV.2018.09.038>.
- Mitchell, Timothy D., and Philip D. Jones. 2005. "An Improved Method of Constructing a Database of Monthly Climate Observations and Associated High-Resolution Grids." *International Journal of Climatology* **25** (6): 693–712. <https://doi.org/10.1002/joc.1181>.
- Moernaut, J, M, van Daele, K, Heirman, K, Fontjin, M, Strasser, M, Pino, R, Urrutia, and M, de Batist. 2014. " Lacustrine turbidites as a tool for quantitative earthquake reconstruction: New evidence for a variable rupture mode in south central Chile". *Journal of Geophysical Research: Solid Earth* **119**: 1607-1633. DOI:10.1002/2013JB010738.
- Morales, E. 2005. " Observations of the morphology of some known and new fragiliarioid

- diatoms (Bacillariophyceae) from rivers in the USA". *Phycological Research* **53** (2): 113-133. DOI: 10.1111/j.1440-183.2005.00378.x.
- Morales, E, and P, Hamilton. 2002. "Seventh NAWQA Workshop on Harmonization of Algal Taxonomy". Report No. 02-21. Philadelphia: Patrick Center for Environmental Research, ANSP.
- Morales, E, P, Siver, and F, Trainor. 2001 "Identification of diatoms during ecological assessments: Comparison between light and scanning electron microscopy". *Proceedings of the Academy of Natural Sciences of Philadelphia* **151**: 29-37. DOI: 10.1635/0097-3157(2001)151[0095:IOBDE]2.0.CO;2.
- Morales, E, M, Edlund, and S, Spaulding. 2010. " Description and ultrastructure of araphid diatom species (Bacillariophyceae) morphologically similar to *Pseudostaurosira elliptica* (Schumann) Edlund et al.". *Phycological Research* **58** (2): 97-107. DOI: 10.1111/j.1440-1835.2010.00567.x.
- Moy, C, G, Seltzer, and D, Rodbell et al. 2002. "Variability of El Niño/Southern Oscillation activity at millennial timescales during the Holocene epoch". *Nature* **420**: 162–165. <https://doi.org/10.1038/nature01194>
- Müller, Meinard. 2007. "Dymamic Time Warping." In *Information Retrieval for Music and Motion*, 69–84. Berlin, Heidelberg: Springer Berlin Heidelberg. <https://doi.org/10.1007/978-3-540-74048-3>.
- Müller, O. (1905). "Bacillariaceen aus dem Nyassaland und einigen benachbarten Gebieten. III Folge". Naviculoideae-Naviculeae-Gomphoneminae-Gomphocymbellinae-Cymbellinae. Nitzschioideae-Nitzschieae (Engler's) *Botanische Jahrbucher fur Systematik, Pflanzengeschichte, und Pflantengeographie* 36(1/2): 137-206, 2 pl.
- Myrbo, A. 2007. "Smear Slides." 2007. <http://lrc.geo.umn.edu/laccore/assets/pdf/sops/smearslides.pdf>.
- Nash, David J., and George C. D. Adamson. 2014. "Recent Advances in the Historical Climatology of the Tropics and Subtropics." *Bulletin of the American Meteorological Society* **95** (1): 131–46. <https://doi.org/10.1175/BAMS-D-12-00030.1>.
- Nash, David J., Gijs De Cort, Brian M. Chase, Dirk Verschuren, Sharon E. Nicholson, Timothy M. Shanahan, Asfawossen Asrat, Anne-Marie Lézine, and Stefan W. Grab. 2016. "African Hydroclimatic Variability during the Last 2000 Years." *Quaternary Science Reviews* **154**: 1–22. <https://doi.org/10.1016/j.quascirev.2016.10.012>.

- Niang, Isabelle, Oliver C Ruppel, Mohamed A Abdrabo, Pauline Dube, Neil Leary, Lena Schulte-Uebbing, DJ Dokken, et al. 2014. "Africa." In *Climate Change 2014: Impacts, Adaptation, and Vulnerability. Part B: Regional Aspects. Contribution of Working Group II to the Fifth Assessment Report of the Intergovernmental Panel on Climate Change*, edited by V Barros, C Field, D Dokken, M Mastrandrea, K Mach, T Bilir, K Chatterjee, et al., 1199–1265. Cambridge, New York: Cambridge University Press.
- Nicholson, S. 1996. "Environmental change within the historical period". In: "The physical geography of Africa". Edited by Adams W, A, Goudie, and A, Orme: 60-87. Oxford: Oxford University Press.
- NMA. 2013. "Annual Climate Bulletin: For the Year 2013." Addis Ababa: NMA.
- Norton, Stephen A., Randall H. Perry, Jasmine E. Saros, George L. Jacobson, Ivan J. Fernandez, Jiří Kopáček, Tiffany A. Wilson, and Michael D. SanClements. 2011. "The Controls on Phosphorus Availability in a Boreal Lake Ecosystem since Deglaciation." *Journal of Paleolimnology* **46** (1): 107–22. <https://doi.org/10.1007/s10933-011-9526-9>.
- Jari Oksanen, F. Guillaume Blanchet, Michael Friendly, Roeland Kindt, Pierre Legendre, Dan McGlinn, Peter R. Minchin, R. B. O'Hara, Gavin L. Simpson, Peter Solymos, M. Henry H. Stevens, Eduard Szoecs and Helene Wagner. 2018. "vegan: Community Ecology Package". R package version 2.5-3. <https://CRAN.R-project.org/package=vegan>.
- Oladipo, E. Olukayode. 1986. "Spatial Patterns of Drought in the Interior Plains of North America." *Journal of Climatology* **6** (5): 495–513. <https://doi.org/10.1002/joc.3370060505>.
- Olsen, Jesper, N. John Anderson, and M Leng. 2013. "Limnological Controls on Stable Isotope Records of Late-Holocene Palaeoenvironment Change in SW Greenland: A Paired Lake Study." *Quaternary Science Reviews* **66**: 85–95. <https://doi.org/10.1016/J.QUASCIREV.2012.10.043>.
- Orlóci, L, V, Pillar, and M, Anand. 2006. " Multiscale analysis of palynological records: New possibilities". *Community Ecology* **7** (1): 53-67. DOI: 10.1556/ComEc.7.2006.1.6.
- Osmaston, Henry A., Wishart A. Mitchell, and J. A. Nigel Osmaston. 2005. "Quaternary Glaciation of the Bale Mountains, Ethiopia." *Journal of Quaternary Science* **20** (6): 593–606. <https://doi.org/10.1002/jqs.931>.
- Ossendorf, G, A, Groos, T, Bromm, M, Tekelemariam, B, Glaser et al. 2019. "Middle Stone Age foragers resided in high elevations of the glaciated Bale Mountains, Ethiopia". *Science* **365** (6453): 583-587. DOI: 10.1126/science.aaw8942.

- O'Sullivan, P. 1983. " Annually-laminated lake sediments and the study of Quaternary environmental changes — a review". *Quaternary Science Reviews* **1** (4): 245-313. [https://doi.org/10.1016/0277-3791\(83\)90008-2](https://doi.org/10.1016/0277-3791(83)90008-2).
- Oswald, W Wyatt, Patricia M Anderson, Thomas A Brown, Linda B Brubaker, J Feng, Sheng Hu, Anatoly V Lozhkin, Willy Tinner, and Petra Kaltenrieder. 2005. "Effects of Sample Mass and Macrofossil Type on Radiocarbon Dating of Arctic and Boreal Lake Sediments." *The Holocene* **15** (5): 758–67. <http://journals.sagepub.com/doi/pdf/10.1191/0959683605hl849r>.
- Owen, R, R Lee, and R Renaut. 2012. "Early Pleistocene Lacustrine Sedimentation and Diatom Stratigraphy at Munya Wa Gicheru, Southern Kenya Rift Valley." *Palaeogeography, Palaeoclimatology, Palaeoecology* **331–332**: 60–74. <https://doi.org/10.1016/J.PALAEO.2012.02.033>.
- Padisák, Judit, Gábor Borics, Gizella Fehér, István Grigorszky, Imre Oldal, Antal Schmidt, and Zsuzsa Zábóné-Doma. 2003. "Dominant Species, Functional Assemblages and Frequency of Equilibrium Phases in Late Summer Phytoplankton Assemblages in Hungarian Small Shallow Lakes." *Hydrobiologia* **502** (1–3): 157–68. <https://doi.org/10.1023/B:HYDR.0000004278.10887.40>.
- Panizzo, Virginia, Anson, Mackay, Neil, Rose, Patrick, Rioual, and Melanie, Leng. 2013. " Recent palaeolimnological change recorded in Lake Xiaolongwan, northeast China: Climatic versus anthropogenic forcing". *Quaternary International* **290–291**: 322-334. <https://doi.org/10.1016/j.quaint.2012.07.033>.
- Pante, Eric, and Benoit Simon-Bouhet. 2013. "Marmap: A Package for Importing, Plotting and Analyzing Bathymetric and Topographic Data in R." Edited by Guy J.-P. Schumann. *PLoS ONE* **8** (9): e73051. <https://doi.org/10.1371/journal.pone.0073051>.
- Parmesan, Camille, and Gary Yohe. 2003. "A Globally Coherent Fingerprint of Climate Change Impacts across Natural Systems." *Nature* **421** (6918): 37–42. <https://doi.org/10.1038/nature01286>.
- Pasche, Natacha, Georges Alunga, Keely Mills, Fabrice Muvundja, David B. Ryves, Michael Schurter, Bernhard Wehri, and Martin Schmid. 2010. "Abrupt Onset of Carbonate Deposition in Lake Kivu during the 1960s: Response to Recent Environmental Changes." *Journal of Paleolimnology* **44** (4): 931–46. <https://doi.org/10.1007/s10933-010-9465-x>.
- Paull, T, P, Hamilton, K, Gajewski, and M, LeBlanc. 2008. "Numerical analysis of small Arctic diatoms (Bacillariophyceae) representing the *Stausosira* and *Stausosirella* species complexes". *Phycologia* **47**:213–224.

- Pérez, L., J. Lorenschat, Julieta Massafarro, Christine Pailles, Florence Sylvestre, Werner Hollwedel, Gerd-Oltmann Brandorff, et al. 2013. "Bioindicators of Climate and Trophic State in Lowland and Highland Aquatic Ecosystems of the Northern Neotropics." *Revista de Biología Tropical* **61** (2): 603–44. https://www.scielo.sa.cr/scielo.php?pid=S0034-77442013000300012&script=sci_arttext.
- Perren, B., R. Bradley, and F. Pierre. 2003. "Rapid Lacustrine Response to Recent High Arctic Warming: A Diatom Record from Sawtooth Lake, Ellesmere Island, Nunavut." *Arctic, Antarctic, and Alpine Research* **35** (3): 271–78. <https://doi.org/10.1080/15230430.2002.12003477>.
- Peterson, Christopher G., and R. Jan Stevenson. 1992. "Resistance and Resilience of Lotic Algal Communities: Importance of Disturbance Timing and Current." *Ecology* **73** (4): 1445–61. <https://doi.org/10.2307/1940689>.
- Peterson, B, and Peter, Carl. 2018. "PerformanceAnalytics: Econometric Tools for Performance and Risk Analysis". R package version 1.5.2. <https://CRAN.R-project.org/package=PerformanceAnalytics>.
- Peyron, Odile, Dominique Jolly, Raymonde Bonnefille, Annie Vincens, and Joël Guiot. 2000. "Climate of East Africa 6000 14C Yr B.P. as Inferred from Pollen Data." *Quaternary Research* **54** (1): 90–101. <https://doi.org/10.1006/qres.2000.2136>.
- Podrifske, Brandi, and Konrad Gajewski. 2007. "Diatom Community Response to Multiple Scales of Holocene Climate Variability in a Small Lake on Victoria Island, NWT, Canada." *Quaternary Science Reviews* **26** (25–28): 3179–96. <https://doi.org/10.1016/J.QUASCIREV.2007.06.009>.
- Potapova, Marina, and Donald F. Charles. 2007. "Diatom Metrics for Monitoring Eutrophication in Rivers of the United States." *Ecological Indicators* **7** (1): 48–70. <https://doi.org/10.1016/J.ECOLIND.2005.10.001>.
- Powers, Lindsay A., Thomas C. Johnson, Josef P. Werne, Isla S. Castañeda, Ellen C. Hopmans, Jaap S. Sinninghe Damsté, and Stefan Schouten. 2005. "Large Temperature Variability in the Southern African Tropics since the Last Glacial Maximum." *Geophysical Research Letters* **32** (8): L08706. <https://doi.org/10.1029/2004GL022014>.
- Prell, Warren L., and John E. Kutzbach. 1987. "Monsoon Variability over the Past 150,000 Years." *Journal of Geophysical Research* **92** (D7): 8411. <https://doi.org/10.1029/JD092iD07p08411>.

- Railsback, L, F, Liang, G, Brook, N, Voarintsoa, H, Sletten, E, Marais, B, Hardt, H, Cheng, and R, Edwards. 2018. "The timing, two-pulsed nature, and variable climatic expression of the 4.2 ka event: A review and new high-resolution stalagmite data from Namibia". *Quaternary Science Reviews* **186**: 78-90. <https://doi.org/10.1016/j.quascirev.2018.02.015>.
- Ravallion, Martin. 2012. "Benchmarking Global Poverty Reduction." 6205. World Bank. <https://openknowledge.worldbank.org/handle/10986/12095> License: CC BY 3.0 IGO.
- Reimer, Paula J, Edouard Bard, Alex Bayliss, J Warren Beck, Paul G Blackwell, Christopher Bronk Ramsey, Caitlin E Buck, et al. 2013. "IntCal13 and Marine13 Radiocarbon Age Calibration Curves 0–50,000 Years Cal BP." *Radiocarbon* **55** (04): 1869–87. https://doi.org/10.2458/azu_js_rc.55.16947.
- Richardson, J. L., and R. A. Dussinger. 1986. "Paleolimnology of Mid-Elevation Lakes in the Kenya Rift Valley." *Hydrobiologia* **143** (1): 167–74. <https://doi.org/10.1007/BF00026659>.
- Rimet, F., and A. Bouchez. 2012. "Life-Forms, Cell-Sizes and Ecological Guilds of Diatoms in European Rivers." *Knowledge and Management of Aquatic Ecosystems* **406** (July): 1–12. <https://doi.org/10.1051/kmae/2012018>.
- Roberts, Helen M., Charlotte L. Bryant, Dei G. Huws, and Henry F. Lamb. 2018. "Generating Long Chronologies for Lacustrine Sediments Using Luminescence Dating: A 250,000 Year Record from Lake Tana, Ethiopia." *Quaternary Science Reviews* **202** (December): 66–77. <https://doi.org/10.1016/J.QUASCIREV.2018.10.037>.
- Rodbell, Donald T., Geoffrey O. Seltzer, David M. Anderson, Mark B. Abbott, David B. Enfield, and Jeremy H. Newman. 1999. "An ~15,000-Year Record of El Niño-Driven Alluviation in Southwestern Ecuador." *Science* **283** (5401): 516–20.
- Rothwell, R, and I, Croudace. 2015. "Micro-XRF Studies of Sediment Cores: A Perspective on Capability and Application in the Environmental Sciences". In: "Micro-XRF Studies of Sediment Cores. Developments in Paleoenvironmental Research, vol 17". Edited by Croudace I. and Rothwell R: 1-21. Dodrecht: Springer.
- Roubeix, Vincent, Françoise Chalié, and Françoise Gasse. 2014. "The Diatom *Thalassiosira Faurii* (Gasse) Hasle in the Ziway–Shala Lakes (Ethiopia) and Implications for Paleoclimatic Reconstructions: Case Study of the Glacial–Holocene Transition in East Africa." *Palaeogeography, Palaeoclimatology, Palaeoecology* **402**: 104–12. <https://doi.org/10.1016/j.palaeo.2014.03.014>.
- Roubeix, Vincent, and Françoise, Chalié. 2018. "New insights into the termination of the

- African Humid Period (5.5 ka BP) in central Ethiopia from detailed analysis of a diatom record". *Journal of Paleolimnology* **61**: 99–110. <https://doi.org/10.1007/s10933-018-0047-7>.
- Round, F, E, R, M, Crawford, and D, G, Mann. 1990. "The Diatoms - Biology & Morphology of the genera". Cambridge: Cambridge University Press.
- Rucina, Stephen M., Veronica M. Muiruri, Rahab N. Kinyanjui, Katy McGuinness, and Rob Marchant. 2009. "Late Quaternary Vegetation and Fire Dynamics on Mount Kenya." *Palaeogeography, Palaeoclimatology, Palaeoecology* **283** (1): 1–14. <https://doi.org/10.1016/j.palaeo.2009.08.008>.
- Rueden, Curtis T., Johannes Schindelin, Mark C. Hiner, Barry E. DeZonia, Alison E. Walter, Ellen T. Arena, and Kevin W. Eliceiri. 2017. "ImageJ2: ImageJ for the next Generation of Scientific Image Data." *BMC Bioinformatics* **18** (1): 529. <https://doi.org/10.1186/s12859-017-1934-z>.
- Russell, J. M., D. Verschuren, and H. Eggermont. 2007. "Spatial Complexity of 'Little Ice Age' Climate in East Africa: Sedimentary Records from Two Crater Lake Basins in Western Uganda." *The Holocene* **17** (2): 183–93. <https://doi.org/10.1177/0959683607075832>.
- Russell, J.M., and T.C. Johnson. 2007. "Little Ice Age Drought in Equatorial Africa: Intertropical Convergence Zone Migrations and El Niño–Southern Oscillation Variability." *Geology* **35** (1): 21–24. <https://doi.org/10.1130/G23125A.1>.
- Russell, James M., and Thomas C. Johnson. 2005. "A High-Resolution Geochemical Record from Lake Edward, Uganda Congo and the Timing and Causes of Tropical African Drought during the Late Holocene." *Quaternary Science Reviews* **24** (12): 1375–89. <https://doi.org/10.1016/j.quascirev.2004.10.003>.
- Ryner, Maria A., Raymonde Bonnefille, Karin Holmgren, and Alfred Muzuka. 2006. "Vegetation Changes in Empakaai Crater, Northern Tanzania, at 14,800–9300 Cal Yr BP." *Review of Palaeobotany and Palynology* **140** (3): 163–74. <https://doi.org/10.1016/j.revpalbo.2006.03.006>.
- Ryves, D, S, Juggins, S, Fritz, and R, Battarbee. 2001. " Experimental diatom dissolution and the quantification of microfossil preservation in sediments". *Palaeogeography, Palaeoclimatology, Palaeoecology* **172** (1–2): 99–113. [https://doi.org/10.1016/S0031-0182\(01\)00273-5](https://doi.org/10.1016/S0031-0182(01)00273-5).
- Sagnotti, Leonardo, and Chiara Caricchi. 2018. "StratFit: An Excel Workbook for Correlation of Multiple Stratigraphic Trends." *Annals of Geophysics* **61** (3): DA341.

<https://doi.org/10.4401/ag-7619>.

Sakoe, H., and S. Chiba. 1978. "Dynamic Programming Algorithm Optimization for Spoken Word Recognition." *IEEE Transactions on Acoustics, Speech, and Signal Processing* **26** (1): 43–49. <https://doi.org/10.1109/TASSP.1978.1163055>.

Salomoni, S. E., O. Rocha, V. L. Callegaro, and E. A. Lobo. 2006. "Epilithic Diatoms as Indicators of Water Quality in the Gravataí River, Rio Grande Do Sul, Brazil." *Hydrobiologia* **559** (1): 233–46. <https://doi.org/10.1007/s10750-005-9012-3>.

Sandweiss, Daniel H., James B. Richardson, Elizabeth J. Reitz, Harold B. Rollins, and Kirk A. Maasch. 1996. "Geoarchaeological Evidence from Peru for a 5000 Years B.P. Onset of El Niño." *Science* **273** (5281): 1531–33.

Saros, Jasmine E., Kristin E. Strock, Joan Mccue, Erika Hogan, and N. John Anderson. 2014. "Response of Cyclotella Species to Nutrients and Incubation Depth in Arctic Lakes." *Journal of Plankton Research* **36** (2): 450–60. <https://doi.org/10.1093/plankt/fbt126>.

Schindelin, Johannes, Ignacio Arganda-Carreras, Erwin Frise, Verena Kaynig, Mark Longair, Tobias Pietzsch, Stephan Preibisch, et al. 2012. "Fiji: An Open-Source Platform for Biological-Image Analysis." *Nature Methods* **9** (7): 676–82. <https://doi.org/10.1038/nmeth.2019>.

Schmidt, Roland, Christian Kamenik, Horst Lange-Bertalot, and Rolf Klee. 2004. "Fragilaria and Staurosira (Bacillariophyceae) from Sediment Surfaces of 40 Lakes in the Austrian Alps in Relation to Environmental Variables, and Their Potential for Palaeoclimatology." *Journal of Limnology* **63** (2): 171. <https://doi.org/10.4081/jlimnol.2004.171>.

Schnurrenberger, D, J, Russell, and K, Kelts. 2003. "Classification of lacustrine sediments abased on sedimentary components". *Journal of Paleolimnology* **29**: 141–154. <https://doi.org/10.1023/A:1023270324800>.

Selig, Uwe, and Günter Schlungbaum. 2003. "Characterisation and Quantification of Phosphorus Release from Profundal Bottom Sediments in Two Dimictic Lakes during Summer Stratification." *Journal of Limnology* **62** (2): 151. <https://doi.org/10.4081/jlimnol.2003.151>.

Shala, Shyhrete, Karin F. Helmens, Krister N. Jansson, Malin E. Kylander, Jan Risberg, and Ludvig Löwemark. 2014. "Palaeoenvironmental Record of Glacial Lake Evolution during the Early Holocene at Sokli, NE Finland." *Boreas* **43** (2): 362–76. <https://doi.org/10.1111/bor.12043>.

- Shanahan, Timothy M., Jonathon, T. Overpeck, W. E. Sharp, Christopher A. Scholz, and Justice, A. Arko. 2006. "Simulating the response of a closed-basin lake to recent climate changes in tropical West Africa (Lake Bosumtwi, Ghana)". *Hydrological processes* **21** (13): 1678-1691. <https://doi.org/10.1002/hyp.6359>.
- Shanahan, Timothy M., Nicholas P. McKay, Konrad A. Hughen, Jonathan T. Overpeck, Bette Otto-Bliesner, Clifford W. Heil, John King, Christopher A. Scholz, and John Peck. 2015. "The Time-Transgressive Termination of the African Humid Period." *Nature Geoscience* **8** (2): 140–44. <https://doi.org/10.1038/ngeo2329>.
- Simpson, G.L. 2007. "Analogue Methods in Palaeoecology: Using the analogue Package". *Journal of Statistical Software* **22** (2), 1-29. DOI: 10.18637/jss.v022.i02.
- Simpson, G.L and H. Birks. 2012. "Statistical learning in Palaeolimnology". In: "Tracking Environmental Change Using Lake Sediments". Edited by Birks, H, André F. Lotter, Steve Juggins, John P. Smol. Netherlands: Springer:
- Simpson, G.L. and Oksanen, J. 2018. "analogue: Analogue matching and Modern Analogue Technique transfer function models". (R package version 0.17-1). (<https://cran.r-project.org/package=analogue>).
- Smol, J., and M. Douglas. 2010. "Freshwater Diatoms as Indicators of Environmental Change in the High Arctic." In *The Diatoms: Applications for the Environmental and Earth Sciences*, edited by J. Smol and E. Stoermer, 2nd ed. Cambridge University Press.
- Smol, J., A. Wolfe, J. Birks, M. Douglas, V. Jones, A. Korhola, R. Pienitz, et al. 2005. "Climate-Driven Regime Shifts in the Biological Communities of Arctic Lakes." *Proceedings of the National Academy of Sciences of the United States of America* **102** (12): 4397–4402. <https://doi.org/10.1073/pnas.97.4.1406>.
- Smol, J.P, and E. F., Stoermer 2010. "The Diatoms: Applications for the Environmental and Earth Sciences" (2nd ed.). Cambridge: Cambridge University Press, 667 p.
- Stager, J. Curt, B. Cumming, and L.D. Meeker. 2003. "A 10,000 year high-resolution diatom record from Pilkington Bay, Lake Victoria East Africa". *Quat. Res.* **59**: 172–181. [https://doi.org/10.1016/S0033-5894\(03\)00008-5](https://doi.org/10.1016/S0033-5894(03)00008-5).
- Stager, J. Curt, Christine Cocquyt, Raymonde Bonnefille, Constanze Weyhenmeyer, and Nicole Bowerman. 2009. "A Late Holocene Paleoclimatic History of Lake Tanganyika, East Africa." *Quaternary Research* **72** (1): 47–56. <https://doi.org/10.1016/j.yqres.2009.04.003>.
- Stager, J.Curt, D, Ryves, B, Chase, and F, Pausata. 2011. "Catastrophic drought in the Afro-

- Asian monsoon region during Heinrich Event 1". *Science* **331** (6022): 129-132. DOI: 10.1126/science.1198322.
- Stager, J Curt, David Ryves, Brian F Cumming, L David Meeker, and Juerg Beer. 2005. "Solar Variability and the Levels of Lake Victoria, East Africa, during the Last Millenium." *Journal of Paleolimnology* **33** (2): 243–51.
- Stager, J. Curt, Paul A Mayewski, and L.David Meeker. 2002. "Cooling Cycles, Heinrich Event 1, and the Desiccation of Lake Victoria." *Palaeogeography, Palaeoclimatology, Palaeoecology* **183** (1): 169–78. [https://doi.org/10.1016/S0031-0182\(01\)00468-0](https://doi.org/10.1016/S0031-0182(01)00468-0).
- Stager, J. Curt, and T. C. Johnson. 2008. "The late Pleistocene desiccation of Lake Victoria and the origin of its endemic biota". *Hydrobiologia* **596**: 5-16. <https://doi.org/10.1007/s10750-007-9158-2>.
- Steffen, Will, Katherine Richardson, Johan Rockström, Sarah E. Cornell, Ingo Fetzer, Elena M. Bennett, Reinette Biggs, et al. 2015. "Planetary Boundaries: Guiding Human Development on a Changing Planet." *Science* **347** (6223): 1259855.
- Stone, Jeffery R., Karlyn S. Westover, and Andrew S. Cohen. 2011. "Late Pleistocene Paleohydrography and Diatom Paleoecology of the Central Basin of Lake Malawi, Africa." *Palaeogeography, Palaeoclimatology, Palaeoecology* **303** (1–4): 51–70. <https://doi.org/10.1016/J.PALAEO.2010.01.012>.
- Street-Perrott, F. A, and R. Alan, Perrott. 1990. "Abrupt climate fluctuations in the tropics: the influence of Atlantic Ocean circulation". *Nature* **343**: 607-612. <https://doi.org/10.1038/343607a0>.
- Street-Perrott, F.A., D.S. Marchand, N. Roberts, and S.P Harisson. 1989. "Global Lake-Level Variations from 18,000 to 0 Years Ago: A Paleoclimatic Analysis". U.S. Department of Energy Technical Report 46, Washington, D.C. 20545. Distributed by National Technical Information Service, Springfield, VA 22161.
- Stuiver, Minze., and Paula. Reimer. 1993. "Extended 14C Data Base and Revised CALIB 3.0 14C Age Calibration Program." *Radiocarbon* **35** (1): 215–30. <http://citeseerx.ist.psu.edu/viewdoc/download?doi=10.1.1.471.8760&rep=rep1&type=pdf>.
- Swinton, M, L, Eichler, J, Farrell, and C, Boylen. 2015. "Evidence for water temperature increase in LakeGeorge, NY: impact on growing season durationand degree days". *Lake and Reservoir Management* **31** (3): 241-253. DOI:10.1080/10402381.2015.1067660.
- Tadesse, Solomon, Jean-Pierre Milesi, and Yves Deschamps. 2003. "Geology and Mineral

- Potential of Ethiopia: A Note on Geology and Mineral Map of Ethiopia." *Journal of African Earth Sciences* **36** (4): 273–313. [https://doi.org/10.1016/S0899-5362\(03\)00048-4](https://doi.org/10.1016/S0899-5362(03)00048-4).
- Talbot, Michael R., Maria Letizia Filippi, Niels Bo Jensen, and Jean-Jacques Tiercelin. 2007. "An Abrupt Change in the African Monsoon at the End of the Younger Dryas." *Geochemistry, Geophysics, Geosystems* **8** (3). <https://doi.org/10.1029/2006GC001465>.
- Talbot, Michael R., and Tine Lærdal. 2000. "The Late Pleistocene - Holocene Palaeolimnology of Lake Victoria, East Africa, Based upon Elemental and Isotopic Analyses of Sedimentary Organic Matter." *Journal of Paleolimnology* **23** (2): 141–64. <https://doi.org/10.1023/A:1008029400463>.
- Taylor, J., W., Harding, and C. Archibald. 2007. "An Illustrated Guide to Some Common Diatom Species from South Africa". Report number: TT282/07. Pretoria: Water Research Commission.
- Telford, R. 1998. "Diatom Stratigraphies of Lakes Awassa and Tilo, Ethiopia: Holocene Records of Groundwater Variability and Climate Change." PhD thesis, Aberystwyth University.
- Telford, R. 2018. "ggpalaeo: ggplot2 Plots For analogue and rioja Packages". R package version 0.0.0.9002.
- Telford, R., and H. Birks. 2011. "A novel method for assessing the statistical significance of quantitative reconstructions inferred from biotic assemblages". *Quaternary Science Reviews* **30** (9–10): 1272-1278. <https://doi.org/10.1016/j.quascirev.2011.03.002>.
- Telford, R., and Henry, F. Lamb. 1999. "Groundwater-Mediated Response to Holocene Climatic Change Recorded by the Diatom Stratigraphy of an Ethiopian Crater Lake". *Quaternary Research* **52** (1): 63-75. <https://doi.org/10.1006/qres.1999.2034>.
- Telford, R., Henry F. Lamb, and Mohammed Umer Mohammed. 1999. "Diatom-Derived Palaeoconductivity Estimates for Lake Awassa, Ethiopia: Evidence for Pulsed Inflows of Saline Groundwater." *Journal of Paleolimnology* **21** (4): 409–22. <https://doi.org/10.1023/A:1008092823410>.
- Telford, R., P. Barker, S. Metcalfe, and A. Newton. 2004. "Lacustrine responses to tephra deposition: Examples from Mexico". *Quaternary Science Reviews* **23** (23-24): 2337-2353. DOI: 10.1016/j.quascirev.2004.03.014.
- Thompson, Lonnie G., Ellen Mosley-Thompson, Mary E. Davis, Keith A. Henderson, Henry H. Brecher, Victor S. Zagorodnov, Tracy A. Mashiotta, et al. 2002. "Kilimanjaro Ice Core

Records: Evidence of Holocene Climate Change in Tropical Africa." *Science* **298** (5593): 589-593.

Tiercelin, J.-J., E. Gibert, M. Umer, R. Bonnefille, J.-R. Disnar, A.-M. Lézine, D. Hureau-Mazaudier, Y. Travi, D. Keravis, and H.F. Lamb. 2008. "High-Resolution Sedimentary Record of the Last Deglaciation from a High-Altitude Lake in Ethiopia." *Quaternary Science Reviews* **27** (5): 449–67. <https://doi.org/10.1016/j.quascirev.2007.11.002>.

Tierney, J.E., C. Ummenhofer, and P. deMenocal. 2013. "Past and future rainfall in the Horn of Africa". *Science Advances* **1** (9): e1500682. DOI: 10.1126/sciadv.1500682.

Tierney, J. E., and P. B. deMenocal. 2013. "Abrupt Shifts in Horn of Africa Hydroclimate Since the Last Glacial Maximum." *Science* **342** (6160): 843–46. <https://doi.org/10.1126/science.1240411>.

Tierney, J. E., J. M. Russell, Y. Huang, J. S. S. Damste, E. C. Hopmans, and A. S. Cohen. 2008. "Northern Hemisphere Controls on Tropical Southeast African Climate During the Past 60,000 Years." *Science* **322** (5899): 252–55. <https://doi.org/10.1126/science.1160485>.

Tierney, Jessica E., Sophie C. Lewis, Benjamin I. Cook, Allegra N. LeGrande, and Gavin A. Schmidt. 2011a. "Model, Proxy and Isotopic Perspectives on the East African Humid Period." *Earth and Planetary Science Letters*. **307** (1-2): 103-112. <https://doi.org/10.1016/j.epsl.2011.04.038>.

Tierney, Jessica E., James M. Russell, and Yongsong Huang. 2010. "A Molecular Perspective on Late Quaternary Climate and Vegetation Change in the Lake Tanganyika Basin, East Africa." *Quaternary Science Reviews* **29** (5): 787–800. <https://doi.org/10.1016/j.quascirev.2009.11.030>.

Tierney, Jessica E., James M. Russell, Jaap S. Sinninghe Damsté, Yongsong Huang, and Dirk Verschuren. 2011b. "Late Quaternary Behavior of the East African Monsoon and the Importance of the Congo Air Boundary." *Quaternary Science Reviews* **30** (7): 798–807. <https://doi.org/10.1016/j.quascirev.2011.01.017>.

Tierney, Jessica E., Caroline C. Ummenhofer, and Peter B. deMenocal. 2015. "Past and Future Rainfall in the Horn of Africa." *Science Advances* **1** (9): e1500682.

Timm, Oliver, Peter Köhler, Axel Timmermann, and Laurie Menviel. 2010. "Mechanisms for the Onset of the African Humid Period and Sahara Greening 14.5–11 Ka BP*." *Journal of Climate* **23** (10): 2612–33. <https://doi.org/10.1175/2010JCLI3217.1>.

Tjallingii, Rik, Ursula Röhl, Martin Kölling, and Torsten Bickert. 2007. "Influence of the Water

- Content on X-Ray Fluorescence Core-Scanning Measurements in Soft Marine Sediments.” *Geochemistry, Geophysics, Geosystems* **8** (2). <https://doi.org/10.1029/2006GC001393>.
- Tormene, Paolo, Toni Giorgino, Silvana Quaglini, and Mario Stefanelli. 2009. “Matching Incomplete Time Series with Dynamic Time Warping: An Algorithm and an Application to Post-Stroke Rehabilitation.” *Artificial Intelligence in Medicine* **45** (1): 11–34. <https://doi.org/10.1016/J.ARTMED.2008.11.007>.
- Törnqvist, T., A. de Jong, W. Oosterbaan, and K. van der Borg. 1992. “Accurate Dating of Organic Deposits by AMS 14C Measurement of Macrofossils.” *Radiocarbon* **34** (3): 566–77.
- Trauth, M, A Bergner, V Foerster, A Junginger, M Maslin, and F Schaebitz. 2015. “Episodes of Environmental Stability versus Instability in Late Cenozoic Lake Records of Eastern Africa.” *Journal of Human Evolution* **87**: 21–31. <https://doi.org/10.1016/J.JHEVOL.2015.03.011>.
- Trauth, Martin H., Verena Foerster, Annett Junginger, Asfawossen Asrat, Henry F. Lamb, and Frank Schaebitz. 2018. “Abrupt or Gradual? Change Point Analysis of the Late Pleistocene–Holocene Climate Record from Chew Bahir, Southern Ethiopia.” *Quaternary Research* **90** (2): 321–330. <https://doi.org/10.1017/qua.2018.30>.
- Trobajo, R., E. Clavero, V. Chepurinov, K. Sabbe, D. Mann, S. Ishihara, and E. Cox. 2009. “Morphological, genetic and mating diversity within the widespread bioindicator *Nitzschia palea* (Bacillariophyceae)”. *Phycologia* **48** (6): 443–459. DOI: 10.2216/08-69.1.
- Trobajo, R., L. Rovira, L. Ector, C. Wetzel, M. Kelly, and D. Mann. 2013. “Morphology and identity of some ecologically important small *Nitzschia* species”. *Diatom Research* **28** (1): 37–59. DOI: 10.1080/0269249X.2012.734531.
- Tuchman, Nancy C., Marc A. Schollett, Steven T. Rier, and Pamela Geddes. 2006. “Differential Heterotrophic Utilization of Organic Compounds by Diatoms and Bacteria under Light and Dark Conditions.” *Hydrobiologia* **561** (1): 167–77. <https://doi.org/10.1007/s10750-005-1612-4>.
- Umer, M., H. F. Lamb, R. Bonnefille, A. M. Lézine, J. J. Tiercelin, E. Gibert, J. P. Cazet, and J. Watrin. 2007. “Late Pleistocene and Holocene Vegetation History of the Bale Mountains, Ethiopia.” *Quaternary Science Reviews* **26** (17–18): 2229–46. <https://doi.org/10.1016/j.quascirev.2007.05.004>.
- Umer, M, and R Bonnefille. 1998. “A Late Glacial/Late Holocene Pollen Record from a Highland Peat at Tamsaa, Bale Mountains, South Ethiopia.” *Global and Planetary Change*

16–17: 121–29. [https://doi.org/10.1016/S0921-8181\(98\)00025-3](https://doi.org/10.1016/S0921-8181(98)00025-3).

Ummenhofer, C., A, Gupta, M, England, and C, Reason. 2009. "Contributions of Indian Ocean Sea Surface Temperatures to Enhanced East African Rainfall". *Journal of Climate* **22**: 993-1013. DOI: 10.1175/2008JCLI2493.1.

Ureggo, D., M, Bush, M, Silman, A, Correa-Metrio, M-P, Ledru, F, Mayle, G, Paduano, and B, Valencia. 2009. "Millennial-Scale Ecological Changes in Tropical South America Since the Last Glacial Maximum". In: "Past Climate Variability in South America and Surrounding Regions". Edited by F. Vimeux, S, Florence, and M, Khodri. Netherlands: Springer.

Urrutia, R., A, Araneda, F, Cruces, L, Torres, L, Chirinos, H, Treutler, N, Fagel, S, Bertrand, I, Alvial, R, Barra, and E, Chapron. 2007. "Changes in diatom, pollen, and chironomid assemblages in response to a recent volcanic event in Lake Galletué (Chilean Andes)". *Limnologia*, **37** (1): 49-62. <https://doi.org/10.1016/j.limno.2006.09.003>.

van Dam, Herman, Adrienne Mertens, and Jos Sinkeldam. 1994. "A Coded Checklist and Ecological Indicator Values of Freshwater Diatoms from The Netherlands." *Netherlands Journal of Aquatic Ecology* **28** (1): 117–33. <https://doi.org/10.1007/BF02334251>.

Vanneste, T., O, Michelsen, B, Graae, M, Kyrkjeeide, H, Holien, K, Hassel, S, Lindmo, R, Kapas, and P, De Frenne. 2017. "Impact of climate change on alpine vegetation of mountain summits in Norway". *Ecological Research* **32** (4): 579-593. <https://doi.org/10.1007/s11284-018-1596-y>.

Vélez-Agudelo, C., M, Espinosa, R, Fayo, and F, Isla. 2017. "Modern diatoms from a temperate river in South America: the Colorado River (North Patagonia, Argentina)". *Diatom Research* **32** (2): 133-152. <https://doi.org/10.1080/0269249X.2017.1321046>.

Verschuren, D., and J. Russell. 2009. "Paleolimnology of African Lakes: Beyond the Exploration Phase." *PAGES News* **17** (3): 112–14.

Verschuren, Dirk. 2003. "Lake-Based Climate Reconstruction in Africa: Progress and Challenges." *Hydrobiologia* **500** (1–3): 315–30. <https://doi.org/10.1023/A:1024686229778>.

Verschuren, Dirk, Kathleen R. Laird, and Brian F. Cumming. 2000. "Rainfall and Drought in Equatorial East Africa during the Past 1,100." *Nature* **403** (6768): 410–14. <https://doi.org/10.1038/35000179>.

Vincens, Annie, Yannick Garcin, and Guillaume Buchet. 2007. "Influence of Rainfall Seasonality on African Lowland Vegetation during the Late Quaternary: Pollen Evidence from Lake Masoko, Tanzania." *Journal of Biogeography* **34** (7): 1274–88.

<https://doi.org/10.1111/j.1365-2699.2007.01698.x>.

Viste, Ellen, Diriba Korecha, and Asgeir Sorteberg. 2013. "Recent Drought and Precipitation Tendencies in Ethiopia." *Theoretical and Applied Climatology* **112** (3–4): 535–51. <https://doi.org/10.1007/s00704-012-0746-3>.

Votava, Jillian E, Thomas C Johnson, and Robert E Hecky. 2017. "Holocene Carbonate Record of Lake Kivu Reflects the History of Hydrothermal Activity." *Proceedings of the National Academy of Sciences of the United States of America* **114** (2): 251–56. <https://doi.org/10.1073/pnas.1609112113>.

Wagner, B., V, Weinrich, F, Viehberg, A, Junginger, A, Kolvenbach, J, Rethemeyer, F, Schaebitz, and G, Schmiedl. 2018. " Holocene rainfall runoff in the central Ethiopian highlands and evolution of the River Nile drainage system as revealed from a sediment record from Lake Dendi". *Global and Planetary Change*, **163**: 29-43. DOI: 10.1016/j.gloplacha.2018.02.003.

Walker, M, M. Berkelhammer, S. Björck, L. C. Cwynar, D. A. Fisher, A. J. Long, J. J. Lowe, R. M. Newnham, S. O. Rasmussen, and H. Weiss. 2012. " Formal subdivision of the Holocene Series/Epoch: a Discussion Paper by a Working Group of INTIMATE (Integration of ice-core, marine and terrestrial records) and the Subcommittee on Quaternary Stratigraphy (International Commission on Stratigraphy)". *Journal of Quaternary Science* **27** (7): 649-659. <https://doi.org/10.1002/jqs.2565>.

Wang, Luo, Patrick Rioual, Virginia N. Panizzo, Houyuan Lu, Zhaoyan Gu, Guoqiang Chu, Deguang Yang, Jingtai Han, Jiaqi Liu, and Anson W. Mackay. 2012. "A 1000-Yr Record of Environmental Change in NE China Indicated by Diatom Assemblages from Maar Lake Erlongwan." *Quaternary Research* **78** (1): 24–34. <https://doi.org/10.1016/J.YQRES.2012.03.006>.

Weldeab, Syee, David W Lea, Ralph R Schneider, and Nils Andersen. 2007. "55,000 Years of West African Monsoon and Ocean Thermal Evolution." *Science* **316** (5829): 1303–7.

Weldeab, Syee, R, Schneider, M, Kolling, and G, Wefer. 2005. "Holocene African droughts relate to eastern equatorial Atlantic cooling". *Geology* **33** (12): 981-984. <https://doi.org/10.1130/G21874.1>.

Weldeab, Syee, V, Menke, and G, Schmiedl. 2014. " The pace of East African monsoon evolution during the Holocene". *Geophysical Research Letters* **41** (5): 1724-1734. <https://doi.org/10.1002/2014GL059361>.

- Werdecker, J. 1962. "Eine Durchquerung des Goba-Massivs in Südäthiopien". Hermann von Wissmann-Festschr. pp. 132–144.
- Wickham, H. 2016. "ggplot2: Elegant Graphics for Data Analysis". New York: Springer-Verlag.
- Wiik, E., H, Bennion, C, Sayer, T, Davidson, S, Clarke, S, McGowan, S, Prentice, G, Simpson, and L, Stone. 2015. " The coming and going of a marl lake: multi-indicator palaeolimnology reveals abrupt ecological change and alternative views of reference conditions". *Frontiers in Ecology and Evolution* **3**. doi:10.3389/fevo.2015.00082.
- Wilke, C. 2018. "cowplot: Streamlined Plot Theme and Plot Annotations for 'ggplot2'". R package version 0.9.3. <https://CRAN.R-project.org/package=cowplot>.
- Williams, David. M., D, Chudaev, and M, Gololobova. 2009. " *Punctatstriata Glubokoensis* spec. nov., a new species of "Fragilarioid" diatom from Lake Glubokoe, Russia". *Diatom Research* **24** (2): 479-485. <https://doi.org/10.1080/0269249X.2009.9705814>.
- Williams, David M., and Frank E. Round. 1987. "Revision of the Genus *Fragilaria*." *Diatom Research* **2** (2): 267–88. <https://doi.org/10.1080/0269249X.1987.9705004>.
- Williams, David. M., and J. Patrick, Kocielek. 2007. " Pursuit of a natural classification of diatoms: History, monophyly and the rejection of paraphyletic taxa". *European Journal of Phycology* **42** (3): 313-319.
- Winder, Monika, John E Reuter, and S. Geoffrey Schladow. 2009. "Lake Warming Favours Small-Sized Planktonic Diatom Species." *Proceedings of the Royal Society B: Biological Sciences* **276** (1656): 427–35. <https://doi.org/10.1098/rspb.2008.1200>.
- Winkler, D., Kenneth J. Chapin, and Lara M. Kueppers. 2016. "Soil moisture mediates alpine life form and community productivity responses to warming". *Ecology* **97** (6): 1553-1563. <https://doi.org/10.1890/15-1197.1>.
- Wolfenden, Ellen, Cynthia Ebinger, Gezahegn Yirgu, Alan Deino, and Dereje Ayalew. 2004. "Evolution of the Northern Main Ethiopian Rift: Birth of a Triple Junction." *Earth and Planetary Science Letters* **224**: 213–28. <https://doi.org/10.1016/j.epsl.2004.04.022>.
- Wolff, C, G, Haug, A, Timmermann, J, Damste, A, Brauer, D, Sigman, M, Cane, and D, Verschuren. 2011. " Reduced Interannual Rainfall Variability in East Africa During the Last Ice Age". *Science* **333** (6043): 743-747. DOI: 10.1126/science.1203724.
- Wolin, J, and J Stone. 2010. "Diatoms as Indicators of Water-Level Change in Freshwater

- Lakes." In *The Diatoms Applications to the Environmental and Earth Sciences*, edited by E Stoermer and J Smol, 183–202. Cambridge: Cambridge University Press.
- Woltering, Martijn, Thomas C Johnson, Josef P Werne, Stefan Schouten, and Jaap S Sinninghe Damsté. 2011. "Late Pleistocene Temperature History of Southeast Africa: A TEX 86 Temperature Record from Lake Malawi." *Palaeogeography, Palaeoclimatology, Palaeoecology* **303**: 93–102. <https://doi.org/10.1016/j.palaeo.2010.02.013>.
- Wood, R. B., R. M. Baxter, and M. V. Prosser. 1984. "Seasonal and Comparative Aspects of Chemical Stratification in Some Tropical Crater Lakes, Ethiopia." *Freshwater Biology* **14** (6): 551–73. <https://doi.org/10.1111/j.1365-2427.1984.tb00176.x>.
- Wood, R. B., M. V. Prosser, and R. M. Baxter. 1976. "The Seasonal Pattern of Thermal Characteristics of Four of the Bishoftu Crater Lakes, Ethiopia." *Freshwater Biology* **6** (6): 519–30. <https://doi.org/10.1111/j.1365-2427.1976.tb01643.x>.
- Wood, R. B., and J. F. Talling. 1988. "Chemical and Algal Relationships in a Salinity Series of Ethiopian Inland Waters." *Hydrobiologia* **158** (1): 29–67. <https://doi.org/10.1007/BF00026266>.
- Woodbridge, Jessie, and Neil Roberts. 2010. "Linking Neo- and Palaeolimnology: A Case Study Using Crater Lake Diatoms from Central Turkey." *Journal of Paleolimnology* **44** (3): 855–71. <https://doi.org/10.1007/s10933-010-9458-9>.
- Wooller, M., D. L. Swain, K. J. Ficken, A. D. Q. Agnew, F. A. Street-Perrott, and G. Eglinton. 2003. "Late Quaternary vegetation changes around Lake Rutundu, Mount Kenya, East Africa: evidence from grass cuticles, pollen and stable carbon isotopes." *Journal of Quaternary Science* **18** (1): 3-15. <https://doi.org/10.1002/jqs.725>.
- Wright, H. E., D. H. Mann, and P. H. Glaser. 1984. "Piston Corers for Peat and Lake Sediments." *Ecology* **65** (2): 657–659.
- Yin, Jeffrey H, and David S Battisti. 2001. "The Importance of Tropical Sea Surface Temperature Patterns in Simulations of Last Glacial Maximum Climate*." *American Meteorological Society* **14**: 565–81.
- Zervas, Dimitrios, Gary J. Nichols, Robert Hall, Helen R. Smyth, Charlotta Lühthje, and Fionn Murtagh. 2009. "SedLog: A Shareware Program for Drawing Graphic Logs and Log Data Manipulation." *Computers & Geosciences* **35** (10): 2151–59. <https://doi.org/10.1016/J.CAGEO.2009.02.009>.
- Zha, Y., J. Gao, and Y. Zhang. 2005. "Grassland productivity in an alpine environment in

response to climate change". *Area* **37** (3): 332-340. <https://doi.org/10.1111/j.1475-4762.2005.00637.x>.

Zhang, Y., C, Peng, Z, Wang, J, Zhang, L, Li, S, Huang, and D, Li. 2018. " The Species-Specific Responses of Freshwater Diatoms to Elevated Temperatures Are Affected by Interspecific Interactions". *Microorganisms* **6** (3): 82. DOI 10.3390/microorganisms6030082.

Zolitschka, Bernd, Pierre Francus, Antti E K Ojala, and Arndt Schimmelmann. 2015. "Varves in Lake Sediments a Review." *Quaternary Science Reviews* **117**: 1–41. <https://doi.org/10.1016/j.quascirev.2015.03.019>.

Appendices

Appendix 1. Confirmation of accepted manuscript (online access as of 2020) by journal editor-in-chief (and full manuscript below) for the taxonomy of *Nitzschia fenestralis* sp. nov. (Grady et al. 2020).

Fottea

Editor: Prof. RNDr. A. Pouličková, CSc., Palacký University Olomouc, Czech Republic
aloisie.poulickova@upol.cz

Confirmation that paper

Nitzschia fenestralis: A new diatom species abundant in the Holocene sediments of an eastern African crater lake

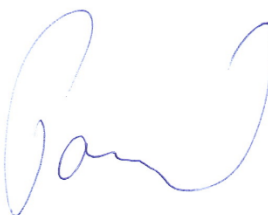
By

D. Grady, D.G. Mann, R. Trobajo

has been accepted for Fottea and will appear in Volume 20 in 2020.

Prof. RNDr. A. Pouličková, CSc.
Editor in chief, Czech Phycological Society

Redakce časopisu FOTTEA
České algologické spol.
Šlechtitelů 11
783 71 Olomouc

9.9.2019 

***Nitzschia fenestralis*: A new diatom species abundant in the Holocene sediments of an eastern African crater lake**

D. GRADY^{1,*}, David G. MANN^{2,3} & Rosa TROBAJO³

¹ *Department of Geography and Earth Sciences, Aberystwyth University, Aberystwyth, SY23 3DB, Wales*

² *Royal Botanic Garden Edinburgh, Edinburgh, EH3 5LR, Scotland*

³ *Marine and Continental Waters, Institute for Food and Agricultural Research and Technology (IRTA), Crta de Poble Nou Km 5.5, Sant Carles de la Ràpita, Catalonia, Spain*

*corresponding author: gradydai524@gmail.com

Abstract

Nitzschia is common in the phytoplankton of several East African lakes. A new species, *Nitzschia fenestralis*, sp. nov. D. GRADY, D.G. MANN & TROBAJO was encountered at numerous depths in a 16 m sediment core from Lake Babogaya, Ethiopia and is described using light and scanning electron microscopy. It is compared with several other morphologically similar taxa described from East and Central Africa (especially *N. aequalis*, *N. mediocris*, *N. obsoleta* and *N. fabiennejansseniana*), and from Europe (*N. fruticosa*). An unusual feature of some of these species (*N. fenestralis*, *N. obsoleta* and *N. fabiennejansseniana*) is that in the raphe canal each stria is represented by two narrower areolae (alternatively interpreted as a single subdivided areola). It is this feature that suggested the name of the new species (through the resemblance to a series of sash windows). Another characteristic of *N. fenestralis* and *N. obsoleta*, apparently never reported previously in any diatom, is that the more advalvar bands end approximately halfway along the frustules, rather than at the poles. In most respects (shape and size, stria and fibula densities, valve and girdle structure), *N. fenestralis* and *N. obsoleta* are very similar, but confusion is unlikely because they differ in whether central raphe endings are present (*N. fenestralis*) or absent (*N. obsoleta*). In *Nitzschia fenestralis*, and perhaps to a lesser extent in *N. obsoleta*, the striae usually become strongly radiate towards the poles. A

preliminary assessment, based on the literature, suggests that *N. fabiennejansseniana* may be synonymous with *N. obsoleta*, which was described earlier.

Key words: Africa, girdle structure, Lake Babogaya, morphology, new species, *Nitzschia*, plankton, taxonomy.

Introduction

Lake sedimentary archives have long been recognized, and regularly used, as the principal source of information in reconstructing the past climate and environments of tropical Africa (VERSCHUREN 2003). The focus of these reconstructions has varied from long-term glacial–interglacial dynamics through the Quaternary, to short-term centennial to inter-annual scales in order to understand the regional responses to natural shifts in climate; these reconstructions are relevant to current anthropogenic climate change and the role of climate in the development and evolution of humans through time.

Since it is not possible to make direct measurements of past environments, palaeoenvironmental proxies are needed and several characteristics of diatoms make them particularly useful. Their utility in understanding and reconstructing environmental conditions in arid and semi-arid environments has been outlined by GASSE et al. (1997). Warmer, tropical waters facilitate plankton communities rich in *Nitzschia* spp., unlike the waters of temperate and polar regions (RICHARDSON 1968; KILHAM et al. 1986). The abundance of *Nitzschia* in modern eastern African assemblages is well documented from surveys in lakes Kivu (SARMENTO et al. 2006), Victoria (KLING et al. 2001; STAGER et al. 2009) and Tanganyika (COCQUYT & VYVERMAN 2005), and more generally across the continent (GASSE 1986; MILLS & RYVES 2012). Their importance has also been documented in fossil assemblages. For example, high abundances of *Nitzschia* spp. have been a feature in the flora of Lake Victoria for 10,000–11,400 years (STAGER et al. 1997; 2003) and for the past 25,000 years in Lake Challa (MILNE 2007; WOLFF et al. 2014).

Nitzschia generally lack many distinguishing features, with their close morphological similarities making them notoriously difficult to accurately identify under the light microscope (LM). However, extensive scanning electron microscope (SEM) work on many

taxa (e.g. references in TROBAJO et al. 2013) have revealed multiple delicate morphological features not visible under LM that are useful in identifying and categorizing *Nitzschia* species. Thus, for example, use of SEM has facilitated the descriptions of several new *Nitzschia* species from lakes Victoria (SITOKI et al. 2013) and Challa (COCQUYT & RYKEN 2017).

Recent palaeolimnological analyses conducted at an eastern African crater lake, Lake Babogaya (GRADY et al. in prep.), have revealed another example of *Nitzschia* dominance (100% of total diatom abundance in some samples) in assemblages through the last 5,000 years of the Holocene. During these analyses, an abundant taxon (>50% abundance in several samples; see results) was observed throughout the record that does not exactly match any previously described *Nitzschia* species, though it resembles a number of species described from Africa and elsewhere by HUSTEDT (1949, 1957). In order to establish the taxonomy of the Babogaya specimens, they were studied in detail by light and scanning electron microscopy (LM and SEM) and compared with the type material of selected other, morphologically similar taxa. The aims of this paper are to: 1) describe a new species, *Nitzschia fenestralis*, from Lake Babogaya; (2) highlight how it differs from similar *Nitzschia* species; (3) comment on the temporal and spatial occurrence of *N. fenestralis*; and (4) highlight particularly unusual features of the new species, including any that may suggest which other species are its closest relatives. In order to help establish how *N. fenestralis* differs from other similar species, we borrowed type material of *N. obsoleta* HUSTEDT, *N. aequalis* HUSTEDT, *N. mediocris* HUSTEDT and *N. fruticosa* HUSTEDT. However, although the results of these analyses update the original works of HUSTEDT (1949) and SIMONSEN (1987) and may be useful for further studies related to the identification of problematic *Nitzschia* taxa, it was not our aim to make a full analysis of these species, which will require much further study. We give the formal description of *N. fenestralis* at the beginning of the Results and Discussion section, so that the name can be used throughout the remainder of the paper.

Methods & materials

Study site

The samples studied came from a core taken at Lake Babogaya, Ethiopia (Fig. 1). Lake Babogaya (also known as Bishoftu Guda or Pawlo), is a 65 m deep maar lake at an altitude of 1860 m above sea level, one of several crater lakes in Bishoftu, ~50 km SE of Addis Ababa. The local climate is monsoonal with distinct, pronounced wet and dry seasons (VISTE et al. 2013). Characteristic of many crater lakes, Lake Babogaya has steep slopes with a very small catchment area and no inflowing rivers or streams. Multiple researchers have conducted comprehensive investigations into the limnology of these crater lakes (BAXTER et al. 1965; WOOD et al. 1976, 1984; WOOD & TALLING 1988; LAMB et al. 2002; LEMMA 2009), and as a result the hydrochemistry and seasonal variations of the relatively fresh (ca. 750–900 $\mu\text{s cm}^{-1}$), alkaline (8.7–9.2 pH) Lake Babogaya are well understood (Table 1).

Lake Babogaya develops thermal stratification during March through to November, leading to the formation of indistinct thermoclines at 11–16 m depth late in the summer wet season. The waters of the lake mix from November to February, during the dry season, associated with the evaporative and night-time radiative cooling under conditions of low humidity and low cloud cover, which is balanced with solar inputs. This mixing likely promotes algal photosynthesis and increased aragonite precipitation by bringing Ca and other nutrients from the hypolimnion to the surface. Presumably, it is this seasonal change in aragonite precipitation that has led to the formation of dark–light laminae in Lake Babogaya, as observed at neighbouring Lake Hora (LAMB et al. 2002). These laminated sediments offer the ability to reconstruct past environmental change at a high resolution. They are currently the subject of ongoing research using diatoms and geochemical data to reconstruct past hydrological conditions (GRADY et al., in prep).

Sample preparation and microscopy

A ca. 16 m core (BA-LC-2011; with a basal ^{14}C date of 5470 cal BP; Table S1) was extracted in October 2011 with a UWITEC corer by a team led by Prof. Frank SCHÄBITZ of Universität zu Köln.

Small 1 cm^3 sediment samples were taken from the Babogaya core where the problematic *Nitzschia* sp. was abundant (>50% of total counted valves) (Aberystwyth DGES palaeoecology sample codes: QDP 2000, QDP 2018, QDP 2056 and QDP 2075). Samples

were prepared for mounting with 70% nitric acid and rinsed (by decanting) with deionized water until samples were pH neutral. Aliquots of both Lake Babogaya sub-samples and type material were transferred to 21 mm and 13 mm coverslips and air-dried for LM and SEM analyses, respectively. Dried samples for SEM were fixed to aluminium stubs and sputtered with platinum for 70–80 s at 5 nm min⁻¹ (at 25 mA) using an Emitech K575X peltier coater.

LM observations and morphometric measurements were performed with a Zeiss Axio Imager M2 using a Plan-Apochromat ×100 objective (nominal numerical aperture: 1.4) with bright field and differential interference contrast optics; photographs were taken using an Axiocam HRc digital camera. Where it was important to obtain maximum resolution, especially to check the visibility of valve pores in LM, the condenser was oiled. Measurements were taken for *N. fenestralis* using the public domain Fiji (ImageJ distribution package) software (SCHINDELIN et al. 2012; RUEDEN et al. 2017).

SEM work was undertaken using a LEO Supra 55 model at 5 kV and 4–5 mm working distance. All samples from Lake Babogaya used in this study, both LM slides and SEM stubs, have been archived at the Royal Botanic Garden Edinburgh (RBGE, herbarium code E).

In order to check that *N. fenestralis* is distinct from species already published, type material (slide and unmounted material) of *N. aequalis* (slides 241/64 and 241/65 of sample A348 and slide 241/74 of sample A354), *N. mediocris* (slide 243/6 and sample A409), and *N. obsoleta* (slides 242/21 and 242/22 and sample A382) was borrowed from the HUSTEDT collection in the Alfred Wegener Institute, Bremerhaven.

Results and Discussion

***Nitzschia fenestralis* D. Grady, D.G. Mann et Trobajo sp. nov. (Figs 2–20, 23, 26, 30, 34, LM; 36–39, 41, 42, 45–49, SEM)**

LM description: Valves are narrow, 1.9–3.3 µm (average = 2.46 ± 0.29 µm), linear-lanceolate with parallel sides centrally in longer valves (Figs 2–4) and acutely rounded, or

sometimes slightly subrostrate poles. The length of the valve is 20–70 μm , but with the mean valve length being $40.65 \pm 9.38 \mu\text{m}$ ($n = 210$). Fibulae short and spaced regularly, with 12–14 in 10 μm ; the central pair of fibulae are no more widely spaced than the others ($n = 210$). Striae (and even the areolae too: Figs 26, 30) are visible under LM with good optics, but counted in this study under SEM, numbering 32–35 in 10 μm ($n = 60$). All morphology metrics are available in Table 2.

SEM observations: The fibulae are squarish and connected on each side of the raphe by a narrow longitudinal ridge ($n = 60$; Figs 46, S5, S6). The areolae adjacent to the raphe (i.e. on the raphe canal) are divided in two, parallel to the raphe ($n = 60$; Figs 45, 47, S1–4). The raphe is continuous from pole to pole (Figs 41, 42, 45, S2, S3), agreeing with the absence of a wider central fibula spacing ($n = 32$), and sits on a shallow keel at the junction between the mantle and the valve face (Figs 42, 45); it curves slightly at the poles (Fig. 47). The striae are uniseriate, composed of small round areolae (Figs 42, 45, 46, 49, S2–6). In all of the 60 samples examined by SEM, the areolae lacked hymenes (e.g. Figs 45–47). We interpret this as a consequence of dissolution and that hymenes are present in intact organisms and frustules (cf. *N. obsoleta*: Fig. 50). The striae continue on to the valve mantle but are interrupted by a small ridge on the junction between the mantle and valve face (Figs 49, S4). The striae are parallel for most of the valve but become strongly radiate at the poles (Figs 36–39, $n = 45$), this feature can also be seen in LM with good optics. There is often a fault in the striation near the centre of the valve (Fig. 36). A small helictoglossa is present at the ends of the raphe internally on the internal side of the valve (Fig. S5; $n = 35$). Many loose or attached girdle bands were observed during SEM, each possessing two rows of small areolae (Figs 48, 49, S7; $n = 14$). Unlike in most diatoms, the open ends of the first two bands were positioned approximately halfway along the side of the frustule, rather than at the poles (Fig. 49).

Holotype: Slide E6092/1 Herbarium, Royal Botanic Garden Edinburgh, Scotland, from 596 cm depth (~3,000 cal BP) in the BA-LC-2011 core. The holotype specimen is shown in Fig. 9 and is located at England Finder J40, between centre and 2. See Fig. S9 for a context image.

Isotype: Slide Zu11/26 Hustedt Collection, Bremerhaven, Germany.

Type locality: Lake Babogaya (08° 47' 08" N, 38° 59' 38.5" E), Ethiopia: sediment core sample (present throughout from ~5400 cal BP at the base of core to the core top at ~600 cal BP). The species is also present at 14.7% relative abundance (slide number QDP 885: Aberystwyth University DGES collection) in the top 1 cm of a surface core taken in 1998 (GRADY, unpublished data) suggesting the species is likely extant; however, further work is required to confirm this.

Distribution: only reported from Lake Babogaya to the authors' knowledge (but see our comments below on a similar diatom reported by GASSE).

Etymology: the specific epithet given to this taxon refers to the resemblance of the divided areolae to small sash windows, with the pores lacking plates looking like multiple rows of the windows when open.

Morphology of *N. fenestralis* and similar species

The samples from the Lake Babogaya core were very rich in *N. fenestralis* and it seems there is a continuous series of valves illustrating what we think are the changes that occur during the life cycle (Figs 2–20). As has been found in many *Nitzschia* species (GEISSLER 1970a, b; TROBAJO et al. 2011, 2013; ROVIRA et al. 2015) the length of *N. fenestralis* varies considerably due to the life cycle whereas the width alters much less (both relatively and absolutely; see Figs 2–15). Consequently, the shape of the cells is rather different at the two ends of the size reduction series and if either end was seen in isolation it would be easy to think they belong to different species.

An unusual feature of *N. fenestralis* is that the striae are obviously oblique to the apical axis towards the poles (Figs 36–39; also detectable in Figs 2–15). This is something that we hadn't noticed before in any other long, linear *Nitzschia* species. Interestingly, it is also present in *N. obsoleta*, though less strongly developed (Figs 40, 43), and perhaps also in the recently described *N. fabiennejansseniana* (COCQUYT & RYKEN 2017; figs 32, 33).

Furthermore, in terms of morphometrics (length, width, stria and fibula density: Table 2, Fig. 51), as well as in valve outline, *N. fenestralis*, *N. obsoleta* and *N. fabiennejansseniana* are similar (Figs 34, 35; COCQUYT & RYKEN 2017, figs 2–29). However, they are clearly

separated by the presence (*N. obsoleta* and *N. fabiennejansseniana*) or absence (*N. fenestralis*) of central raphe endings (Figs 26, 27, 41–44, and see COCQUYT & RYKEN 2017, figs 30, 31). The taxonomic utility of this character was already recognized in the publication where *N. obsoleta* was first described (HUSTEDT 1949, p. 134) and often since (e.g. KRAMMER & LANGE-BERTALOT 1988; TROBAJO et al. 2004; TROBAJO et al. 2013).

Interestingly, under SEM, these three taxa (*N. fenestralis*, *N. obsoleta* and *N. fabiennejansseniana*) also share the distinctive feature of having areolae in the raphe canal divided in two (Figs 42, 45 and 47 for *fenestralis*, Figs 44 and 50 for *obsoleta* and COCQUYT & RYKEN 2017, figs 30–33 for *fabiennejansseniana*). We also observed this feature for *N. mediocris* (not illustrated); however, this taxon, despite the absence of central raphe endings, is separated from *N. fenestralis* by its narrower valves and much higher stria density (Table 2, Figs 24, 25, 33). Although *N. fenestralis* can be separated from *N. obsoleta* and *N. fabiennejansseniana* by the absence of central raphe endings, it is less clear whether *N. obsoleta* and *N. fabiennejansseniana* can be separated from each other. There is no obvious difference between them in valve structure and, as Table 2 shows, these two species cannot be separated by length, width, and fibula and stria density. Comparisons between these two species were not included in COCQUYT & RYKEN's (2017) paper describing *N. fabiennejansseniana* but it seems very likely to us that it is a later synonym of *N. obsoleta*. However, this issue was not the focus of our work and a final decision should await a more complete examination of both species.

When considering general valve outline, *N. aequalis* and *N. fruticosa* are also very similar to *N. fenestralis*, and also have a continuous raphe, however *N. aequalis* (Figs 21, 22) has much longer valves than *N. fenestralis*. Despite measuring 210 valves of *N. fenestralis* and scanning slides for longer specimens, the longest valves we found were ca 70 µm whereas the range recorded for *N. aequalis* by HUSTEDT (1949) was 80–130 µm (Table 2); the two valves that we measured of *N. aequalis* were also more finely striated (37 or 38 striae in 10 µm) than *N. fenestralis*, although HUSTEDT gave a wider range (Table 2). *Nitzschia fruticosa* has slightly wider valves and a higher fibula density than *N. fenestralis* (Table 2). The figures of *N. fruticosa* given by SIMONSEN (1987, pl. 661, figs 7–11) and KRAMMER &

LANGE-BERTALOT (1988, pl. 60, figs 8–12) show a diatom with more attenuated, narrower ends than *N. fenestralis* and striae that are parallel throughout.

Other somewhat similar taxa are:

In terms of valve outline, *N. pseudoaequalis* COCQUYT ET RYKEN, *N. intermissa* HUSTEDT, *N. bacata* HUSTEDT (especially *N. bacata* f. *linearis* HUSTEDT) are also similar to *N. fenestralis*. However, alongside morphometrics such as different stria density or valve width, critically all these taxa possess central raphe endings. Conversely, numerous taxa, such as *N. abonensis* FOGED, *N. etoshensis* CHOLNOKY, *N. asterionelloides* O. MÜLLER, share the lack of central raphe endings with *N. fenestralis* and are also similar in terms of valve outline (FOGED 1966; CHOLNOKY 1966). However, the stria and fibula density of these taxa are finer (*N. etoshensis* and *N. asterionelloides*) or coarser (*N. abonensis*) than those of *N. fenestralis*. Additionally, the widths of *N. etoshensis* (4–5.5 µm) and *N. asterionelloides* (1.6–1.8 µm) separate these species from *N. fenestralis* (1.9–3.3 µm).

In her seminal work on the diatoms of East Africa, GASSE (1986, pl. 35, fig. 13) illustrated a specimen with somewhat similar morphology to *N. fenestralis* which she placed in the broad *N. palea* complex as *N. aff. palea*, despite the taxa of this complex normally having rostrate apices (e.g. KRAMMER & LANGE-BERTALOT 1988; MORALES & HAMILTON 2002; TAYLOR *et al.* 2007, TROBAJO *et al.* 2009). Further work is needed to confirm whether *N. aff. palea* of GASSE is indeed *N. fenestralis* or not.

Noteworthy morphological features of *N. fenestralis*

As noted above, the radiate orientation of the striae towards the poles in *N. fenestralis* is apparently unusual in *Nitzschia*. However, it is possible that it has been overlooked elsewhere, especially in long delicate species. Whole valves are often illustrated only as LMs, while SEM images show only details of the ultrastructure (e.g. raphe structure, areolae, girdle bands). Thus, in the LMs of whole valves of *N. fabiennejansseniana* given by COCQUYT & RYKEN (2017) the striae are mostly invisible and the poles of this species are shown for only one valve in SEM (*ibid.*, figs 32, 33); this particular valve had radiate polar striae like *N. fenestralis* but it is unclear whether this is characteristic of *N.*

fabiennejansseniana or not and stria orientation is not mentioned in COCQUYT & RYKEN's (2017) description of the species.

The structure of the raphe canal is proving valuable for characterizing species of *Nitzschia* and related genera (e.g. TROBAJO *et al.* 2012, 2013). Several variants are known. In one, the raphe canal walls lack areolae altogether (e.g. in *Pseudo-nitzschia* and *Fragilariopsis*: e.g. MANN 1978). Elsewhere, there may be a single longitudinal row of areolae, one opposite each stria of the valve face (e.g. ROVIRA *et al.* 2015), several longitudinal rows (e.g. *N. sigmoidea*: MANN 1986, figs 3, 4), or a complex structure, in which each valve stria is represented within the raphe canal by a cluster of three or more small areolae (e.g. *N. fonticola*, *N. soratensis*: TROBAJO *et al.* 2006, 2013). The paired areolae in the raphe canal of *N. fenestralis* represent a further type, present also in *N. obsoleta* and *N. fabiennejansseniana* (if this is separate from *N. obsoleta*) and may perhaps be characteristic of a subgroup of *Nitzschia* that has not previously been recognized.

A further interesting feature, which we have never seen reported before in any other diatom, is the presence of short bands in both *N. fenestralis* and *N. obsoleta*, each band reaching from the pole to approximately half way along the girdle on either side. The material of *N. fenestralis* was too fragmented for us to be able to determine how many such bands there are in a theca: there are at least two. In *N. obsoleta* there are four, arranged alternately; only the much narrower fifth band is of normal length, extending around the whole circumference of the cell and open at one pole (Figs 50, S8).

Ecology and associated diatoms

All samples of the core studied contained *Nitzschia* species (Fig. 52) and in most of them they represented >30% of the diatom community; indeed, in a few samples *Nitzschia* made up nearly 100% of the total community (Fig. 52). As discussed above, *Nitzschia*-dominated waterbodies are not as unusual in tropical Africa as elsewhere, with the early classification of African lakes (HUSTEDT 1949; TALLING & TALLING 1965; RICHARDSON 1968) containing a whole class and sub-class of lakes partially characterised by high abundances of *Nitzschia* taxa (class III and subclass IIb) and also by lake alkalinity.

Nitzschia fenestralis was observed throughout the core record but was most abundant (>35% relative abundance) in samples between 300 and 800 cm sediment depth (Figs 52, 53) in association with the freshwater *Nitzschia paleacea* (GRUNOW) VAN HEURCK, *Nitzschia lancettula* O. MÜLLER and *Nitzschia gracilis* HANTZSCH *sensu* GASSE (1986). Among other species present with *Nitzschia fenestralis* in certain sections were predominantly freshwater taxa such as *Nitzschia palea* (KÜTZING) SMITH, *N.* “group latens” (*sensu* GASSE 1986), *Aulacoseira granulata* (EHRENBERG) SIMONSEN and *Fragilaria*-type taxa such as *Pseudostaurosira brevistriata* (GRUNOW) WILLIAMS & ROUND and *Ulnaria ulna* (KÜTZING) COMPÈRE.

Although it is important to note the role of numerous other environmental factors (such as water salinity and turbidity to name a couple), the distribution of diatom taxa in Africa have been linked with hydrochemistry in terms of alkalinity and pH, especially *Nitzschia* spp. (e.g. class IIb lakes in RICHARDSON (1968)). For example, based on their eastern African diatom dataset (initial dataset consisting of 156 samples containing 579 taxa across 98 sites), GASSE & TEKAIA (1983) suggest that *Pseudostaurosira brevistriata* and *Nitzschia lancettula*, taxa common alongside *N. fenestralis* in the Babogaya core, are indicator taxa for a lake pH of around 8 to 8.6, with the combined African dataset (GASSE et al. 1995; 282 samples containing 665 taxa across 164 sites) suggesting pH optima of 7.82 ± 1.02 and 8.51 ± 0.76 pH for *P. brevistriata* and *N. lancettula*, respectively. The same combined African dataset gives an optimum of ~ 7.6 pH for both *N. palea* and *N. paleacea*, species that are also common with *N. fenestralis*. However, the composition of a plankton community (including the abundance of *Nitzschia* species such as *N. paleacea*) is also influenced by nutrient availability (especially N, Si and P; e.g. KILHAM et al. 1986; VAN DAM et al. 1994; BAIER et al. 2004). Furthermore, factors such as lake water temperature and mixing are also important in controlling *Nitzschia* abundance (KILHAM et al. 1986; WOODBRIDGE & ROBERTS 2010), illustrating the complex, multifactorial influences on plankton composition and that further work is required to fully understand the ecology of *N. fenestralis*.

The genus *Nitzschia* is widely distributed and abundant in several types of ecosystems but is taxonomically difficult. *Nitzschia* species often have very few distinguishing

morphological characters that can be seen in LM, making them notoriously difficult to accurately identify. Even in SEM, their recognition can be difficult; not surprisingly, therefore, *Nitzschia* studied under LM are often identified at genus level only (or with “aff.” to similar species) in (palaeo)ecological and taxonomic studies (e.g. GASSE 1986; LEGESSE et al. 2002; MORALES & HAMILTON 2002; KRSTIĆ et al. 2012). However, the ability to recognize and differentiate a species is a prerequisite to fully understand and utilise the ecology of that species. The present study, in which a hitherto unknown diatom has been found to dominate the diatom assemblage of a lake for a large part of its history, illustrates what would be missed by not recognizing it as different from other species such as *N. obsoleta*, *N. aequalis*, etc. Only now that we can discriminate *N. fenestralis* from morphologically similar taxa is it possible to study its ecology and distribution, and therefore its potential use for investigating environmental changes (past and present) in this crater lake and perhaps elsewhere.

Acknowledgements

We are thankful to Professor Schäbitz of Universität zu Köln for use of the BA-LC-2011 core and Dr Bank Beszteri and Dr Andrea Burfeid for very kindly arranging loans of *Nitzschia* types from the Hustedt collection at the Alfred Wegener Institut, Bremerhaven, Holly Wynne, Patrick Robson, Alan Cookson and Frieda Christie are gratefully acknowledged for their assistance and time in preparing samples and operating the equipment required for this research. Dr. Sarah Davies and Professor Henry Lamb are thanked for their time in supervising the PhD of D. Grady and for their helpful comments on this manuscript. We would like to thank the anonymous reviewer whose helpful comments improved the manuscript. We appreciate the support given by the Masonic Charitable Foundation and Aberystwyth University in funding the studentship of D. Grady, including research time at the RBGE. The authors also acknowledge support from the CERCA Programme/Generalitat de Catalunya. The Royal Botanic Garden Edinburgh is supported by the Scottish Government’s Rural and Environment Science and Analytical Services Division.

References

- BAXTER, R.; PROSSER, M.; TALLING, J. & WOOD, R. (1965): Stratification in tropical African lakes at moderate altitude (1500 to 2000 m). – *Limnol. Oceanogr.* 10: 511–520.
- CHOLNOKY, B. (1966): Diatomeen assoziationen aus einigen Quellen in Südwest-Afrika und Bechuanaland. – *Nova Hedwigia, Beih.* 21: 163–244.
- COCQUYT, C. & RYKEN, E. (2017): Two new needle-shaped *Nitzschia* taxa from a deep East African crater lake. – *Diatom Res.* 32: 465–475. doi: 10.1080/0269249X.2017.1401009.
- COCQUYT, C. & VYVERMAN, W. (2005) Phytoplankton in Lake Tanganyika: a comparison of community composition and biomass off Kigoma with previous studies 27 years ago. – *J. Great Lakes Res.* 31: 535–546. doi: 10.1016/S0380-1330(05)70282-3.
- COCQUYT, C.; DE HAAN, M.; JAHN, R. & HINZ, F. (2012): *Nitzschia epiphytica*, *N. epiphyticoides* and *N. pseudepiphytica* (Bacillariophyta), three small diatoms from East and Central Africa. – *Phycologia* 51: 126–134. doi: 10.2216/10-61.1.
- FOGED, N. (1966): Freshwater diatoms from Ghana. – *Biol. Skr. Dan. Vid. Selsk.* 15 (1): 169 pp.
- GASSE, F. (1986): East African diatoms: taxonomy, ecological distribution. – J. Cramer, Berlin and Stuttgart.
- GASSE, F. & TEKAIA, F. (1983): Transfer functions for estimating paleoecological conditions (pH) from East African diatoms. – *Hydrobiologia* 103: 85–90. doi: 10.1007/BF00028433.
- GASSE, F.; JUGGINS, S. & KHELIFA, B. (1995): Diatom-based transfer functions for inferring past hydrochemical characteristics of African lakes. – *Palaeogeogr. Palaeoclimatol. Palaeoecol.* 117: 31–54. doi: 10.1016/0031-0182(94)00122-O.
- GASSE, F.; BARKER, P.; GELL, P.; FRITZ, S. & CHALIE, F. (1997): Diatom-inferred salinity in palaeolakes: an indirect tracer of climate change. – *Quat. Sci. Rev.* 16: 547–563. doi: 10.1016/S0277-3791(96)00081-9.
- GEISSLER, U. (1970a): Die Variabilität der Schalenmerkmale bei den Diatomeen. – *Nova Hedwigia*, 19: 623–773.
- GEISSLER, U. (1970b): Die Schalenmerkmale der Diatomeen. Ursachen ihrer Variabilität und Bedeutung für die Taxonomie. – *Nova Hedwigia, Beih.* 31: 511–35.

- HUSTEDT, F. (1949): Süßwasser-Diatomeen aus dem Albert-Nationalpark in Belgisch-Kongo. – Exploration du Parc National Albert, Mission H. Damas (1935–1936). Institut des Parcs Nationaux du Congo Belge, Bruxelles.
- HUSTEDT, F. (1957): Die Diatomeenflora des Flußsystems der Weser im Gebiet der Hansestadt Bremen. – Abh. Naturwiss. Ver. Bremen 34: 181–440.
- KLING, H.; MUGIDDE, R. & HECKY, R. (2001): Recent changes in the phytoplankton community of Lake Victoria in response to eutrophication. – In: MUNAWAR, M. & HECKY, R. (eds.) The great lakes of the world (GLOW): food-web, health and integrity. – pp. 47–65. Backhuys, Leiden, The Netherlands
- KRAMMER, K. & LANGE-BERTALOT, H. (1988): Bacillariophyceae: Teil 2: Bacillariaceae, Epithemiaceae, Surirellaceae. – In: Ettl, H., Gerloff, J., Heynig, H. & Mollenhauer, D. (eds) Süßwasserflora von Mitteleuropa, Band 2/2. – 596 pp. VEB Gustav Fischer, Jena.
- KRSTIĆ, S.; ZECH, W.; OBREHT, I.; SVIRČEV, Z. & MARKOVIĆ, S. (2012): Late Quaternary environmental changes in Helambu Himal, Central Nepal, recorded in the diatom flora assemblage composition and geochemistry of Lake Panch Pokhari. J. Paleolimnol. 47: 113–124.
- LAMB, H.; KEBEDE, S.; LENG, M.; RICKETTS, D.; TELFORD, R. & UMER, M. (2002): Origin and isotopic composition of aragonite laminae in an Ethiopian crater lake. – In: ODADA, E. & OLAGO, D. (eds) The East African Great Lakes: Limnology, Palaeolimnology and Biodiversity. – pp. 487–508. Springer, Dordrecht. doi: 10.1007/0-306-48201-0_20.
- LEGESSE, D.; GASSE, F.; RADA KOVITCH, O.; VALLET-COULOMB, C.; BONNEFILLE, R.; VERSCHUREN, D.; GIBERT, E. & BARKER, P. (2002): Environmental changes in a tropical lake (Lake Abiyata, Ethiopia) during recent centuries. – Palaeogeogr. Palaeoclimatol. Palaeoecol. 187: 233–258.
- LEMMA, B. (2009): Observations on the relations of some physico-chemical features and DVM of *Paradiaptomus africanus* in Lakes Bishoftu-Guda and Hora-Arsedi, Bishoftu, Ethiopia. – Limnologica 39: 230–243.
- MANN, D.G. (1978): Studies in the Nitzschiaceae (Bacillariophyta). – 2 vols, Ph.D. Dissertation. University of Bristol. Available online at https://rbg-web2.rbge.org.uk/algae/publications_mann_thesis.html
- MANN, D.G. (1986): *Nitzschia* subgenus *Nitzschia* (Notes for a monograph of the Bacillariaceae 2). – In: RICARD, M. (ed.), Proceedings of the 8th International Diatom Symposium. – pp. 215–226. O. Koeltz, Koenigstein.
- MILLS, K. & RYVES, D. (2012): Diatom-based models for inferring past water chemistry in western

- Ugandan crater lakes. – *J. Paleolimnol.* 48: 383–399. doi: 10.1007/s10933-012-9609-2.
- MILNE, I. (2007): Climate and environmental change inferred from diatom communities in Lake Challa (Kenya–Tanzania). – MSc thesis. Department of Biology, Queens University, Kingston, Ontario.
- MORALES, E. & HAMILTON, P. (2002): Seventh NAWQA Taxonomy Workshop on Harmonization of Algal Taxonomy. – Philadelphia, USA.
- RICHARDSON, J.L. (1968): Diatoms and lake typology in East and Central Africa. – *Int. Rev. ges. Hydrobiol. Hydrogr.* 53: 299–338.
- ROVIRA, L.; TROBAJO, R.; SATO, S.; IBÁÑEZ, C. & MANN, D.G. (2015): Genetic and physiological diversity in the diatom *Nitzschia inconspicua*. *J. Euk. Microbiol.* 62: 815–832. doi:10.1111/jeu.12240
- RUEDEN, C.; SCHINDELIN, J.; HINER, M.; DE ZONIA, B.; WALTER, A.; ARENA, E. & ELICEIRI, K. (2017): ImageJ2: ImageJ for the next generation of scientific image data. – *BMC Bioinformatics* 18: 529. doi: 10.1186/s12859-017-1934-z.
- SARMENTO, H.; ISUMBISHO, M. & DESCY, J.-P. (2006): Phytoplankton ecology of Lake Kivu (eastern Africa). – *J. Plankton Res.* 28: 815–829. doi: 10.1093/plankt/fbl017.
- SCHINDELIN, J.; ARGANDA-CARRERAS, I.; FRISE, E.; KAYNIG, V.; LONGAIR, M.; PIETZSCH, T.; PREIBISCH, S.; RUEDEN, C.; SAALFELD, S.; SCHMID, B.; TINEVEZ, J.; WHITE, D.; HARTENSTEIN, V.; ELICEIRI, K.; TOMANCAK, P. & CARDONA, A. (2012): Fiji: an open-source platform for biological-image analysis. – *Nature Methods* 9: 676–682. doi: 10.1038/nmeth.2019.
- SIMONSEN, R. (1987): Atlas and Catalogue of the Diatom Types of Friedrich Hustedt. – 3 vols. J. Cramer, Berlin & Stuttgart.
- SITOKI, L.; KOFLER, W. & ROTT, E. (2013): Planktonic needle-shaped *Nitzschia* species from Lake Victoria, Africa, revisited. – *Diatom Res.* 28: 165–174. doi: 10.1080/0269249X.2013.765509.
- STAGER, J.; COCQUYT, C.; BONNEFILLE, R.; WEYHENMEYER, C. & BOWERMAN, N. (2009): A late Holocene paleoclimatic history of Lake Tanganyika, East Africa. – *Quat. Res.* 72: 47–56. doi: 10.1016/j.yqres.2009.04.003.
- STAGER, J.; CUMMING, B. & MEEKER, L. (1997): A high-resolution 11,400-yr diatom record from Lake Victoria, East Africa. – *Quat. Res.* 47: 81–89. doi: 10.1006/QRES.1996.1863.
- STAGER, J.; CUMMING, B. & MEEKER, L. (2003): A 10,000-year high-resolution diatom record from Pilkington Bay, Lake Victoria, East Africa. – *Quat. Res.* 59: 172–181. doi: 10.1016/S0033-5894(03)00008-5.

- TALLING, J. & TALLING, I. (1965): The chemical composition of African lake waters. – *Int. Rev. ges. Hydrobiol. Hydrogr.* 50: 421–463.
- TAYLOR, J.; HARDING, W. & ARCHIBALD, C. (2007): An illustrated guide to some common diatom species from South Africa. – Pretoria.
- TROBAJO, R.; COX, E. & QUINTANA, X. (2004): The effect of some environmental variables on the morphology of *Nitzschia frustulum* (Bacillariophyta), in relation to its use as a bioindicator. – *Nova Hedwigia* 79: 433–45
- TROBAJO, R.; MANN, D.G.; CHEPURNOV, V.; CLAVERO, E. & COX, E.J. (2006): Taxonomy, life cycle, and auxosporulation of *Nitzschia fonticola* (Bacillariophyta). – *J. Phycol.* 42: 1353–1372. doi: 10.1111/j.1529-8817.2006.00291.x.
- TROBAJO, R., CLAVERO, E., CHEPURNOV, V.A., SABBE, K., MANN, D.G., ISHIHARA, S. & COX, E.J. (2009). Morphological, genetic and mating diversity within the widespread bioindicator *Nitzschia palea* (Bacillariophyceae). – *Phycologia* 48: 443–459. doi: 10.2216/08-69.1
- TROBAJO, R.; ROVIRA, L.; MANN, D.G. & COX, E.J. (2011): Effects of salinity on growth and on valve morphology of five estuarine diatoms. – *Phycol. Res.* 59: 83–90. doi: 10.1111/j.1440-1835.2010.00603.x
- TROBAJO, R.; MANN, D.G. & COX, E.J. (2012): Studies on the type material of *Nitzschia abbreviata* (Bacillariophyta). *Nova Hedwigia, Beih.* 141: 185–200.
- TROBAJO, R.; ROVIRA, L.; ECTOR, L.; WETZEL, C.; KELLY, M. & MANN, D.G. (2013): Morphology and identity of some ecologically important small *Nitzschia* species. – *Diatom Res.* 28: 37–59. doi: 10.1080/0269249X.2012.734531.
- VAN DAM, H.; MERTENS, A. & SINKELDAM, J. (1994): A coded checklist and ecological indicator values of freshwater diatoms from The Netherlands. – *Neth. J. Aquat. Ecol.* 28: 117–133. doi: 10.1007/BF02334251.
- WOLFF, C.; KRISTEN-JENNY, I.; SCHETTLER, G.; PLESSEN, B.; MEYER, H.; DULSKI, P.; NAUMANN, R.; BRAUER, A.; VERSCHUREN, D. & HAUG, G. (2014): Modern seasonality in Lake Challa (Kenya/Tanzania) and its sedimentary documentation in recent lake sediments. – *Limnol. Oceanogr.* 59: 1621–1636. doi: 10.4319/lo.2014.59.5.1621.
- VERSCHUREN, D. (2003): Lake-based climate reconstruction in Africa: progress and challenges. – *Hydrobiologia* 500: 315–330. doi: 10.1023/A:1024686229778.
- WOOD, R. & TALLING, J. (1988): Chemical and algal relationships in a salinity series of Ethiopian inland waters. – *Hydrobiologia* 158: 29–67. doi: 10.1007/BF00026266.

WOOD, R., PROSSER, M. & BAXTER, R. (1976): The seasonal pattern of thermal characteristics of four of the Bishoftu Crater Lakes, Ethiopia. – *Freshw. Biol.* 6: 519–530. doi: 10.1111/j.1365-2427.1976.tb01643.x.

WOOD, R.; BAXTER, R. & PROSSER, V. (1984): Seasonal and comparative aspects of chemical stratification in some tropical crater lakes Ethiopia. – *Freshw. Biol.* 14: 551–573. doi: 10.1111/j.1365-2427.1984.tb00176.x.

Supplementary material

The following supplementary material is available for this article:

Figs S1–S8. *Nitzschia fenestralis* and *N. obsoleta*, extra SEM micrographs.

Fig. S9. Context photograph for the holotype of *N. fenestralis*.

Table S1. AMS radiocarbon dates for the Lake Babogaya core.

Table 1. Hydrochemistry of the Debre Zeit area groundwater (Gr) and Lake Babogaya (BA).

	Conductivity (<i>k20</i> $\mu\text{S}/\text{cm}$)	pH	HCO_3^- - (<i>meq/L</i>)	Cl^- (<i>meq/L</i>)	SO_4^{2-} (<i>meq/L</i>)	CO_3^- (<i>meq/L</i>)	K^+ (<i>meq/L</i>)	Na^+ (<i>meq/L</i>)	Ca^{2+} (<i>meq/L</i>)	Mg^{2+} (<i>meq/L</i>)
Gr ¹	685	7.3	2.62	0.42	–	–	–	0.42	1.98	2.52
BA ¹	776	8.7–9.2	7.67	0.69	–	–	–	3.74	0.22	3.74
BA ²										
0 m	850 (± 30)	–	2.55	0.06	4.09	2.70	0.37	2.33	0.84	3.72
3 m	841 (± 28)	–	4.20	0.11	3.51	3.00	0.72	4.97	0.80	3.92
6 m	829 (± 15)	–	4.30	0.11	2.28	2.90	0.76	4.97	0.60	4.64
16 m	859 (± 14)	–	4.60	0.11	2.68	2.60	0.62	4.58	0.68	4.36
30 m	959 (± 12)	–	5.99	0.10	2.79	1.90	0.45	2.84	0.68	4.72
50 m	–	–	5.49	0.10	2.08	1.70	0.42	2.52	0.60	4.52

¹ Surface water in 1998, from LAMB *et al.* (2002).

² Surface waters to 50 m depth in 2001, from LEMMA (2009).

Table 2. Range (1 d.p; mean \pm s.d: 2 d.p) of *N. fenestralis* measurements in samples dominated by the species, compared to morphologically similar *Nitzschia* species. All measurements are given in μm . *nd* = not determined/documentated.

Taxon	<i>mediocris</i>		<i>fabiennejansseniana</i>	<i>obsoleta</i>		<i>fruticosa</i>	<i>aequalis</i>	<i>fenestralis</i>
Length	40–50		24–48.5	25–45	22.7–44.8 (33.68 \pm 4.83)	38–83	80–130	20–70.2 (40.65 \pm 9.38)
Width	1.5–2		2.1–2.8	2.5–3	2.1–3 (2.58 \pm 0.20)	2.5–4	3	1.9–3.3 (2.46 \pm 0.29)
Stria density (/10 μm)	<i>nd</i>	57–61 (58.36 \pm 1.34)	32–35	32–35	33–36 (34.66 \pm 0.72)	34 ¹	34–40	32–35 (33.25 \pm 0.88; n = 60)
Fibula density (/10 μm)	14–17 (mostly 16)		11–13 (commonly 12)	12–14	11–14 (12.66 \pm 0.75)	16–18	12–14 (mostly 12)	10–14 (12.09 \pm 0.72)
Gap in central fibulae?	no	no	yes	yes	yes	no	no	no
Areolae near raphe divided?	yes	?	yes	–	yes	?	?	yes
n =	–	14	–	–	50	–	?	210
Source	HUSTEDT (1949)	This study	COCQUYT & RYKEN (2017)	HUSTEDT (1949)	This study	HUSTEDT (1957), SIMONSEN (1987)	HUSTEDT (1949)	This study

¹ SIMONSEN (1987, p. 445) notes that, whereas HUSTEDT was apparently unable to resolve the striae of *N. fruticosa*, the striation is “comparatively coarse”, with c. 34 in 10 μm .

Figures

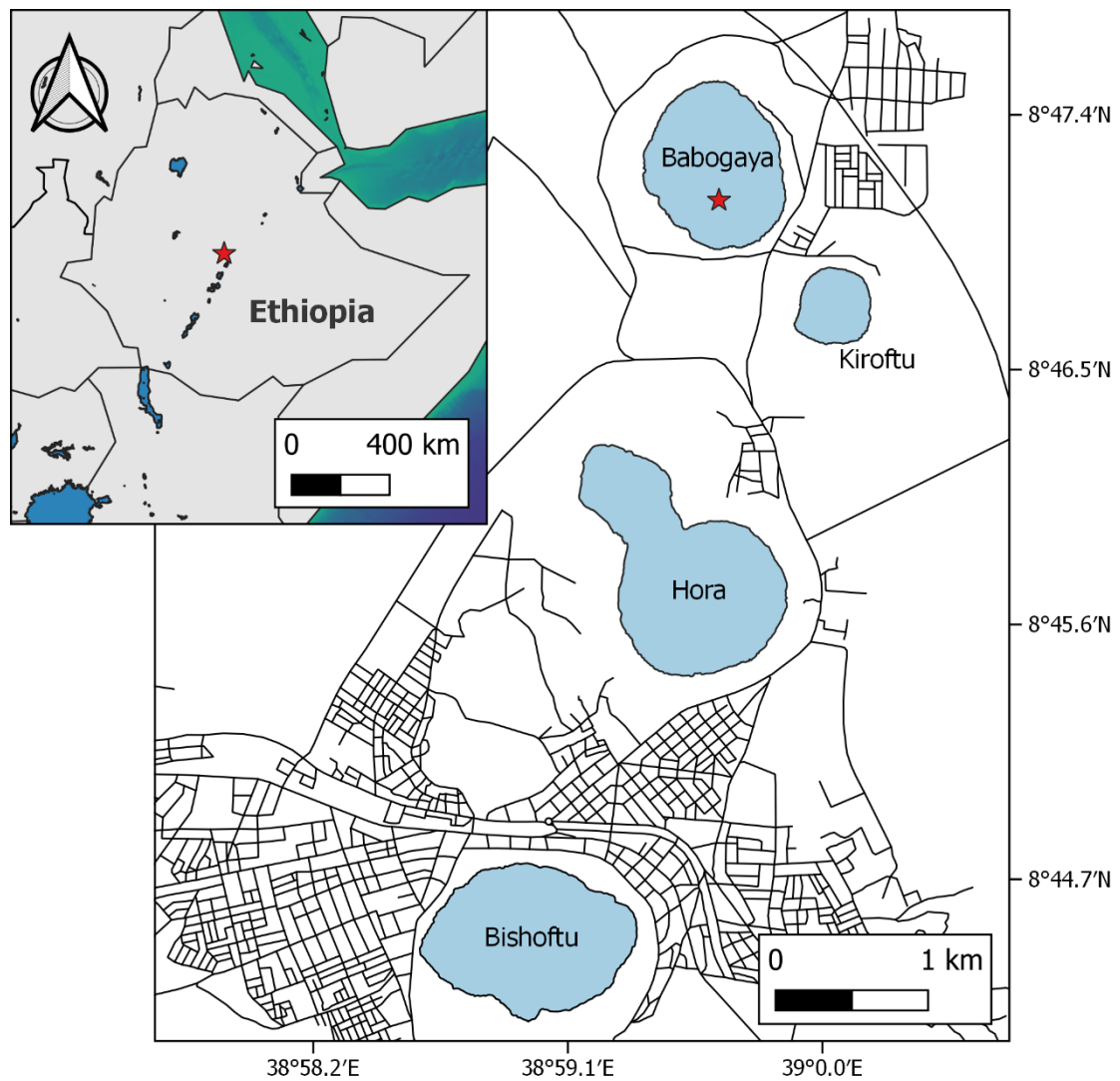
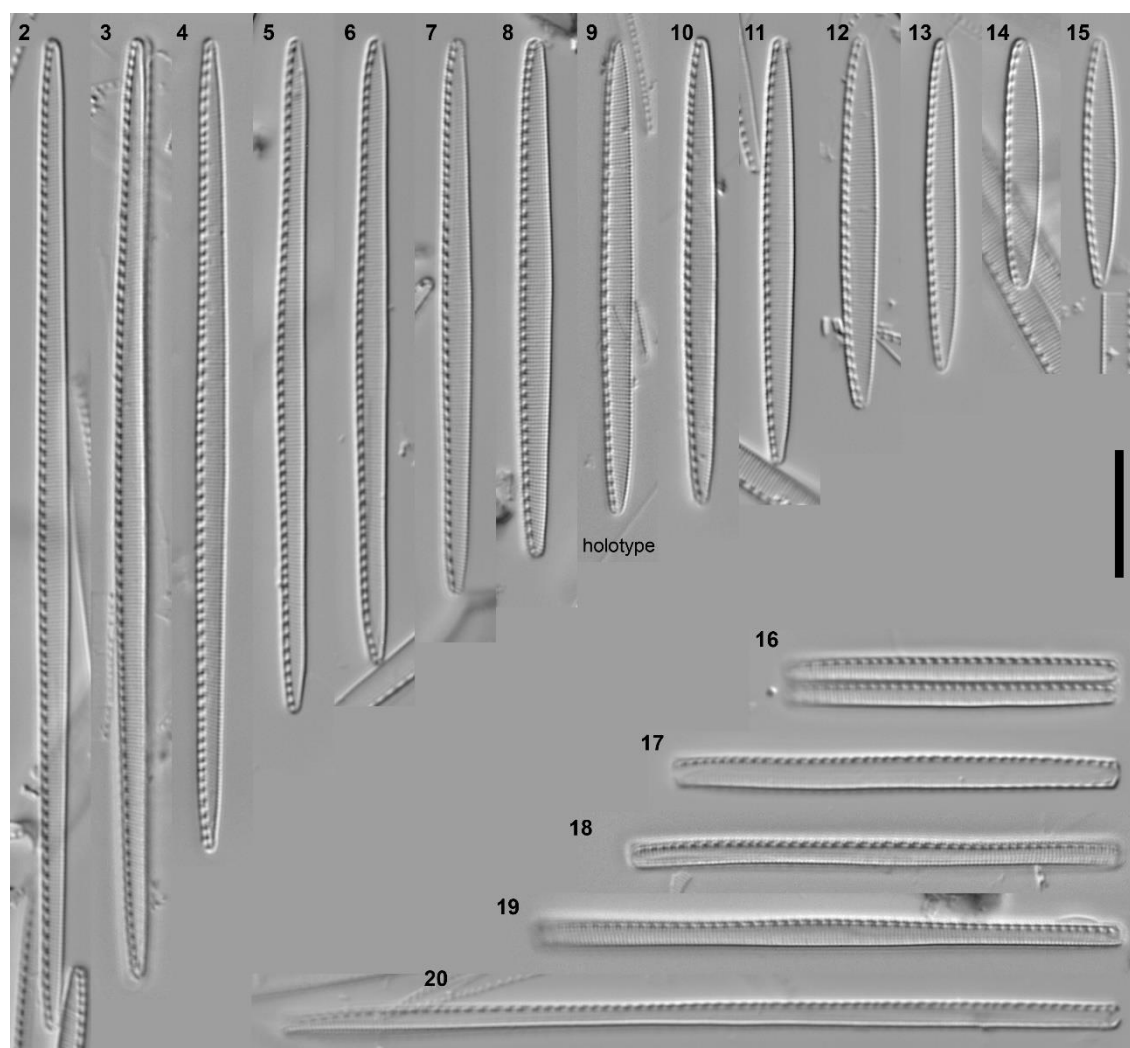
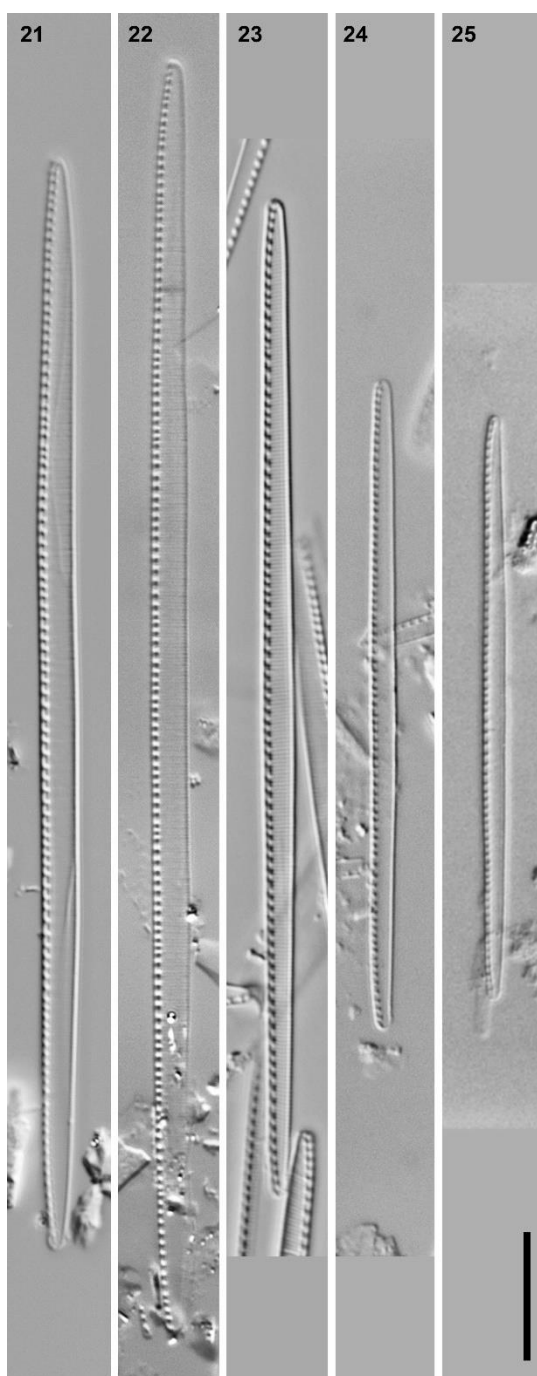


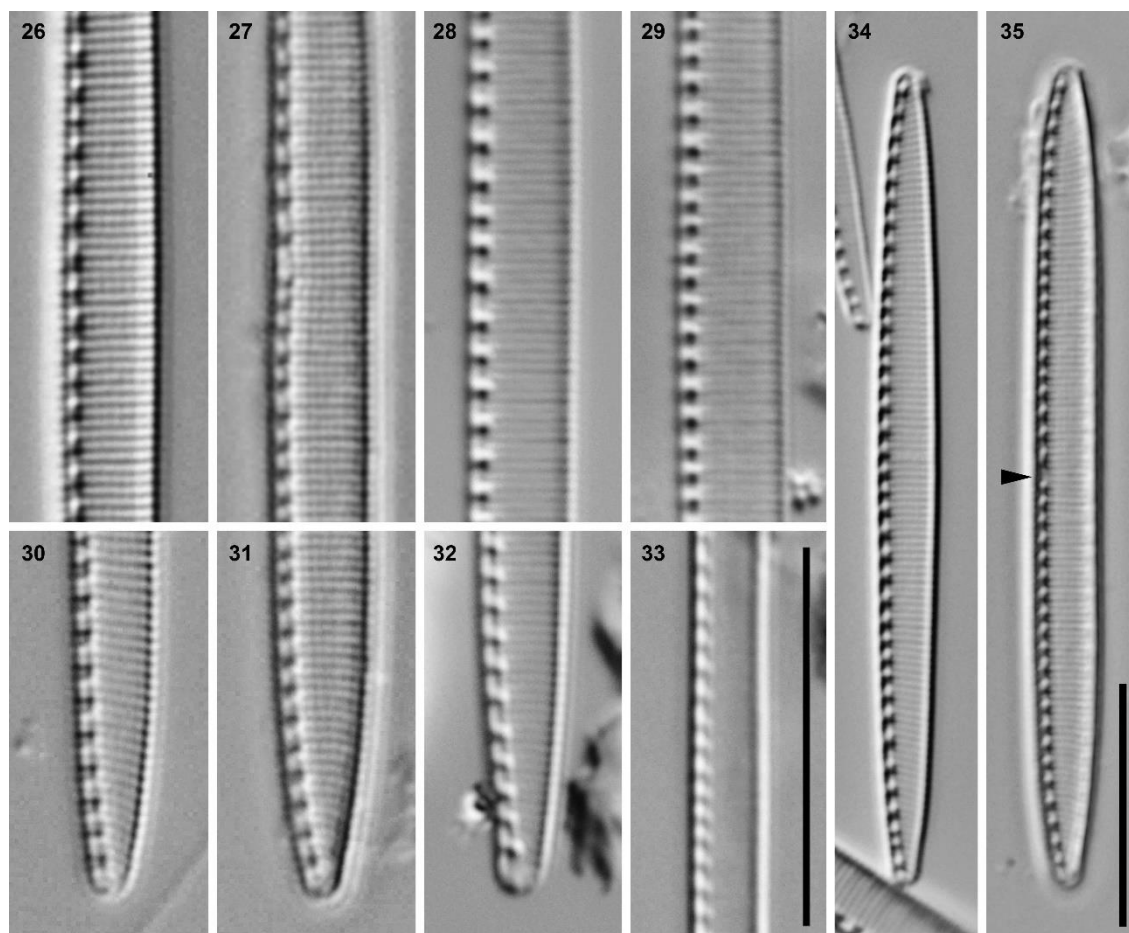
Fig. 1. Location of the Bishoftu crater lakes within Ethiopia (red point in inset map) and the Bishoftu area (black lines indicate roads).



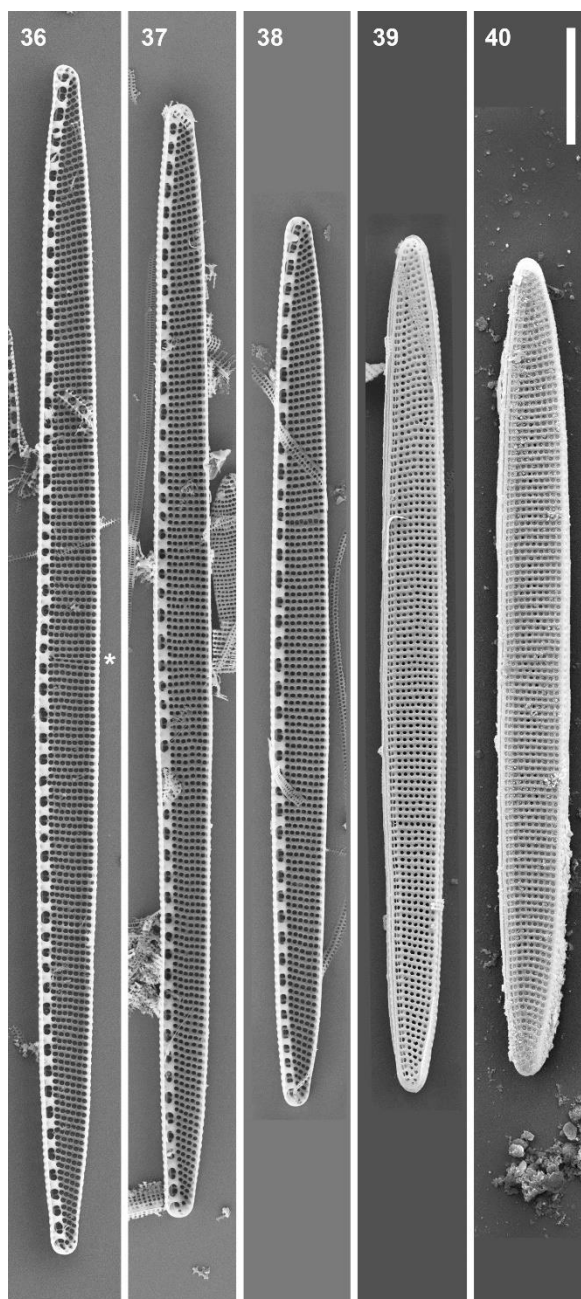
Figs 2–20. *Nitzschia fenestralis* sp. nov.: cleaned valves and frustules from Lake Babogaya: LM, DIC optics. Figs 2–15. Series of valves, interpreted as representing size reduction during the life cycle, in valve view (the holotype of *N. fenestralis* is shown in Fig. 9). Note the even spacing of all the fibulae. Fig. 16. A recently divided vegetative cell in girdle view, showing nitzschioid symmetry of both daughter frustules. Figs 17–20. Frustules of various lengths in girdle view; all are nitzschioid. Scale bar 10 μ m.



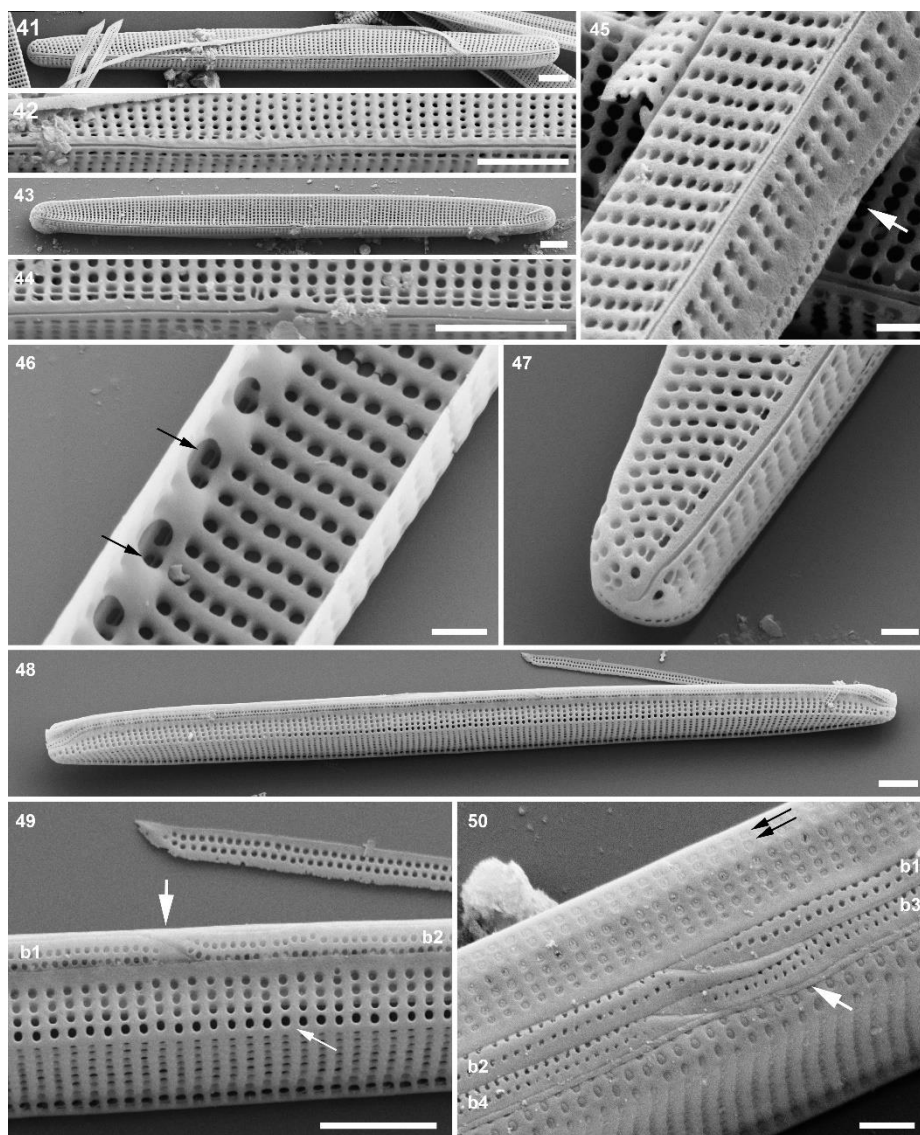
Figs 21–25. Comparison of valves of similar linear *Nitzschia* species lacking a central nodule from tropical African lakes, LM, DIC optics. Fig. 21. Paralectotype of *N. aequalis* (ringed specimen on Hustedt collection slide 241/65 from Lake Edward: this specimen was also photographed by SIMONSEN 1987, pl. 530, Figs 3, 4). Fig. 22. Another specimen of *N. aequalis* (on Hustedt collection slide 241/74, again from Lake Edward). Fig. 23. Long specimen of *N. fenestralis* (also shown in Fig. 1). Figs 24, 25. *Nitzschia mediocris* (Hustedt collection, slide 243/6, Nyamirundi, Lake Kivu). Scale bar 10 μm .



Figs 26–35. Comparison of *Nitzschia fenestralis*, *N. obsoleta*, *N. aequalis* and *N. mediocris*, LM, DIC optics. Figs 26–29. Valve centres of *N. fenestralis* (Fig. 26), *N. obsoleta* (Fig. 27, from Hustedt collection slide 242/21, from off algae in Lake Edward), and *N. aequalis* (paralectotype shown in Fig. 28, a second valve in Fig. 29). Note that the striae are less dense in *N. fenestralis* and *N. obsoleta* (33 and 34.5 in 10 μm respectively) than in *N. aequalis* (38 and 37.5 in 10 μm); in addition, the areolae are resolved in *N. fenestralis* and *N. obsoleta*, but not *N. aequalis*. Figs 30–32. Valve ends of *N. fenestralis*, *N. obsoleta* and *N. aequalis* (paralectotype), respectively. Fig. 33. Centre of *N. mediocris*. Fig. 34. *Nitzschia fenestralis*: note the even spacing of all fibulae and the radiate orientation of the striae towards the poles. Fig. 35. *Nitzschia obsoleta*: the two central fibulae are more widely spaced and a central nodule can be detected between them (arrowhead). Scale bars 10 μm (in Fig. 33 for Figs 26–33, in Fig. 35 for Figs 34, 35).



Figs 36–40. *Nitzschia fenestralis* and *N. obsoleta*, whole valves, SEM, all untitled and presented with the raphe system to the left. Here and in Figs 41–50 and S1–S8, *N. fenestralis* is illustrated from sample QDP 2000 and *N. obsoleta* from Hustedt sample A382 (which is the sample from which LM slide 242/21 in the Hustedt collection was prepared). Figs 36–38. *Nitzschia fenestralis*, internal views, showing more or less evenly spaced fibulae and striae that become strongly radiate towards the apices. Fig. 39. *Nitzschia fenestralis*, external view. Fig. 40. *Nitzschia obsoleta*, external view. Scale bar 10 μm .



Figs 41–50. *Nitzschia fenestralis* and *N. obsoleta*, details of external frustule ultrastructure (except Fig. 46), SEM; all tilted 25°. Figs 41, 42. Whole valve context and centre of *N. fenestralis*: the raphe is continuous. Figs 43, 44. Whole valve context and centre of *N. obsoleta*: central raphe endings are present; this specimen is eroded and has lost its hymenes (contrast Fig. 50). Fig. 45. *Nitzschia fenestralis*, centre, showing continuous raphe, deep valve mantle, the double row of poroids on each side of the raphe within the raphe canal (see also Fig. 47), and a split in the girdle bands at the centre (arrow). Fig. 46. *Nitzschia fenestralis*, internal view. The bases of the fibulae are linked by a longitudinal ridge, creating elliptical portulae linking the raphe canal with the valve interior. The double poroids in the raphe canal are visible (e.g. arrows). Fig. 47. *Nitzschia fenestralis*, valve pole, showing slightly bent terminal fissure and the double row of narrower areolae in the raphe canal. Figs 48, 49.

Figs 41-50 *cont.* Whole valve context and centre of a disassembled, incomplete theca of *N. fenestralis*, showing the open ends (at large arrow) of band 1 (b1) and band 2 (b2), which both bear two rows of closely spaced round poroids; the other end of band 2 is also visible, lying free on the stub (above arrow). Note also the deep valve mantle, where each stria is represented by four areolae, and the slight interruption of the striae at the valve face–mantle junction (narrow arrow). Fig. 50. *Nitzschia obsoleta*, centre of frustule in girdle view. Note the double row of areolae (black arrows) in the raphe canal, deep valve mantle with four areolae in each stria (cf. Fig. 49), open ends of bands 1–4 (b1–b4), each with two rows of small round areolae, and the narrower, imperforate band 5 (white arrow), which is not interrupted at the centre. Note also that each valve areola is occluded by a hymen close to its external aperture. Scale bars 2 μm (Figs 41–44, 48, 49) or 500 nm (Figs 45–47, 50).

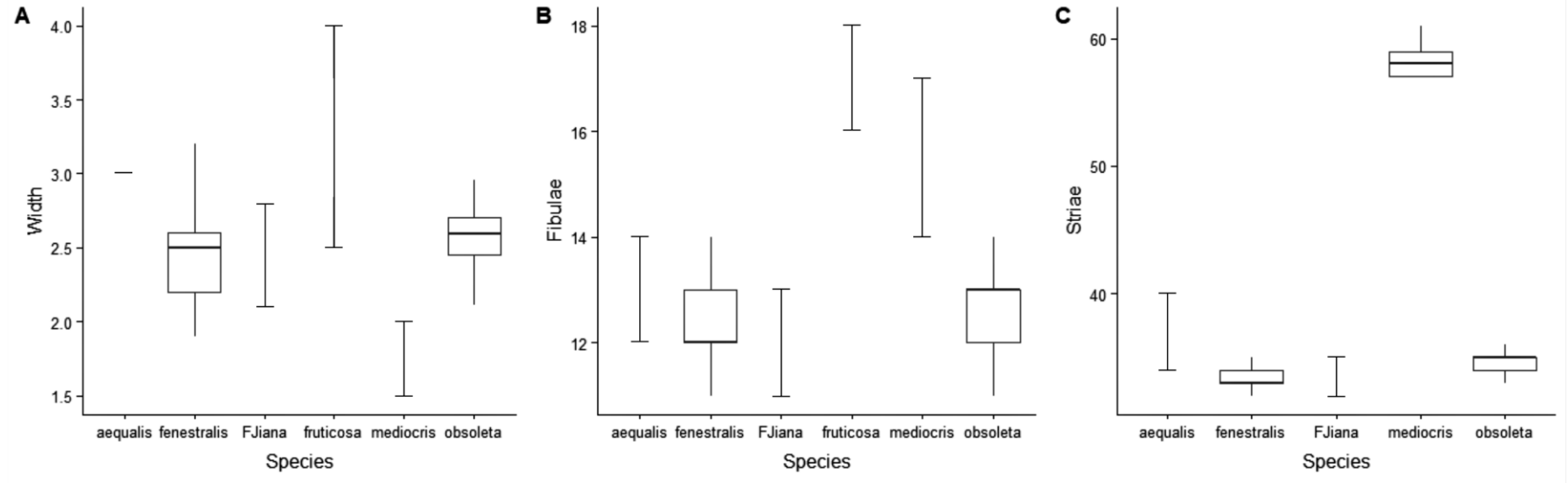


Fig. 51. Width (A), striae (B) and fibulae (C) density of *Nitzschia fenestralis* and similar *Nitzschia* taxa. Box plots are included for metrics measured in this study, with whiskers only for morphometrics published elsewhere cited in text.

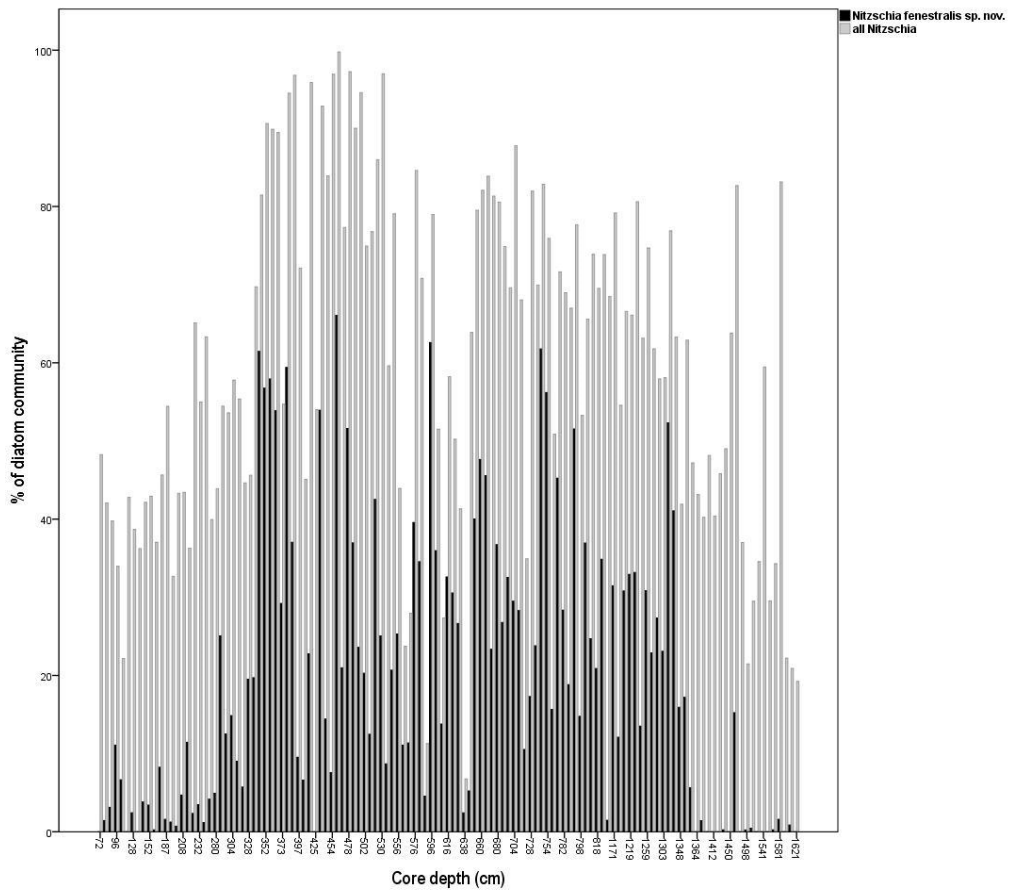


Fig. 52. Abundance of *Nitzschia fenestralis*, and *Nitzschia* in general, in samples taken through the Lake Babogaya core.

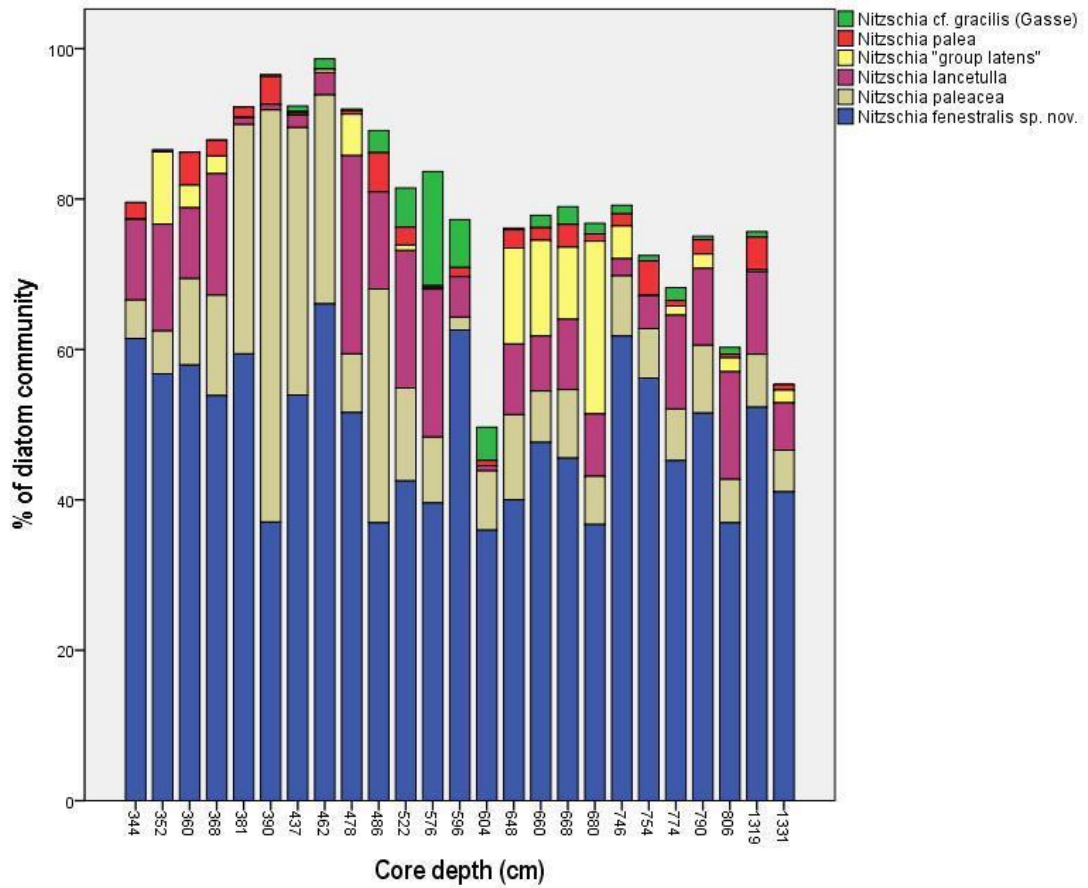
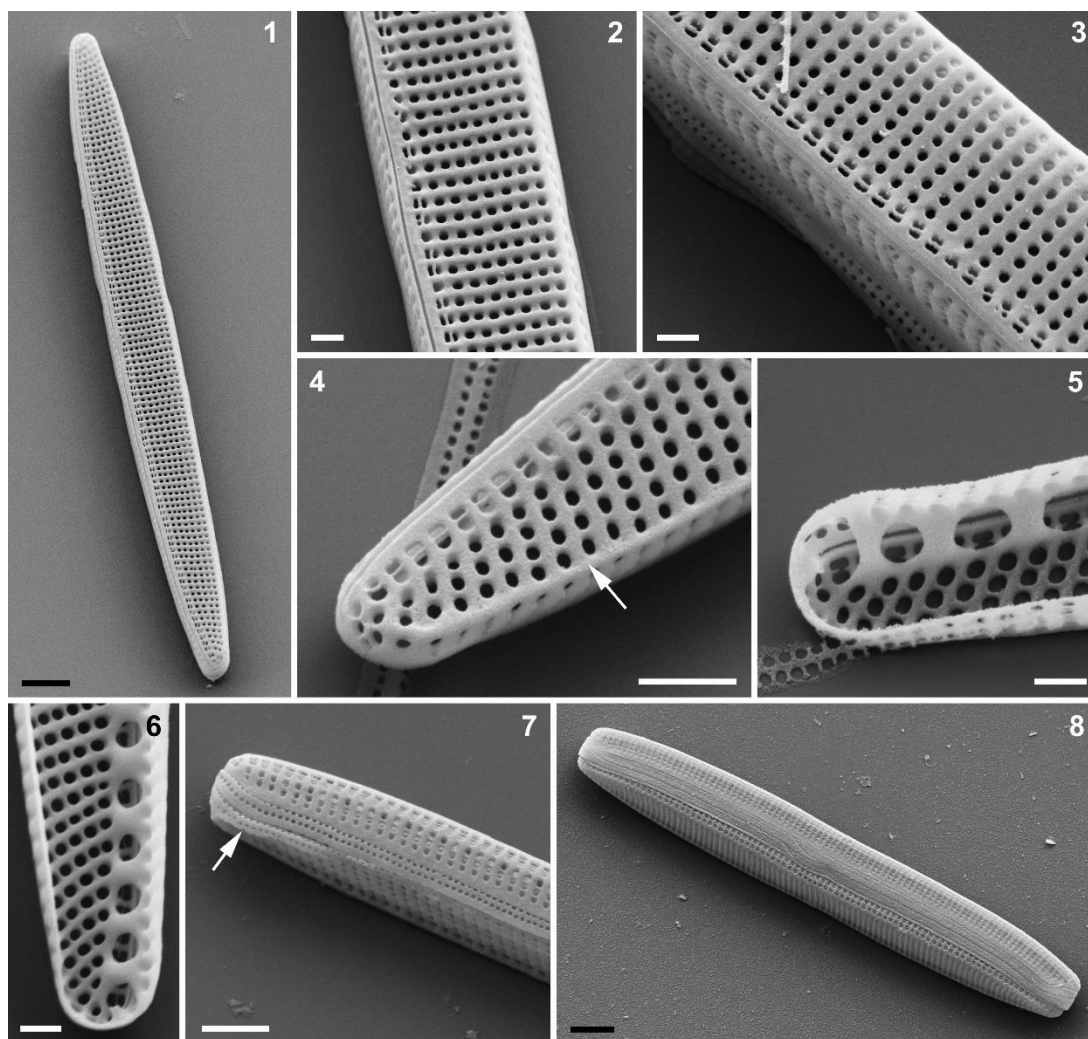


Fig. 53. Abundance of *Nitzschia fenestralis* and other *Nitzschia* taxa when *N. fenestralis* abundance was >35% in a sample.

Supplementary Figures



Figs S1–S8. *Nitzschia fenestralis* and *N. obsoleta*, SEM, all tilted 25°. Figs S1, S2. Whole valve context and centre of *N. fenestralis*; note that in this specimen the arrangement of areolae in the raphe canal is somewhat irregular (contrast Fig. S3). Fig. S3. *Nitzschia fenestralis*, centre, showing the double row of narrower areolae in the raphe canal. Figs S4–S6. *Nitzschia fenestralis*, valve pole in external (Fig. S4) and internal views (Figs S5, 6). Note the slight marginal ridge (arrow, Fig. S4) at the junction of the valve face and mantle. Fig. S7. Theca of *N. fenestralis*. As well as the valvocopula with two rows of areolae (which comprises two half bands: cf. Fig. 49), lying adjacent to the valve, this theca possesses a more abvalvar band with two rows of small areolae, presumably equivalent to band b3 or b4 of *N. obsoleta* (cf. Fig. 50 and Fig. S8). Fig. S8. *Nitzschia obsoleta*: whole frustule in girdle view; this image provides context for Fig. 50. Scale bars 2 μm (Figs S1, S7, S8) or 500 nm (Figs S2–S6).

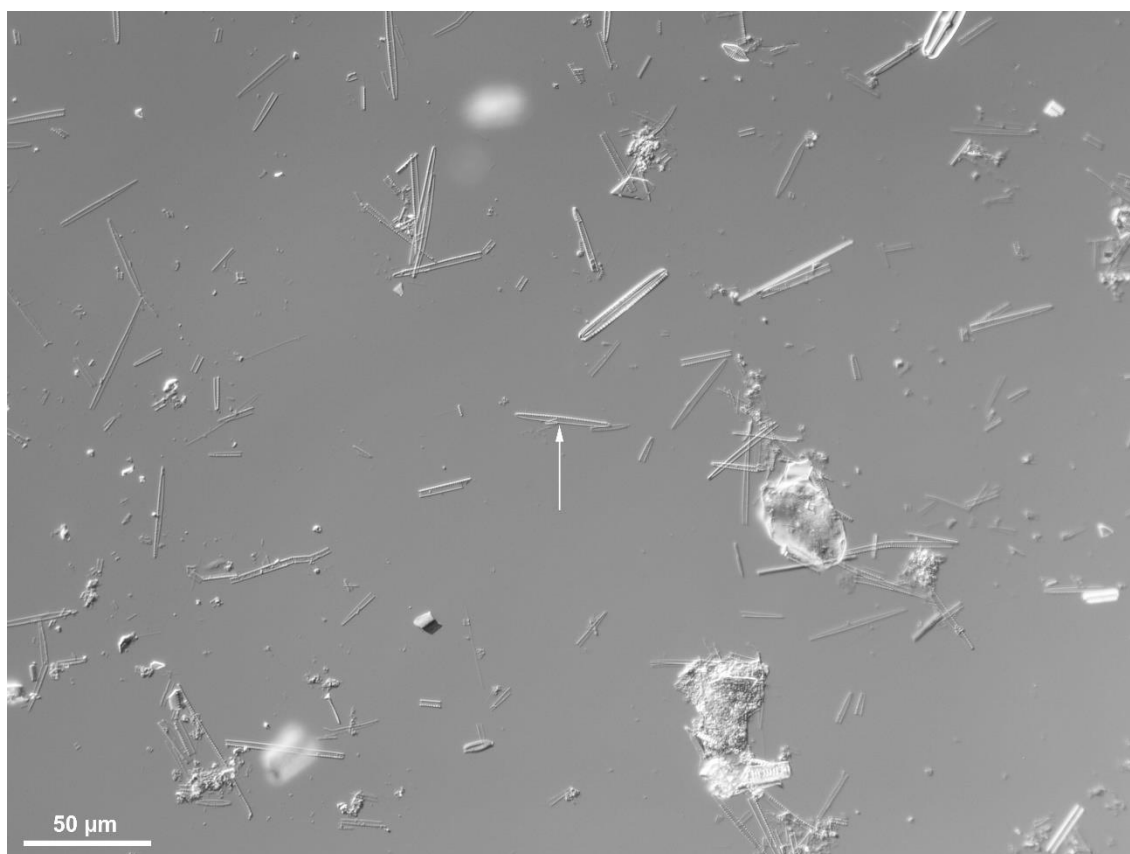


Fig. S9. Context photograph for the holotype (arrow) of *N. fenestralis*, illustrated in Fig. 9.

Appendix 2. Taxonomic authorities for diatom taxa identified (continues over 8 pages).

Name used in thesis	Other name	Authority	Year
<i>Achnanthes conspicua</i>	<i>Platessa conspicua</i>	A. Meyer	1919
<i>Achnanthes delicatula</i>		(Kützing) Grunow	1880
<i>Achnanthes exigua</i>	<i>Achnantheidium exiguum</i>	Grunow	1880
<i>Achnanthes exigua</i> var. <i>elliptica</i>		Hustedt	1937
<i>Achnanthes exilis</i>		Kützing	1833
<i>Achnanthes lanceolata</i>	<i>Planothidium lanceolatum</i>	(Brébisson ex Kützing) Grunow	1880
<i>Achnanthes minutissima</i> var. <i>affinis</i>	<i>Achnantheidium affine</i>	(Grunow) Lange-Bertalot in Lange-Bertalot & Krammer	1989
<i>Achnanthes oblongella</i>	<i>Platessa oblongella</i>	Østrup	1902
<i>Achnanthes reversa</i>	<i>Psammothidium reversum</i>	Lange-Bertalot	1989
<i>Achnanthes rosenstockii</i>	<i>Achnantheidium rosenstockii</i>	Lange-Bertalot in Lange-Bertalot & Krammer	1989
<i>Achnanthes</i> sp.			
<i>Achnanthes stewartii</i>	<i>Platessa stewartii</i>	Patrick	1945
<i>Achnanthes ventralis</i>	<i>Psammothidium ventrale</i>	(Krasske) Lange-Bertalot in Lange-Bertalot & Krammer	1989
<i>Achnantheidium minutissimum</i>	<i>Achnanthes minutissima</i>	(Kützing) Czarnecki	1994
<i>Amphora coffeaeformis</i>	<i>Halamphora coffeaeformis</i>	(C.Agardh) Kützing	1844
<i>Amphora delicatissima</i>		Krasske in Hustedt	1930
<i>Amphora inariensis</i>		Krammer	1980
<i>Amphora libyca</i>		Ehrenberg	1841
<i>Amphora ovalis</i>		(Kützing) Kützing	1844
<i>Amphora pediculus</i>		(Kützing) Grunow	1875
<i>Amphora veneta</i>	<i>Halamphora veneta</i>	Kützing	1844
<i>Anomoneis</i> sp.			
<i>Anomoneis sphaerophora</i>		Pfizer	1871
<i>Anomoneis sphaerophora</i> f. <i>costata</i>	<i>Anomoneis costata</i>	(Kützing) A.-M.Schmid	1977

Name used in thesis	Other name	Authority	Year
<i>Anomoneis sphaerophora</i> f. <i>sculpta</i>	<i>Anomoeoneis sphaerophora</i> var. <i>sculpta</i>	(Ehrenberg) Krammer in Krammer & Lange-Bertalot	1985
<i>Aulacoseira alpigena</i>		(Grunow) Krammer	1991
<i>Aulacoseira ambigua</i>		(Grunow) Simonsen	1979
<i>Aulacoseira distans</i>		(Ehrenberg) Simonsen	1979
<i>Aulacoseira granulata</i>		(Ehrenberg) Simonsen	1979
<i>Aulacoseira granulata</i> var. <i>angustissima</i>		(O.Müller) Simonsen	1979
<i>Aulacoseira granulata</i> var. <i>valida</i>		(Hustedt) Simonsen	1979
<i>Aulacoseira herzogii</i>		(Lemmermann) Simonsen	1979
<i>Aulacoseira</i> sp.			
<i>Caloneis bacillum</i>		(Grunow) Cleve	1894
<i>Caloneis silicula</i>		(Ehrenberg) Cleve	1894
<i>Caloneis</i> sp.			
<i>Cocconeis microscopica</i>	<i>Psammothidium microscopicum</i>	Cholnoky	1959
<i>Cocconeis placentula</i>		Ehrenberg	1838
<i>Cocconeis placentula</i> var. <i>Euglypta</i>		(Ehrenberg) Grunow	1884
<i>Cocconeis placentula</i> var. <i>lineata</i>		(Ehrenberg) Van Heurck	1885
<i>Cyclotella caspia</i>		Grunow	1878
<i>Cyclotella</i> cf. <i>kuetzingia</i>			
<i>Cyclotella cyclopuncta</i>	<i>Cyclotella cretica</i> var. <i>cyclopuncta</i>	Håkansson & J.R.Carter	1990
<i>Cyclotella meneghiniana</i>		Kützing	1844
<i>Cymatopleura librile</i>	<i>Surirella librile</i>	(Ehrenberg) Pantocsek	1902
<i>Cymbella affinis</i>		Kützing	1844
<i>Cymbella</i> cf. <i>cistula</i>			
<i>Cymbella cistula</i>		(Ehrenberg) O.Kirchner	1878
<i>Cymbella descripta</i>	<i>Encyonopsis descripta</i>	(Hustedt) Krammer & Lange-Bertalot	1985
<i>Cymbella ehrenbergii</i>	<i>Cymbopleura inaequalis</i>	Kützing	1844
<i>Cymbella fonticola</i>	<i>Encyonopsis fonticola</i>	Hustedt	1937

Name used in thesis	Other name	Authority	Year
<i>Cymbella gracilis</i>	<i>Encyonema gracile</i>	(Rabenhorst) Cleve	1894
<i>Cymbella hungarica</i>		(Grunow) Pantocsek	1902
<i>Cymbella hustedtii</i>		Krasske	1923
<i>Cymbella leptoceros</i>		(Ehrenberg) Kützing	1844
<i>Cymbella mesiana</i>	<i>Encyonema mesianum</i>	Cholnoky	1955
<i>Cymbella minuta</i>	<i>Encyonema minutum</i>	Hilse in Rabenhorst	1862
<i>Cymbella obscura</i>	<i>Encyonema obscurum</i>	Krasske	1938
<i>Cymbella sinuata</i>	<i>Reimeria sinuata</i>	W.Gregory	1856
<i>Cymbella sp.</i>			
<i>Cymbella tumida</i>		(Brébisson) Van Heurck	1880
<i>Cymbella tumidula</i>		Grunow in A.W.F.Schmidt	1875
<i>Denticula tenuis</i>		Kützing	1844
<i>Diploneis oblongella</i>		(Nägeli ex Kützing) Cleve-Euler	1922
<i>Diploneis subovalis</i>		Cleve	1894
<i>Discostella stelligera</i>	<i>Cyclotella stelligera</i>	(Cleve & Grunow) Houk & Klee	2004
<i>Encyonema muelleri</i>	<i>Cymbella muelleri</i>	(Hustedt) D.G.Mann in Round, R.M.Crawford & D.G.Mann	1990
<i>Encyonema silesiacum</i>	<i>Cymbella silesiaca</i>	(Bleisch) D.G.Mann in Round, R.M.Crawford & D.G.Mann	1990
<i>Encyonopsis microcephala</i>	<i>Cymbella microcephala</i>	(Grunow) Krammer	1997
<i>Epithemia adnata</i>		(Kützing) Brébisson	1838
<i>Epithemia argus</i>		(Ehrenberg) Kützing	1844
<i>Epithemia hyndmanii</i>		W.Smith	1850
<i>Epithemia smithii</i>		Carruthers	1864
<i>Epithemia sores</i>		Kützing	1844
<i>Epithemia sores</i> var. <i>gracilis</i>		Hustedt	1922
<i>Epithemia sp.</i>			
<i>Epithemia turgida</i>		(Ehrenberg) Kützing	1844
<i>Eunotia arcus</i>		Ehrenberg	1837

Name used in thesis	Other name	Authority	Year
<i>Eunotia minor</i>		(Kützing) Grunow in Van Heurck	1881
<i>Eunotia praerupta</i>		Ehrenberg	1843
<i>Fragilaria cf. parasitica</i>			
<i>Fragilaria berlinensis</i>	<i>Belonastrum berlinense</i>	(Lemmermann) Lange-Bertalot	1993
<i>Fragilaria bidens</i>		Heiberg	1863
<i>Fragilaria capucina</i> sp.			
<i>Fragilaria capucina</i> var. <i>mesolepta</i>	<i>Fragilaria mesolepta</i>	(Rabenhorst) Rabenhorst	1864
<i>Fragilaria capucina</i> var. <i>rumpens</i>	<i>Fragilaria capucina</i> subsp. <i>Rumpens</i>	(Kützing) Lange-Bertalot ex Bukhtiyarova	1995
<i>Fragilaria capucina</i> var. <i>vaucheriae</i>	<i>Fragilaria vaucheriae</i>	(Kützing) Lange-Bertalot	1980
<i>Fragilaria exigua</i>		Grunow in Cleve & Möller	1878
<i>Fragilaria famelica</i>	<i>Synedra famelica</i>	(Kützing) Lange-Bertalot	1980
<i>Fragilaria fasciculata</i>	<i>Tabularia fasciculata</i>	(C.Agardh) Lange-Bertalot	1980
<i>Fragilaria leptostauron</i> var. <i>martyi</i>	<i>Martyana martyi</i>	(Héribaud-Joseph) Lange-Bertalot	1991
<i>Fragilaria nanana</i>	<i>Synedra nana</i>	Lange-Bertalot	1993
<i>Fragilaria pinnata</i> var. <i>trigona</i>	<i>Staurosirella pinnata</i> var. <i>trigona</i>	(Brun & Héribaud-Joseph) Hustedt in A.W.F.Schmidt	1913
<i>Fragilaria tenera</i>		(W.Smith) Lange-Bertalot	1980
<i>Fragilaria zeilleri</i>	<i>Pseudostaurosira zeilleri</i>	Héribaud-Joseph	1903
<i>Fragilaria zelleri</i> var. <i>elliptica</i>	<i>Pseudostaurosira medliniae</i>	F.Gasse	1980
<i>Frustulia vulgaris</i>		(Thwaites) De Toni	1891
<i>Gomphonema affine</i>		Kützing	1844
<i>Gomphonema clavatum</i>	<i>Gomphonema olivaceum</i>	Ehrenberg	1832
<i>Gomphonema clevei</i>	<i>Gomphoneis clevei</i>	Frike	1902
<i>Gomphonema gracile</i>		Ehrenberg	1838
<i>Gomphonema insigne</i>		W.Gregory	1856
<i>Gomphonema intricatum</i> var. <i>pusilla</i>		(Cleve-Euler) Mayer	1955
<i>Gomphonema lanceolatum</i>		C.Agardh	1831
<i>Gomphonema minutum</i>		(C.Agardh) C.Agardh	1831
<i>Gomphonema minutum</i> f. <i>syriacum</i>		Lange-Bertalot & Reichardt	

Name used in thesis	Other name	Authority	Year
<i>Gomphonema parvulum</i>		(Kützing) Kützing	1849
<i>Gomphonema pumilum</i>		(Grunow) E.Reichardt & Lange-Bertalot	1991
<i>Gomphonema</i> sp.			
<i>Gomphonema truncatum</i>		Ehrenberg	1832
<i>Gomphonema vibrio</i>		Ehrenberg	1843
<i>Gomphonitzschia</i> sp.			
<i>Hantzschia amphixoys</i>		(Ehrenberg) Grunow	1880
<i>Lindavia ocellata</i>	<i>Cyclotella ocellata</i>	(Pantocsek) T.Nakov <i>et al.</i>	2015
<i>Mastogloia elliptica</i> var. <i>dansei</i>		(C.Agardh) Grunow in van Heurck	1880
<i>Meridion circulare</i>		(Greville) C.Agardh	1831
<i>Navicula cryptocephala</i>		Kützing	1844
<i>Navicula cryptotenella</i>		Lange-Bertalot in Krammer & Lange-Bertalot	1985
<i>Navicula cuspidata</i>	<i>Craticula cuspidata</i>	(Kützing) Kützing	1844
<i>Navicula gastrum</i>	<i>Placoneis gastrum</i>	(Ehrenberg) Kützing	1844
<i>Navicula helensis</i>	<i>Fallacia helensis</i>	Schulz	1926
<i>Navicula microrhombus</i>		(Cholnoky) Schoeman & Archibald	
<i>Navicula minima</i>		Grunow in Van Heurck	1880
<i>Navicula minus</i> var. <i>muralis</i>	<i>Adlafia minuscula</i> var. <i>muralis</i>	(Grunow) Lange-Bertalot ex Lange-Bertalot & Rumrich	1981
<i>Navicula monoculata</i>	<i>Pseudofallacia monoculata</i>	Hustedt	1945
<i>Navicula mutica</i>	<i>Luticola mutica</i>	Kützing	1844
<i>Navicula paramutica</i>	<i>Luticola paramutica</i>	W.Bock	1963
<i>Navicula pelliculosa</i>	<i>Fistulifera pelliculosa</i>	(Kützing) Hilse	1863
<i>Navicula pseudoscutiformis</i>	<i>Cavinula pseudoscutiformis</i>	Hustedt	1930
<i>Navicula radiosa</i>		Kützing	1844
<i>Navicula similis</i>	<i>Placogeia similis</i>	Krasske	1929
<i>Navicula</i> sp.			
<i>Navicula tenera</i>	<i>Pseudofallacia tenera</i>	Hustedt	1936

Name used in thesis	Other name	Authority	Year
<i>Navicula viridula</i> var. <i>rosellatta</i>		(Kützing) Cleve	1895
<i>Naviucla halophila</i>		(Grunow) Cleve	1894
<i>Neidium alpinum</i>		Hustedt	1943
<i>Neidium ampliatum</i>		(Ehrenberg) Krammer in Krammer & Lange-Bertalot	1985
<i>Neidium dubium</i>		(Ehrenberg) Cleve	1894
<i>Nitzschia</i> "group latens"		<i>sensu</i> Gasse	1986
<i>Nitzschia amphibia</i>		Grunow	1862
<i>Nitzschia amphibia</i> f. <i>frauenfeldii</i>		(Grunow) Lange-Bertalot in Lange-Bertalot & Krammer	1987
<i>Nitzschia angustata</i>		(W.Smith) Grunow	1880
<i>Nitzschia</i> cf. <i>acicularis</i>			
<i>Nitzschia</i> cf. <i>flexa</i>			
<i>Nitzschia dissipata</i>		(Kützing) Rabenhorst	1860
<i>Nitzschia epiphytica</i>		O.Müller	1905
<i>Nitzschia epiphyticoides</i>		Hustedt	1949
<i>Nitzschia fenestralis</i>		Grady, D.G.Mann & Trobajo	in press
<i>Nitzschia fonticola</i>		(Grunow) Grunow in Van Heurck	1881
<i>Nitzschia frustulum</i>		(Kützing) Grunow	1880
<i>Nitzschia gracilis</i>		<i>sensu</i> Gasse	1986
<i>Nitzschia inconspicua</i>		Grunow	1862
<i>Nitzschia intermedia</i>		Hantzsch in Grunow	1880
<i>Nitzschia lancettula</i>		O.Müller	1905
<i>Nitzschia latens</i>		Hustedt	1949
<i>Nitzschia linearis</i>		W.Smith	1853
<i>Nitzschia palea</i>		(Kützing) W.Smith	1856
<i>Nitzschia palea</i> var. <i>debilis</i>		(Kützing) Grunow	1880
<i>Nitzschia paleacea</i>		(Grunow) Grunow in Van Heurck	1881
<i>Nitzschia perminuta</i>		Grunow in Van Heurck	1881

Name used in thesis	Other name	Authority	Year
<i>Nitzschia sinuata</i> var. <i>delognei</i>		(Grunow) Lange-Bertalot	1980
<i>Nitzschia sinuata</i> var. <i>tabellaria</i>		(Grunow) Grunow in Van Heurck	1881
<i>Nitzschia tropica</i>		Hustedt	1949
<i>Nitzschia umbonata</i>		(Ehrenberg) Lange-Bertalot	1978
<i>Nitzschia valdecostata</i>		Lange-Bertalot & Simonsen	1978
<i>Opephora olsenii</i>	<i>Opephora mutabilis</i>	M.Møller	1950
<i>Pinnularia borealis</i> var. <i>rectangularis</i>		G.W.F. Carlson	1913
<i>Pinnularia brauniana</i>		(Grunow) Studnicka	1888
<i>Pinnularia major</i>		(Kützing) Rabenhorst	1853
<i>Pinnularia microstauron</i>		(Ehrenberg) Cleve	1891
<i>Pinnularia obscura</i>		Krasske	1932
<i>Pinnularia</i> sp			
<i>Pinnularia stomatophora</i>		(Grunow) Cleve	1895
<i>Pinnularia viridis</i>		(Nitzsch) Ehrenberg	1843
<i>Pseudostaurosira brevistriata</i>	<i>Fragilaria brevistriata</i>	(Grunow) D.M. Williams & Round	1988
<i>Pseudostaurosira elliptica</i>	<i>Fragilaria elliptica</i>	(Schumann) Edlund, Morales & Spaulding	2006
<i>Pseudostaurosira parasitica</i>	<i>Fragilaria parasitica</i>	(W. Smith) E. Morales in E. Morales & Edlund	2003
<i>Pseudostaurosira pseudoconstruens</i>	<i>Fragilaria pseudoconstruens</i>	(Marciniak) D.M. Williams & Round	1988
<i>Rhoicosphenia curvata</i>		(Kützing) Grunow	1860
<i>Rhopalodia gibba</i>	<i>Epithemia gibba</i>	(Ehrenberg) O. Müller	1895
<i>Rhopalodia gibba</i> var. <i>parallela</i>	<i>Epithemia parallela</i>	(Grunow) Holmboe	1899
<i>Rhopalodia gibberula</i>		(Ehrenberg) O. Müller	1895
<i>Rhopalodia gracilis</i>		O. Müller	1895
<i>Rhopalodia operculata</i>	<i>Epithemia operculata</i>	(C. Agardh) Håkanasson	1979
<i>Rhopalodia vermicularis</i>		O. Müller	1895
<i>Sellaphora pupula</i>	<i>Navicula pupula</i>	(Kützing) Mereschkovsky	1902
<i>Stauroneis phoenicenteron</i>		(Nitzsch) Ehrenberg	1843
<i>Stauroneis smithii</i>		Grunow	1860

Name used in thesis	Other name	Authority	Year
<i>Stauroneis</i> sp.			
<i>Staurosira construens</i>	<i>Fragilaria construens</i>	Ehrenberg	1843
<i>Staurosira construens</i> var. <i>venter</i>	<i>Fragilaria construens</i> var. <i>venter</i>	(Ehrenberg) P.B.Hamilton in Hamilton <i>et al.</i>	1992
<i>Staurosira construens</i> var. <i>binodis</i>	<i>Neidiomorpha binodis</i>	(Ehrenberg) M.Cantonati, Lange-Bertalot & N.Angeli	2010
<i>Staurosirella pinnata</i>	<i>Fragilaria pinnata</i>	(Ehrenberg) D.M.Williams & Round	1988
<i>Stephanodiscus hantzschii</i>		Grunow in Cleve & Grunow	1880
<i>Stephanodiscus minutulus</i>		(Kützing) Cleve & Möller	1882
<i>Stephanodiscus niagarae</i>		Ehrenberg	1845
<i>Stephanodiscus</i> sp.			
<i>Surirella amphioxys</i>		W.Smith	1856
<i>Surirella angusta</i>		Kützing	1844
<i>Surirella engleri</i>	<i>Iconella engleri</i>	O.Müller	1904
<i>Surirella nyassae</i>		O.Müller	1904
<i>Surirella ovata</i>	<i>Surirella minuta</i>	Kützing	1844
<i>Surirella venusta</i>		Østrup	1910
<i>Tabellaria binalis</i> var. <i>elliptica</i>	<i>Oxyneis binalis</i> var. <i>elliptica</i>	R.J.Flower	1986
<i>Thalassiosira faurii</i>		(Gasse) Hasle	1978
<i>Ulnaria acus</i>	<i>Synedra acus</i>	(Kützing) Aboal	2003
<i>Ulnaria oxyrhynchus</i>	<i>Fragilaria ulna</i> var. <i>oxyrhynchus</i>	(Kützing) Aboal in Aboal <i>et al.</i>	2003
<i>Ulnaria ulna</i>	<i>Syndera ulna</i>	(Nitzsch) Compère	2001

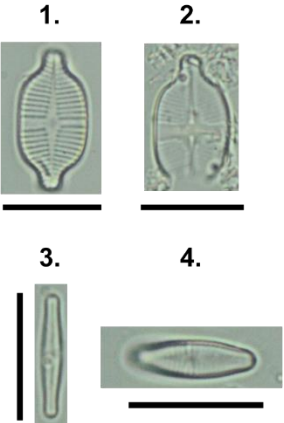
Thesis Plates

Plate I

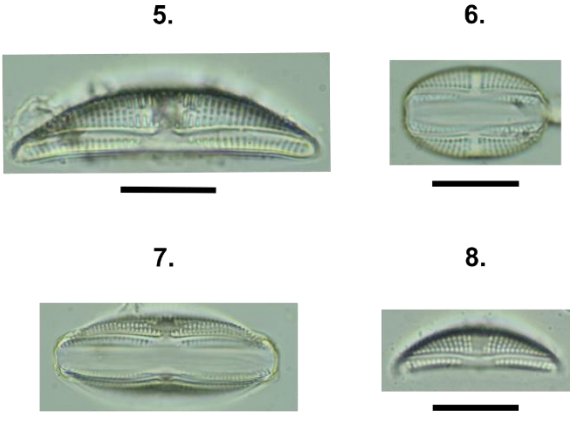
1. *Achnanthydium exiguum* (rapheless side of valve)
2. *Achnanthydium exiguum* (side with raphe)
- 3-4. *Achnanthydium minutissimum*
5. *Amphora libyca*
6. *Amphora libyca* (girdle view)
7. *Amphora pediculus* (girdle view)
8. *Amphora pediculus*
9. *Aulacoseira granulata* var. *angustissima* (girdle view showing separation spine)
10. *Aulacoseira granulata* var. *angustissima* (girdle view)
11. *Cymbella affinis*
- 12-14. *Cymbella hustedtii*
- 15-16. *Cymbella leptoceros*
- 17-18. *Discostella stelligera*

All scale bars shown represent 10 μ m unless stated otherwise

Achnanthydium Kützing



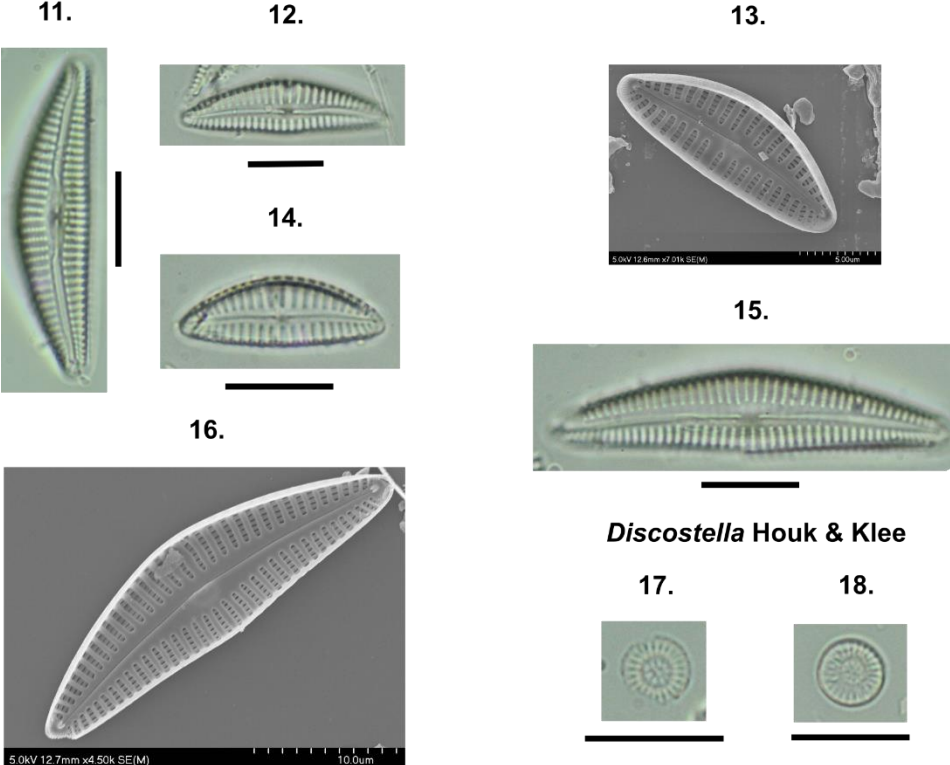
Amphora (Ehrenberg) Kützing



Aulacoseira Thwaites



Cymbella Agardh



Discostella Houk & Klee

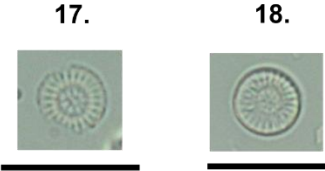


Plate II

1. *Encyonema muelleri*
2. *Encyonema silesiacum*
- 3-4. *Encyonopsis fonticola*
- 5-6. *Encyonopsis microcephala*
7. *Epithemia adnata*
8. *Epithemia argus*
9. *Epithemia sorex*
10. *Fragilaria nanana* (centre of valve)
11. *Fragilaria nanana* (pole of valve)
12. *Gomphonema clevei*
13. *Gomphonema intricatum* var. *pusilla*
14. *Gomphonema parvulum*
15. *Gomphonema pumilum*

All scale bars shown represent 10 μ m unless stated otherwise

***Encyonema* Kützing**

1.



2.



***Encyonopsis* Krammer**

3.



4.



5.



6.



***Epithemia* Kützing**

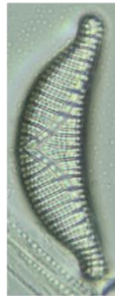
7.



8.



9.



***Fragilaria* Lyngbye**

10.



11.



***Gomphonema* Ehrenberg**

12.



13.



14.



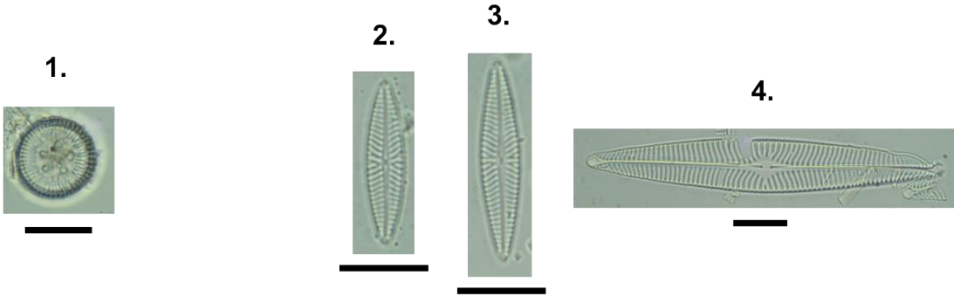
Plate III

1. *Lindavia ocellata*
- 2-3. *Navicula cryptotenella*
4. *Navicula radiosa*
- 5-6. *Nitzschia amphibia*
7. *Nitzschia* cf. *gracilis*
- 8-9. *Nitzschia epiphytica*
- 10-12. *Nitzschia* "group latens"
- 13-16. *Nitzschia lancettula*
17. *Nitzschia palea*
- 18-19. *Nitzschia paleacea*
20. *Nitzschia tropica*
21. *Nitzschia tropica* (girdle view)

All scale bars shown represent 10 μ m unless stated otherwise.

Lindavia
(Schutt) De Toni & Forti

Navicula Bory de Saint-Vincent



Nitzschia Hassall

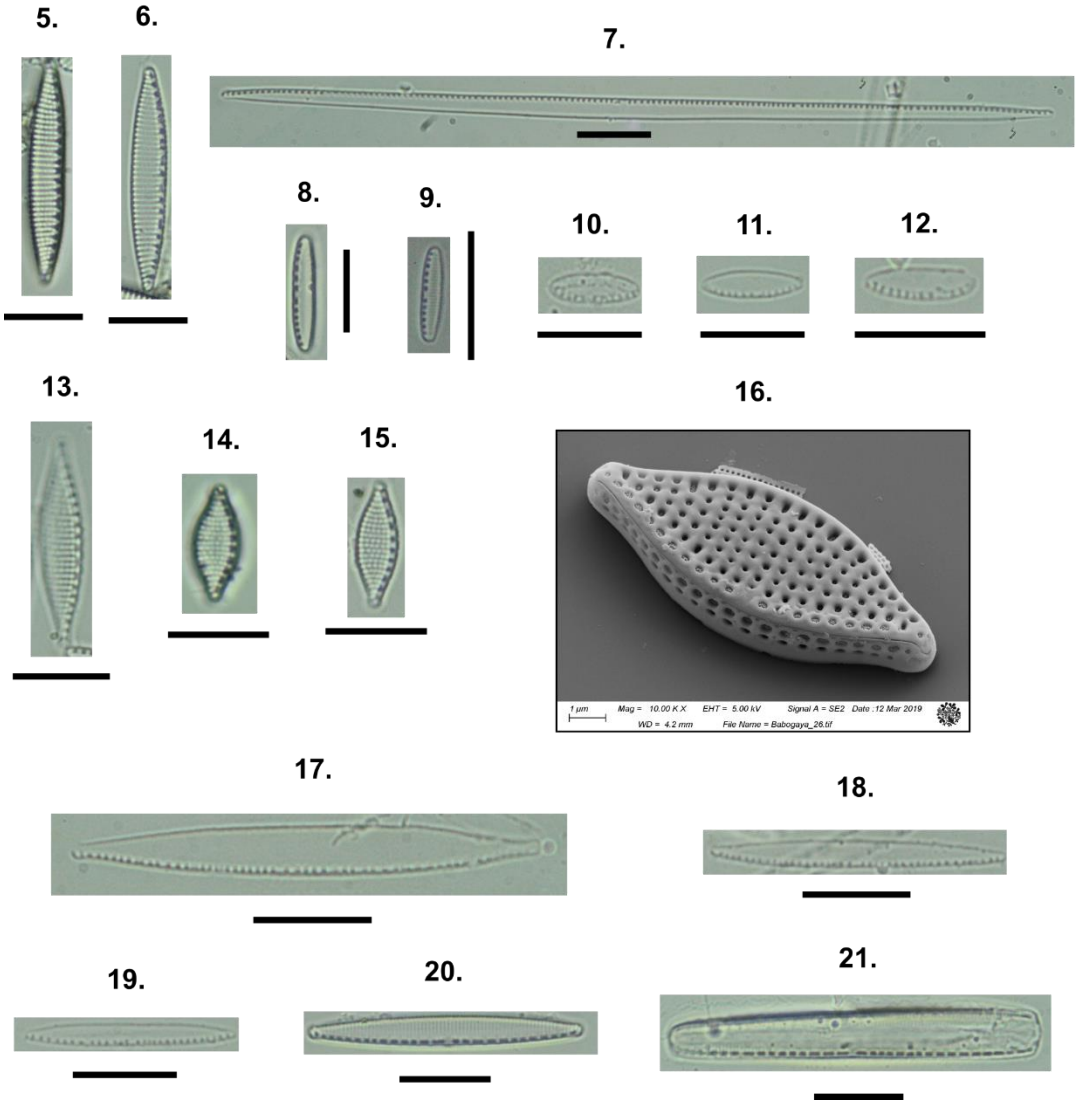
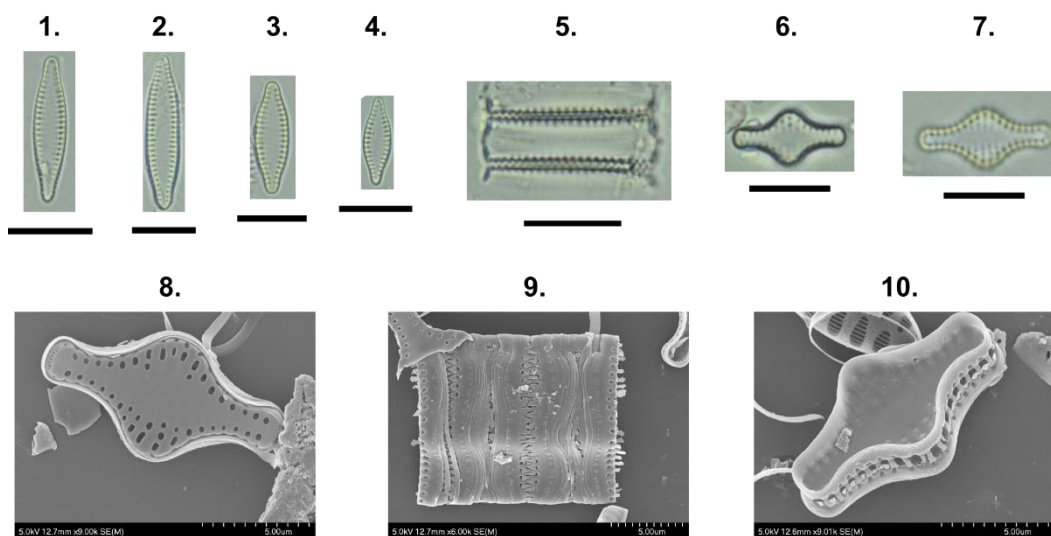


Plate IV

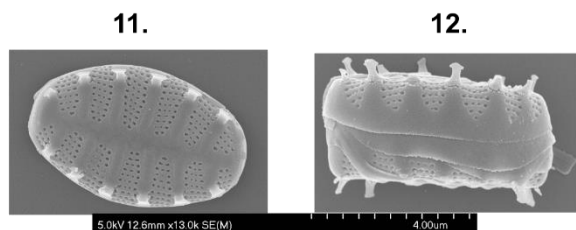
- 1-4. *Pseudostaurosira brevistriata*
5. *Pseudostaurosira brevistriata* (girdle view)
6-8. *Pseudostaurosira pseudoconstruens*
9-10. *Pseudostaurosira pseudoconstruens* (girdle view)
11-12. *Punctastriata* sp.
13. *Sellaphora pupula*
14-16. *Staurosira construens*
17-19. *Staurosira construens* var. *venter*
20. *Staurosira construens* var. *venter* (girdle view)
21. Morphotype between *Staurosira construens* var. *venter* and *Fragilaria elliptica*

All scale bars shown represent 10 μ m unless stated otherwise.

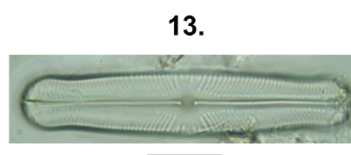
Pseudostaurosira Williams & Round



Punctastriata Williams & Round



Sellaphora Mereschkowsky



Staurosira Ehrenberg

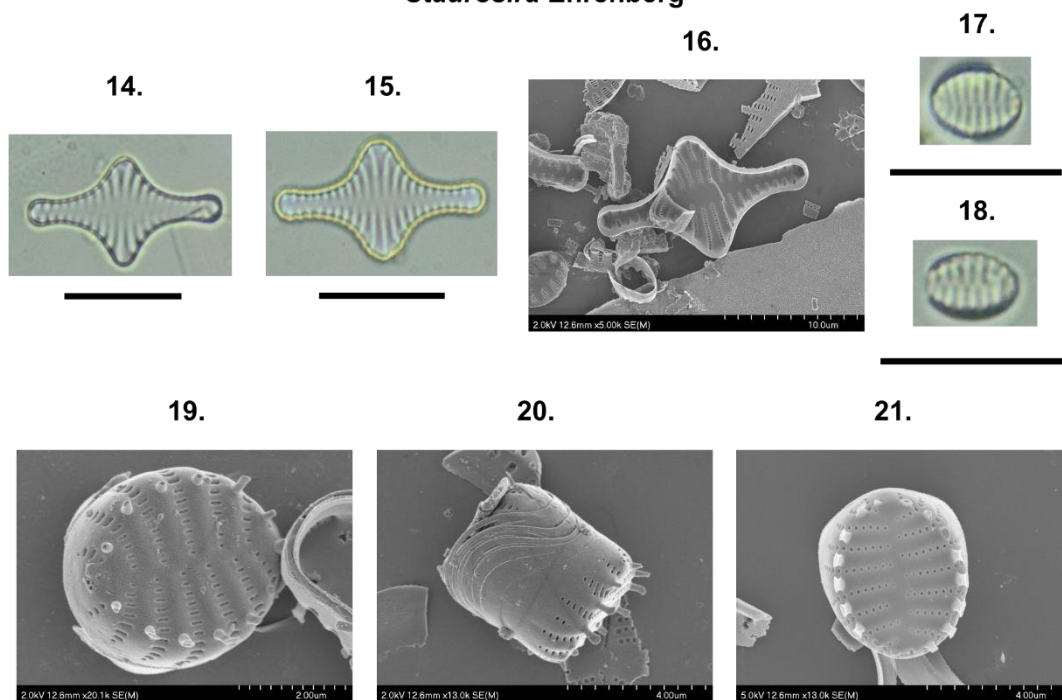


Plate V

1-6. *Staurosirella pinnata*

7-9. *Staurosirella pinnata* (girdle view)

10. Comparison of the considerably similar *Staurosirella pinnata* (black arrow) and *Punctastriata* sp. (red arrow)

9-10. *Pseudostaurosira pseudoconstruens* (girdle view)

11. *Ulnaria acus*

12. Comparison of the central areas of *Ulnaria acus* (upper valve) and *Fragilaria nanana* (lower valve) showing the similarity of these morphotypes

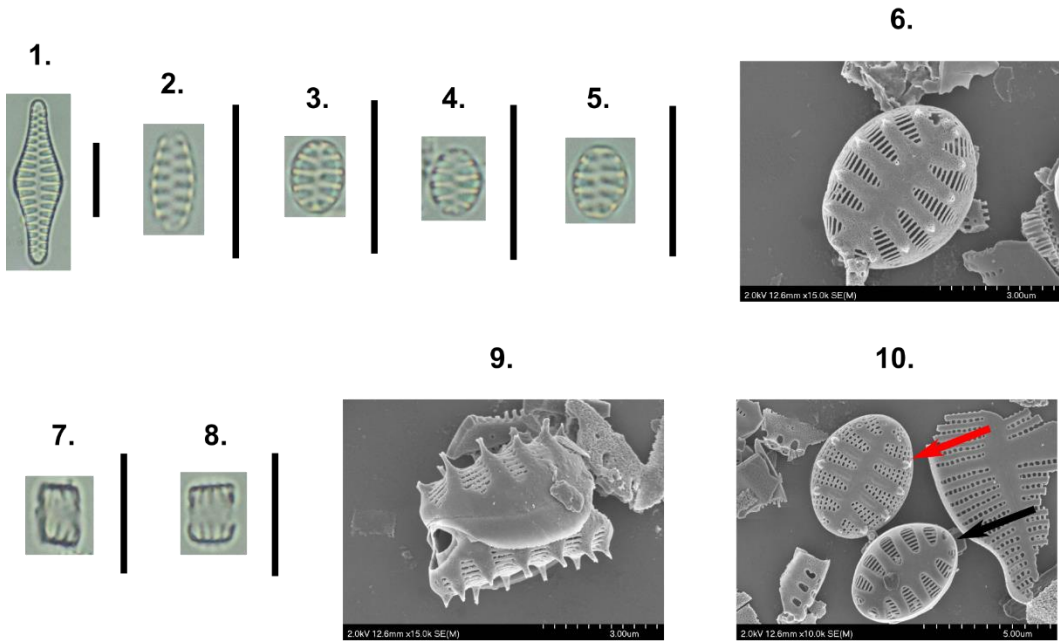
13-14. *Ulnaria ulna*

15. *Phacotus* sp. loricae (circled) in bright field

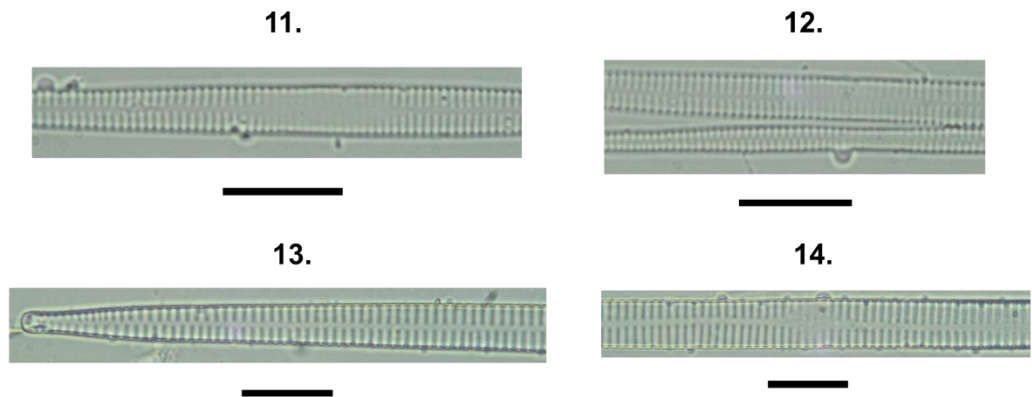
16. Same *Phacotus* sp. loricae (circled) as 15 under polarised light microscope

All scale bars shown represent 10 μ m unless stated otherwise.

Staurosirella Williams & Round



Ulnaria (Kützing) Compère



Other microfossils

